

T 153

49646

CENTRAL LIBRARY
TEZPUR UNIVERSITY

Accession No. 49646
14/9/11

CENTRAL LIBRARY, T. U.
New ACC. NO. T 153

REFERENCE BOOK
NOT TO BE ISSUED
TEZPUR UNIVERSITY LIBRARY

**DEVELOPMENT OF POLYURETHANE
NANOCOMPOSITES**

**A THESIS SUBMITTED IN PARTIAL FULFILLMENT OF THE
REQUIREMENTS FOR THE DEGREE OF
Doctor of Philosophy**

By

Harekrishna Deka

Registration Number 016 of 2009



**School of Science & Technology
Department of Chemical Sciences
Tezpur University
Napaam 784028
Assam, India**

Dedicated to my

Beloved parents

ABSTRACT

Background

The 'polymer nanocomposite' has attracted almost all the scientists and technologists within a short span of time. This is because of the dramatic improvements of many desirable properties by proper incorporation of a small fraction of nanofillers in polymer systems. Notably, these improvements are attained without impairing the fascinating properties of pristine polymers such as light weight characteristic, flexibility, transparency etc. However, despite of considerable progress of this technology, researchers are still in search of the answers of some fundamental questions that are yet to decipher.

Again, polyurethane (PU) being a versatile polymer of contemporary time is demanding its popularity in a diversified field of applications such as coatings, adhesives, foams, sealants, elastomers, fibres, composites, biomaterials and many other niches. This is the result of inherent micro biphasic domain morphology with block copolymeric nature of PU. Further this is added by the possibilities for tailor making properties by varying the composition, structure and domain size of hard and soft segments of PU.

Over the last two decades, polymer science has carried out a significant growth in the field of non-linear highly branched polymers such as dendritic polymers. These polymers possess unique architectural features and have large numbers of surface functionalities. The dendritic polymer includes dendrimer and hyperbranched polymer. The hyperbranched polymers have the feasibilities of industrial production due to easier preparative techniques compared to the dendrimers. Thus it is worth thinking to utilize the hyperbranched polyurethanes (HBPU) as matrices for the preparation of different nanocomposites and to investigate the same.

Further the stringent environmental rules and regulations, gradual exhaustion of petroleum reserves insist the scientists to utilize naturally renewable resources as the feed stocks for polymers. In this regard vegetable oil, a renewable resource, is worth to be mentioned here. A variety of oil bearing seeds are being produced in the vast forest resources and farm lands. Few of such oils have been explored and successfully utilized for the development of various types of polymeric materials. Castor, sunflower, linseed, soybean, palm, rapeseed, canola, corn, tung, coconut, safflower, peanut, cottonseed, rubber seed oil, kamala seed oil, mahua, karanj, neem, tobacco seed oil,

melon seed oil, jatropha seed oil etc. are few such examples. *Mesua ferrea* L. is a plant available abundantly in the countries such as India, Sri Lanka, Bangladesh, Nepal, Indochina (Southeast Asia), Malay Peninsula etc. This is a non-drying oil and the fatty acid compositions have claimed to utilize it as raw material for the preparation of different industrial polymers.

Scopes and Objectives of the Present Investigation

Although *Mesua ferrea* L. seed oil has remarkable potential as a renewable resource based feed stock but only a few reports described its utilization in the fields of medicine, biodiesel and polymer to prepare resinous products such as polyester, PU, poly(ester amide) and epoxy resins. Thus, there is no study on this oil for development of thermoplastic HBPU. Hence, the following questions may arise in this area.

- (i) Whether this oil can be utilized for the preparation of HBPU?
- (ii) Whether the performance characteristics of the hyperbranched polymer can be improved by any physical or chemical means?
- (iii) Whether the modified polymer can be utilized as matrix for the preparation of different types of nanocomposites?
- (iv) Whether the incorporation of different nanofillers into the hyperbranched matrix can lead to the genesis of advanced materials?

Under the above background, the main objectives of the present investigation are as follows-

- (i) To synthesize, characterize and evaluate various properties of *Mesua ferrea* L. seed oil based HBPU.
- (ii) To study the effect of hard and soft segment ratio on the performance of the above PUs.
- (iii) To improve the performance of the synthesized hyperbranched polymer by modifying with other suitable commercial polymer.
- (iii) To improve the performance characteristics of the HBPU systems by nanocomposite formation.
- (iv) To utilize various nanofillers for the preparation of nanocomposite to achieve desirable properties.
- (v) To study the rheological behavior for better understanding of nano-reinforcing mechanism in the nanocomposites.

(vi) To utilize the prepared nanocomposites as advanced materials in the field of surface coating, adhesive, shape memory application, biodegradable biomaterial, antimicrobial, free radical scavenger etc.

The Thesis

Chapter one deals with the general introduction of vegetable oil based PU nanocomposites. A brief review on PU nanocomposites with special emphasis on vegetable oil based polyols for PUs, the importance of such nanocomposites, history, general techniques for preparation, characterization, properties and applications have been described in this chapter. This chapter also focuses the scopes and objectives along with the plans and methodologies of the present investigation.

Chapter two reports the synthesis, characterization and properties evaluation of HBPU with varying hard and soft segment ratios using monoglyceride of *Mesua ferrea* L. seed oil as one of the components. The linear analog (LPU) of HBPU was also synthesized for comparison purpose. The synthesized polymers were characterized by measurement of physical properties like hydroxyl value, inherent viscosity and specific gravity, and other characterization techniques such as FTIR, ¹HNMR, XRD, SEM and GPC analyses. The characterization revealed the hyperbranched nature of the polymers. The performance characteristics such as hardness, flexibility, gloss, adhesion, impact resistance and chemical resistance in different media were determined. Thermal stabilities were found to be increased with the increase of hard segment content. The HBPU with 30% hard segment exhibited the optimum performance characteristics and thus this ratio was maintained in the further investigations. The chapter concludes that *Mesua ferrea* L. seed oil based HBPU can be utilized as thermoplastic materials for various applications as these can be solution as well as melt casted.

Chapter three describes the enhancement in performance characteristics of the HBPU (30% hard segment content) by modifying it with commercially available bisphenol-A based epoxy resin and poly(amido amine) hardener at different weight ratios (HBPU:epoxy = 100:5, 100:10 and 100:20). FTIR spectra were utilized to study the crosslinking reactions. The physical properties such as measurement of density, swelling test, sol fractions, XRD analysis and rheological study were performed. The various performance characteristics like tensile strength, impact resistance, hardness, thermal stability and chemical resistance in different media showed improvement over the pristine HBPU. The morphological study was done by SEM, which revealed good

compatibility between the components. The shape memory property measured at different temperatures exhibited very good shape recovery of 90-98%. Among the three ratios the HBPU:epoxy, 100:20 ratio exhibited the optimum performance and it was chosen as the matrix for nanocomposite formation in further studies.

Chapter four reports the formation of organo montmorillonite (OMMT) nanocomposites using the aforementioned epoxy modified HBPU matrix through an *ex-situ* technique. The formation of the nanocomposites was characterized by FTIR, XRD, SEM and TEM analyses. The physical as well as rheological properties were also studied. The mechanical properties such as tensile strength, impact resistance, scratch hardness and thermal properties were much improved compared to the pristine matrix system. The study showed the high potentiality of the nanocomposites as adhesive materials for a variety of substrates.

Chapter five describes the formation of the OMMT nanocomposites with the same matrix as stated in Chapter 4 by an *in-situ* technique. The formation of the nanocomposites was thoroughly studied by FTIR, XRD and TEM techniques. The physical and rheological properties were also investigated in the same way as done in Chapter 4. It was observed that the various properties such as thermal stability, melting point, tensile strength, scratch hardness, impact resistance etc. were higher than not only the matrix but also the nanocomposites prepared by *ex-situ* technique. Thus other properties such as water vapor barrier, shape memory property, chemical resistance test and more importantly biodegradation study was carried out for these systems.

Chapter six illustrates the effect of modification of OMMT and the properties on the nanocomposites with the same matrix used in Chapter 4 and 5. The highly branched poly(amido amine) (HBPAA) was synthesized using relatively cheap reagents urea and cyanuric chloride with the help of $A_2 + B_3$ approach. The synthesized HBPAA was characterized by the measurements of inherent viscosity, density, solubility test, degree of branching and FTIR, UV, 1H NMR and XRD analyses. Further this HBPAA was utilized to modify the OMMT by two different ways via ion exchanged and sonication processes. Out of the two processes, the sonication based process is more effective as confirmed from XRD and FTIR studies. Therefore, the dose dependency study of the modified OMMT on the nanocomposites was carried out by using sonication modified OMMT only. The formation of modified OMMT nanocomposites was characterized by FTIR, XRD, SEM and TEM analyses. The various properties such as mechanical, thermal, rheological and flame retardancy of the

nanocomposites were tested. The noticeable enhancements in mechanical properties such as impact resistance and scratch hardness, in thermal stability and especially in flame retardancy were achieved compared to the nanocomposites prepared by *in-situ* technique. The performance characteristics of the sonication modified OMMT nanocomposites showed better performance than the ion exchanged modified OMMT nanocomposite of same concentration.

Chapter seven demonstrates the suitability of the HBPU as matrix for silver and iron based nanoparticles. The silver nanocomposites were prepared with both HBPU and LPU matrices to confirm the superiority of the hyperbranched moiety. The formation and distribution of silver nanocomposites were proved by FTIR, XRD and TEM analyses. The mechanical properties such as tensile strength and impact resistance were found to be improved without affecting the flexibility and elongation at break value of the pristine polymers. Excellent improvements in thermal properties were obtained in the prepared nanocomposites. The nanocomposite exhibited remarkable antimicrobial activities towards *Staphylococcus aureus*, *Escherichia coli* and *Candida albicans*, along with the sufficient bacterial biodegradation as proved by the broth culture technique taking the *P. aeruginosa* strains (MTCC 7814 and MTCC 7815). The RBC hemolysis inhibition assay indicates cytocompatibility nature of the materials. The well dispersed iron based nanoparticles in HBPU matrix was characterized by the same techniques as silver nanocomposites. The iron based nanocomposite exhibited remarkable free radical scavenging capability towards DPPH. The iron based nanoparticles had super-paramagnetic behavior and the magnetization was found to be increased after annealing. Thus this chapter directed the high potential of the HBPU/metal nanocomposites in various field of applications.

Chapter eight includes the effect of insertion of modified MWCNT in the hyperbranched matrix on various properties like mechanical, thermal, shape recovery, biodegradation and cytocompatibility. The homogeneous distribution of the MWCNT in the matrix was proved by FTIR, XRD, SEM and TEM analyses. The mechanical and thermal properties were much improved after nanocomposite formation compared to the pristine HBPU. With the increase of concentration of MWCNTs the shape memory property of the nanocomposites was enhanced relatively with reference to the HBPU. The biocompatibility nature in terms of non-toxicity at the cellular level and biodegradability of the nanocomposites indicate their high potentiality in biomedical applications.

Chapter nine, the last chapter of the thesis includes the concluding remarks, highlights of the findings and future scopes of the present investigation. The major achievements of the present investigation are as follows-

- (i) A low cost non-edible vegetable oil, *Mesua ferrea* L. seed oil was successfully utilized for the first time to prepare highly potential HBPU.
- (ii) The synthesized PUs were successfully characterized by the conventional analytical and spectroscopic techniques.
- (iii) The modification of HBPU with commercially available epoxy resin and poly(amido amine) hardener system significantly improved the properties especially mechanical properties, thermal stability, chemical resistance and shape memory behavior.
- (iv) Modified HBPU/OMMT nanocomposites were successfully prepared by *ex-situ* and *in-situ* techniques. The nanocomposites exhibited improvements in performance characteristics. It was noticed that most of the properties of the nanocomposites prepared by *in-situ* technique were superior to that of the nanocomposites prepared by *ex-situ* technique.
- (v) The modes of modification of OMMT by HBPU and their consequent nanocomposites have profound influence on the performance characteristics. The prepared nanocomposites possess enhanced properties especially, the improvements in thermal and flame retardancy was remarkable.
- (vi) HBPU is better matrix for the preparation of silver nanocomposites than the linear analog. The well dispersed and highly stable silver, and iron based nanoparticle nanocomposites showed better properties than the pristine HBPU. The antimicrobial silver nanocomposites also exhibited adequate biodegradation.
- (vii) The HBPU/MWCNT nanocomposites showed excellent improvements in the properties like mechanical, thermal, rheological and shape memory behavior. They also showed higher biodegradation and more cytocompatibility nature compared to the pristine HBPU.
- (viii) The rheological behaviors of the above nanocomposites confirmed the presence of strong interactions between fillers and the matrices.
- (ix) The different nanocomposites have high potential to be used as advanced surface coating materials, adhesive, highly thermo-stable materials, free radical scavenging, biodegradable biomaterials and shape memory materials.

DECLARATION

I do hereby declare that the thesis entitled "*Development of Polyurethane Nanocomposites*", submitted to the Department of Chemical Sciences, Tezpur University, is a record of original research work carried out by me. All sources of assistance have been assigned due acknowledgment. I also declare that neither this work as a whole nor a part of it has been submitted to any other University or Institute for any other degree, diploma or award.

Place: Tezpur University, Tezpur


(Harekrishna Deka)

Date: 10/08/2010



TEZPUR UNIVERSITY

Ph: 03712-267004

(A Central University established by an Act of Parliament) 03712-267005

NAPAAM, TEZPUR-784028

Fax: 03712-267006

DISTRICT: SONITPUR:: ASSAM:: INDIA

03712-267005

E-mail: nkarak@tezu.ernet.in

CERTIFICATE

This is to certify that the thesis entitled "*Development of Polyurethane Nanocomposites*" submitted to the Tezpur University in the Department of Chemical Sciences under the School of Science & Technology, in partial fulfillment for the award of the Degree of Doctor of Philosophy in Science, is a record of research work carried out by Harekrishna Deka under my personal supervision and guidance.

All helps received by him from various sources have been duly acknowledged.

No part of this thesis has been reproduced elsewhere for award of any other degree.

Place: Tezpur University

Date: 10/08/10

(Dr. Niranjana Karak)

Professor

Department of Chemical Sciences
School of Science & Technology



TEZPUR UNIVERSITY

Ph: 03712-267004

(A Central University established by an Act of Parliament) 03712-267005

NAPAAM, TEZPUR-784028

Fax: 03712-267006

DISTRICT: SONITPUR:: ASSAM :: INDIA

03712-267005

CERTIFICATE

This is to certify that the thesis entitled "*Development of Polyurethane Nanocomposites*" submitted to the Tezpur University in the Department of Chemical Sciences under the School of Science and Technology, in partial fulfillment for the award of the Degree of Doctor of Philosophy in Science, has been examined by us on and found to be satisfactory.

The committee recommends for the award of the degree of Doctor of Philosophy.

Principal Supervisor

External Examiner

Date:

Date:

PREFACE

The emergence of polymer nanocomposite has opened up new avenues to cope up with the contemporary problems. The growth rate of polymer nanocomposites would certainly lead to the genesis of a new era in Material Science. At the same time, replacement of petroleum based raw materials by renewable resource based feed stocks for the production of polymers is thriving all around. One of such renewable resource is *Mesua ferrea* L. seed oil, a vegetable oil, having ample potential to design various polymers for its suitable fatty acid compositions. Again, the novel and inimitable architectural features of hyperbranched polymers with large numbers of active surface functionalities have attracted a considerable attention as advanced frontier macromolecules in Polymer Science and Technology.

Thus the foremost objective of this thesis is to utilize this vegetable oil in the development of hyperbranched polyurethanes and their different nanocomposites. The thesis describes the synthesis, characterization, property and application of *Mesua ferrea* L. seed oil based thermoplastic hyperbranched polyurethanes. Attempts have been made to modify the hyperbranched polyurethane by commercially available epoxy resin to improve its performance characteristics. The properties of this thermoset matrix were further enhanced by formation of clay nanocomposites by using different techniques. The clay was also modified by highly branched poly(amido amine) to improved better compatibility with the matrix. The pristine thermoplastic hyperbranched polyurethane was also exploited as the matrix for the different nanofillers such as carbon nanotube, silver and iron based nanoparticles. The prepared nanocomposites exhibited high potential to be applicable in a spectrum of applications such as advanced surface coating materials, adhesive, highly thermo-stable materials, free radical scavengers, biodegradable biomaterials and shape memory materials.

Date: 10/08/2010

Place: Napaam, Tezpur


(Harekrishna Deka)

CONTENTS

<i>Content</i>	<i>Page No.</i>
Abstract	i
Declaration	vii
Certificate of Supervisor	viii
Certificate of External Examiner	ix
Preface	x
Contents	xi
List of Abbreviations and Symbols	xviii
List of Tables	xx
List of Figures	xxi
List of Schemes	xxv
Acknowledgement	xxvi

CHAPTER 1

General introduction

1.1. Introduction	1
1.2. Background	3
1.3. Classification of polymer nanocomposites	4
1.4. Materials and methods	5
1.4.1. Materials	5
1.4.1.1. Polyurethane	5
1.4.1.1.1. Macroglycol	6
1.4.1.1.2. Diisocyanate	8
1.4.1.1.3. Chain extender	9
1.4.1.1.4. Catalyst	11
1.4.1.2. Nano-dimensional reinforcing agents	12
1.4.2. Methods	16
1.4.2.1. Solution method	16
1.4.2.2. <i>In-situ</i> polymerization	17
1.4.2.3. Melt mixing	17
1.5. Characterization	20
1.6. Properties	22

1.6.1. Mechanical	22
1.6.2. Dynamic mechanical	23
1.6.3. Barrier	23
1.6.4. Thermal	24
1.6.5. Flame retardancy	24
1.6.6. Rheological	25
1.6.7. Optical	25
1.6.8. Electrical	25
1.6.9. Magnetic	26
1.6.10. Catalytic activity	26
1.6.11. Biodegradation	26
1.7. Applications	26
1.8. A short review on vegetable oil based polyurethane nanocomposites	29
1.9. Scopes and objectives of the present investigation	45
1.10. Plans of work	46
References	47

CHAPTER 2

Synthesis, characterization and properties of *Mesua ferrea* L. seed oil based hyperbranched polyurethanes

2.1. Introduction	59
2.2. Experimental	60
2.2.1. Materials	60
2.2.2. Instruments and methods	62
2.2.2.1. Preparation of monoglyceride of <i>Mesua ferrea</i> L. seed oil	63
2.2.2.2. Synthesis of hyperbranched polyurethanes	63
2.2.2.3. Sample preparation for performance studies	64
2.3. Results and discussions	65
2.3.1. Synthesis	65
2.3.2. Characterization	66
2.3.3. Physical properties	68
2.3.4. Morphological study	70
2.3.5. Mechanical properties	71
2.3.6. Thermal properties	72

2.3.7. Chemical resistance test	73
2.4. Conclusions	73
References	74

CHAPTER 3

Modification of HBPU by epoxy resin

3.1. Introduction	77
3.2. Experimental	78
3.2.1. Materials	78
3.2.2. Instruments and methods	79
3.2.2.1. Preparation of the HBPU and its modification with epoxy resin	80
3.2.2.2. Sample preparation for performance studies	80
3.3. Results and discussions	81
3.3.1. Curing study	81
3.3.2. Physical properties	83
3.3.3. Rheological properties	84
3.3.4. Morphological study	85
3.3.5. Mechanical properties	86
3.3.6. Thermal properties	87
3.3.7. Shape memory study	89
3.3.8. Chemical resistance test	89
3.4. Conclusions	90
References	90

CHAPTER 4

MHBPU/clay nanocomposites prepared by *ex-situ* technique

4.1. Introduction	94
4.2. Experimental	95
4.2.1. Materials	95
4.2.2. Instruments and methods	96
4.2.2.1. Preparation of the HBPU and its modification with epoxy resin	96
4.2.2.2. Preparation of nanocomposites	97
4.2.2.3. Sample preparation for performance studies	97
4.3. Results and discussions	97

4.3.1. Formation of nanocomposites	97
4.3.2. Characterization	97
4.3.3. Physical properties	101
4.3.4. Rheological properties	101
4.3.5. Mechanical properties	108
4.3.6. Adhesion study	110
4.3.7. Thermal properties	112
4.4. Conclusions	113
References	113

CHAPTER 5

MHBPU/clay nanocomposites prepared by *in-situ* technique

5.1. Introduction	118
5.2. Experimental	119
5.2.1. Materials	119
5.2.2. Instruments and methods	119
5.2.2.1. Preparation of the HBPU and its modification with epoxy resin	119
5.2.2.2. Preparation of nanocomposites	120
5.2.2.3. Sample preparation for performance studies	120
5.2.2.4. Biodegradation by broth culture technique	120
5.3. Results and discussions	121
5.3.1. Formation of nanocomposites	121
5.3.2. Characterization	121
5.3.3. Physical properties	124
5.3.4. Rheological properties	125
5.3.5. Mechanical properties	130
5.3.6. Water vapor barrier property	133
5.3.7. Thermal properties	133
5.3.8. Shape memory study	135
5.3.9. Chemical resistance test	135
5.3.10. Biodegradation study	135
5.4. Conclusions	137
References	137

CHAPTER 6

Highly branched poly(amido amine) modified clay/MHBPU nanocomposites

6.1. Introduction	141
6.2. Experimental	143
6.2.1. Materials	143
6.2.2. Instruments and methods	144
6.2.2.1. Synthesis of highly branched poly(amido amine)	144
6.2.2.2. Preparation of the HBPU and its modification with epoxy resin	145
6.2.2.3. Modification of OMMT by HBPAA	145
6.2.2.4. Preparation of nanocomposites	145
6.2.2.5. Sample preparation for performance studies	145
6.3. Results and discussions	146
6.3.1. Synthesis of HBPAA	146
6.3.2. Characterization of HBPAA	147
6.3.3. Modification of OMMT	149
6.3.4. Characterization of the nanocomposites	150
6.3.5. Rheological properties of the nanocomposites	153
6.3.6. Mechanical properties of the nanocomposites	154
6.3.7. Thermal properties of the nanocomposites	155
6.3.8. Flame retardancy of the nanocomposites	157
6.4. Conclusions	158
References	158

CHAPTER 7

HBPU/metal nanocomposites

7.1. Introduction	162
7.2. Experimental	164
7.2.1. Materials	164
7.2.2. Instruments and methods	165
7.2.2.1. Preparation of HBPU, LPU	165
7.2.2.2. Preparation of silver nanocomposites	165
7.2.2.3. Preparation of iron based nanocomposite	165
7.2.2.4. Antimicrobial assay	166

7.2.2.5. Biodegradation of silver nanocomposites by broth culture technique	166
7.2.2.6. RBC hemolysis protection assay of silver nanocomposites for cytocompatibility	166
7.2.2.7. Free radical scavenging activity of iron based nanocomposite	167
7.2.2.8. Sample preparation for performance studies	167
7.3. Results and discussions	167
7.3.1. Formation of nanocomposites	167
7.3.2. Characterization of silver nanocomposites	168
7.3.3. Characterization of iron based nanocomposite	171
7.3.4. Antimicrobial activity of silver nanocomposites	174
7.3.5. Mechanical properties of silver nanocomposites	176
7.3.6. RBC hemolysis protection assay for cytocompatibility of silver nanocomposites	177
7.3.7. Free radical scavenging activity of iron based nanocomposite	178
7.3.8. Magnetic behavior of iron based nanocomposite	178
7.3.9. Thermal properties of the nanocomposites	179
7.3.10. Biodegradation of silver nanocomposites	181
7.4. Conclusions	182
References	183

CHAPTER 8

HBPU/MWCNT nanocomposites

8.1. Introduction	187
8.2. Experimental	188
8.2.1. Materials	188
8.2.2. Instruments and methods	189
8.2.2.1. Preparation of HBPU	190
8.2.2.2. Preparation of HBPU/MWCNT nanocomposites	190
8.2.2.3. Biodegradation study by broth culture technique	190
8.2.2.4. RBC hemolysis protection assay for cytocompatibility	190
8.3. Results and discussions	190
8.3.1. Formation of nanocomposites	190
8.3.2. Characterization	190

8.3.3. Rheological properties	194
8.3.4. Mechanical properties	200
8.3.5. Thermal properties	201
8.3.6. Shape memory study	204
8.3.7. RBC hemolysis protection assay	205
8.3.8. Biodegradation	206
8.4. Conclusions	208
References	208

CHAPTER 9

Conclusions and future directions

9.1. Summary and conclusions	213
9.2. Future directions	215
List of Publications	216

LIST OF ABBREVIATIONS AND SYMBOLS

b.p.	boiling point
c.c.	cubic centimeter
cm	centimeter(s)
DBTDL	dibutyl tin dilaurate
deg C/°C	degree centigrade
dia.	diameter
dL	deci liter(s)
DSC	differential scanning calorimetry
FTIR	Fourier transform infrared
F _w	Formula weight
g	gram(s)
GPC	gel permeation chromatography
h	hour(s)
K	Kelvin
kN	kilo-Newton
kV	kilo-volt
L	liter(s)
lb	pound(s)
m	meter(s)
mA	mili ampear
min	minute(s)
mL	mili liter(s)
mm	mili meter(s)
mol	mole
m.p.	melting point
M _n	number average molecular weight
M _w	weight average molecular weight
MPa	mega pascal
N	Newton
NMR	nuclear magnetic resonance
nm	nano meter(s)
OMMT	organically modified montmorillonite

PCL	Poly(ϵ -caprolactone) diol
PP	polypropylene
ppm	parts per million
RBC	red blood cell
s	second(s)
SEM	scanning electron microscope
TDI	toluene diisocyanate
TEM	transmission electron microscopy
T_g	glass transition temperature
TGA	thermogravimetric analysis
TMS	tetramethyl silane
UTM	universal testing machine
UV	ultraviolet
v	volume
w	weight
XRD	X-ray diffraction
μm	micro meter(s)
μM	micro molar(s)
μL	micro liter(s)
%	percentage
η_{inh}	inherent viscosity
λ_{max}	wavelength maximum
θ	scattering angle

LIST OF TABLES

- Table 1.1: Frequently used macroglycols in PU synthesis
- Table 1.2: Frequently used diisocyanates in PU synthesis
- Table 1.3: Frequently used chain extenders in PU synthesis
- Table 1.4: Commonly used catalysts in PU synthesis
- Table 1.5: Commercially available polymer nanocomposites and their applications
- Table 1.6: Chemical structure and physical properties of some fatty acids present in vegetable oils
- Table 1.7: Few important vegetable oils with their fatty acid compositions
- Table 2.1: Composition of reactants for the hyperbranched and linear PUs
- Table 2.2: FTIR spectral data of the hyperbranched and linear PUs
- Table 2.3: Physical properties of the hyperbranched and linear PUs
- Table 2.4: Mechanical properties of the hyperbranched and linear PUs
- Table 2.5: The characteristic thermal decomposition temperatures
- Table 3.1: Technical specifications of epoxy resin and hardener
- Table 3.2: Composition and curing time of the modified systems at 120 °C
- Table 3.3: Physical and mechanical properties of the MHBPU
- Table 3.4: Thermal properties of MHBPU
- Table 3.5: Shape memory data of MHBPU and HBPU at various temperatures
- Table 4.1: Physical and mechanical properties of the nanocomposites
- Table 4.2: T_g , T_m and ΔH_m values of the nanocomposites
- Table 4.3: Thermal stability data of the nanocomposites
- Table 5.1: McFarland Nephelometer standards
- Table 5.2: Physical and mechanical properties of the nanocomposites
- Table 5.3: Thermal properties and shape memory data of the nanocomposites
- Table 5.4: Thermal stability data of the nanocomposites
- Table 5.5: Chemical resistance in terms of percentage of weight loss in grams
- Table 6.1: Mechanical properties, LOI values and UL 94 rating of the nanocomposites
- Table 6.2: Thermal properties of the nanocomposites
- Table 7.1: Mechanical properties of the silver nanocomposites
- Table 7.2: Thermal properties of the silver nanocomposites
- Table 8.1: Mechanical properties and characteristic thermal decomposition temperature
- Table 8.2: T_m , ΔH_m and shape recovery of the nanocomposites

LIST OF FIGURES

- Fig. 1.1: Different states of polymer/clay nanocomposites
- Fig. 1.2: Different types of nanomaterials
- Fig. 1.3: (a) SWCNT, (b) MWCNT and (c) cellulose chain structure
- Fig. 1.4: Crystal structure of 2:1 layered silicate
- Fig. 1.5: Different application fields of polymer nanocomposites
- Fig. 1.6: Scientific publications vs. year of publication searched by Scopus
- Fig. 1.7: Representation of triglyceride
- Fig. 1.8: General structure of castor oil triglyceride
- Fig. 2.1: Structure of glycerol (1,2,3-propane triol)
- Fig. 2.2: Structure of poly(ϵ -caprolactone) diol
- Fig. 2.3: Structure of toluene diisocyanate
- Fig. 2.4: FTIR spectra of HBPU30 and linear analog
- Fig. 2.5: FTIR spectra of all the HBPU s in the $-\text{NH}$ and $-\text{CO}$ stretching region
- Fig. 2.6: ^1H NMR spectrum of HBPU30
- Fig. 2.7: WAXD patterns of all the HBPU s and linear analog
- Fig. 2.8: SEM micrographs of HBPU s
- Fig. 2.9: Stress-strain profile of HBPU s and linear analog
- Fig. 2.10: TGA thermograms of HBPU s and linear analog
- Fig. 3.1: FTIR spectra of (a) MHBPU20, (b) MHBPU10, (c) MHBPU5 before curing and (d) MHBPU10 after curing
- Fig. 3.2: XRD diffractograms of MHBPU s
- Fig. 3.3: Dependence of (a) G' , (b) G'' , (c) η^* with respect to frequency and (d) variation of G' as a function of time
- Fig. 3.4: SEM micrographs of MHBPU s
- Fig. 3.5: TGA thermograms of MHBPU s and HBPU
- Fig. 3.6: DSC curves of MHBPU s and HBPU
- Fig. 3.7: Pictorial diagram of the shape memory behavior of MHBPU s
- Fig. 4.1: FTIR spectra of MHBPU and MHPUNCE1
- Fig. 4.2: WAXD of the nanocomposites and OMMT
- Fig. 4.3: SEM micrographs of (a) MHPUNCE1, (b) MHPUNCE2.5 and (c) MHPUNCE5
- Fig. 4.4: TEM images of (a) MHPUNCE1, (b) MHPUNCE2.5 and (c) MHPUNCE5

- Fig. 4.5: Shear viscosity as a function of time
- Fig. 4.6: Shear viscosity as a function of shear rate
- Fig. 4.7: Temperature dependence of shear viscosity
- Fig. 4.8: Time dependence plot of (a) G' , (b) G'' and (c) η^*
- Fig. 4.9: Plot of (a) G' and (b) G'' against frequency
- Fig. 4.10: Plot of G' against G'' for the nanocomposites
- Fig. 4.11: Frequency dependence η^* of MHBPU and nanocomposites
- Fig. 4.12: Variation of $\tan\delta$ with frequency of the nanocomposites and MHBPU
- Fig. 4.13: Plot of (a) G' and (b) G'' as a function of temperature sweep
- Fig. 4.14: Temperature dependence η^* of the nanocomposites and MHBPU
- Fig. 4.15: Variation of adhesive strength for different substrates of the nanocomposites
- Fig. 4.16: TGA thermograms of the nanocomposites
- Fig. 5.1: FTIR spectra of the MHBPU and nanocomposites
- Fig. 5.2: WAXD of the OMMT and nanocomposites
- Fig. 5.3: TEM micrograph of MHPUNCI2.5 (representative one)
- Fig. 5.4: A photograph showing the retention of transparency of the nanocomposites
- Fig. 5.5: Shear viscosity as a function of time
- Fig. 5.6: Shear viscosity as a function of shear rate
- Fig. 5.7: Temperature dependence shear viscosity of the nanocomposites
- Fig. 5.8: Time dependence plot of (a) G' , (b) G'' and (c) η^* of the nanocomposites
- Fig. 5.9: Plot of (a) G' and (b) G'' against frequency
- Fig. 5.10: Plot of G' against G'' of the nanocomposites
- Fig. 5.11: Frequency dependence η^* of the nanocomposites
- Fig. 5.12: Variation of $\tan\delta$ with frequency of the nanocomposites
- Fig. 5.13: Plot of (a) G' and (b) G'' as a function of temperature sweep
- Fig. 5.14: Temperature dependence η^* of the nanocomposites
- Fig. 5.15: Water vapor permeability of the MHBPU and nanocomposites
- Fig. 5.16: Thermogravimetric curves of the nanocomposites
- Fig. 5.17: Statistics for the growth of *P. aeruginosa* strain (a) MTCC 7815, (b) MTCC 7814 and SEM pictures of the degraded nanocomposite films: (a) MHPUNCI1 and (b) MHPUNCI5
- Fig. 6.1: Structure of cyanuric chloride
- Fig. 6.2: Structure of urea
- Fig. 6.3: Structure of diisopropylethylamine

- Fig. 6.4: FTIR spectra of (a) HBPA, (b) OMMT, (c) modified OMMT (sonicated) and (d) modified OMMT (exchanged)
- Fig. 6.5: ^1H NMR spectrum of HBPA (T=terminal, L=linear and D=dendritic unit)
- Fig. 6.6: XRD diffractograms of OMMT, modified OMMT and nanocomposites
- Fig. 6.7: FTIR spectra of the nanocomposites
- Fig. 6.8: Representative TEM images of (a) MHPUMNC1 and (b) MHPUMNC5
- Fig. 6.9: SEM images of (a) MHPUMNC1, (b) MHPUMNC2.5, (c) MHPUMNC2.5(E) and (d) MHPUMNC5
- Fig. 6.10: Variation of (a) G' , (b) G'' and (c) η^* with frequency
- Fig. 6.11: TGA thermograms of the MHBPU and nanocomposites
- Fig. 6.12: DSC thermograms of the nanocomposites
- Fig. 7.1: UV-visible absorption spectra of (a) nanocomposites and pristine polymers, (b) time evolution curves starting from formation to maximum stability period
- Fig. 7.2: FTIR spectra of the silver nanocomposites
- Fig. 7.3: XRD patterns of the silver nanocomposites
- Fig. 7.4: Typical TEM micrographs of (a) LPUAg2.5 and (b) HBPUAg2.5 and corresponding histograms for distribution of particle size
- Fig. 7.5: UV spectra of iron-HBPU-PANI nanocomposite after (a) 0.5 h and (b) 24 h
- Fig. 7.6: FTIR spectra of (a) iron-HBPU-PANI nanocomposite and (b) annealed iron-HBPU-PANI nanocomposite
- Fig. 7.7: XRD patterns of (a) pure HBPU, (b) iron-HBPU-PANI nanocomposite and (c) annealed iron-HBPU-PANI nanocomposite
- Fig. 7.8: TEM micrograph and histogram of the iron-HBPU-PANI nanocomposite
- Fig. 7.9: SEM image of iron-HBPU-PANI nanocomposite
- Fig. 7.10: The comparative bar-graphs of antimicrobial efficiency of the silver nanocomposites against (a) *Staphylococcus aureus*, (b) *Escherichia coli*, and (c) *Candida albicans* with standard antibiotics and antifungal
- Fig. 7.11: The RBC hemolysis inhibition assay of the silver nanocomposites
- Fig. 7.12: Scavenging capacity (%) of different systems
- Fig. 7.13: Magnetization curve of the nanocomposites (a) iron-HBPU-PANI and (b) annealed iron-HBPU-PANI
- Fig. 7.14: Thermogravimetric curves of the silver nanocomposites
- Fig. 7.15: TGA curve of iron-HBPU-PANI nanocomposite

- Fig. 7.16: Statistics for the growth of *P. aeruginosa* strain (a) MTCC 7814, (b) MTCC 7815 and SEM pictures of the degraded nanocomposite films: (c) LPUAg2.5 (d) HBPUGAg2.5
- Fig. 8.1: FTIR spectra of (a) acid modified MWCNT, (b) HBPUMWCNT1, (c) HBPUMWCNT2.5 and (d) HBPUMWCNT5
- Fig. 8.2: XRD diffractograms of MWCNT, HBPU and the nanocomposites
- Fig. 8.3: SEM micrographs of (a) HBPUMWCNT1, (b) HBPUMWCNT2.5 and (c) HBPUMWCNT5
- Fig. 8.4: TEM images of (a) magnified single MWCNT and (b) HBPUMWCNT2.5
- Fig. 8.5: Stability of dispersed MWCNT in (a) HBPU matrix after seven months and (b) DMF after one week
- Fig. 8.6: Shear viscosity as a function of time
- Fig. 8.7: Shear viscosity as a function of shear rate
- Fig. 8.8: Temperature dependence shear viscosity of the nanocomposites and HBPU
- Fig. 8.9: Frequency dependence of (a) G' and (b) G'' of the nanocomposites and HBPU
- Fig. 8.10: Time dependence plot of (a) G' , (b) G'' and (c) η^* of the nanocomposites and HBPU
- Fig. 8.11: Plot of (a) η^* against frequency of the nanocomposites and HBPU, (b) shear and η^* against shear rate or frequency
- Fig. 8.12: Variation of $\tan\delta$ with frequency
- Fig. 8.13: Plot of (a) G' and (b) G'' as a function of temperature sweep
- Fig. 8.14: Temperature dependence η^* of the nanocomposites and HBPU
- Fig. 8.15: TGA thermograms of MWCNT and nanocomposites
- Fig. 8.16: Shape recovery behavior of the nanocomposites measured at 60 °C: (a) initial shape, (b) intermediate shape and (c) permanent shape after recovery
- Fig. 8.17: The RBC hemolysis protection assay of the nanocomposites
- Fig. 8.18: Statistics for the growth of *P. aeruginosa* strain (a) MTCC 7814, (b) MTCC 7815 and SEM images of degraded nanocomposites: (c) HBPUMWCNT1 and (d) HBPUMWCNT5

LIST OF SCHEMES

- Scheme 1.1: Formation of urethane linkage
- Scheme 1.2: Schematic presentation for the preparation of polymer nanocomposites by solution method
- Scheme 1.3: Schematic diagram for the preparation of polymer nanocomposites by *in-situ* polymerization technique
- Scheme 1.4: Flow chart diagram for different steps of the melt mixing technique
- Scheme 1.5: General scheme of the formation of vegetable oil based PU/epoxy systems
- Scheme 2.1: Synthesis of HBPU
- Scheme 3.1: Proposed crosslinking reactions of HBPU with epoxy and hardener
- Scheme 4.1: Schematic representation of interface interactions of MHBPU with nanoclay
- Scheme 5.1: Proposed mechanism for interactions between clay and *in-situ* formed HBPU
- Scheme 6.1: Chemoselective reactivity of cyanuric chloride
- Scheme 6.2: Synthesis of highly branched poly(amido amine)
- Scheme 6.3: Possible interactions of modified OMMT with the matrix
- Scheme 8.1: Possible interactions of MWCNTs with HBPU matrix

ACKNOWLEDGMENT

It is my greatest pleasure to express my gratitude to large numbers of people who have been directly or indirectly influence and encourage over the course of my studies and my life in general.

First of all, I would like to express my deep sense of gratitude and indebtedness to my research guide Prof. Niranjan Karak, Department of Chemical Sciences, Tezpur University for his invaluable guidance, support, advice and a wonderful companion throughout my Ph.D. work. His dedication towards research and indomitable spirit would ever remain as a source of inspiration for me.

It is my pleasant duty to acknowledge with thanks the co-operation and support extended to me by the authority of Tezpur University and entire community of the Department of Chemical Sciences, for allowing me to use the administrative and technical facilities required for my research work.

It is my greatest pleasure to acknowledge the present and former Heads of the Department Prof. T. K. Maji, Prof. N. S. Islam (Dean, Research and Development) and Dr. R.K. Dutta for giving me the opportunity to work on my topic and valuable advises throughout my stay at Tezpur University.

I would also like to express my sincere gratitude and humble respect to Prof. S. K. Dolui and Dr. R. Borah, members of my doctoral research committee for their timely help and advises.

I am immensely grateful to Prof. R.C. Deka, Dr. A.K. Phukan, Dr. A.J. Thakur, Dr. P. Puzari and Mr. K.K. Bania faculty members of Department of Chemical Sciences, Tezpur University for valuable suggestions and advices. Words fall short as I extend my gratitude to Prof. A.K. Buragohain, Registrar, Tezpur University for his cooperation during the course of my work.

My heartfelt thanks go to my senior lab-mates Dr. Nandini Dutta, Dr. Jyotishmoy Borah, Dr. Sibdas Singha Mahapatra and Dr. Suvanghu Dutta for their manifold help and active co-operation over all these years. I would also like to thank my junior group members Uday Konwar, Gautam Das, Buddhadeb Roy, Rocktotpal Konwarh for their constant inspiration and help during my Ph.D. years.

I would like to offer my sincere thanks to Dr. Biren Gohain, Dr. Binoy Saikia, Mr. Ranjan D. Kalita, Mr. Nipu Dutta, Mr. Raju K. Borah, Mr. Sankur Phukan, Dr. Kishor K. Baruah, Mr. Ratan Baruah and Mr. Jayanta Bora for instrumental and

experimental helps. IIT Guwahati, NEIST Jorhat, NEHU Shillong and other institutions are highly acknowledged for their help in analyzing and testing works.

A heartfelt bouquet of appreciation is due to Dr. S. Baruah, Scientist, Petroleum and Natural Gas Division, North Eastern Institute of Science and Technology (NEIST), Assam, Dr. S.K. Bharadwaj, Mr. Rupam Sarmah, Mr. Nitul Kakati, Mr. Chandan Borgohain for their precious support in parts of experimental work.

I would also like to express my sincere thanks to Mr. D. Bharali, Mr. P. Nath, Mr. H. Gogoi and Mr. B.G. Chetry.

I wish to thank all my research scholar friends for their help and support during the course of my work.

I am also grateful to DST, New Delhi for financial support to me as JRF and SRF.

I am grateful to Mrs. Sushmita Karak for her encouragement and co-operation.

Finally, I owe heartfelt gratitude to my mother for her blessings and support, my elder sister- Nilakshi ba and brother Achyut Krishna for constantly inspiring me to carry out my research work to completion. I am thankful to all my relatives and well-wisher for their encouragement. The endless love of them will always be in my heart that will inspire me in every step of my future life.

Unique thoughts of gratitude go to my wonderful late father. I wish I would had the opportunity to share all this achievement with you.

Place : Tezpur University, Tezpur

Date : 10/08/2010

Harekrishna Deka
(Harekrishna Deka)

CHAPTER 1

General introduction

1.1. Introduction

Polymer nanocomposites have carved a unique position in the niche of advanced materials. Modification of pristine polymers by various physico-chemical means is indispensable in the context of their low level of various desired properties. However, the filled systems and conventional composites may not always represent the ideal means due to the disproportionate property improvement in relation to the incorporation of a high amount of reinforcing agent(s). It is pertinent to mention that nanoscience and nanotechnology has opened up a new avenue of structure-property tailoring in the domain of polymers¹ for multifaceted advanced applications. The “nano-effect” leads to tremendous property enhancement with a low level of reinforcing agent. This explains the genesis of polymer nanocomposites.

Polymer nanocomposites are combination of multi-phasic materials with different compositions and structures, where at least one of the dimensions of a phase is in nanoscale regime. Starting from the Toyota's research works in 1988^{2,3} the popularity of polymer nanocomposites has reached a pinnacle with colossal application oriented utilities. This exponential growth of interest in the field of polymer nanocomposites is due to the remarkable improvement in properties like moduli, mechanical strength, thermal, gas barrier, flame retardant, biodegradability⁴⁻⁹ of pristine polymers etc. Although the sparking research thrust to unravel the mechanism of improvements, but it is still in mist. It is thought that the altered properties of nanocomposites are associated with the changes in polymer molecular dynamics and crystallinity on addition of nano-dimensional reinforcing agents.¹⁰ The geometrical shape and size of nanomaterials also play important roles in tuning the interactions and hence the properties of such systems.¹¹

In so far large varieties of polymeric systems have been investigated as matrices for preparation of nanocomposites, in which segmented copolymers attracted a significant interest. Polyurethane (PU) is a versatile multi-block copolymer that can be efficiently tailored to give a diverse range of products in the domain of coatings,

Parts of this work is under communication

fibers, adhesives, rubber and thermoplastic elastomers, sealants, foams, biomedical and so on.¹²⁻¹⁴ The repeating unit in PU is the urethane linkages but other moieties such as urea, ester, ether, aromatic groups etc. may also present in the structure.¹⁵ PU consists of two incompatible structural units viz. soft and hard segments. The soft segments comprise of linear long chain diols or polyols and the hard segments form from diisocyanate and short chain extender molecules such as diols or diamines. While the soft segments are flexible and weakly polar in nature, the hard segments are rigid and highly polar.¹⁶ Soft segments provide flexibility and hard segments impart strength and high elasticity to PU due to the stabilization by the H-bonding among themselves. The unique possibility of tailor making the properties of PU is attributing to its versatility.¹⁷ The perfection and degree of phase separation have ample contributions to the properties of PU and are dependent on molar composition, synthetic procedure and thermal history.¹⁸ The influence of structure and intra and inter interactions of hard and soft segments on various properties like physical, thermal and chemical properties of this material is well documented.^{19,20}

Recently, the used of hyperbranched polymers have opened up the avenue for production of advanced polymeric materials. Hyperbranched polymers are 3D highly branched macromolecules with some missing branches and defects in their structures. The easy and one step synthetic procedures make the hyperbranched polymers more industrially acceptable compared to the dendrimers, other class of dendritic polymer. The hyperbranched polymers show unique properties like low melt and solution viscosity, high solubility and reactivity, easy modification to optimize the properties for special applications etc., as they possess peculiar structural features such as high surface functionality, non entanglement and confined geometry.²¹ Two synthetic procedures were adopted for the synthesis of hyperbranched polymers. Most of the hyperbranched polymers have been synthesized by the polycondensation of AB₂ type of monomers. However the availability of suitable AB₂ type monomers is difficult or rare. A₂ + B₃ approach is also used largely for the same purpose, where the properties can be regulated by changing the reaction parameters. Thus synthesis of hyperbranched polyurethane (HBPU) using A₂ + B₃ approach may offer a unique route and the resulted polymer may exhibit uniqueness of hyperbranched character.

There is a continuous declination of the use of petroleum based feedstock in *manufacturing different industrial products including polymers*. The emerging environmental issues such as volatile organic solvent emissions and recycling or waste disposal problems, spiraling rise in prices and fast exhaustion of world oil pools

compelled the scientists for the use of renewable natural resources as eco-friendly and cost effective alternative materials.^{22,23} Vegetable oil is one of such renewable resources drawing enormous attention in the production of different polymeric materials such as epoxy, alkyd, poly(ester amide), PU etc.²⁴⁻³³ There are also reports on utilization of such oils in different industrial applications like surface coatings including paints, varnishes etc., printing inks, lubricants, emulsifiers, plasticizers, multipurpose additives etc.²⁸⁻³⁶ These oils possess several advantages viz. low toxicity, physical and chemical stability, aptitude to facile chemical modification, ease of handling and transport, possibility of recycling, renewability and biodegradability, easily availability in large quantities, and most importantly environmentally benign in nature.²⁵⁻²⁷ A variety of oil bearing seeds have been found in the forest resources and farm lands of India and so far about 350 oil bearing crops are identified. Linseed, castor, soybean, sunflower, safflower, tung, coconut etc. are a few seed oils that are used traditionally for the preparation of polymeric materials. Non-traditional rubber seed oil, neem oil, karanja oil, jatropha seed oil, kamala seed oil, lesquerella oil, melon seed oil, apricot oil, *Annona squamosa*, African mahogany seed oil, African locust bean seed oil etc. are also used for the same reason. Therefore, investigation of vegetable oil based HBPU may lead to the genesis of new avenues in the field of PU.

1.2. Background

In 1970 the term “nanocomposite” was first proposed by Theng.³⁷ The terms like “hybrid nanocomposite”, “nano structural composite”, “nano biocomposite” etc. are also used to describe the different types of polymer nanocomposite. One of the earliest reports described by Hess and Parker in 1966 was the stable dispersion of metallic cobalt particles of uniform size of 1-100 nm range in the polymer solutions.³⁸ Although the mile stone of polymer/clay nanocomposite started from the work of Toyota’s research^{2,3}, the research on polymer/clay intercalation can be trace back to before 1980.^{39,40} But these earlier works failed to report the remarkable improvement in the properties of polymers. Since then the number of literatures on polymer nanocomposite have been increasing continuously every year.

The history of PU chemistry dates back to 1937 when Otto Bayer developed PU fiber.⁴¹⁻⁴³ However, it had to wait till 1950’s to come into the general market. Nowadays, the PU made products are flourishing the nook and corner of markets. The first successful preparation of HBPU was reported by Spindler and Frechet using AB₂ monomers which contained one hydroxyl group (A) and two blocked isocyanate groups

(B).⁴⁴ The condensation of $A_2 + CB_n$ ($n \geq 2$) monomers for preparation of hyperbranched poly(urea urethane)s was reported by Gao and Yan.⁴⁵ The A_2 -type monomers were diisocyanates and CB_n -type monomers were compounds containing one amino group and multihydroxyl groups for the above reaction. The $AA^* + B^*B_2$ technique for the preparation of hyperbranched poly(urea urethane)s was proposed by Bruchmann et al. in 2003.⁴⁶ All the monomers, A_2 and B_3 (or B^*B_2) are of low molar mass and have short distances between the branch points. Therefore the HBPU lack of entanglement and they exhibit inferior mechanical properties. This problem was first solved by Unal et al. work.⁴⁷ They reported the incorporation of oligomeric poly(tetramethylene oxide) and amine terminated poly(propylene oxide) (as A_2 monomers) in the preparation of hyperbranched poly(urethane urea)s. This revealed the facile approach of obtaining hyperbranched product with improved mechanical properties. Most of the works on HBPU nanocomposites are recent only.

1.3. Classification of Polymer Nanocomposites

Polymer nanocomposite is a combination of multi phasic material where the continuous phase, polymer, is reinforced by organic or inorganic nano-dimensional reinforcing agent (at least one) and the resultant system becomes uniphasic. Depending on the dimension of nanofillers, polymer nanocomposite can broadly be divided into three categories. In first category, iso-dimensional nanofillers (all dimensions within 100 nm) are present in the matrix. The spherical silica, silica or titania oxides synthesized by the sol-gel process, dispersion of metal nanoparticles etc. fall in this category.

In the second class, the nanocomposites have nanofillers with two dimensions in nanometer and the third one is larger in size. Such nanofillers possess elongated structure. Nanotube, nanofibers, cellulose whiskers reinforced polymer matrices are the examples of this category. The polymer/carbon nanotube nanocomposites belong to this class.

Third type of nanocomposites corresponds to the case where the nanofillers have only one dimension in nanometer range. The extensively studied polymer/clay and polymer/layer double hydroxide (LDH) nanocomposites represent this group. On the basis of the nature and extent of interactions between nanofillers and polymer, two different types of nanocomposites are thermodynamically achievable viz. intercalated and exfoliated nanocomposites (Fig. 1.1). In intercalated nanocomposite, the polymer chains are inserted into the galleries of the nanofillers at a regular fashion, regardless of nanofillers to polymer ratio. In an ideal intercalated nanocomposite, the polymer chains

are intercalated between the nanofillers resulting in a well ordered multilayer with alternating polymer layered nanofillers and the repeating distance within a few nanometers. However, in the exfoliated nanocomposite the nanofillers are delaminated and dispersed in the continuous polymer matrix.

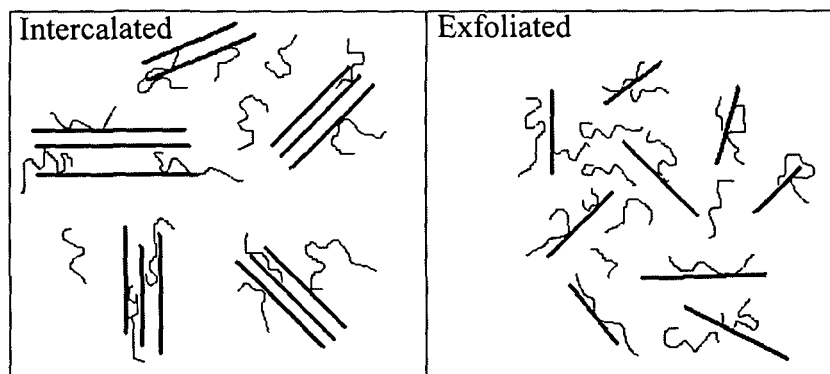


Fig. 1.1: Different states of polymer/clay nanocomposites

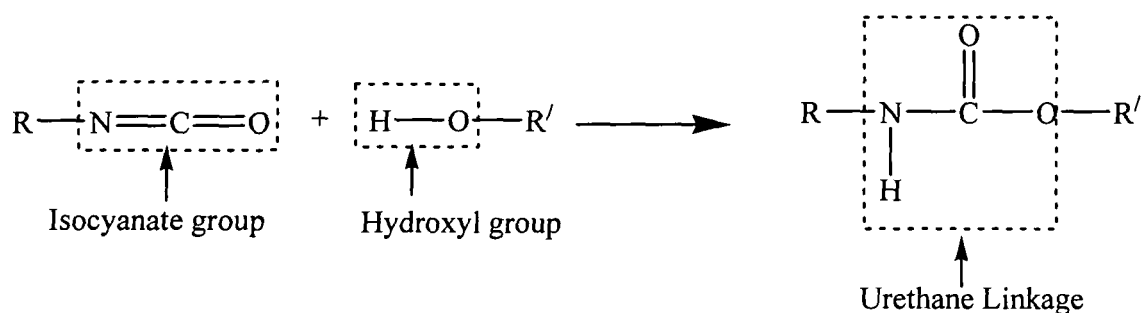
1.4. Materials and Methods

1.4.1. Materials

In polymer nanocomposite, there are nanofillers/nanomaterials and other necessary additives along with the polymer matrix. Depending on the technique of preparation, sometimes solvent or other auxiliary chemicals are also required. It has already been stated that a large number of polymer matrices and nanomaterials are utilized to obtain a variety of polymer nanocomposites. In the present investigation, as PU will be used as the matrix and nanoclay, metal nanoparticles and carbon nanotube shall be the nanofillers, so the discussion is restricted within these materials only.

1.4.1.1. Polyurethane

PUs have high reputation over the years as matrices for both conventional composites as well as nanocomposites. Urethanes are produced by the reaction of organic isocyanates with hydroxyl group containing compounds as shown in Scheme 1.1. In



Scheme 1.1: Formation of urethane linkage

general, thus PUs are produced by the reaction of di/polyols with di/polyisocyanates. Again, di/polyols that are used in preparation of PUs are of two types, viz. macroglycol and chain extender. Brief descriptions on these components are presented below.

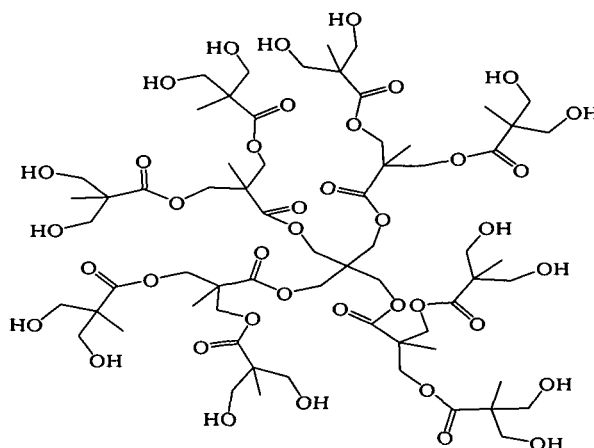
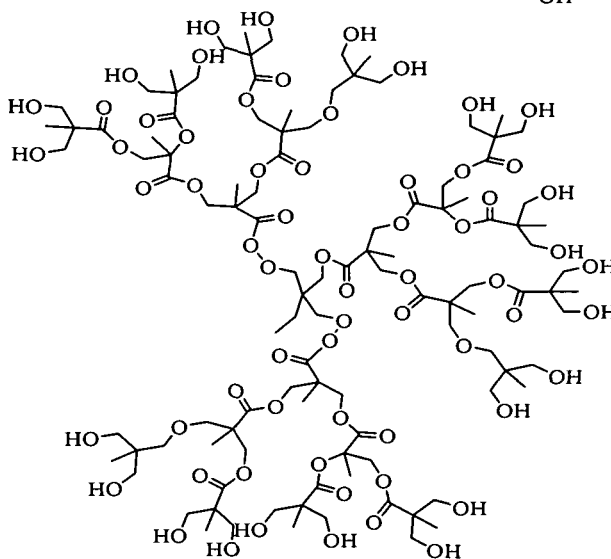
1.4.1.1.1. Macroglycol

Mainly the aliphatic diols or polyols of molecular weight 400 to 5000 g/mol are used as the macroglycol in the preparation of PU. The flexibility of PUs comes from this segment and many properties of PUs depend on the molecular weight and structure of the macroglycol. While the long chain macroglycols containing low functionality yield elastomeric soft PUs, the short chain macroglycols with high functionality result rigid crosslinked materials.⁴⁸ A variety of macroglycol such as polycaprolactone diol, polyether and polyester based diol/polyol, polycarbonates etc. are used and a few are listed in Table 1.1.

Table 1.1: Frequently used macroglycols in PU synthesis

Name	Chemical Structure	Ref.
Polycaprolactone diol		15
Polyhydrocarbon	$\text{HO} \left[\text{CH}_2 - \text{CH} = \text{CH} - \text{CH}_2 \right]_n \text{OH}$	15
Polyester	Hydroxy terminated polybutadiene glycol (HTPB) 	15
	where R = hydrocarbon part that may contain ether linkages also	
Polycarbonate	$\text{HO} \left[\text{CH}_2 \right]_6 \text{O} - \text{C}(=\text{O}) - \text{O} - \left[\text{CH}_2 \right]_6 \text{OH}$	15
Polyacrylic	$\text{CH}_3 \left[\text{CH}(\text{COOR}) - \text{CH}_2 - \text{CH}(\text{COOCH}_2\text{CH}_2\text{OH}) \right]_n \text{CH}_3$	48
Polyhydroxyl	$\begin{array}{c} \text{CH}_2\text{-OROH} \\ \\ (\text{CH-OROH})_x \\ \\ \text{CH}_2\text{-OROH} \end{array}$	15
	where x = 1 for triol and 6 for hexol	
Polyether (Polyalkylene oxide)	$\text{HO} \left[\left(\text{CH}_2 \right)_x \text{CH}(\text{R}) - \text{O} \right]_n \text{H}$	48
	where, x = 1,3 for R = H and x = 1 only for R = Me and Et	

Continued

Hyperbranched -
olHyperbranched -
ol

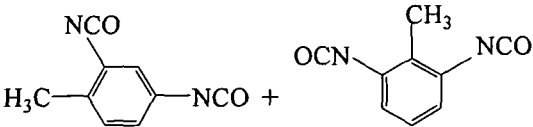
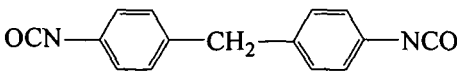
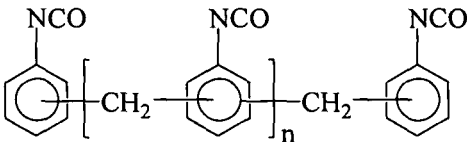
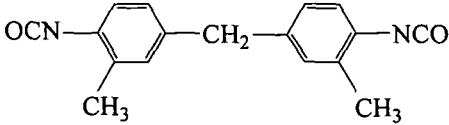
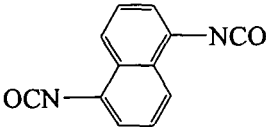
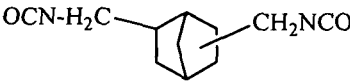

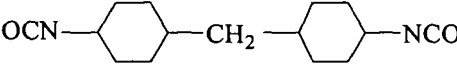
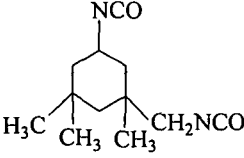

Polyester polyols are widely used macroglycols as they confer high strength, heat stability and adhesion to the PUs. But they show poor chemical resistance as the ester groups suffer easy hydrolysis especially by alkali. Also an autocatalytic effect is caused by the *in-situ* formation of carboxylic acid that catalyzes the hydrolysis of esters and thus weakens the performance of the polymer.⁴⁹ At the same time some of the polyester polyol like polycaprolactone, polycarbonate, hydroxyl terminated polybutadiene etc. possess high hydrolytic stability. The polyether polyols may confer to the polymers with some specific properties such as metal chelation, hydrophilicity, crystallinity, surface activity etc.

Nowadays, the dendritic or hyperbranched polyols are often used to prepare the dendritic or HBPU as these polymers show better performance than their linear analogs. “BoltonTM” is the trade name of hyperbranched polyester polyols and a variety of grades are available commercially.

1.4.1.1.2. Diisocyanate

The structure of isocyanate component is one of the influencing factors in determining the properties of PUs. The suitable selection of isocyanate component predicts the final structure of the products. The most commonly used diisocyanates are listed in Table 1.2.

Table 1.2: Frequently used diisocyanates in PU synthesis

Name	Abbreviation	Chemical Structure	Ref.
Toluene diisocyanate	TDI		15, 50
4,4-Diphenyl methane diisocyanate	MDI		15
Hexamethylene diisocyanate	HDI	$\text{OCN}-(\text{CH}_2)_6\text{NCO}$	51,52
Polymeric methylene diphenyl diisocyanate	PMDI		50
3,3-Dimethyl diphenyl methane diisocyanate	DDI		52
Naphthalene diisocyanate	NDI		52
Norbornane diisocyanate	NBDI		52
p-Phenylene diisocyanate	PPDI		51
Dicyclohexyl methane diisocyanate	HMDI		15,52
Isophorone diisocyanate	IPDI		15
Cyclohexyl diisocyanate	CDI		15

TDI and MDI are most common widely used diisocyanates.^{50,51} The first commercially available isocyanate was TDI. It is available as a mixture of 80% of 2,4- and 20% of 2,6-TDI isomers, though it can also be found as pure single isomer.⁵⁰ Similarly, MDI has three isomers namely 4,4'-, 2,4'- and 2,2'-MDI. However, only 4,4'- isomer is used in commercial purposes⁵⁰ though in PMDI, all the isomers are present and is used in PU preparation.

The aromatic diisocyanates are more reactive than the cycloaliphatic or linear aliphatic diisocyanates. The improvements in most of the properties of PUs and the rigidity of PU network are found to be in the order; aromatic diisocyanate > cycloaliphatic diisocyanate > aliphatic diisocyanate.⁵² But the properties like elongation at break and impact resistance are found to be in the opposite order. The PUs made of aromatic diisocyanates have lower oxidative and ultraviolet stabilities than the same of aliphatic diisocyanates. Also the formers have the tendency to become yellowish with time on exposure to light. This nature may be attributed to the presence of aromatic or benzenoid structures and hence capable to undergo resonance.^{48,53} Therefore the aliphatic and cycloaliphatic diisocyanates are extensively used in elastomer and coating applications than their aromatic analogs. HDI and HMDI are the most common aliphatic diisocyanates used commercially. It was also found that the cycloaliphatic diisocyanates based polymers showed superior retention of hardness, modulus, resistance to water uptake and hydrolysis and thermal degradation compared to aromatic diisocyanate based PUs. The cycloaliphatic diisocyanates like CDI and HMDI based PUs possess high strength and thermal stability.¹⁵ Aromatic triisocyanate (e.g., Desmodur RF^R and Desmodur CB 75N^R) based PUs exhibit excellent properties.⁵⁴ The greater density of aromatic triisocyanate based PU as compared to the cycloaliphatic and aliphatic diisocyanates may be the reason of this observation.⁵⁴

1.4.1.1.3. Chain Extender

Chain extenders are low molecular weight (generally, below 400 g/mol) active hydrogen containing difunctional compounds. The chain extender is used to extend the chain length of the hard segment and the molecular weight of PU. The low molecular weight aliphatic/aromatic diols, diamines and amino alcohols are used for this purpose. In general, aliphatic chain extender renders more softness to PUs than aromatic chain extender. The most commonly used chain extenders are mentioned in Table 1.3.

Table 1.3: Frequently used chain extenders in PU synthesis

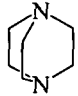
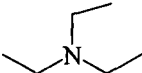
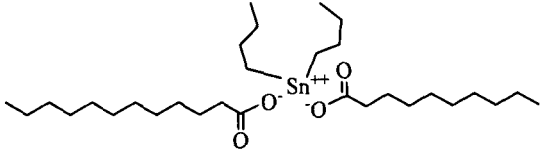
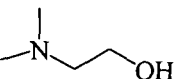
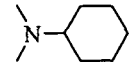
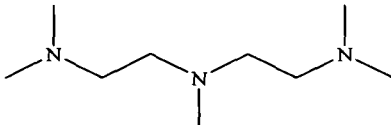
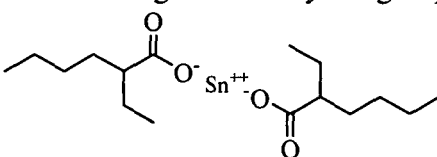
Name	Chemical Structure	Ref.
Ethylene glycol	$\text{HO}-\text{CH}_2-\text{CH}_2-\text{OH}$	51
1,4-Butanediol	$\text{HO}-\text{CH}_2-\text{CH}_2-\text{CH}_2-\text{CH}_2-\text{OH}$	15
1,6-Hexanediol	$\text{HO}-\left(\text{CH}_2\right)_6-\text{OH}$	51
Ethanolamine	$\text{H}_2\text{N}-\text{CH}_2-\text{CH}_2-\text{OH}$	52
Diethylene triamine	$\text{H}_2\text{N}-\text{CH}_2-\text{CH}_2-\text{NH}-\text{CH}_2-\text{CH}_2-\text{NH}_2$	55
Ethylene diamine	$\text{H}_2\text{N}-\text{CH}_2-\text{CH}_2-\text{NH}_2$	15,61
4,4-Methylene bis(2-chloroaniline) (MOCA)		51
1,4-Cyclohexane dimethanol		15
Glycerol		51
1,2,3-Propanetriol		52
Trimethylol propane		52
N,N,N,N-tetrakis (2-hydroxyethyl)ethyl diamine		50

The amine chain extenders rapidly react and increase the crosslinking density of PUs by bridging with biuret linkages and resulted thermoset materials. In contrast, diol chain extenders have the difficulties like limited solubility in polyol and sometimes required organometallic catalysts to prompt the urethane reaction.⁵⁵ Aromatic and cyclic chain extenders generally result materials with better performance characteristics. Trifunctional and highly branched chain extenders like trimethylol propane, glycerol, triglyceride ricinolate, hyperbranched polyol etc. are used as branching or crosslinking agents.⁵³

1.4.1.1.4. Catalyst

The low temperature syntheses of PUs need variety of catalysts. The use of catalyst increases the reaction rate much faster as compared to the uncatalyzed reaction. A list of commonly used catalyst is given in the Table 1.4.

Table 1.4: Commonly used catalysts in PU synthesis

Name	Abbreviation	Chemical Structure	Ref.
Triethylenediamine	TEDA/ DABCO		48
Triethylamine	TEA/TEN		48
Dibutyltindilaurate	DBTDL		15
Dimethylethanol-amine	DMEA		48
Dimethylcyclohexyl-amine	DMCHA		48
N,N,N',N',N''-pentamethyldiethylenetriamine	PMDTA		15
Tetravalent tin compounds	-	$R_nSnX_{(4-n)}$ where R=alkyl, aryl etc. and X= halogen/ carboxylate group	15
Stannous octoate	-		48

These catalysts can broadly be divided into two classes namely, amine (basic) compounds and organometallic compounds. The pioneering works on catalysis of urethane reactions were done by Baker and Gaunt⁵⁶ and Baker and Bailey⁵⁷ using tertiary amine, and still it is one of the most often used urethane catalysts. The commonly used amine catalysts are triethylenediamine (TEDA) also known as 1,4-diazabicyclo [2.2.2] octane (DABCO), triethylamine (TEA), dimethylethanolamine (DMEA), dimethylcyclohexylamine (DMCHA) etc.⁴⁸ As suggested by Lenz,⁵⁸ the catalysis mechanism of tertiary amine catalyzed urethane reaction involves complexation of the amine with isocyanate groups followed by reaction of the complex with ols to produce PU.

Mercury, lead, tin, bismuth and zinc based organometallic complexes are also used as catalyst for the urethane reaction.^{48,51} But the toxicity and disposal problems of such compounds limit their uses. The bismuth and zinc carboxylates have been used as alternative since 1990's. Nowadays, alkyl tin carboxylates, oxides and mercaptide oxides such as dibutyl tin dilaurate (DBTDL), dioctyltin mercaptide, stannous octoate, dibutyltin oxide etc. are used successfully in all types of PU applications.⁵¹ Among these DBTDL is found to be the most widely used catalyst.

1.4.1.2. Nano-dimensional Reinforcing Agents

The fillers that have one or more dimensions below 100 nm and aspect ratio more than 100 are generally known as nano-dimensional reinforcing fillers. The physical and chemical properties of such fillers have markedly different than those of the bulk. The nanomaterials including metal nanoparticles are used in preparation of polymer nanocomposites to improve the desired performance of pristine polymers are discussed below. Depending on the dimension of the nanomaterials, they are of three types (Fig. 1.2).

i) Nanoparticles

The nanoparticles have all three dimensions are in the order of nanometer range. They often named as equi-axed or nanoparticles or nanogranules or nanocrystals. The nanoparticles have different shapes as shown in Fig. 1.2. There are various routes for preparation of the nanoparticles. These include- vapor deposition, pyrolysis, chemical precipitation, sol-gel process, hydrothermal/solvothermal synthesis, reaction in confined space etc. All these techniques give stress to avoid the so called “run away” into the macroscopic world. Different shape and size of nanoparticles can be formed by controlling the rate of addition and other reaction parameters. The same nanoparticles may have different shape, size and hence behavior. Silver, copper, magnetic iron nanoparticles are widely studied examples of this category.

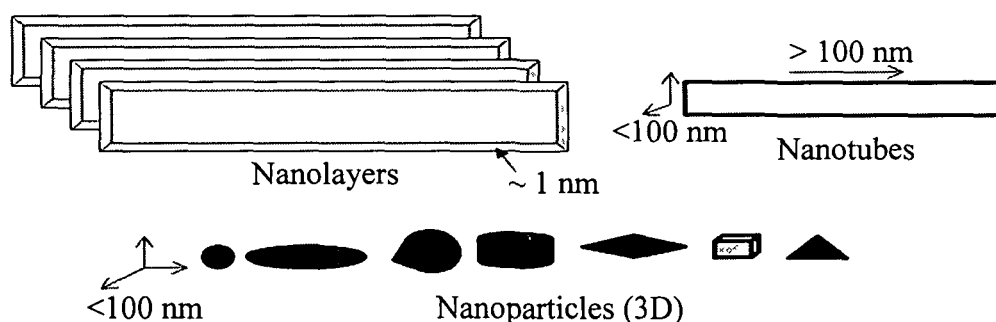
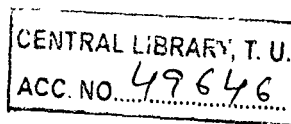
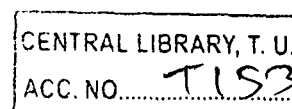


Fig. 1.2: Different types of nanomaterials

ii) *Nanotubes*

The nanotubes possess two dimensions in the nanometer scale and the third is larger, and thus formed an elongated structure. They are generally cylindrical or tubular in form and known as nanotubes or nanofibers or whiskers or nanorods. For example, carbon nanotube, cellulose whiskers etc.

Carbon nanotubes, which belong to this category, are the tubular structure of fullerenes. Carbon nanotubes can be visualized as a graphite sheet where each carbon atom is sp^2 hybridized and covalently bonded to three neighboring carbon atoms in such a way to form a seamless shell. This graphite sheet can roll into cylindrical form to shape the nanotubes.⁵⁹ It may be from one (single-walled carbon nanotube, SWCNT) or more (multi-walled carbon nanotube, MWCNT) graphite sheets as shown in Fig. 1.3 (a, b). The atomic arrangements, diameter and length of the nanotubes, morphology or nanostructure predict the properties of the carbon nanotubes. Carbon nanotubes are the stiffest and strongest (modulus- 1TPa, tensile strength- 60 GPa) man made material known to date. In addition, they show high thermal and electrical properties. Various reported methods for enabling the growth of carbon nanofibers and nanotubes include the use of chemical vapor deposition, laser ablation, arc discharge, thermal chemical vapor deposition, sol-gel process, substrate supported catalyst, catalyst particles suspended as an aerosol etc.⁶⁰ The increase of chemical affinity of carbon nanotubes to polymer matrices is a crucial topic. The modification strategies assist in effective processing to prepare well dispersed and stable polymer carbon nanotube composites with enhanced properties. On the basis of the bonding between carbon nanotube and polymer whether covalent or non-covalent the modification may be divided into two categories. In the non-covalent carbon nanotube modification the surface of the carbon nanotubes are polymer coated through physical adsorption. In this modification the conjugation of the carbon nanotube sidewalls remains same and therefore it does not affect the final structural properties of the material. The second modification concerns covalent chemical bonding (grafting) of polymer chains to carbon nanotubes. There are two main techniques for grafting of carbon nanotubes on the basis of formation of polymer chains- "grafting to" and "grafting from".⁶¹ In "grafting to" approach, firstly, a polymer is synthesized with terminal reactive groups or radical precursor and subsequently the polymer chain is attached to the surface of nanotubes by addition reaction. On the other hand, in the "grafting from" approach polymer chains start to grow from the surface of carbon nanotubes via *in-situ* polymerization of monomers



initiated by chemical species immobilized on the sidewalls and edges of carbon nanotubes.

Another important example in this category is cellulose whiskers [Fig. 1.3(c)]. Cellulose is a linear condensation of β -1-4-linked D-anhydroglucopyranose. It is available in plants, animals, bacteria etc. Degree of polymerization (DP) of cellulose ranges from 2,500 to 15,000 depending on the sources. The strong inter and intra molecular H-bonds in the cellulose chains confer linearity, stiffness, rigidity and strength. This ultimately leads to form thread like structure known as microfibrils that are apparently bound to form natural fibers.⁶²

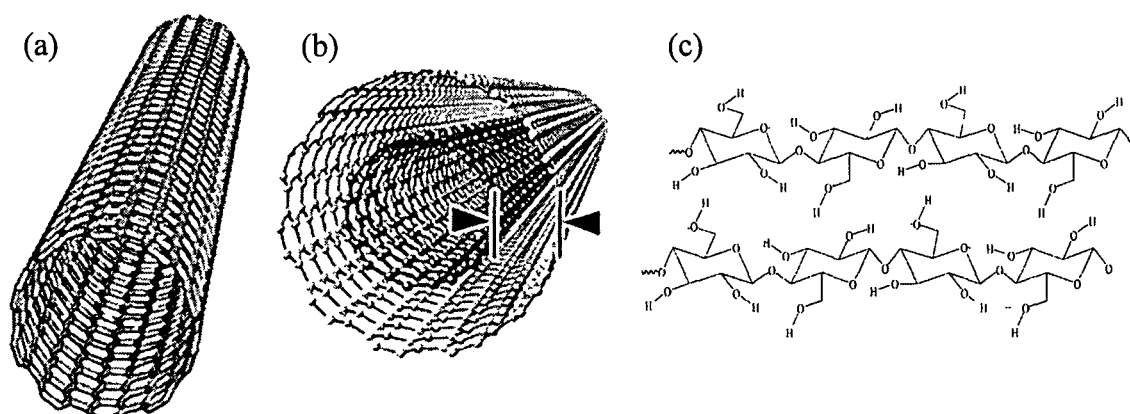


Fig. 1.3: (a) SWCNT, (b) MWCNT and (c) cellulose chain structure

iii) Nanolayers

The nanolayers possess only one dimension in the nanometer range. They present in the form of sheets or layers with one to few nanometers thick and hundred to several microns long. For example, phyllosilicates (clay), oxides (graphite oxide), layered silicic acids (magadite), mineral layered hydroxides (brucite), layered double hydroxides, layered alumino-phosphates (berlinite), metal (M^{4+}) phosphates, metal chalcogenides (TiS_2), cyanides [$Ni(CN)_2$] etc.

The plate like nanoclay, which is incorporated in polymer matrices to enhance their strength, hardness, flame retardancy etc., is important nanofiller of this category. The high aspect ratio (ratio of length to thickness > 1000) and large surface area of the clay layers are apt for reinforcement of polymeric matrices. The clay used in the nanocomposite preparation belongs to 2:1 layered silicates (or 2:1 phyllosilicates). Their crystal lattice consists of two dimensional layers where a central octahedral sheet of alumina is merged at the top with two external silica tetrahedrals, so that the oxygen ions of octahedral sheet also belong to tetrahedral sheets (Fig. 1.4). The layer thickness is ~ 1 nm and the lateral dimension varies from 300 Å to several microns depending on the particulate silicate, source of clay and method of preparation.⁶³ Synthetic clay can

be prepared by various routes such as template synthesis, hydrothermal process etc. The Na^+ or K^+ ions in the clay layers can be replaced with the cationic surfactant like primary, secondary and quaternary ammonium ions by ion exchange reactions to render the hydrophobicity to hydrophilic clay. The cationic surfactants lower the surface energy of clay and increases the inter layer distances resulting enhancement of wetting characteristics by the polymers. Further, the functional groups of alkyl ammonium cations can react with polymer or initiate polymerization of monomers to improve the strength of interface between inorganic clay surface and polymer.⁶⁴

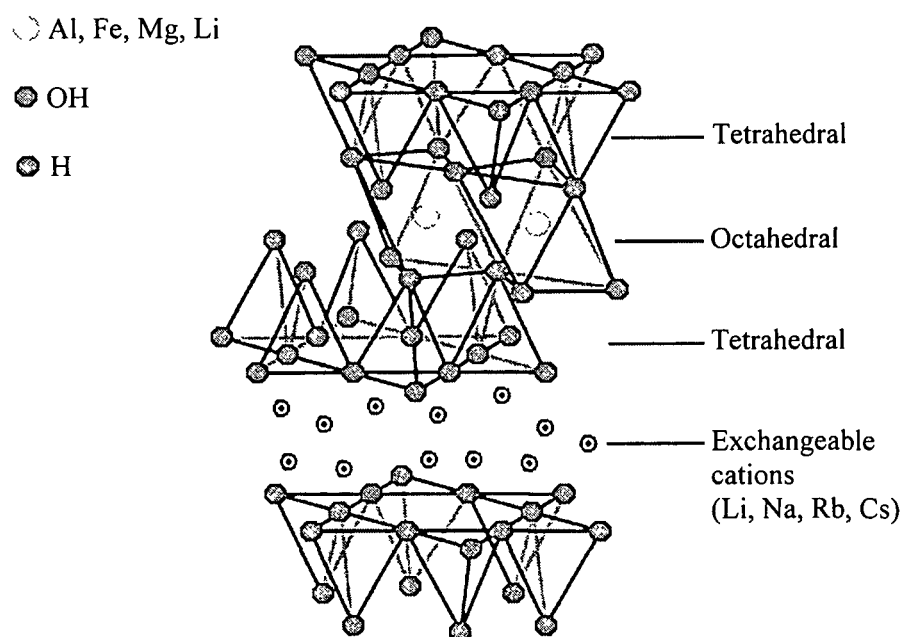


Fig. 1.4: Crystal structure of 2:1 layered silicate

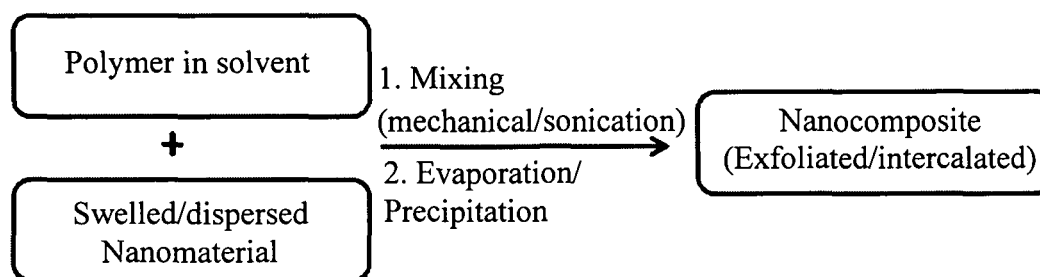
Again, depending on the occurrence pathway these nanomaterials can be categorized into three types- natural, incidental and engineered nanoparticles. Natural nanoparticles are formed through natural processes like volcanic dust, lunar dust, magneto-tactic bacteria, minerals etc. The incidental nanoparticles arise from the man made industrial processes such as diesel exhaust, coal combustion, welding fumes etc. They are also known as waste or anthropogenic particles. The nanoparticles are produced in the laboratory either by “top down” approach (from large sample to obtained nanosized particles) or “bottom up” (assembling smaller subunits through crystal growth or chemical synthesis to grow nanoparticles of the desired size and configuration) approaches.

1.4.2. Methods

The preparative methods of polymer nanocomposite can broadly be categorized into three sub categories namely solution, *in-situ* polymerization and melt-mixing. Briefly, these methods are discussed below.

1.4.2.1. Solution Method

This method involves dissolution of polymer and swelling of nanomaterials in the appropriate solvent for mixing followed by evaporation of solvent or precipitation (Scheme 1.2). Initially the solvent molecules help to swell and/or disperse the



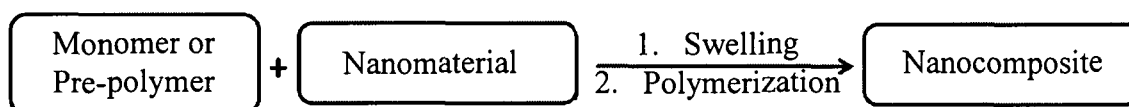
Scheme 1.2: Schematic presentation for the preparation of polymer nanocomposites by solution method

nanomaterials into the polymer solution. The intercalation of nanomaterials in this case is a two-stage process, where the polymer chains substitute the solvent molecules in the final stage. In such replacement the decrease of entropy due to confinement of polymer is compensated by an increase of the same due to desorption of solvent molecules that are utilized for intercalation.⁶⁵ Thus the entropy gained by desorption of solvent molecules is the driving force for such intercalations. In case of polymer/layered silicate nanocomposites, at first the weakly stack layers are easily dispersed in a suitable solvent. Polymer chains can penetrate into the delaminated sheets only in the second stage. The resultant structure may be either intercalated or exfoliated depending of the interactions between polymer and clay layers. However, during solvent evaporation (or the mixture precipitated), the layers can reassemble to reform an ordered multilayer structure with polymer chains sandwiched in between forming a well ordered intercalated nanocomposite. The chance of forming exfoliated nanocomposites is very low by this technique. Though this technique is used in many cases for preparation of nanocomposite, from the commercial production point of view it is not a well accepted method. This is due to the copious use of organic solvents and phase separation of the prepared products from those solvents, which is usually environmentally unfavorable and economically prohibitive.⁶⁶ On the other hand, it is a stunning way for water soluble polymers as water is used as solvent in this case. Also

there is no need of modification of clay as the polymers are polar in nature and thus hydrophilic enough to interact with the silicate layers.

1.4.2.2. *In-situ* Polymerization

In *in-situ* polymerization, the nanomaterials are first dispersed in liquid monomer or pre-polymer solution, which is then polymerized. The polymerization can be initiated by appropriate inorganic or organic initiators, by heat or radiation, or catalyst fixed through cationic exchange inside the interlayer before swelling step by the monomer. This is much effective and easy technique to break down the particle agglomerates using a high shear device and also possible to achieve more uniform mixing of nanomaterials in the monomer, because of low viscosity of the monomer or pre-polymer compared to polymer as in other techniques. In addition, the low viscosity and high diffusivity result high rate of monomer or pre-polymer diffusion into the nanomaterials. This method is capable of producing well exfoliated nanocomposite and has been applied to a wide range of polymer systems. The driving force of this technique is related to the secondary interactions of the monomers. In the swelling state due to the high surface energy, the nanomaterials attract the monomer molecules so that they diffuse between the layers or tube structure of nanomaterials. After reaching the equilibrium the diffusion of the monomer is stop and the nanomaterials are swelled. On starting of the polymerization, the polymer chains start to grow within the nanomaterials and ultimately result the exfoliated structure.⁶⁷ *In-situ* polymerization was the first reported method to prepare the polymer/clay nanocomposites.⁶⁸ A schematic diagram for preparation of nanocomposite through *in-situ* polymerization technique is shown in Scheme 1.3.



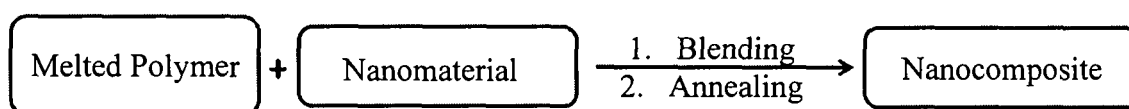
Scheme 1.3: Schematic diagram for the preparation of polymer nanocomposites by *in-situ* polymerization technique

1.4.2.3. Melt Mixing

This technique consists of blending of nanomaterials with the polymer matrix in molten state to form the intercalated or exfoliated structure either static or under shear condition. At the melting state the chosen polymer should be sufficiently compatible with the nanomaterials to form the nanocomposite. Therefore to optimize the interaction, the process may require several judicious experiments with different

compatibilizers. Generally the temperature is kept below the decomposition temperature of all the components of the nanocomposite. In this technique, processing conditions play important roles on the structure/property of polymer nanocomposite. The melt mixing method may not be as efficient as that of *in-situ* polymerization and solution technique and often produces partially exfoliated structures. But at the same time, this approach can be applied by the polymer processing industry to produce nanocomposite based on traditional polymer processing techniques, such as extrusion and injection molding. Another significant advantage is the elimination of the use of hazardous solvents. Thus this technology has an ample contribution in spreading up the process for commercial production of polymer nanocomposite.

The fact that polymer chains can undergo centre of mass transport in between the nanomaterials is surprising because, the unperturbed radius of gyration of the polymer is roughly an order of magnitude greater than the interlamellar spacing. The polymer chains possess a dramatic loss of conformational entropy during the intercalation. In this case, the believed driving force is the enthalpic contribution that comes from the interaction between the matrix and nanomaterials during blending and annealing steps. The different steps of melt mixing process are presented in Scheme 1.4.



Scheme 1.4: Flow chart diagram for different steps of the melt mixing technique

Besides the above methods there are other techniques too, which are used sometimes to prepare polymer nanocomposites. Among these template synthesis and sol-gel process are the most important and hence discussed below.

Template Synthesis

This is a bottom up approach and is different from above described methods. This method is also called as *in-situ* hydrothermal crystallization. In this method, nanomaterials are synthesized from precursor solution using polymers as template and hence the nanocomposites are formed *in-situ*. This method is widely used for the synthesis of double layered hydroxide based nanocomposites. Theoretically this method has potential of promoting the dispersion of nanomaterials in the polymer matrix in a one-step process. But this does not hold for all the nanomaterials. For example, clay can be synthesized within the polymer matrix, using an aqueous solution or gel containing the polymer and the silicate building blocks. The precursors used for

clay synthesis include silica sol, magnesium hydroxide sol and lithium fluoride. The polymer assists the nucleation and growth of inorganic host crystals in the process and gets trapped within the layers as they grow. But the major problem associated is the requirement of high temperatures to synthesize the clay, which may decompose the polymers. An exception is the synthesis of hectorite type clay minerals which can be performed under relatively mild conditions. Another problem is the aggregation tendency of the growing silicate layers. However, several reports described the successful preparation of the polymer nanocomposites applying this method.^{63,67}

Sol-gel Process

The sol-gel process has attracted considerable interest in the preparation of new materials by combining inorganic and organic precursors. This is a wet chemical technique, also known as chemical solution deposition. It is a combination of hydrolysis and condensation polymerization reaction of molecular precursors that provide the way to synthesize organic-inorganic nanocomposites. Such nanocomposites prepared by sol-gel process are impossible to prepare by conventional high temperature process due to the decomposition of the organic compounds. Most of the colloidal nanocomposites are prepared by sol-gel process, where the silica precursors are precipitated in controlled manner onto the polymer core particles to form silica coated hybrid colloids, which is termed as 'sol-gel nanocoating'. Polymer latexes are commonly used as colloidal templates and therefore the surface modification of the polymer particles is carried out to increase the chemical affinity with the shell.

Again, the preparation of polymer/metal nanocomposites fall either in *in-situ* (nanoparticles are prepared inside the matrix system) or *ex-situ* (nanoparticles are prepared outside the matrix system) approaches, where metal nanoparticles are incorporated in the polymer matrix by using solution, *in-situ* or melt mixing techniques. Indeed, large varieties of other techniques are also employed for the preparation of polymer nanocomposites. These include cryogenic ball milling, thermal spraying, plasma induced polymerization, evaporation of elemental metal with its deposition on polymeric matrices, thermal decompositions of metal ions using different procedures etc. However, to achieve the uniform distribution of the nanoparticles through these techniques is very difficult and thus they are not used, in general. Sonication is often used for better homogenization of the nanomaterials in the polymer matrix.

1.5. Characterization

Various techniques are used to characterize the polymer nanocomposites. The structural morphology is evaluated by X-ray diffraction techniques such as wide angle X-ray diffraction (WAXD) and small angle X-ray scattering (SAXS). Due to the easy availability and simple analysis method, WAXD is frequently used to analyze the nanocomposite structure, and occasionally to study the kinetics of polymer melt intercalation.⁶⁸ In case of polymer/nanolayer nanocomposite the shape, size, position and intensity of XRD pattern indicate the intercalated or exfoliated structure of the nanocomposite. Again appearance of new desired peaks proves the formation of polymer/metal nanoparticle nanocomposite. The interlayer spacing of nanolayers in the nanocomposite can also be evaluated from Bragg's equation ($2d \sin \theta = n\lambda$, where λ is the wavelength of the X-ray radiation used in the diffraction experiment, d is the spacing between the diffractive lattice planes also known as the basal spacing, n is the diffraction number and θ is the measured half diffraction angle or glancing angle). The shifting or disappearance of the peaks may convince the formation of intercalated or exfoliated structure but it is not conclusive, as several factors affect the accuracy of this analysis.⁶⁹ If the sensitivity and scanning time is low, concentration of the nanolayers are beyond the detection capacity and the presence of strong absorbing atom may result loss of diffraction peaks. Thus the analyses may mislead and are not quantitative.⁷⁰ The SAXS is used to obtain information about the nanomaterials in terms of parameters such as average particle size, shape, distribution and surface to volume ratio at very low angles (typically $<3-5^\circ$). Using the concept of fractal geometry the scattering methods can also give geometrical descriptions of the structures as the random processes of polymerization or aggregation usually result in formation of fractal objects.⁷¹ This method is accurate, non destructive and usually requires only a minimum of sample preparation. The combine study of WAXD and SAXS yield quantitative characterization of nanostructure and crystallite structure in the nanocomposites.

Transmission electron microscopy (TEM) is a powerful microscopy technique, which provides qualitative understanding on internal structure, spatial distribution of various phases and views the defect structure through direct visualization. However, TEM is time intensive and gives only localized qualitative information of the sample as a whole. In some instances the organic components of the sample may decompose under electron beam. In such condition cryogenic microscopy (cryo-TEM) is used where the specimen is measured at liquid nitrogen or liquid helium temperature in a

frozen state. In recent time, the high resolution TEM (HRTEM) is used to obtain a much closer look at the samples.⁷¹ The application of electron energy loss spectroscopy imaging techniques to TEM (ESI-TEM) can provide information on the composition of polymer surface and proved to be a powerful technique for the characterization of colloidal nanocomposites.⁷² TEM in combination to SAXS is a useful method to characterize the morphology of nanocomposite. While the TEM analysis gives visible information on the extent of particle separation in the nanocomposites, SAXS analysis enable acquisition of more detailed information about size distributions of primary particles and “mean” size aggregates in the real nanosize range below 20 nm.

The scanning electron microscopy (SEM) is an electron microscopy technique for analysis and imaging of micro and nanostructures. SEM creates characteristic 3D appearance of images and therefore useful for judging the surface morphology of the samples. The samples may also produce X-rays under SEM investigation. These can be detected in SEM combined with energy dispersive X-ray (EDX) spectroscopy.⁷¹ The atomic force microscopy (AFM) or scanning force microscopy (SFM) is also used for imaging, measuring and manipulating nanomaterials.

The chemical structure of the nanocomposites can generally be identified with the help of FTIR and solid state NMR (¹H, ¹³C, ²⁹Si etc.). FTIR spectroscopy is widely used to prove the formation of nanocomposites. For example, the appearance of the bands $\sim 1130\text{ cm}^{-1}$ and $\sim 820\text{ cm}^{-1}$ corresponds to the Si-O-Si and Si-OH bond stretching in the polymer/clay nanocomposites.⁷¹ These spectra are also useful to predict existence/disappearance of H-bonding between the nanomaterials and matrix. Attenuated total reflection infrared (ATR-IR) spectroscopy is used to characterize the IR spectra of nanocomposites of too thick or too strong absorbing samples.⁷³ Further the more structural information can be drawn from solid state NMR study. It provides greater insight about the surface chemistry and to a very limited extent the dynamics of polymer nanocomposites. The homogeneity of the dispersion level within the polymer matrix is very important for determining the physical properties and therefore in solid-state NMR, it is tried to link the measured longitudinal relaxations of proton (and ¹³C nuclei) with the quality of nanomaterial dispersion.⁷⁴ The ²⁹Si solid state NMR further gives the information on the distribution of silica nanoparticles in silica based polymer nanocomposites.⁷⁵ Due to the high polarizability, the xenon atom is particularly sensitive to the density of its microenvironment and thus ¹²⁹Xe NMR spectroscopy was used to investigate the enhancement of free volume in polymer nanocomposites.⁷⁶

Positron annihilation lifetime spectroscopy (PALS) technique is also used for the same purpose.

Differential scanning calorimetry (DSC) is a valuable tool to evaluate the thermal properties of the nanocomposites.⁷⁷ The change of glass transition temperature (T_g), crystallization behavior, crosslinking kinetics in thermosetting polymers etc. on incorporation of the nanomaterials can be studied by DSC.

The rheometric study and dynamic mechanical analysis (DMA) are utilized to measure the viscous and elastic components of polymer nanocomposite in terms of storage (G') and loss modulus (G''), which in turn help in determination of state of dispersion of nanofillers in matrix. The well dispersed nanofillers caused shifting of G' and T_g values of the nanocomposite. They also measure the stiffness of nanocomposite quantitatively.⁷⁸

Neutron scattering especially small angle neutron scattering (SANS), dynamic light scattering (DLS), disk centrifuge photosedimentometry (DCP) are also sometime used to unveil the structural aspect as well as conformation of the nanocomposites. X-ray photoelectron spectroscopy (XPS) is a surface analytical technique for assessing surface compositions. The XPS data combined with TEM studies of the ultramicrotomed particles can shed further light on particle morphology. The other techniques such as determination of mechanical properties, chemical resistance, flame retardancy, water vapor barrier property etc., are same as that of the conventional polymer composites.

1.6. Properties

The dramatic improvement of many desired properties of the polymer nanocomposites, on incorporation of a very small amount of nanofillers, is the central attraction to the scientific community. Various properties of polymer nanocomposites are briefly presented here.

1.6.1. Mechanical

The mechanical properties of polymer nanocomposites are of foremost concerned as nanolayers and nanofibers are added to polymers primarily to improve their mechanical properties.⁷⁹ The mechanical properties include tensile strength, elongation at break, impact resistance, flexural strength, hardness, fracture toughness etc. Tensile test is the most widely used method to evaluate the mechanical properties. Generally with the increase of amount of nanofillers, the tensile strength increases to a level and then starts

to fall. This is usually described by the state of dispersion of nanofillers whether intercalated or exfoliated. At higher concentration the nanomaterials have the tendency to form agglomerates. As degree of exfoliation increases, the effective surface volume and aspect ratio of the nanofillers increases and hence reinforcement effect improves. The effective stress transfer through the interface between nanofillers and polymers is dependent on factors like wettability and interfacial strength which in turn predict the mechanical properties.⁸⁰ On the other hand, the elongation at break values of nanocomposites generally decreases but sometimes it remains constant or even increased.⁸¹ The increased restricted movement of polymer chains attributed to decrease of elongation at break but the increase of elongation at break value may be due to formation of nanodomain shear zones under stress and strain. Impact resistance is another important mechanical property for many end application of polymers. It is a combined effect of flexibility and strength of materials.

Hardness of polymer nanocomposites is important from application point of view as it refers to the resistant to change of shape when force is applied. There are three major types of hardness- scratch hardness, indentation hardness and rebound hardness. The hardness of polymer nanocomposite depends on type of nanofillers.

1.6.2. Dynamic Mechanical

Dynamic mechanical properties of nanocomposites are measured by dynamic mechanical analysis (DMA). It reveals the response of nanocomposite to a cyclic deformation as a function of temperature. Three parameters- G' (or E'), G'' (or E'') and phase angle ($\tan\delta$) predict the change in transitions of molecular mobility such as T_g after nanocomposite formation.⁶³ The G' increases with the formation of exfoliated and well dispersed nanocomposite. Enhancement of G'' has also been reported for different nanocomposites. The $\tan\delta$ values depend not only on the dispersion state of nanofillers but also on the type of matrix used.

1.6.3. Barrier

Polymer nanocomposites generally possess enhanced barrier properties. This spectacular improvement of barrier properties can be explained on the basis of formation of maze structure or tortuous paths. The impermeable nanomaterials force the permeating molecules to wiggle around them in a random walk and hence diffuse by a tortuous pathway in the polymer matrix.⁸² In this regard sheet like morphology is particularly efficient to maximize the path length due to large length to width ratio as

compared to other shape of nanofillers.⁶³ There are several models for predicting this behavior. Nielsen, Fredrickson and Bicerano etc. models can be exemplified, for instance. The different polymer nanocomposites show enhanced barrier property to various gases, liquids, water vapor and chemical molecules. Improvements in capability of the polymer nanocomposite based membranes for gas separation have also been achieved.⁸³

1.6.4. Thermal

Thermal properties are important aspect of nanocomposites describing the response of materials with temperature. Various thermal analytical techniques are available such as thermal-gravimetric analysis (TGA), differential scanning calorimetry (DSC), thermo-mechanical analysis (TMA), dielectric thermal analysis (DETA) etc. TGA is used to demonstrate the thermal stability of nanocomposite and percent of nanofillers incorporated in matrix. Generally, the incorporation of nanofillers like nanolayers and nanofibers into the polymer matrix was found to enhance the thermal stability by acting as a superior insulator and mass transport barrier to the volatile masses produced during decomposition and assisting in formation of char after thermal decomposition.⁸⁴ However, the thermal stability may deteriorate after nanocomposite formation.⁸⁵ DSC is used to determine the thermal transition behavior such as T_g , melting temperature (T_m) etc. of nanocomposite. Generally T_g shifted or disappeared due to the restricted motion of the polymer chains by the nanofillers. Meanwhile, DETA and TMA are useful to measure the coefficient of thermal expansion and to have better understanding the viscoelastic behavior of nanocomposite respectively. Thermally stimulated depolarization current is a recent dielectric technique used extensively to study relaxation mechanisms in polymeric nanocomposites to characterize the T_g in more details.

1.6.5. Flame Retardancy

The flame retardant polymer nanocomposites are attracting a great deal as the traditionally used intrinsic flame retardant polymers or the flame retardant additives possess severe environmental problems. The flame retardant property of nanocomposite is studied by measuring limiting oxygen index (LOI), UL-94 test and cone calorimetry. Parameters like burning rates, spread rates, ignition characteristics etc. defined the flammability behavior of a polymer nanocomposite. The improved flame retardancy of nanocomposite is described on the basis of formation of char

residue. This effectively reduces the amount of flammable small molecules into vapor phase and decreasing the heat release rate.¹ The char also holds the material structural integrity and preventing fire spreading. The char creates a protective layer that impedes oxygen penetration and creates an insulating layer between heat and fuel. Synergistic effect on enhancing flame retardancy can also be achieved by incorporation of atoms like phosphorus, sulfur into polymer precursor along with nanofillers.

1.6.6. Rheological

The study of rheology is the deformation and flow of matter under the influence of an applied external stress. The measurement of rheological properties of a nanocomposite is helpful to know the physical properties during and after processing. Since the rheological properties of polymer nanocomposite are sensitive to the shape, size and surface characteristics of the fillers, thus rheology can be envisaged to assess the state of dispersion of fillers in matrix.⁸⁶ Generally nanocomposites show increased viscosity at low shear rates known as solid-like behavior and shear thinning behavior at high shear rates. The alignment of nanofillers towards the flow direction at high shear rates attributed to this fact.⁸⁶

1.6.7. Optical

The optical properties include transparency, refractive index, fluorescence, luminescence etc. Polymer containing optical functional group or material shows interesting optical properties after nanocomposite formation.⁸⁷ In polymer nanocomposite, the nanofillers enhance the optical properties while the polymer acts as stabilizer to the fillers. The transparent pristine polymers remain optically clear after nanocomposite formation as there is no marked decrease in the clarity due to the nano dispersed fillers.

1.6.8. Electrical

Electrical properties of polymer nanocomposite refer to conductivity and dielectric properties. The electrical properties are expected to be different when the polymer is filled with nanofillers. The quantum effects become prominent at nano region and the interparticle spacing decreases for the same volume fraction compared with the bulk. In addition, the decrease of rate of resistivity is lower than in micrometer scale fillers.

1.6.9. Magnetic

Intense research on magnetic nanoparticles is going on especially in the medical sectors. For example, magnetic nanoparticles are used in drug delivery systems as they can be manipulated by an external magnetic field gradient to control a targeted delivery. The polymer coated magnetic nanoparticles have attracted more and more attention in the fields such as in cell separation, drug targeting, enzyme immunoassay and so on. This is because of the fact that the magnetic separations are comparatively easy, rapid, and require simple equipment as compared to other separation procedures.⁸⁸

1.6.10. Catalytic Activity

Polymer nanocomposite possesses different catalytic activity. For example vegetable oil based HBPU/ silver nanocomposites can act as heterogeneous catalyst to convert the 4-nitrophenol to 4-aminophenol.⁸⁹ However catalytic activity of nanoparticles decreases with the number of cycles used. Polymer/clay nanocomposite has been known for its catalytic activity.⁹⁰ The highly active and large surface area of nanomaterials result their effective catalytic activity.

1.6.11. Biodegradation

One of the interesting and exciting aspects of polymer nanocomposite is their significant improvement of biodegradability often reported after nanocomposite formation. The improved biodegradability of the nanocomposites may be attributed to catalytic role of the nanomaterials in biodegradation process. A typical biodegradation process involves four main steps viz. water absorption, ester cleavage and formation of oligomer fragments, solubilization of oligomer fragments, and ultimately removal of soluble oligomers by microorganisms.⁹¹ Therefore any factor which influences the hydrolysis tendency may control the biodegradation process. In case of polymer/clay nanocomposites the terminal hydroxyl groups of silicate layers is one of the reasons for improvement of biodegradation ability of polymers.

1.7. Applications

The incorporation of nanomaterials into polymer matrices leads to the genesis of a myriad of application possibilities. Besides using as mechanical reinforcing agent of polymer matrix, the nanofillers can bestow some unique properties to the final nanocomposites and thus nanocomposites have attracted considerable interest in many industries. A few applications of polymer nanocomposites are shown in Fig. 1.5.

The increasing demands of polymer nanocomposite in automobile industries are due to the light weight, relatively low cost and thus large fuel and energy savings. The first example of using nanocomposite in automotive industry was reported by Toyota research group in 1991 with a Nylon/nanoclay component. PU nanocomposites have their own niche in automotive industries. PU/clay nanocomposites having high dielectric constant and high breakdown voltage are used to prepare spark plug caps for automobiles.⁹² The research on PU nanocomposite based linings for armed vehicles is under progress. Ahmadi et al. reported the potential automotive refinish clear coat based on PU/silicate layer nanocomposite.⁹³

Polymer nanocomposites are using as advanced food packaging material as they can respond to the external stimulus and alert the presence of pathogens or contamination along with their lightness and recyclability. Recently the Nanocor company has released the beer bottle made up of polymer nanocomposites. Wu et al. described the potentiality of PU/cellulose nanocomposites as packaging material.⁹⁴

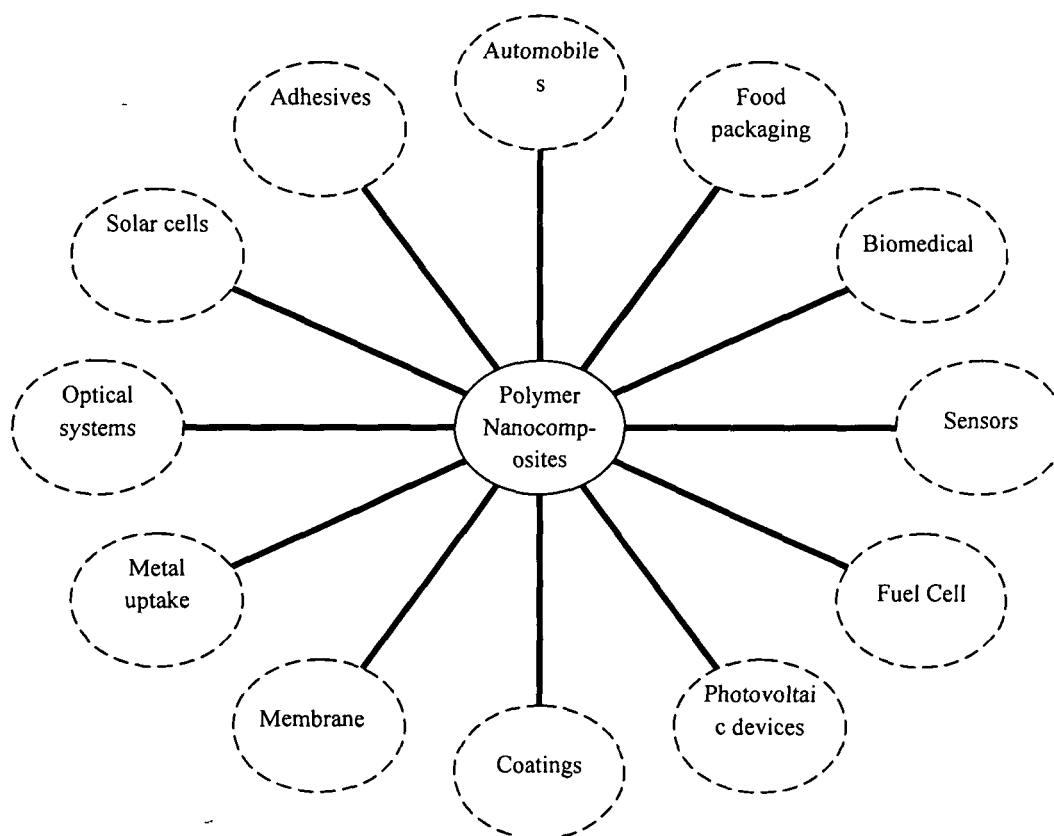


Fig. 1.5: Different application fields of polymer nanocomposites

One of the most demanding applications of polymer nanocomposites is in medical field. Starting from biosensors to medical implants polymer nanocomposites are being used. As the PUs are biocompatible hence PU nanocomposites are occupying

a vast sector of this field. The PU nanocomposites have the high potential to be applicable as artificial capillary bed,⁹⁵ antimicrobial agent,⁹⁶ soft tissue engineering,⁹⁷ catheters and other medical tubing,⁸⁹ low permeability biomedical,⁹⁸ fibroblast applications⁹⁹ etc. On the other hand the improved shape memory property of PU nanocomposites can be utilized as biomaterial in clinical applications, in vascular, orthopedic and in dental applications.¹⁰⁰ Mamunya et al. reported the potentiality of PU/silicate nanocomposites to find applications as gel electrolytes and as hydrogels in drug delivery systems.¹⁰¹

The polymer nanocomposites are also used as adhesive, sealant and surface coating materials. The PU/clay nanocomposites not only enhance the adhesive character but also reduce the gas permeation rate.¹⁰² Corcione et al. described a typical adhesive formulation used in laminated films for food packaging.¹⁰³ There are other reports describing the adhesive character of PU nanocomposites.¹⁰⁴ Since the ancient time the coating practices include the nanofillers in the paints. PU nanocomposites with different type of nanofillers such as nanoclay, metals nanoparticles etc. are used to obtain highly hydrophobic, antimicrobial, flame retardant, high performance and thermostable surface coatings.¹⁰⁵⁻¹⁰⁷

The sensor technology is highly utilizing the advantages of nanotechnology. The polymer nanocomposites are utilized for sensitivity of gas, humidity, toxic chemicals, metals etc. The factors like accuracy of sensitivity, selectivity, reproducibility, scanning time etc. are depend directly on the sensing capability of the membrane. Cho et al. described the PU/MWCNT composites acting as the smart actuators.¹⁰⁸

PU nanocomposites can also be used in the foam industry. A lot of reports reveal the use of PU/clay nanocomposites as foam.^{109,110} The versatility and improved properties of PU nanocomposites are the main reasons for receiving importance in daily applications. Few of the commercially available nanocomposite products are listed in Table 1.5.

Table 1.5: Commercially available polymer nanocomposites and their applications *

Trade Name/ General name	Producer	Applications
M9 TM	Mitsubishi Gas Chemical Company	Container, juice or beer bottle, multi-layer films
Curad [®] Imperm TM	Medline Industries Nanocor	Wound care/bandage Beverage container

Continued

Nylon Nanocomposites	Bayer, Toyota Motors, Ube, Unitika	Automotive parts, packaging, barrier film
Aegis™ OX	Honeywell Polymer	High barrier beer bottles
Aegis™ NC	Honeywell Polymer	Medium barrier bottles and films
SET™	Foster Corporation	Catheter shafts and balloons, tubing
Nitro Hybtonite®	Montreal	Hockey sticks
Epoxy/CNT nanocomposites	Babolat	Tennis rackets
Forte™	Noble Polymer	Automotive, furniture, appliance
Durethan KU2- 260	Bayer	Barrier films, paper coating
MWCNT nanocomposites	Hyperion	Electrostatic dissipation
SBR rubber nanocomposites	Pirelli	Winter tires

*Data are collected from company website and industrial magazine

1.8. A Short Review on Vegetable Oil Based Polyurethane Nanocomposites

The recent time demands urge to establish novel and innovative technologies to produce products from renewable resources that can reduce the worldwide dependence on fossil fuels. The continuous exhaustion of oil reserves, the fluctuating price of petroleum based products, the increasing global warming and stringent environmental rules and regulations compelled the scientific society to make renewable resources indispensable. Among the various renewable resources, vegetable oil is drawing a considerable attention as they possess some advantages. These include easy availability in large quantities with varieties of compositions and structure, relatively low cost, easy handling, reducing green house gas and overall environmental benignness.²⁴⁻²⁷ Therefore there is a steady growth in the utilization of vegetable oils in production of non-food value added products such as paints and coatings, shampoos, soaps, cosmetics, lubricants, emulsifiers, plasticizers, biodiesels, pharmaceuticals etc.²⁸⁻³³ The structural composition of vegetable oil has also tempted the scientist to make use of it to develop different polymeric materials. The reported literature described the use of different vegetable oils such as castor, sunflower, soybean, linseed, palm, etc. to synthesize different type of PUs.¹¹¹⁻¹¹⁴

Again, formation of polymer nanocomposites is proving to be the most efficient approach to improve the material properties of polymers. The polymer nanocomposites have attracted a great deal of interest both in academic and industries for their synergistical properties of constituent's beneficial properties or newly induced one. The

desired properties of polymer nanocomposites can be achieved on the incorporation of very small volume fractions of fillers. This is mainly due to their extremely small interparticles distance and the interaction lies between the polymer and fillers in nano scale. Consequently, the nanocomposites retain the macroscopic homogeneity and low density of the polymer.

Background

J.G. Kane is known as the father of vegetable oils. He was the first person to demonstrate the potential of vegetable oil for edible and industrial purposes.¹¹⁵ The first vegetable oil based resins were reported by Kienle and Hovey in 1925.¹¹⁶ They synthesized a series of polyester resins for surface coating applications. Development of vegetable oil based polyols for manufacturing PUs was put forwarded in early nineteen-fifties originally from castor oil.¹¹⁷ But from the late nineteenth century when the rising cost of petroleum feed stocks and the demand for environment friendly green products raises the popularity of vegetable oil based PUs.^{43, 118} Castor oil was first used as trifunctional vegetable oil based polyol to synthesize HBPU by Karak et al.¹¹⁹ Though the first vegetable oil modified hyperbranched polyol based PUs was reported by Petrovic et al. in 2008 from soybean oil.¹²⁰ The amalgamation of peculiar structural characteristic of hyperbranched polymer and the benefit of green vegetable oils are described in these reports. Oil derived PU nanocomposite was first reported in 2002 by Dongyan et al.¹²¹ The number of literature on vegetable oil based polymer nanocomposites have been publishing in ascending order in the last few years which is reflected from Fig. 1.6.

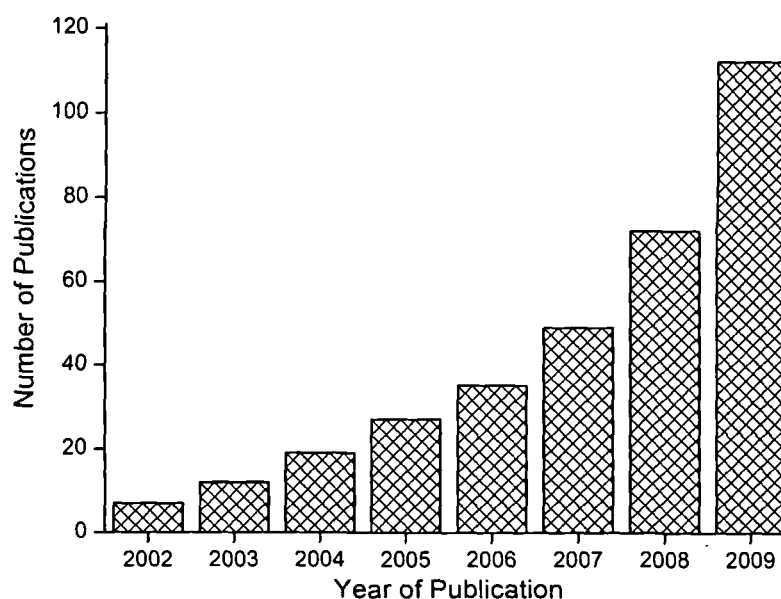


Fig. 1.6: Scientific publications vs. year of publication searched by Scopus

Preparation of Vegetable Oil Based Polyurethane Nanocomposites

The versatility of PU nanocomposites has further enhanced when they are prepared from renewable vegetable oil based polymers. The incorporation of the triglyceride moiety into the matrix imparts increased chemical and physical properties. Also the vegetable oil based PU matrix itself exhibit excellent properties such as mechanical strength, adhesion, flexibility, abrasion resistance, toughness, chemical and corrosion resistance etc. which make them sometimes superior to conventional petrochemical based PUs. Importantly, since one of the raw materials is naturally renewable and available in large quantities, so the cost involve in the raw materials and processing are relatively lower compared to the petroleum based PUs. These materials are also environment friendly and are biodegradable in nature.

The preparative techniques of vegetable oil based PU nanocomposites are almost similar to the aforesaid techniques for PUs as described in the general section. The components required for synthesis of such PUs are the same but at least one of the polyol components must be vegetable oil based. Therefore the details of vegetable oils and their polyols are only described here.

Vegetable Oils

Vegetable oils possess high degree of unsaturation compared to mineral oils (petroleum fractions, obtained from mines) and thus the formers are less stable. Unlike volatile essential oils found in the stems, leaves, flowers, fruits etc. of plants, vegetable oils (another category of plant oils) are non-volatile. They have fixed composition and boiling point (b.p.) and are commonly known as fixed oils. Generally vegetable oils are triglycerides or triacylglycerols (esters of glycerol) with long chain fatty acids (Fig. 1.7). The fatty acid consists of 94-96% of the total weight of the triglyceride oil.¹²² The combinations of the different types of fatty acids lead to a great variety of triglycerides in vegetable oils. Depending on the fatty acid distribution, different vegetable oils

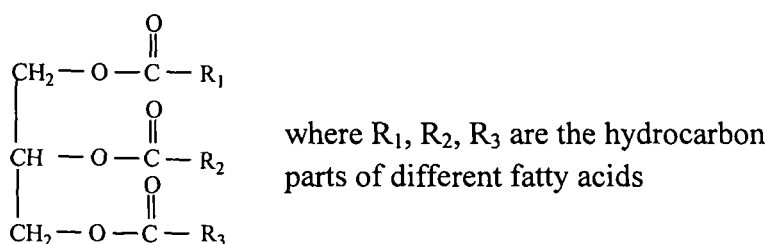


Fig. 1.7: Representation of triglyceride

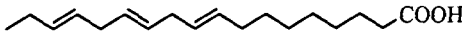
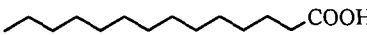
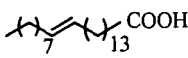
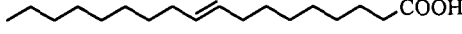
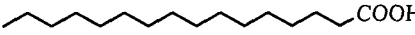
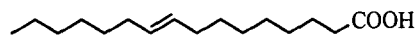
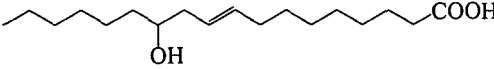
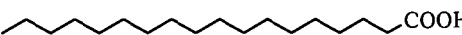
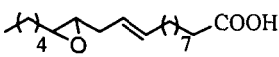
possess different physical and chemical properties (Table 1.6). Different types of saturated fatty acids such as arachidic, lauric, palmitic, stearic etc. and oleic, linoleic,

linolenic etc., as unsaturated fatty acids are generally found in different triglycerides. The certain vegetable oils also contain ricinoleic, myristic, behenic, capric, caproic, eleostearic, erucic, licanic, isanic, caprylic etc. fatty acids. Besides the regular carboxylic, saturated or unsaturated moieties, these fatty acids contain some special functionalities like ketonic, hydroxyl, epoxy, triene etc. Very little amounts of phospholipids, hydrocarbons, some fat soluble vitamins, tocopherols, tocotrienols, sterols, stanols, fatty acyl esters etc. are also present in vegetable oils along with the triglycerides.^{51,123} The structures and physical properties like density, b.p. and melting point (m.p.) of some important fatty acid^{116,124} are given in Table 1.6. The fatty acid composition of the vegetable oils is fixed and acts as its “finger print” (Table 1.7) that can be used to differentiate the vegetable oils from one another.

Table 1.6: Chemical structure and physical properties of some fatty acids present in vegetable oils

Name of fatty acid	Structure	Density (g/cc) at 25 °C	m.p. (°C)	b.p. (°C)
Arachidic		0.8240	74-76	328
Behenic		0.822	75-80	306
Capric		0.888	31-32	269
Caproic		0.92	-3	202
Caprylic		0.910	16-17	237
Eleostearic		-	-	-
Erucic		-	-	-
Eicosenoic		-	25-32	-
Gadoleic		-	-	-
Heptadecan- -oic		0.853	59-61	227
Heptadecen- -oic		-	-	-
Isanic		-	-	-
Lauric		0.880	44-46	299
Licanic		-	-	-
Lignoceric		-	74-78	306
Linoleic		0.9	-5	229

Continued

Linolenic		0.914	-11	230-232
Myristic		0.862	58.8	250
Nervonic		0.918	42-44	398
Oleic		0.895	13-14	360
Palmitic		0.853	63-64	351
Palmitoleic		-	33	162
Ricinoleic		0.94	5.5	245
Stearic		0.83-0.94	66-70	365-370
Vernolic*		-	-	-

* Reference has been taken from [124]

Extraction and Purification of Vegetable Oils

Oil extraction and purification are important steps before its use. Four methods are used to extract the oil viz. mechanical pressing, solvent extraction, enzymatic process and high pressure CO₂ extraction processes.^{125,126} In the mechanical pressing method, the pretreated seeds are squeezed by hydraulic press or screw press to get the oil from protein meal of the seeds. In solvent extraction technique, the pretreated seeds are first immersed in a suitable solvent system for a sufficient period at 60-80 °C and then distillation is done to collect the oil. This process needs lot of solvent and thus unfavorable from the green chemistry point of view. In enzymatic process, the pretreated seeds are first boiled in water and mixed up with suitable enzymes which digest the solid part of the seed leaving the oils. The oil is then extracted by liquid-liquid centrifugal method. In the high pressure CO₂ method, the pretreated seeds are mixed with CO₂ under high pressure to dissolve the oil. On releasing the pressure liquid CO₂ goes to gaseous state and the oil gets separated. Amongst the four, the last two methods viz., enzymatic and high pressure CO₂ method yield quite high and hence are favorable in commercial scale. After extraction, the oils are preserved at low temperature and preferably in inert atmosphere to avoid the contamination by O₂ and hydrolysis of the oil to free fatty acids by moisture present in the atmosphere.

Table 1.7: Few important vegetable oils with their fatty acid compositions

Vegetable Oil	Fatty Acids (in approximate %)						Worldwide Production**	Ref.
	Palmitic	Stearic	Oleic	Linoleic	Linolenic	Others		
Castor	2.0	1.0	7.0	3.0	-	87 (ricinoleic)	0.45	128,129
Coconut	9.1	2.8	6.8	1.9	0.1	47.1 (Lauric), 32.2*	3.32	129
Corn	10.9	2.0	25.4	59.6	1.2	0.9*	2.01	128
Cottonseed	21.6	2.6	18.6	54.4	0.7	0.7 (Myristic), 0.6 (Palmitoleic), 0.8*	3.93	128
Linseed	6.0	4.0	22	16	52	-	0.64	120
Olive	9.0	2.7	80.3	6.3	0.7	0.6 (Palmitoleic), 0.4 (Arachidic)	2.82	128,129
Palm	44.4	4.1	39.3	10	0.4	1.0 (Myristic), 0.8*	28.14	120, 128
Peanut	11.1	2.4	46.7	32	-	2.9 (Behenic), 1.6 (Eicosenoic), 1.5 (Lignoceric), 1.8*	4.82	128
Rapeseed	3.8	1.2	18.5	14.5	11.0	41.1 (Erucic), 6.6 (Eicosenoic), 1.0 (Lignoceric), 0.7 (Arachidic), 1.6*	13.04	128
Soybean	11	4.0	23	53	7.0	2.0*	31.87	120, 129
Sunflower	7.0	4.5	18.7	67.5	0.8	0.7 (Behenic), 0.4 (Arachidic), 0.4*	9.5	120
Safflower	6.8	2.3	12	77.7	0.4	0.3 (Arachidic), 0.5*	-	120
Tung	-	4.0	8.0	4.0	-	84 (α -elaeostearic)	-	128

* Other fatty acid compositions **Data in million metric tons (2006 figures)

The extracted oils generally contain certain impurities such as phosphatides, free fatty acids, colored substances, gums and resins. By simple filtration or settling technique dirt can be removed.¹¹⁶ Gums are removed by degumming which renders the affinity of phosphatides towards water by converting them to hydrated gums. As a consequence, the gums coagulate and are separated by a centrifugal separator. The most effective technique is the alkali refining technique where a caustic soda solution is used in sufficient quantity to neutralize the free fatty acids. The required amount of caustic soda depends upon the type of oil, impurities present and the final color required.⁵¹ In this technique free fatty acid and color components are removed without excessive saponification of the oil and without loss of oil by emulsification.¹¹⁶ The acid refining technique is also used where the cold oil is stirred with concentrated sulphuric acid solution. On settling, the impurities are drawn off and the oil is washed to make free from mineral acids. But the color removal in this process is not suitable as in alkali refining technique. After the refining process, bleaching is done for partial or complete removal of color.⁵¹ There are two ways either by chemical or physical means. The chemical method suffers the disadvantage as the oil may undergo oxidation during the process. In the physical method, the oil is heated in the presence of adsorbent such as fullers earth, activated carbon, silica, bentonite etc. under abiotic condition. Generally the process is carried out at about 110 °C with 0.2-2.5% solution of the adsorbent for 30-60 min.^{51,127}

Preparation of Polyols from Vegetable Oils

The industrially important polyols are of low viscosity with high hydroxyl content. Generally vegetable oil based polyols are oligomers having a wide distribution of molecular weight and substantial degree of branching as reported by many literatures.^{24-33,120,128} They are multifunctional materials with mostly heterogeneous triglyceride structures. The polyols are obtained either by direct polymerization or by functionalization of the oil through double bond reactions such as hydroformylation, epoxidation and metathesis or through ester bond breaking reactions.

The first utilized and one of the most explored vegetable oils in the preparation of PU is castor oil (Fig. 1.8). It consists of glyceryl esters of ~90% with ricinoleic acid and rest 10% with oleic, linoleic and other fatty acids (Table 1.6).¹²⁸⁻¹³⁰ Castor oil is approximately 70% trifunctional and 30% difunctional. In nineteen fifties Metz et al. observed that 50 °C was desired temperature for the urethane reaction as a better control of the reaction.¹¹⁸ But the trifunctionality in castor oil created a lot of trouble as

the polyol is highly reactive towards diisocyanates. Controlling of the reaction was a challenge for that time. Therefore different attempts were taken to achieve the control

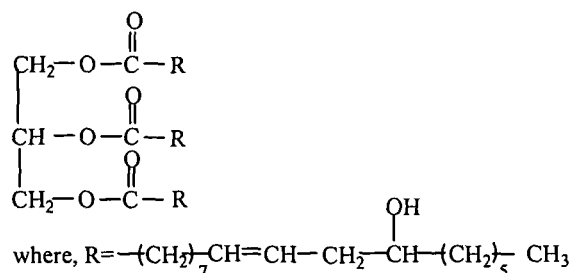


Fig. 1.8: General structure of castor oil triglyceride

by converting the trifunctional part of castor oil into difunctional moieties. Castor oil was reacted with different compounds such as phenyl isocyanate, maleic anhydride to obtain modified difunctional castor oil (MCO).¹³¹ According to another report ricinoleic acid was isolated from castor oil and treated with ethylene glycol, diethylene glycol and triethylene glycol at 230 °C to obtain a series of difunctional polyester polyols.¹²

The double bonds in the unsaturated fatty acids and the ester groups linking the fatty acid to the glycerol moiety is the two major reactive sites for conversion of vegetable oils into polyols. Direct oxidation of the double bonds present in vegetable oils, containing sufficient unsaturation, resulted the polyols. However, to limit the formation of side products such as peroxides, aldehydes, ketones, carboxyls and other low molecular weight species produced by chain scission is really a difficult task. This oxidation related problems can be overcome by introducing epoxy groups at the double bond through epoxidation reaction. Epoxidation of soybean, rapeseed, linseed, olive, corn, safflower, karanja, melon seed and cottonseed is carried out on an industrial scale.¹³²⁻¹³⁶ In general, four approaches are used for epoxidation of vegetable oils. These are (i) use of peracids like peracetic acid or perbenzoic acid in presence of acid catalyst¹³³, (ii) use of organic and inorganic peroxides including transition metal catalysts¹³⁷, (iii) utilization of halohydrins using hypohalous acids (HOX) and their salts¹³⁸ and (iv) use of molecular O₂.¹³⁸ These epoxy groups are highly reactive and readily cleaved by alcoholysis in the presence of alcohols/thiols, hydrolysis in the presence of acid catalysts and by hydrogenation¹³⁴ to generate the polyols. Petrovic et al. reported the oxirane ring cleavage by HCl or HBr to obtain halogenated polyols.¹³⁹ Interestingly, Guo and coworkers synthesized soybean polyols by ring opening of the corresponding epoxides with water in the presence of phosphoric acid.¹⁴⁰ After catalysis reaction, phosphoric acid chemically binds with the polyol and confers some

special properties to the end product.¹⁴⁰ It was observed that the reactivity of these polyols having secondary hydroxyl groups was lower as compared to petrochemical based polyols due to shielding by the long fatty acid chains. Petrovic et al. for the first time suggested the improvement of reactivity by converting secondary hydroxyl groups into primary via ethoxylation with ethylene oxide at 35-45 °C in the presence of a super acid (HBF₄) as the catalyst.¹⁴¹

Hydroformylation, also known as the oxo synthesis, is another route to convert the vegetable oils to polyols. It is a Fischer Tropsch reaction that involves the conversion of alkenes to aldehydes. Hydroformylation route was demonstrated by Petrovic et al. to obtain polyols with primary hydroxyl groups by reacting triglycerides with carbon monoxide and hydrogen followed by conversion of resulting aldehyde groups to hydroxyls by hydrogenation.¹²⁰ The conversion to polyaldehydes can also be accompanied in the presence of either rhodium or cobalt as catalyst. Guo et al. reported the hydroformylation of soybean oil with a hydroxyl functionality of 4.1 (more than 95% conversion) if the reaction is rhodium catalyzed, whereas a hydroxyl functionality of 2.7 is obtained (about 65% conversion), when the reaction is cobalt catalyzed.¹⁴²

While the epoxidation followed by ring opening results polyols with secondary hydroxyl groups, the hydroformylation procedure gives primary hydroxyl groups located generally within the fatty acid chains. The ozonolysis is a route that can produce polyols having terminal hydroxyl groups. This technique is cost effective and ozone is used to cleave the double bonds present in the unsaturated vegetable oils oxidatively. Followed by the pioneering work of Pryde's group in 1960's, soybean oil was first subjected to ozonolysis to prepare aldehyde oils.¹⁴³ Petrovic et al. also reported the utilization of ozonolysis reaction followed by reduction by hydrogenation to develop a triol from triolein, soybean oil and canola oil which is then treated with diisocyanates to obtain PUs.¹⁴⁴ Low viscosity polyols by ozonolysis using glycols as esterification agents was reported by Graiver et al.¹⁴⁵ The processes so far discussed for polyol synthesis, epoxidation/hydroxylation, hydroformylation/hydrogenation and ozonolysis/hydrogenation are restricted only to the vegetable oils containing unsaturated fatty acids. The undesirable aldehyde and epoxy groups are also sometimes found in the polyols and purification of the products makes the process more tedious and costlier.

In this context transesterification technique has made a remarkable progress in realizing the development of polyols. In the technique vegetable oil is reacted with an

alcohol and hence is often called alcoholysis. The process is catalyzed by acids, bases and enzymes.

Reaction of vegetable oils with polyfunctional alcohols such as glycerol results partial glycerides i.e., a mixture of monoglyceride and diglyceride.¹⁴⁶ The solubility of the resulting glyceride in methanol gives the idea about the extent of alcoholysis. In a typical reaction, alcoholysis produces a mixture of monoglyceride (51%), diglyceride (40%), unreacted triglyceride (4%) and free glycerol (5%). Roy et al. studied the glycerolysis process for a number of vegetable oils.¹⁴⁷ They observed that the yield of the monoglyceride solely depends on the solubility of glycerol in the oil rather than on the fatty acid composition. The reaction that carried out without catalyst needs very high temperature which may cause darkening of the oil. Generally the catalysts used are bases and acids but the base catalysts are far better than acid. Some of the base catalysts are metal oxides, metal hydroxides and metal salts. The commercially available catalysts are oxides or alkoxides of lead, lithium, cadmium, zinc, tin etc.¹⁴⁸

Transesterification or alcoholysis is also done with monohydric alcohol such as methanol. This produces a mixture of fatty acid methyl esters and a molecule of glycerol⁵¹ in the presence of acid (sulphonic and sulphuric acids), base (sodium and potassium methoxide) or an enzyme catalyst. The produced glycerol is separated by solvent extraction technique. The progress of the reaction is influenced by several factors such as type of catalyst, temperature, alcohol/vegetable oil molar ratio and free fatty acid content etc.⁵¹ The ultrasonic measurement can utilize for monitoring the glycerol settling which on the other way useful for evaluating the effect of parameters like amount of catalyst, mixing time and temperature on transesterification reactions.¹⁴⁹ Ahmad et al. reported the preparation of a diol linseed fatty amide (DLFA) via aminolysis of linseed oil directly with diethanolamine and NaOCH₃ as the catalyst.¹⁵⁰ Transesterification of different vegetable oils with glycerol, trimethylol propane and ethylene glycols¹⁵¹ were reported among which trimethylol propane gives the best results if the reaction can be carried out at 120 °C in presence of *p*-toluene sulphonic acid as the catalyst. In a recent literature, Perin et al. suggested transesterification of castor oil with methanol or ethanol by microwave irradiation at 60 °C for 3 h.¹⁵²

Hyperbranched Polyols from Vegetable Oils

Hyperbranched polyols contain high functionality and high degree of branching and therefore they are much better than the conventional linear polyols in many aspects. The common route to synthesize hyperbranched polymer is the

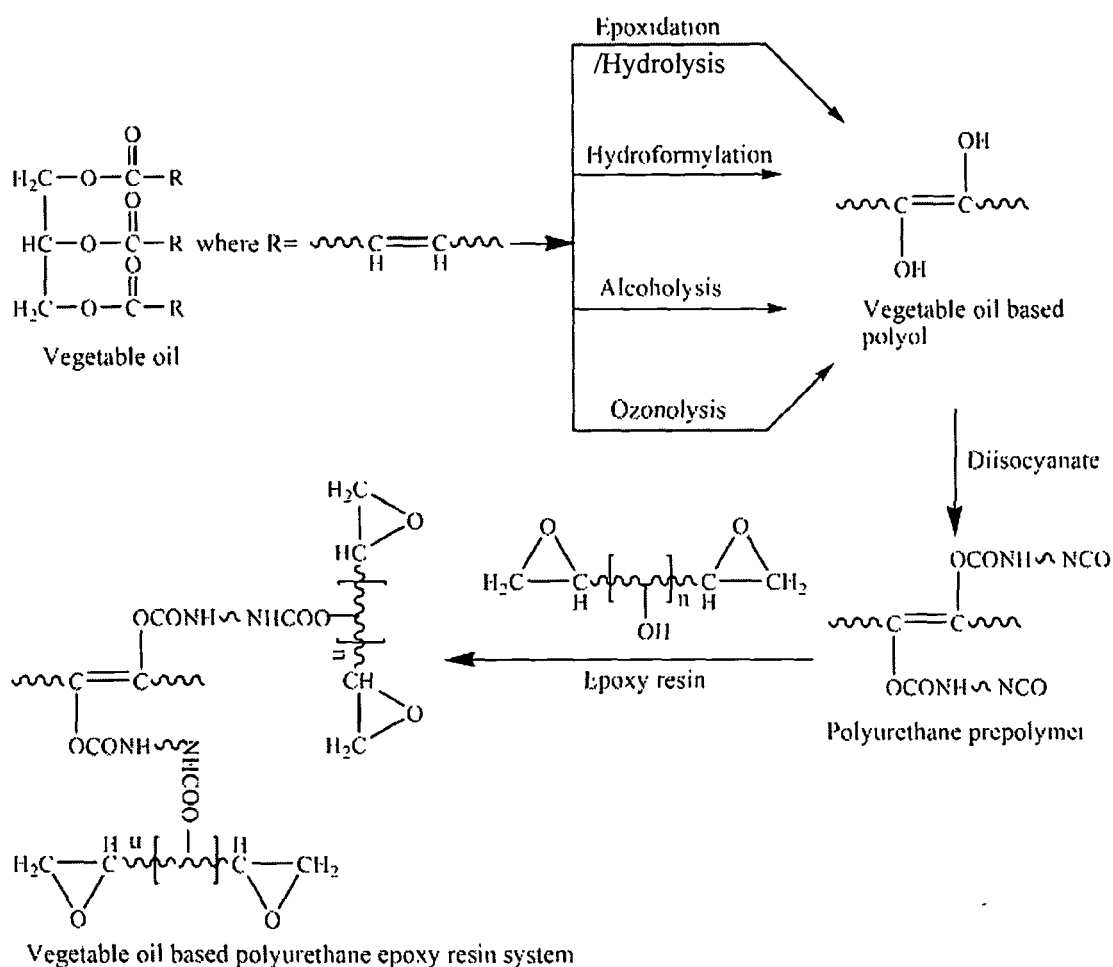
polycondensation of AB_x type monomers where $X \geq 2$. There is also possibility to prepare hyperbranched polyols using a non-stoichiometric ratio of polyfunctional components or by stopping the reaction before the gel point. Recently Petrovic et al. emphasized on development of vegetable oil based hyperbranched polyols.¹²⁰ They prepared two soybean oil based hyperbranched polyols as pre-polymers from hydrogenated epoxidized soybean oil and from hydroformylated polyol by reacting them with HMDI or adipoyl dichloride followed by liquid-liquid extraction of unreacted monomeric species. The obtained polyols had a wide distribution of molecular weight and functionality with a fairly irregular structure. One of the most significant aspects of hyperbranched polyols is increase of functionality but decrease of hydroxyl number and equivalent weight with the increase of molecular weight. The length of the branches like short branches for rigid applications or long branches for flexible applications, can be controlled depending upon the requirement. The hyperbranched polyols have the tendency to produce foams with undesirable closed cell structure although it can be regulated by the proper choice of surfactants.¹²⁰

Preparation of Nanocomposites

The vegetable oil based polyol PU nanocomposites are also prepared by utilizing similar preparative techniques as discussed earlier. For example, Dongyan et al. described the preparation of $BaTiO_3$ superfine fiber/castor oil based PU and poly(methyl methacrylate) interpenetrating polymer network (IPN) nanocomposites.¹²¹ They grind the superfine fibers, coupling agent and IPN system together for 25 min and exposed to supersonic device for 20 min, which was finally casted in mold.

The other vegetable oil based PU INP nanocomposite systems are reported to deal with epoxy resins.⁴⁻⁶ This is because of the attractive performance such as high strength, modulus, thermal stability and creep resistance etc. exhibited by epoxy resins and a good compatibility with the PU systems. All the nanocomposites are prepared by *in-situ* method. Lei et al. used ultrasonication for half an hour for the better dispersion of the organically modified palygorskite (o-PGS) in the matrix.⁷ A general scheme of the formation of vegetable oil based PU/epoxy systems is given below (Scheme 1.5).

The use of sonication in the preparation of nanocomposites has also been reported by other authors.^{5-9,153-158} Dutta and Karak prepared *Mesua ferrea* L. seed oil based PU/clay nanocomposites.¹⁵³ Following two different methods, oil based polyols were prepared via monoglyceride and diethanolamide of the fatty acids of the oil. The dispersion as well as delamination of the organo clay in PU/epoxy blend system was



Scheme 1.5: General scheme of the formation of vegetable oil based PU/epoxy systems assisted by sonication for half an hour in an *ex-situ* technique. Turunc et al. also reported the soybean oil based PU/silica nanocomposites.⁹ The PU was prepared through non-isocyanate route using epoxidized soybean oil modified in a closed vessel at 110 °C and 4.6 kg/cm² of CO₂ in presence of TBAB catalyst followed by the reaction of butylenediamine. In another report the three hydroxyl groups of castor oil was utilized successfully to prepare HBPU where this vegetable oil was act as a B₃ monomer in the A₂ + B₃ technique.⁸ Sonication was also employed in the preparation of modified MWCNT/HBPU nanocomposite for improved homogenization in *in-situ* technique. In all the nanocomposite preparation the sonication time was not exceeded more than half an hour. Use of excess sonication may result degradation of the matrix systems or aggregation of nanofillers and ultimately deteriorated the performance characteristics of nanocomposites.

Akram et al. reported the tetraethoxyorthosilane modified linseed oil based polyol to obtain PU subsequently silica nanocomposites through *in-situ* process.¹⁵⁴

Very recently Karak et al. described a successful way incorporating the s-triazine moiety in the sunflower oil based thermoplastic hyperbranched and linear PU

followed by preparation of silver nanocomposites.⁸⁹ At first a pre-polymer was formed by reacting monoglyceride of sunflower oil and poly(ϵ -caprolactone) diol with MDI. This pre-polymer was finally reacted with s-triazine-butanediol based hyperbranched polyether polyol to form the HBPU. The silver nanocomposites were prepared by *in-situ* catalytic reduction of organic silver salt using organic Sn-catalyst.

Characterization

Vegetable oil based PU nanocomposites are characterized by the same way as discussed in the earlier sections (Sections 1.5). Vegetable oil based polymer nanocomposites are easily characterized by XRD technique. The shift of the [001] diffraction peak of nanoclay to lower value reveals the intercalation of the PU chains into the clay galleries.^{4,5,156-158} The disappearance of this peak may also indicate the formation of the exfoliated structure.¹⁵³ It was also observed that above 5 weight% of clay, it always results intercalated structure rather than exfoliated. In the XRD pattern of sunflower oil based HBPU/ silver nanocomposites there was no effect on the peak position for PCL crystallinity.⁸⁹ On the other hand sharpening of the peak position for PCL crystallinity was observed in case of castor oil based HBPU/MWCNT nanocomposites.⁸ In the FTIR spectra of vegetable oil based PU nanocomposites, besides the presence of characteristic bands for the nanomaterials, the bands for fatty acid compositions were also distinct. The bands for ester carbonyl $-C=O$, ether oxygen $-C-O-C-$ etc. are observed in the FTIR spectra of *Mesua ferrea* L. seed oil based PU/ clay nanocomposites as well as bands for stretching vibration of Si-O, Al-O and Si-O-Si for nanoclay.¹⁵³

Thermal characterization of vegetable oil based PU nanocomposites is carried out by TGA and DSC techniques in a similar manner as for general polymer nanocomposites. Higher thermal stability compared to the pristine PU matrix after incorporation of nanoclay was reported by several authors.^{5,110,159} This is because of the fact that nanoclay is acting as a thermal insulator and mass transport barrier to the volatile products produced during decomposition by providing tortuous path way to escape. Similarly the melting enthalpy (ΔH_m) and T_g are also enhanced after nanocomposite formation.^{9,154}

Different types of transitions and relaxations (variation of G' and G'' with temperature) related to the structure and morphology are generally analyzed by DMA (DMTA) and TMA analyses. In a typical DMA behavior of vegetable oil based PUs show a very broad transition from glassy to rubbery state at room temperature which

indicates a wider distribution of crosslinking density and lower homogeneity in the network¹²⁰ and hence in the nanocomposites. The factors responsible for such broad glass transition are the formation of triglyceride rich regions and the plasticizing effect of the long fatty acid chains.¹⁶⁰ The G' are found to be increased for the HBPU/silver nanocomposites compared to the linear analog from the same vegetable oil.⁸⁹

Dongyan et al. studied the electrical resistivity and I-V characteristic for BaTiO₃ superfine fiber castor oil PU/PMMA IPN nanocomposites.¹²¹ The resistance value decreases with increasing nanofillers concentration. Up to 10 weight% of nanofillers the material behaves like insulator while above that it acts as conductive system. The I-V characteristic study also supports the above observation.

Properties

Vegetable oil based PU nanocomposites exhibited similar and in some cases better than the petroleum based PU nanocomposites. The properties described earlier (Section 1.6) are also valid for vegetable oil based PU nanocomposites.

The physical properties such as specific gravity retains almost same as that of the matrix.¹⁵³ The specific gravity of thermoset matrix was 0.95, while 0.98 for the nanocomposite with 5 weight% nanoclay loading in *Mesua ferrea* oil based PU nanocomposites.¹⁵³ Interestingly, the drying time (time for optimum crosslinking) reduces gradually with the increase of clay loadings from 1 to 5 weight%.

Incorporation of nanofillers results the improvement in the tensile strength, toughness etc. while the elongation at break value decreases due to the imposed restricted chain motion in general. On the other hand, the increasing trend in elongation at break values with the increase of clay loadings was observed by Li.⁵ The vegetable oil based PU exhibited enhanced flexibility and it retains in the nanocomposites. The long chain of fatty acid may attribute to this flexibility.¹⁵³ The critical stress intensity factor (K_{IC}) as measured in three-point bending mode was found to be enhanced in the nanocomposites.⁵ This is due to the improved interfacial properties and unique morphology of the nanocomposites.

In general vegetable oil based PUs show three step degradation patterns in TGA thermograms. The first step from 180-230 °C is due to the degradation of the urethane bonds depending on the type of substituent on the diisocyanate and polyol. The second and third steps start at more than 350 °C and 500 °C respectively. The second and third decomposition steps correspond to decomposition of ester, amide and hydrocarbon chains respectively. However, two step degradations are also observed in certain cases.

Most of the nanocomposites exhibited one step degradation pattern in TGA thermograms rather than two or three steps.¹⁵³ The flame retardant property of castor oil based PU/epoxy IPN with o-PGS nanocomposites was evaluated by LOI test.⁷ It was stated that the addition of o-PGS or epoxy was advantageous for the enhancement of the flame retardancy of the vegetable oil based PU.

The properties of PU nanocomposites are significantly affected by the water absorption characteristics. Some of the properties like mechanical, modulus etc. decreases greatly with water absorption. The nanocomposites show much lower water absorption rate and attain the balance of water absorption much slowly relative to the matrix systems.^{4,7} The hydrophobic fatty acid chain contributes a lot to this fact.

Although the rheological property of vegetable oil based highly branched polyester¹⁶¹ and linear epoxy nanocomposites¹⁶² are available in literature, still there is no such consensus on vegetable oil based PU nanocomposites.

Ashraf et al. studied the electrical conductivity of linseed oil based poly(urethane amide) nanostructured poly(1-naphthylamine) (PNA).¹⁶³ The conductivity was observed in the semiconducting range. The conductivity was much higher at low loading of PNA compared to polyaniline (PANI). While the 30 weight% loading of PANI resulted the conductivity value of $4 \times 10^{-4} \text{ Scm}^{-1}$, the incorporation of 2.5 weight% PNA into PU matrix produced conductivity value of $6.7 \times 10^{-4} \text{ Scm}^{-1}$. The nanoscale PNA chains crosslinked to PU molecules through H-bonding and urea type linkages provide the path to charge condition.

The vegetable oil based PU nanocomposites sometime also possess antibacterial activity. Akram et al. observed the antibacterial property linseed oil based PU/silica nanocomposites.¹⁵⁴ The nanocomposites showed mild antibacterial behavior against *Escherichia coli* while sufficient antibacterial activity against *Staphylococcus aureus*.

The PUs are known for their biocompatibility and hence the nanocomposites. The porous nano-hydroxyapatite castor oil based PU nanocomposite foam was found to be biocompatible.⁴⁶ The cytocompatibility of the foam was evaluated by *in-vitro* cell culture study. There was no negative effect on the cell morphology, viability, proliferation and differentiation which reveal the good cellular affinity and cytocompatibility of the nanocomposite foam. MMT assay was also reported to confirm the cytotoxicity. Dutta and Karak reported the RBC hemolysis inhibition capacity of the *Mesua ferrea* oil based PU/clay nanocomposites to state the cytocompatibility of the materials.¹⁵³ Further the bacterial degradation of the same was

tested conveniently by broth culture technique where the nanocomposites were exposed to microbial degradation.

Jia et al. studied the influence of tribological performance such as coefficient of friction and rate of wear loss with respect to the clay loading in a castor oil based PU/epoxy system.⁶ Addition of the nanoparticles resulted in the improvement of wear resistance of the matrix systems.

The catalytic activity of the nanocomposites is an interesting domain for exploration. Due to the high surface area, the nanofillers can effectively catalyzed the reactions where the matrix acts as support. In this regard for the first time, Karak et al. explored the catalytic activity of the sunflower oil based HBPU/silver nanocomposite.⁸⁹ The catalytic reduction of 4-nitrophenol to 4-aminophenol in presence of the nanocomposites were studied photometrically and the catalytic potential was statistically optimized through response surface method.

The vegetable oil based PUs exhibit poor chemical resistance as they are susceptible to hydrolysis due to the presence of ester bonds. However, the addition of the nanofillers and formation of IPN induced enhanced chemical resistant to the nanocomposites.⁹

The shape memory properties of vegetable oil based PU nanocomposites depend upon a number of factors such as conjugation present in the vegetable oil, curing temperature, physical or chemical crosslink present in the PU etc.¹⁶⁴ The shape memory behavior of vegetable oil based HBPU nanocomposites were reported for first time with MWCNT nanofillers.⁸

Applications

The emergence of vegetable oil based polymer nanocomposites is to partially or fully replace petroleum based polymers and to reduce the environmental havocs. Vegetable oil based PU nanocomposite is gaining vast popularity due to its diversified potential application fields. The matrix, PU itself is a unique class of material as it can be prepared from a large variety of polyols and diisocyanates depending upon the requisite properties of the final products. One example of its growing popularity can be realized from the estimation for soy polyols in urethane market is estimated to be more than 800 million pounds per year in US.¹⁶⁵

Vegetable oil based PU nanocomposites can be used as a direct replacement of petrochemical polyol based PU nanocomposites in various fields like adhesives, foams and surface coatings etc. The potentiality of linseed oil based poly(urethane amide)/

PNA nanocomposites as anti-static and corrosive-protective coatings was described by Ashraf et al.¹⁶³ Silica reinforced linseed oil based PU nanocomposites may be used in the field of thermal resistant protective coatings and paints.¹⁵⁴ In another report, environment friendly route was elaborated to prepare soybean oil based PU/silica nanocomposites coatings.⁹ Heidarian et al. also reported anti-corrosive PU/OMMT coatings for carbon steel.¹⁵⁵ They observed improvement of corrosion resistance with the increase of clay content on the measurement of impedance parameters, polarization studies and water absorption test.

Vegetable oil based PU/clay nanocomposites possess improved thermal stability. Different types of nanoclay such as cloisite, montmorillonite etc. are used for this purpose. Several reports utilized the palm oil, soybean oil, castor oil to prepare the PU nanocomposite foam.^{110,156}

Castor oil modified polyol based PU/nano-hydroxyapatite with tunable biodegradable properties has been reported to be utilized in biomedical implants and tissue engineering.⁴⁶ These nanocomposite scaffolds showed non-toxic behavior and good cytocompatibility and have the potential to be applied in repair and substitute of human menisci of the knee-joint and articular cartilage. Epoxy modified *Mesua ferrea* oil based biocompatible and biodegradable PU nanocomposites hold the immense potential as biomaterials.¹⁵³

Vegetable oil based PUs exhibit shape memory property.¹⁶⁶ Incorporation of nanofillers effectively enhances the shape memory property of PUs. Castor oil based HBPU/MWCNT nanocomposites showed improved shape memory behavior.⁸ The large number of surface functional groups of HBPU contribute a lot in better dispersion of the MWCNT into the matrix which in turn improve the thermal, mechanical and shape memory properties.

Vegetable oil based hyperbranched and linear PU/silver nanocomposites can also be utilized as heterogeneous catalyst.⁸⁹ The use of hyperbranched structure is advantageous over linear in stabilization and better homogenization of the nanoparticles in the matrix with a narrow size-window.

1.9. Scopes and Objectives of the Present Investigation

From the main features of the above discussion, it has been found that many vegetable oils are widely used in place of petroleum based products as the raw materials. Among the vast varieties of widely grown plants and herbs that are available in India, *Mesua ferrea* L. (Nahar) is a plant that produces exceptionally high oil containing seeds. It is

also copious in different countries such as Sri Lanka, Bangladesh, Nepal, Indochina (Southeast Asia), Malay Peninsula etc. Few reports deal with the utilization of this oil in the fields of medicine and biodiesel¹¹⁶ and in the field of polymer including PU synthesis.¹⁴⁶ Nevertheless, there is no report on utilization of this oil for synthesis of HBPU and its nanocomposites. Hence, the following questions may arise in this area.

- (i) Whether this oil can be utilized for the preparation of HBPU?
- (ii) Whether the performance characteristics of the hyperbranched polymer can be improved by any physical or chemical means?
- (iii) Whether the modified polymer can be utilized as the matrix for the preparation of different types of nanocomposites?
- (iv) Whether the incorporation of different nanofillers into the hyperbranched matrix can lead to the genesis of advanced materials?

Under the above background, the main objectives of the present investigation are as follows:

- (i) To synthesize, characterize and evaluate various properties of *Mesua ferrea* L. seed oil based HBPU.
- (ii) To study the effect of hard and soft segment ratio on the performance of the above PUs.
- (iii) To improve the performance of the vegetable oil based hyperbranched polymer by blending with other suitable commercial polymer.
- (iii) To improve the performance characteristics of the HBPU systems by nanocomposites formation.
- (iv) To utilize various nanofillers for nanocomposite formation to achieve the desirable properties.
- (v) To study the rheological behavior for better understanding of nano-reinforcing mechanisms in the nanocomposites.
- (vi) To utilize the prepared nanocomposites as advanced materials in the field of surface coating, adhesive, shape memory application, biodegradable biomaterial, antimicrobial, free radical scavenger etc.

1.10. Plans of Work

To fulfill the above objectives, the following plans of work have been adopted.

The plans of work for the proposed research are as follows.

- i) A state of art literature survey on the field of vegetable oil based PUs and their nanocomposites.

- ii) The HBPU's from vegetable oil will be synthesized by the standard literature procedure.
- iii) The synthesized PU's will be characterized by different analytical and spectroscopic techniques such as determination of hydroxyl value, isocyanate value, FTIR, UV, NMR, TGA, DSC etc.
- iv) PU nanocomposites will be prepared by the *in-situ* polymerization technique as reported in the literature using vegetable oil based PU and organophilic nanoclay/nanometals/CNT etc.
- v) The prepared nanocomposites will be characterized by UV, FTIR, XRD, TEM, SEM, rheometer etc. to study the structure, morphology and rheological behaviors.
- vi) The performance characteristics of the characterized nanocomposites will be investigated by determination of mechanical properties like, tensile strength, modulus, elongation at break, impact resistance; thermal properties such as T_g , thermostability, flame retardancy; chemical resistance characteristics in different chemical media etc. The special properties like adhesive, shape memory, antimicrobial test, cytocompatibility, radical scavenging etc. will be conducted depending on requirement.
- vii) The performance characteristics of the nanocomposite will be optimized by manipulation of composition of raw materials, processing parameters etc. to find out the best nanocomposite in each category.

References

1. Karak, N. Polymer (epoxy) clay nanocomposites. *J. Polym. Mater.* **23**, 1-20 (2006)
2. Okada, A. et al. US Pat. 4,739,007 (1988)
3. Kojima, Y. et al. Sorption of water in nylon 6-clay hybrid. *J. Apply. Polym. Sci.* **49**, 1259-1264 (1993)
4. Jia, Q.M.; Zheng, M.; Chen, H.X.; Shen, R.J. Synthesis and characterization of polyurethane/epoxy interpenetrating network nanocomposites with organoclays. *Polym. Bullet.* **54**, 65-73 (2005)
5. Li, J. High performance epoxy resin nanocomposites containing both organic montmorillonite and castor oil-polyurethane. *Polym. Bullet.* **56**, 377-384 (2006)
6. Jia, Q.; Shan, S.; Wang, Y.; Gu, L.; Li, J. Tribological performance and thermal behavior of epoxy resin nanocomposites containing polyurethane and organoclay. *Polym. Adv. Technol.* **19**, 859-864 (2008)

7. Lei, Z.; Yang, Q.; Wu, S.; Song, X. Reinforcement of polyurethane/epoxy interpenetrating network nanocomposites with an organically modified palygorskite. *J. Apply. Polym. Sci.* **111**, 3150-3162 (2009)
8. Rana, S.; Karak, N.; Cho, J.W.; Kim, Y.H. Enhanced dispersion of carbon nanotubes in hyperbranched polyurethane and properties of nanocomposites. *Nanotechnol.* **19**, 495707(pp8) (2008)
9. Turunc, O.; Kayaman-Apohan, N.; Kahraman, M.V.; Menciloglu, Y.; Gungor, A. Nonisocyanate based polyurethane/silica nanocomposites and their coating performance. *J. Sol. Gel. Sci. Technol.* **47**, 290-299 (2008)
10. Finnigan, B.; Martin, D.; Halley, P.; Truss, R.; Campbell, K. Morphology and properties of thermoplastic polyurethane nanocomposites incorporating hydrophilic layered silicates. *Polymer* **445**, 2249-2260 (2004)
11. Barmar, M.; Barikani, M.; Fereidounnia, M. Study of polyurethane/clay nanocomposites produced via melt intercalation method. *Iran. Polym. J.* **15**, 709-714 (2006)
12. Guan, J.; Wagner, W.R. Synthesis, Characterization and cytocompatibility of polyurethane urea elastomers with designed elastase sensitivity. *Biomacromolecules* **6**, 2833-2842 (2005)
13. Kojio, K.; Nakashima, S.; Furukawa, M. Microphase-separated structure and mechanical properties of norbornane diisocyanate-based polyurethanes. *Polymer* **48**, 997-1004 (2007)
14. Pierce, B.F.; Brown, A.H.; Sheares, V.V. Thermoplastic poly(ester urethane)s with novel soft segments. *Macromolecules* **41**, 3866-3873 (2008)
15. Hepburn, C. *Polyurethane Elastomers*, 2nd edn. (Elsevier Applied Science, London, 1992)
16. Petrovic, Z.S.; Ferguson, J. Polyurethane elastomers. *Prog. Polym. Sci.* **16**, 695-836 (1991)
17. Paik Sung, C.S.; Hu, C.B.; Wu, C.S. Properties of segmented poly(urethane ureas) based on 2,4-toluene diisocyanate. 1. Thermal transitions, X-ray studies, and comparison with segmented poly(urethanes). *Macromolecules* **13**, 111-116 (1980)
18. Lin, S.B.; Hwang, K.S.; Tsay, S.Y.; Cooper, S.L. Segmental orientation studies of polyether polyurethane block copolymers with different hard segment lengths and distributions. *Colloid Polym. Sci.* **263**, 128-140 (1985)
19. Zhang, C.; Feng, S. Effect of glycols on the properties of polyester polyols and of room-temperature-curable casting polyurethanes. *Polym. Int.* **53**, 1936-1940 (2004)

20. Chu, B. et al. Microphase separation kinetics in segmented polyurethanes: Effects of soft segment length and structure. *Macromolecules* **25**, 5724-5729 (1992)
21. Karak, N.; Maiti, S. *Dendrimers and Hyperbranched Polymers—Synthesis to Applications* (MD publication Pvt. Ltd., New Delhi, 2008)
22. Ahmad, S.; Ashraf, S.M.; Naqvi, F.; Yadav, S.; Hasnat, A. A polyesteramide from *Pongamia glabra* oil for biologically safe anticorrosive coating. *Prog. Org. Coat.* **47**, 95-102 (2003)
23. Aigbodion, A.I.; Pillai, C.K.S.; Bakare, I.O.; Yahaya, L.E. Synthesis, characterisation and evaluation of heated rubber seed oil and rubber seed oil-modified alkyd resins as binders in surface coatings. *Ind. J. Chem. Technol.* **8**, 378-384 (2001)
24. Sharmin, E.; Ashraf, S.M.; Ahmad, S. Synthesis, characterization, antibacterial and corrosion protective properties of epoxies, epoxy-polyols and epoxy-polyurethane coatings from linseed and *Pongamia glabra* seed oils. *Int. J. Bio. Macromol.* **40**, 407-422 (2007)
25. Ikhuoria, E.U.; Aigbodion, A.I.; Okiemen, F.E. Preparation and characterisation of water-reducible alkyds with fumarized rubber seed oil. *Prog. Org. Coat.* **52**, 238-240 (2005)
26. Blayo, A.; Gandini, A.; Nest, J.F.L. Chemical and rheological characterizations of some vegetable oils derivatives commonly used in printing inks. *Ind. Crop. Prod.* **14**, 155-167 (2001)
27. Carrick, L.L. Vegetable oil paints. *J. Am. Oil. Chem. Soc.* **27**, 513-522 (1950)
28. Aigbodion, A.I.; Pillai, C.K.S. Preparation, analysis and applications of rubber seed oil and its derivatives in surface coatings. *Prog. Org. Coat.* **38**, 187-192 (2000)
29. Sabin, P.; Benjelloun-Mlayah, B.; Delmas, M. Offset printing inks based on rapeseed and sunflower oil: Synthesis and characterization of rapeseed oil- and sunflower oil-modified alkyd resins. *J. Am. Oil. Chem. Soc.* **74**, 481-489 (1997)
30. Erhan, S.Z.; Bagby, M.O. Vegetable-oil-based printing ink formulation and degradation. *Ind. Crop. Prod.* **3**, 237-246 (1995)
31. Akram, D.; Sharmin, E.; Ahmad, S. Synthesis and characterization of boron incorporated polyester polyol from linseed oil: A sustainable material. *Macromol. Symp.* **277**, 130-137 (2009)
32. Joseph, R.; Alex, R.; Vinod, V.S.; Premalatha, C.K.; Kuriakose, B. Studies on epoxidized rubber seed oil as plasticizer for acrylonitrile butadiene rubber. *J. Apply. Polym. Sci.* **89**, 668-673 (2003)

33. Nandan, V.; Joseph, R.; George, K.E. Rubber seed oil: A multipurpose additive in NR and SBR compounds. *J. Apply. Polym. Sci.* **72**, 487-492 (1999)
34. Bisht, R.P.; Sivasankaran, G.A.; Bhatia, V.K. Vegetable oils as lubricants and additives. *J. Sci. Ind. Res.* **48**, 174-180 (1989)
35. Ramadhas, A.S.; Jayaraj, S.; Muraleedharan, C. Use of vegetable oils as I.C. engine fuels - A review. *Renew. Energy* **29**, 727-742 (2004)
36. Ajiwe, V.I.E.; Okeke, C.A.; Ogbuagu, J.O.; Ojukwu, U.; Onwukeme, V.I. Characterization and applications of oils extracted from *Canarium schweinfurttii*, *Vitex doniana* and *Xylopiya aethiopia* fruits/seeds. *Bioresour. Technol.* **64**, 249-252 (1998)
37. Theng, B.K.G. Interactions of clay minerals with organic polymers. Some practical applications. *Clay Miner.* **18**, 357-362 (1970)
38. Hess, P.H.; Parker, P.H. Jr., Polymers for stabilization of colloidal cobalt particles. *J. Apply. Polym. Sci.* **10**, 1915-1927 (1966)
39. Cater, L.W.; Hendricks, J.G.; Don, S. US Pat. 2,531,396 (1950)
40. Greenland, D.J. Adsorption of polyvinyl alcohols by montmorillonite. *J. Colloid Sci.* **18**, 647-664 (1963)
41. Bayer, O. Das di-isocyanat-polyadditionsverfahren (polyurethane). *Angew. Chem.* **59**, 257-272 (1947)
42. Bayer, O.; Rinke, H.; Orthner, B.; Schild, H. German Pat. 728,981 (1942)
43. Bayer, O.; Rinke, H.; Schild, H. German Pat. 28,381 (1944)
44. Spindler, R.; Frechet, J.M.J. Synthesis and characterization of hyperbranched polyurethanes prepared from blocked isocyanate monomers by step-growth polymerization. *Macromolecules* **26**, 4809-4813 (1993)
45. Gao, C.; Yan, D. "A₂ + CB_n" approach to hyperbranched polymers with alternating ureido and urethano units. *Macromolecules* **36**, 613-620 (2003)
46. Dong, Z.; Li, Y.; Zou, Q. Degradation and biocompatibility of porous nano-hydroxyapatite/polyurethane composite scaffold for bone tissue engineering. *Appl. Surf. Sci.* **255**, 6087-6091 (2009)
47. Unal, S. et al. A new generation of highly branched polymers: Hyperbranched, segmented poly(urethane urea) elastomers. *Macromolecules* **37**, 7081-7084 (2004)
48. Chattopadhyay, D.K.; Raju, K.V.S.N. Structural engineering of polyurethane coatings for high performance applications. *Prog. Polym. Sci.* **47**, 352-418 (2007)
49. Brown, D.W.; Lowry, R.E.; Smith, L.E. Kinetics of hydrolytic aging of polyester urethane elastomers. *Macromolecules* **13**, 248-252 (1980)

50. Salamore, J.C. (Ed.), *Concise Polymeric Materials Encyclopedia* (CRC press, Boca Ranton, 1999)
51. Oil and Colour Chemist's Association of Australia, *Surface Coatings*, Vol 1 (Chapman and Hall, London, 1981)
52. Ulrich, H. *Chemistry and Technology of Isocyanates* (Wiley, New York, 1996)
53. Lamba, N.M.K.; Woodhouse, K.A.; Cooper, S.L. *Polyurethanes in Biomedical Applications* (CRC Press, Boca Ranton, 1998)
54. Javni, I.; Zhang, W.; Petrovic, Z.S. Effect of different isocyanates on the properties of soy-based polyurethanes. *J. Apply. Polym. Sci.* **88**, 2912-2916 (2003)
55. Szycher, M. *Szycher's Handbook of Polyurethanes* (CRC press, Boca Ranton, 1999)
56. Baker, J.W.; Gaunt, J. The mechanism of the reaction of aryl isocyanates with alcohols and amines. Part II. The base-catalysed reaction of phenyl isocyanate with alcohols. *J. Chem. Soc.* **7**, 9-18 (1949)
57. Baker, J.W.; Bailey, D.N. The mechanism of the reaction of aryl isocyanates with alcohols and amines. Part VI. Preliminary investigations with amines: Complex-formation by amines and ureas in benzene solution. *J. Chem. Soc.* **17**, 4649-4651 (1957)
58. Lenz, R.W. *Organic Chemistry of Synthetic High Polymers* (Wiley Interscience, New York, 1967)
59. Grobert, N. Carbon nanotubes-becoming clean. *Mater. Today* **10**, 28-35 (2007)
60. Spitalsky, Z.; Tasis, D.; Papagelis, K.; Galiotis, C. Carbon nanotube-polymer composites: Chemistry, processing, mechanical and electrical properties. *Prog. Polym. Sci.* **35**, 357-401 (2010)
61. Homenick, C.M.; Lawson, G.; Adronov, A. Polymer grafting of carbon nanotubes using living free-radical polymerization. *Polym. Rev.* **47**, 265-290 (2007)
62. Tasis, D.; Tagmatarchis, N.; Bianco, A.; Prato, M. Chemistry of carbon nanotubes. *Chem. Rev.* **106**, 1105-1136 (2006)
63. Alexandre, M.; Dubois, P. Polymer-layered silicate nanocomposites: Preparation, properties and uses of a new class of materials. *Mater. Sci. Eng. R* **28**, 1-63 (2000)
64. Pavlidou, S.; Papaspyrides, C.D. A review on polymer-layered silicate nanocomposites. *Prog. Polym. Sci.* **33**, 1119-1198 (2008)
65. Vaia, R.A.; Giannelis, E.P. Lattice model of polymer melt intercalation in organically-modified layered silicates. *Macromolecules* **30**, 7990-7999 (1997)

66. Ray, S.S.; Bousima, M. Biodegradable polymers and their layered silicate nanocomposites: In greening the 21st century materials world. *Prog. Mater. Sci.* **50**, 962-1079 (2005)
67. McNally, T.; Murphy, W.R.; Lew, C.Y.; Turner, R.J.; Brennan, G.P. Polyamide-12 layered silicate nanocomposites by melt blending. *Polymer* **44**, 2761-2772 (2003)
68. Vaia, R.A.; Jant, K.D.; Kramer, E.J.; Giannelis, E.P. Microstructural evolution of melt intercalated polymer-organically modified layered silicates nanocomposites. *Chem. Mater.* **8**, 2628-2635 (1996)
69. Morgan, A.B.; Gilman, J.W. Effects of organoclay Soxhlet Extraction on mechanical properties, flammability properties and organoclay dispersion of polypropylene nanocomposites. *J. Apply. Polym. Sci.* **87**, 2313-2320 (2003)
70. Davis, C.H. et al. Effects of melt-processing conditions on the quality of poly(ethylene terephthalate) montmorillonite clay nanocomposites. *J. Polym. Sci., Part B: Polym. Phys.* **40**, 2661-2666 (2002)
71. Zou, H.; Wu, S.; Shen, J. Polymer/silica nanocomposites: Preparation, characterization, properties, and applications. *Chem. Rev.* **108**, 3893-3957 (2008)
72. Amalvy, J.I.; Percy, M.J.; Armes, S.P.; Leite, C.A.P.; Galembeck, F. Characterization of the nanomorphology of polymer-silica colloidal nanocomposites using electron spectroscopy imaging. *Langmuir* **21**, 1175-1179 (2005)
73. <http://www.nuance.northwestern.edu/keckii/ftir2.asp> (accessed on 23.02. 2010)
74. VanderHart, D.L.; Asano, A.; Gilman, J.W. NMR measurements related to clay-dispersion quality and organic-modifier stability in nylon-6/clay nanocomposites. *Macromolecules* **34**, 3819-3822 (2001)
75. Bauer, F. et al. Preparation of scratch and abrasion resistant polymeric nanocomposites by monomer grafting onto nanoparticles, 1: FTIR and multi-nuclear NMR spectroscopy to the characterization of methacryl grafting. *Macromol. Chem. Phys.* **201**, 2654-2659 (2000)
76. Merkel, T.C.; Toy, L.G.; Andrady, A.L.; Gracz, H.; Stejskal, E.O. Investigation of enhanced free volume in nanosilica-filled poly(1-trimethylsilyl-1-propyne) by ^{129}Xe NMR spectroscopy. *Macromolecules* **36**, 353-358 (2003)
77. Kim, S.H.; Ahn, S.H.; Hirai, T. Crystallization kinetics and nucleation activity of silica nanoparticle poly(ethylene 2,6-naphthalate). *Polymer* **44**, 5625-5634 (2003)
78. Liu, X.; Wu, Q. PP/clay nanocomposites prepared by grafting-melt intercalation. *Polymer* **42**, 10013-10019 (2001)

79. Crosby, A.J.; Lee, J.Y. Polymer nanocomposites: The "nano" effect on mechanical properties. *Polym. Rev.* **47**, 217-229 (2007)
80. Paul, D.R.; Robeson, L.M. Polymer nanotechnology: Nanocomposites. *Polymer* **49**, 3187-3204 (2008)
81. Chen, B.; Evans, J.R.G. Poly(ϵ -caprolactone)-clay nanocomposites: Structure and mechanical properties. *Macromolecules* **39**, 747-754 (2006)
82. Fredrickson, G.H.; Bicerano, J. Barrier properties of oriented disk composites. *J. Chem. Phys.* **110**, 2181-2188 (1999)
83. Cong, H.; Radosz, M.; Towler, B.F.; Shen, Y.Q. Polymer-inorganic nanocomposite membranes for gas separation. *Sep. Purif. Technol.* **55**, 281-291 (2007)
84. Becker, O.; Varley, R.J.; Simon, G.P. Thermal stability and water uptake of high performance epoxy silicate nanocomposites. *Eur. Polym. J.* **40**, 187-195 (2004)
85. Xia, X.; Cai, S.; Xie, C. Preparation, structure and thermal stability of Cu/LDPE nanocomposites. *Mater. Chem. Phys.* **95**, 122-129 (2006)
86. Cho, J.W.; Paul, D.R. Nylon 6 nanocomposites by melt compounding. *Polymer* **42**, 1083-1094 (2001)
87. Beecroft, L.L.; Ober, C.K. Nanocomposite materials for optical applications. *Chem. Mater.* **9**, 1302-1317 (1997)
88. Wei, S.; Zhu, Y.; Zhang, Y.; Xu, J. Preparation and characterization of hyperbranched aromatic polyamides/Fe₃O₄ magnetic nanocomposites. *React. Funct. Polym.* **66**, 1272-1277 (2006)
89. Karak, N.; Konwarh, R.; Voit, B. Catalytically active vegetable-oil-based thermoplastic hyperbranched polyurethane/silver nanocomposites. *Macromol. Mater. Eng.* **295**, 159-169 (2010)
90. Dubey, A.; Mishra, B.G. Selective liquid phase oxidation of aromatics over silica-polymer nanocomposite materials. *Catal. Commun.* **8**, 1507-1510 (2007)
91. Liu, J.W.; Zhao, Q.; Wan, C.X. Research progresses on degradation mechanism *in vivo* and medical applications of polylactic acid. *Space Med. Med. Eng.* **14**, 308-312 (2001)
92. <http://www.freshpatents.com/High-dielectric-constant-nanocomposites-methods-of-manufacture-thereof-and-articles-comprising-the-same-dt20070524ptan20070117886.php> (accessed on 25.02. 2010)
93. Ahmadi, B.; Kassiriha, M.; Khodabakhshi, K.; Mafi, E.R. Effect of nano layered silicates on automotive polyurethane refinish clear coat. *Prog. Org. Coat.* **60**, 99-104 (2007)

94. Wu, Q.; Henriksson, M.; Liu, X.; Berglund, L.A. A high strength nanocomposite based on microcrystalline cellulose and polyurethane. *Biomacromolecules* **8**, 3687-3692 (2007)
95. Kannan, R.Y.; Salacinski, H.J.; Edirisinghe, M.J.; Hamilton, G.; Seifalian, A.M. Polyhedral oligomeric silsesquioxane-polyurethane nanocomposite microvessels for an artificial capillary bed. *Biomaterials* **27**, 4618-4626 (2006)
96. Shah, S.A.S.; Nag, M.; Kalagara, T.; Singh, S.; Manorama, S.V. Silver on PEG-PU-TiO₂ polymer nanocomposite films: An excellent system for antibacterial applications. *Chem. Mater.* **20**, 2455-2460 (2008)
97. <http://gow.epsrc.ac.uk/ViewGrant.aspx?GrantRef=GR/S56115/01> (accessed on 27.02.2010)
98. Xu, R.; Manias, E.; Snyder, A.J.; Runt, J. Low permeability biomedical polyurethane nanocomposites. *J. Biomed. Mater. Res. A* **64**, 114-119 (2003)
99. Styan, K.E.; Martin, D.J.; Poole, W.L.A. *In vitro* fibroblast response to polyurethane silicate nanocomposites. *J. Biomed. Mater. Res. A* **86**, 571-582 (2008)
100. Fare, S. et al. *In vitro* interaction of human fibroblasts and platelets with shape-memory polyurethane. *J. Biomed. Mater. Res. A* **73**, 1-11 (2005)
101. Mamunya, Ye.P. et al. Structure and water sorption of polyurethane nanocomposites based on organic and inorganic components. *Eur. Polym. J.* **40**, 2323-2331 (2004)
102. Osman, M.A.; Mittal, V.; Morbidelli, M.; Suter, U.W. Polyurethane adhesive nanocomposites as gas permeation barrier. *Macromolecules* **36**, 9851-9858 (2003)
103. Corcione, C.E.; Prinari, P.; Cannoletta, D.; Mensitieri, G.; Maffezzoli, A. Synthesis and characterization of clay-nanocomposite solvent-based polyurethane adhesives. *Int. J. Adhes. Adhes.* **28**, 91-100 (2008)
104. Vega-Baudrit, J. et al. Properties of thermoplastic polyurethane adhesives containing nanosilicas with different specific surface area and silanol content. *Int. J. Adhes. Adhes.* **27**, 469-479 (2007)
105. Devaux, E.; Rochery, M.; Bourbigot, S. Polyurethane/clay and polyurethane/POSS nanocomposites as flame retarded coating for polyester and cotton fabrics. *Fire Mater.* **26**, 149-154 (2002)
106. Chattopadhyay, D.K.; Raju, K.V.S.N. Structural engineering of polyurethane coatings for high performance applications. *Prog. Polym. Sci.* **32**, 352-418 (2007)

107. Sreedhar, B.; Chattopadhyay, D.K.; Swapna, V. Thermal and surface characterization of polyurethane-urea clay nanocomposite coatings. *J. Apply. Polym. Sci.* **100**, 2393-2401 (2006)
108. Cho, J.W.; Kim, J.W.; Jung, Y.C.; Goo, N.S. Electroactive shape-memory polyurethane composites incorporating carbon nanotubes. *Macromol. Rapid. Commun.* **26**, 412-416 (2005)
109. Cao, X.; Lee, L.J.; Widya, T.; Macosko, C. Polyurethane/clay nanocomposites foams: Processing, structure and properties. *Polymer* **46**, 775-783 (2005)
110. Chuayjuljit, S.; Maungcharreon, A.; Saravari, O. Preparation and properties of palm oil-based rigid polyurethane nanocomposite foams. *J. Reinf. Plast. Comp.* **29**, 218-225 (2010)
111. Yeganeh, H.; Mehdizadeh, M.R. Synthesis and properties of isocyanate curable millable polyurethane elastomers based on castor oil as a renewable resource polyol. *Eur. Polym. J.* **40**, 1233-1238 (2004)
112. Ahmad, S.; Ashraf, S.M.; Hasnat, A.; Yadav, S.; Jamal, A. Studies on urethane-modified alumina-filled polyesteramide anticorrosive coatings cured at ambient temperature. *J. Apply. Polym. Sci.* **82**, 1855-1865 (2001)
113. Gast, L.E.; Scheinder, W.J.; Cowan, J.C. Polyesteramides from linseed oil for protective coatings. *J. Am. Oil. Chem. Soc.* **46**, 534-536 (1968)
114. Thames, S.F.; Yu, H.; Wang, M.D. Air-dry primer coatings from dehydrated lesquerella oil. *Ind. Crop. Prod.* **6**, 169-175 (1997)
115. Bringi, N.V. (Ed.), *Non-Traditional Oil Seeds and Oils in India* (Oxford & IBH Publishing Co. Pvt. Ltd., New Delhi, 1987)
116. Dutta, N. *Development of Polyester Resins from Mesua ferrea L. Seed Oil*, (PhD Thesis, Tezpur University, India, 2006)
117. http://en.wikipedia.org/wiki/Natural_oil_polyols (accessed on 01.03. 2010)
118. Dutta, S. *Development of Mesua ferrea L. Seed Oil Based Polyurethane Resins* (PhD Thesis, Tezpur University, India, 2009)
119. Karak, N.; Rana, S.; Cho, J.W. Synthesis and characterization of castor-oil-modified hyperbranched polyurethanes. *J. Apply. Polym. Sci.* **112**, 736-743 (2009)
120. Petrovic, Z.S. Polyurethanes from vegetable oils. *Polym. Rev.* **48**, 109-155 (2008)
121. Dongyan, T.; Liangsheng, Q.; Zheng, J.; Weimin, C. Preparation, morphology, and thermoelectric property studies of BaTiO₃ superfine fiber/castor oil polyurethane-based IPN nanocomposites. *J. Apply. Polym. Sci.* **84**, 709-715 (2002)

122. Gultekin, G. et al. Fatty acid-based polyurethane films for wound dressing applications. *J. Mater. Sci. Mater. Med.* **20**, 421-431 (2009)
123. Hayes, D.G. Enzyme-catalyzed modification of oilseed materials to produce eco-friendly products. *J. Am. Oil. Chem. Soc.* **81**, 1077-1103 (2004)
124. Grinberg, S.; Kolot, V.; Mills, D. New chemical derivatives based on Vernonia galamensis oil. *Ind. Crop. Prod.* **3**, 113-119 (1994)
125. Gunstone, F.D. *The Chemistry of Oils and Fats* (Blackwell Pub. Ltd., UK, 1988)
126. Karleskind, A. (Ed.), *Oils & Fats*, Vol. 1 (Intercept Ltd., UK, 1996)
127. Becker, W. Solvent extraction of soybeans. *J. Am. Oil. Chem. Soc.* **55**, 751-753 (1978)
128. Zlatanovic, A.; Lava, C.; Zhang, W.; Petrovic, Z.S. Effect of structure on properties of polyols and polyurethanes based on different vegetable oils. *J. Polym. Sci., Part B: Polym. Phys.* **42**, 809-816 (2004)
129. Guner, F.S.; Yagci, Y.; Erciyes, A.T. Polymers from triglyceride oils. *Prog. Polym. Sci.* **31**, 633-670 (2006)
130. Derksen, J.T.P.; Cuperus, F.P.; Kolster, P. Renewable resources in coatings technology: A review. *Prog. Org. Coat.* **27**, 45-53 (1996)
131. Bao, L.H.; Lan, Y.J.; Zhang, S.F. Effect of NCO/OH molar ratio on the structure and properties of aqueous polyurethane from modified castor oil. *Iran. Polym. J.* **15**, 737-746 (2006)
132. Borden, G.W.; Smith, O.W.; Trecker, D.J. US Pat. 1975/3,876,518 (1975)
133. Ahmad, S.; Ashraf, S.M.; Hasnat, A.; Noor, A. Studies on epoxidised oil and its blend with polystyrene and poly(methyl methacrylate). *Ind. J. Chem. Technol.* **8**, 176-180 (2001)
134. Okieimen, F.E.; Bakare, O.I.; Okieimen, C.O. Studies on the epoxidation of rubber seed oil. *Ind. Crop. Prod.* **15**, 139-144 (2002)
135. Goud, V.V.; Pradhan, N.C.; Patwardhan, A.V. Epoxidation of karanja (*Pongamia glabra*) oil by H₂O₂. *J. Am. Oil. Chem. Soc.* **83**, 635-640 (2006)
136. Scala, J.L.; Wool, R.P. Property analysis of triglyceride-based thermosets. *Polymer* **46**, 61-69 (2005)
137. Sharpless, K.B.; Woodard, S.S.; Finn, M.G. On the mechanism of titanium-tartrate catalyzed asymmetric epoxidation. *Pure. Appl. Chem.* **55**, 1823-1836 (1983)
138. Guenter, S.; Rieth, R.; Rowbottom, K.T. *Ullmann's Encyclopedia of Industrial Chemistry* 6th edn., Vol. 12 (John Wiley and Sons, 2003)

139. Petrovic, Z.S.; Guo, A.; Zhang, W. Structure and properties of polyurethanes based on halogenated and nonhalogenated soy-polyols. *J. Polym. Sci., Part A: Polym. Chem.* **38**, 4062-4069 (2000)
140. Guo, Y.; Mannari, V.M.; Massingill, J.L. Hydrolysis of epoxidized soybean oil in the presence of phosphoric acid. *J. Am. Oil. Chem. Soc.* **84**, 929-935 (2007)
141. Ionescu, M.; Petrovic, Z.S.; Wan, X. Ethoxylated soybean polyols for polyurethanes. *J. Polym. Environ.* **15**, 237-243 (2007)
142. Guo, A.; Demydov, D.; Zhang, W.; Petrovic, Z.S. Polyols and polyurethanes from hydroformylation of soybean oil. *J. Polym. Environ.* **10**, 49-52 (2002)
143. Pryde, E.H.; Anders, D.E.; Teeter, H.M.; Cowan, J.C. Ozonization of soybean oil. The preparation and some properties of aldehyde oils. *J. Am. Oil. Chem. Soc.* **38**, 375-379 (1961)
144. Petrovic, Z.S.; Zhang, W.; Javni, I. Structure and properties of polyurethanes prepared from triglyceride polyols by ozonolysis. *Biomacromolecules* **6**, 713-719 (2005)
145. Phuong Tran, Daniel Graiver and Ramani Narayan Ozone-mediated polyol synthesis from soybean oil. *J. Am. Oil. Chem. Soc.* **82**, 653-659 (2005)
146. Dutta, S.; Karak, N. Effect of the NCO/OH ratio on the properties of *Mesua Ferrea* L. seed oil-modified polyurethane resins. *Polym. Int.* **55**, 49-56 (2006)
147. Choudhury, R.B.R. The preparation and purification of monoglycerides I. Glycerolysis of oils. *J. Am. Oil. Chem. Soc.* **37**, 483-486 (1960)
148. Saunders, J. H.; Frisch, K. C. *Polyurethanes: Chemistry and Technology, Part II* (Interscience Publishers, New York, 1964)
149. A.B. Koc, Ultrasonic monitoring of glycerol settling during transesterification of soybean oil. *Bioresour. Technol.* **100**, 19-24 (2009)
150. Ahamad, S.; Naqvi, F.; Verma, K.L.; Yadav, S. Studies on a newly developed linseed oil-based alumina-filled polyesteramide anticorrosive coating. *J. Appl. Polym. Sci.* **72**, 1679-1687 (1999)
151. Nagakura, M. Fat and oil products in urethane polymers. *Prog. Org. Coat.* **5**, 35-78 (1977)
152. Perin, G.; Alvaro, G.; Lenardao, E.J.; D'Oca, M.G.M. Transesterification of castor oil assisted by microwave irradiation. *Fuel* **87**, 2838-2841 (2008)
153. Dutta, S.; Karak, N.; Saikia, J.P.; Konwar, B.K. Biocompatible epoxy modified bio-based polyurethane nanocomposites: Mechanical property, cytotoxicity and biodegradation. *Bioresour. Technol.* **100**, 6391-6397 (2009)

154. Akram, D.; Ahmad, S.; Sharmin, E.; Ahmad, S. Silica reinforced organic-inorganic hybrid polyurethane nanocomposites from sustainable resource. *Macromol. Chem. Phys.* **211**, 412-419 (2010)
155. Heidarian, M.; Shishesaz, M.R.; Kassiriha, S.M.; Nematollahi, M. Characterization of structure and corrosion resistivity of polyurethane/organoclay nanocomposite coatings prepared through an ultrasonication assisted process. *Prog. Org. Coat.* **68**, 180-188 (2010)
156. Liu, M.; Petrovic, Z.S.; Xu, Y. Bio-based polyurethane-clay nanocomposite foams: Syntheses and properties. *Materials Research Society Symposium Proceedings* **1188**, 95-102 (2009)
157. Rihayat, T. et al. Mechanical characterisation of polyurethane/clay nanocomposites. *Polym. Polym. Compos.* **15**, 647-652 (2007)
158. Etekallpalli, R.K.R.; Ibeh, C.C. Bio-based polyurethane nanocomposites. *Annual Technical Conference-ANTEC, Conference Proceedings*, 273-277 (2006)
159. Rihayat, T. et al. Synthesis and thermal characterization of polyurethane/clay nanocomposites based on palm oil polyol. *Polym.-Plast. Technol.* **45**, 1323-1326 (2006)
160. Can, E.; Wool, R.P.; Kusefoglu, S. Soybean- and castor-oil-based thermosetting polymers: Mechanical properties. *J. Appl. Polym. Sci.* **102**, 1497-1504 (2006)
161. Konwar, U.; Karak, N.; Mandal, M. *Mesua ferrea* L. seed oil based highly thermostable and biodegradable polyester/clay nanocomposites. *Polym. Degrad. Stab.* **94**, 2221-2230 (2009)
162. Das, G.; Karak, N. Vegetable oil-based flame retardant epoxy/ clay nanocomposites. *Polym. Degrad. Stab.* **94**, 1948-1954 (2009)
163. Ashraf, S.M.; Ahmad, S.; Riaz, U. Development of novel conducting composites of linseed-oil-based poly(urethane amide) with nanostructured poly(1-naphthylamine). *Polym. Int.* **56**, 1173-1181 (2007)
164. Li, F.; Larock, R.C. New soybean oil-styrene-divinylbenzene thermosetting copolymers. VI. Time-temperature-transformation cure diagram and the effect of curing conditions on the thermoset properties. *Polym. Int.* **52**, 126-132 (2003)
165. Guzman, D. US agribusiness eyes China's oilseed market potential. *Chemical Market Reporter* **264**, 12-14 (2003)
166. Yeganeh, H.; Shamekhi, M.A. Novel polyurethane insulating coatings based on polyhydroxyl compounds, derived from glycolysed PET and castor oil. *J. Appl. Polym. Sci.* **99**, 1222-1233 (2006)

CHAPTER 2

Synthesis, characterization and properties of *Mesua ferrea* L. seed oil based hyperbranched polyurethanes

2.1. Introduction

The unique structural characteristics of HBPU have drawn a significant attention for the utilization of such materials in different advanced applications.¹ The single step one pot polymerization technique has paved the way for large scale production of the low polydispersed hyperbranched polymers at a reasonable cost.² The hyperbranched polymer possesses higher solubility, lower hydrodynamic diameter and lower melt as well as solution viscosity than its linear analog.³ This is due to the compact, non-entangled, globular and highly branched structure with large number of active surface functional groups of the hyperbranched polymer. Therefore hyperbranched polymers have many advantages over linear analogs. Besides the determination of degree of branching, the hyperbranched polymer can also be distinguished from its linear analog of equivalent molecular weight by studying the properties such as viscosity, solubility and hydrodynamic diameter.¹ Due to the unavailability of desired AB_X (where $X \geq 2$) type monomers, most of the cases the $A_2 + B_3$ preparative technique is a favorable choice. Reports on synthesis of HBPU using commercially available A_2 and B_3 type monomer have been found in literature.⁴⁻⁷ Nevertheless, the HBPU exhibit inferior mechanical strength due to the lack of entanglement and crystallinity. This was first addressed by Unal et al. using simple oligomeric $A_2 + B_3$ approach to overcome the drawback.⁸ In the present investigation an oligomeric diol is used as a macroglycol to achieve desirable mechanical strength.

On the other hand, the exhaustion of petroleum reserves, variable price of petroleum based products and the stringent environmental rules and regulations have provoked the utilization of natural renewable resources in both scientific and industrial communities.^{9,10} Among these, vegetable oils have drawn immense attention because of their advantages like easy availability, sustainability, versatility in structure and properties, relatively low and stable cost. Most importantly they are biodegradable and eco-friendly in nature.¹¹ A wide spectrum of application fields including surface

coating and paint, illumination, lubrication, automotive, biomedical, oil field etc. are covered by vegetable oils.^{12,13} Traditional vegetable oils such as linseed, soybean, coconut, castor, sunflower, palm oils along with seeds like cashew nut, natural rubber, *Pongamia glabra*, *Pongamia pinnata*, rapeseed, *Annona squamosa*, *Moringa oleifera* have been successfully utilized to produce different types of industrial polymers in addition to other products. In India, a wide variety of wildy grown plants and herbs are available. *Mesua ferrea* L. (Nahar) plant is available in different countries as mentioned in the earlier chapter, in addition to India.¹⁴ It is adequately produced in different parts of our country especially in the north-eastern region. The seeds possess surprisingly high oil content (~70%).^{15,16} The utilization of this oil has been reported from the same laboratory in the preparation of polymers such as polyesters,¹⁶ poly(ester amide)s,¹⁷ poly(urethane ester)s¹⁸ and poly(urethane amide)s.¹⁹ Among these PUs are found to be most exciting. Further, because of the superiority of hyperbranched polymers over the linear analogs, it is worthwhile to utilize this oil for synthesis of high performance HBPU. In addition to the above, in the realm of material science, PU has captured a unique niche of its own, instigating research in both industry and academic panorama.²⁰ The presence of separated microphase morphology and strong H-bonding between the hard segments, with alternative hard and soft segments structure, PU shows attractive physical, mechanical, chemical and thermal properties.^{21,22} These properties can also be manipulated by judicious variations of structure, molecular weight, distributions of the segments and the hard/soft segmental ratios.²³ Thus the versatility of PU is attributed to the unique possibilities for tailor making their properties. The influence of hard and soft segments ratio on the properties of PUs is well documented.^{24,25} Therefore in this chapter, the synthesis, characterization and properties of *Mesua ferrea* L. seed oil modified HBPU are discussed.

2.2. Experimental

2.2.1. Materials

The vegetable oil was isolated from *Mesua ferrea* L. seeds. The seeds were collected from Darrang, Assam, India. *Mesua ferrea* L. is a plant with a conical crown shape and is about 3-15 m in height. The average yield of seeds per tree is around 10-15 kg per annum. The seed oil is characteristic of slightly viscous liquid having brown color and smell. The oil was extracted from the dried powder of seeds by solvent soaking technique using n-hexane (Merck, India) as the solvent. Subsequently it was purified by

alkali refining technique using 0.01% aqueous NaOH solution and then washed with distilled water and finally dried under vacuum. The *Mesua ferrea* L. seed oil is non-drying oil with fatty acid composition of 52.3% oleic and 22.3% linoleic acids as unsaturated fatty acids and 15.9% palmitic and 9.5% stearic acids as saturated fatty acids.²⁶

Glycerol was purchased from Merck, India (Fig. 2.1). Its density is 1.26 g/mL, maximum 0.005% sulphated ash and minimum assay 99%. Other impurities present are 0.05% glycerol tributryrate, 0.0001% chloride, 0.0005% sulphate and 0.0002% heavy metals. In the present investigation, glycerol was used for two purposes, firstly, as a triol (alcoholizing reagent) for converting triglyceride into monoglyceride and secondly, as a B₃ monomer for hyperbranched polymer. It was used after drying under vacuum at 45 °C.

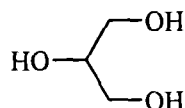


Fig. 2.1: Structure of glycerol (1,2,3-propane triol)

Lead mono-oxide (PbO) was obtained from S.D. Fine Chemical Ltd., India. The minimum assay is 99% and the impurities present are 0.02% chloride, 0.005% copper and 0.01% iron. Herein, it was used as a catalyst for transesterification reaction of triglyceride with glycerol. It was used as received.

Poly(ϵ -caprolactone) diol (PCL) (Fig. 2.2) was obtained from Solvay Co., UK. In the present investigation, it was used as a macroglycol in the synthesis of PUs. PCL has the density 1.071 g/c.c., hydroxyl number 37 mg KOH/g and number average molecular weight (M_n) 3000 g/mol. It was used after drying under vacuum at 45 °C.

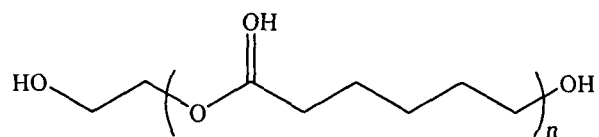


Fig. 2.2: Structure of poly(ϵ -caprolactone) diol

Toluene diisocyanate (TDI) (Fig. 2.3) was purchased from Sigma-Aldrich, Germany. It has formula weight (F_w) 174.16 g/mol, where 80% 2,4-isomer and 20% 2,6-isomer are present. It has density 1.214 g/c.c., m.p. 21.8 °C and b.p. 251 °C. Herein, TDI was used as a diisocyanate in the PU synthesis. It was used as received. Since TDI is highly reactive towards moisture, so while handling it needs caution.

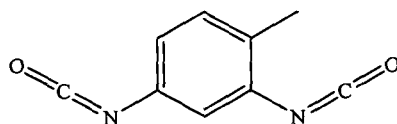


Fig. 2.3: Structure of toluene diisocyanate

N,N'-dimethylformamide (DMF) was purchased from Merck, India. It was used as a solvent after drying over CaO (Merck, India) and distilled under reduced pressure. It has F_w 73.09 g/mol, purity $\geq 98.0\%$, density 0.94 g/c.c. and b.p. 153 °C.

Methanol (CH₃OH) obtained from Merck, India has F_w 58.0 g/mol, purity $\geq 99.5\%$, density 0.971 g/c.c. and b.p. 56-57 °C. Here, it was used as a solvent.

Molecular sieve of 4A type was obtained from Merck, India. They often consist of alumino-silicate minerals, clays, porous glasses, microporous charcoals, zeolites, active carbons or synthetic compounds that have porous structure through which small molecules can diffuse. Its equilibrium capacity for water at 30 °C and 75% relative air humidity is $\geq 20\%$ and bulk density is 650-700 g/c.c. It was used as received to trap trace amount of moisture present in solvents.

2.2.2. Instruments and Methods

The viscosity of the polymer solutions (0.5 g/dL in DMF) was measured at (27±0.1) °C by the help of Ubbelohde capillary viscometer (suspended-level viscometer). The molecular weight of HBPU and the linear analog were determined by GPC analysis (Waters, Model 515, USA) using THF as the solvent. The density of the polymers was evaluated by pycnometer at room temperature (~27 °C) using the conventional liquid displacement method (Archimedes principle).²⁷ Hydroxyl value was determined by the standard procedure.²⁷

FTIR spectra of the PUs were recorded by a Nicolet, Impact 410, USA spectrometer using KBr pellets. Very small quantities of finely powdered nanocomposite samples were dispersed and grounded in KBr to a fine mixture in a mortar to form transparent KBr pellets for FTIR analysis. The UV spectra were recorded by UV spectrophotometer (Hitachi, U2001, Japan) with 0.001% polymer solution in DMF. ¹HNMR spectra of the polymers were also recorded by a 400 MHz, Varian, USA NMR spectrometer using d₆-DMSO as the solvent and TMS as the internal standard. The X-ray diffraction study was carried out at room temperature (~27 °C) by a Rigaku, Miniflex, UK X-ray diffractometer at scanning rate of 2.0/min over the range of $2\theta = 10-70^\circ$. The X-ray was derived from nickel-filtered Cu-K α ($\lambda = 0.154$ nm) radiation in a sealed tube operated at 40 kV and 40 mA. The thermal

analysis was done by TGA, (Shimadzu, TG 50, USA) with a nitrogen flow rate of 30 mL/min and heating rate of 10 °C/min. The surface morphology of the samples was observed by SEM of JEOL, JSM-6390LV, Japan. The surface of the fractured tensile test samples was platinum coated before testing.

The mechanical properties such as tensile strength and elongation at break were measured with the help of Universal Testing Machine, UTM, (Zwick, Z010, Germany) with a 10 kN load cell and crosshead speed of 50 mm/min. The gloss of the films was measured by using mini glossmeter (Sheen instrument Ltd., Ref: 262, UK). The hardness of the samples was measured by using Shore A durometer model SHR-MARK-III as per the ASTM D 676-59 standard. Impact and adhesion (using the lap shear adhesion method and taking plywood sheet as the substrate, ASTM D3165-95) were performed using the standard techniques.¹² The lap shear test was carried out with the help of the UTM machine at jaw separation speed of 50 mm/min. The flexibility was determined by bending test of the samples coated on tin plate and examining any crack or damage in the substrate while bending around a cylindrical mandrel.²⁸

The chemical resistance tests were performed in different chemical media as per the ASTM D 543-67 standard procedure²⁹ by taking polymer coated glass plates in 250 mL beakers containing 150 mL of the individual chemical medium for 10 days. The chemical resistance was determined by visual changes in the films as well as calculation of percent weight loss.

2.2.2.1. Preparation of Monoglyceride of *Mesua ferrea* L. Seed Oil

In a three neck round bottom flask equipped with a mechanical stirrer, thermometer and a nitrogen gas inlet, 15.0 g (0.017 mol) *Mesua ferrea* L. seed oil, 3.14 g (0.034 mol) glycerol and 0.05 weight% lead mono-oxide (with respect to the oil) was charged with continuous stirring. The reaction mixture was heated up to (240±5) °C for 30-40 min until the monoglyceride was formed. The formation of the monoglyceride was confirmed by solubility in methanol (monoglyceride : methanol = 1: 3 v/v) at ambient temperature.

2.2.2.2. Synthesis of Hyperbranched Polyurethanes

Required amount of PCL and monoglyceride of the oil were taken in a three-neck round bottom flask equipped with a nitrogen gas inlet, mechanical stirrer and a dropping funnel. The reactants were dissolved in 30 mL of DMF with constant stirring. A requisite amount of TDI was added drop-wise into the reaction mixture at room

temperature. The reaction was allowed to stir for 4 h at temperature of (70 ± 2) °C to obtain a viscous mass, which was treated as pre-polymer.

The obtained pre-polymer was then cooled to $(0-5)$ °C followed by addition of glycerol (dissolved in DMF) with the help of dropping funnel. The temperature was raised to (110 ± 2) °C and stirred continuously for about 2.5 h under the same condition. A part of the viscous product was precipitated in water and then dried in vacuum oven at 50 °C for 48 h for further analyses and the rest amount was solution casted on different substrates for various tests. The exact mole compositions of all PUs are given in Table 2.1.

The synthesis of linear PU followed the same procedure except monoglyceride of the oil was used in second stage instead of glycerol.

Table 2.1: Composition of reactants for the hyperbranched and linear PUs

Code*	Monoglyceride (mol)	PCL (mol)	TDI (mol)	Glycerol (mol)	NCO/OH ratio (mol)
HBPU20	1.5	2.5	6.5	2.5	0.89
HBPU30	3	2	7.5	2.5	0.96
HBPU38	5	2	9.75	2.75	1.01
HBPU47	6	1.5	10	2.5	1.05
LPU30	4	2	6	-	1.0

*The number in the code indicates the hard segment content in the polymers

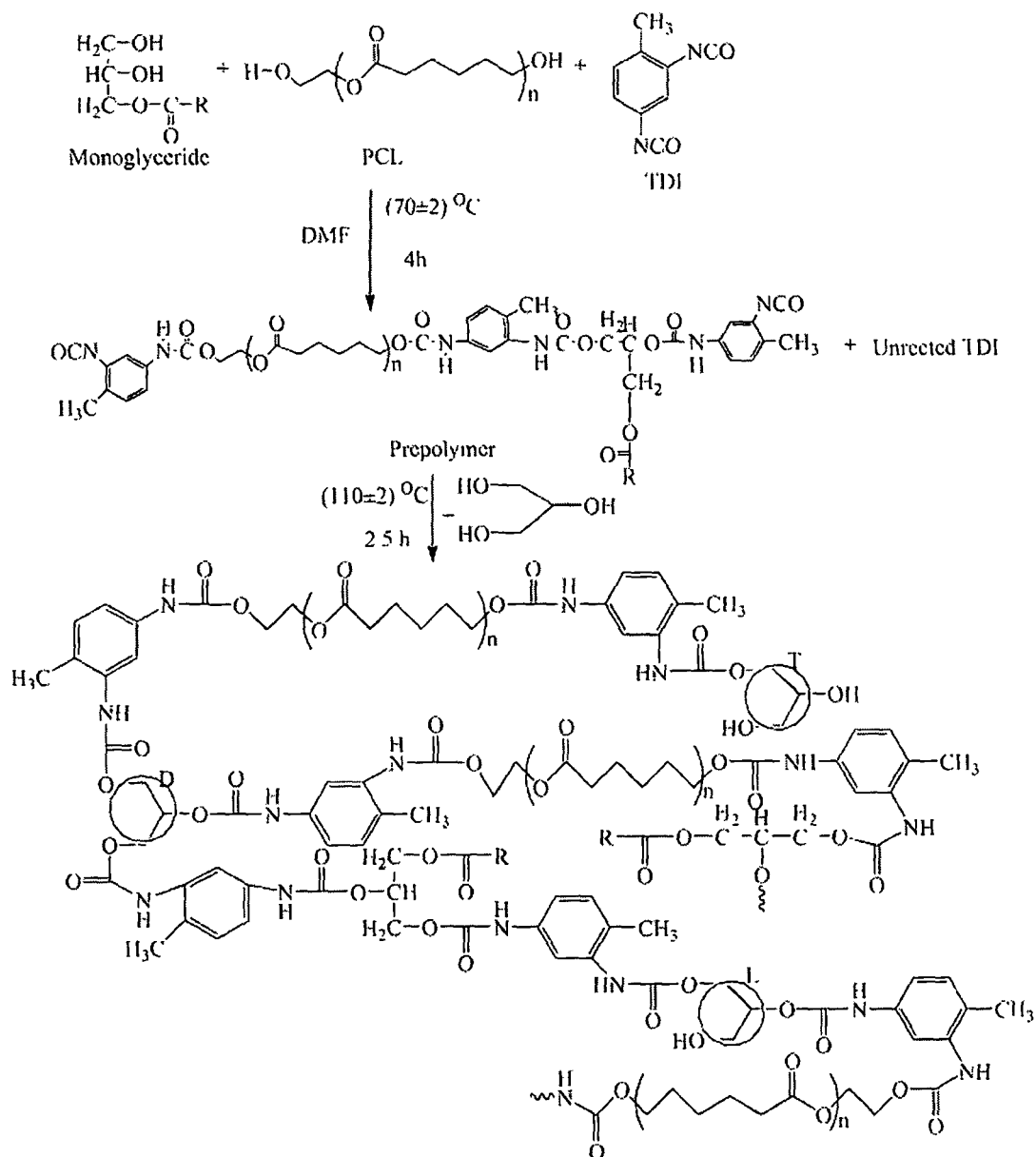
2.2.2.3. Sample Preparation for Performance Studies

The polymer solutions were casted on different substrates for different studies. The mild steel strips ($150 \times 100 \times 1.44 \text{ mm}^3$), tin strips ($150 \times 50 \times 0.19 \text{ mm}^3$) and glass strips ($75 \times 25 \times 1.39 \text{ mm}^3$) were coated by the polymers for gloss, impact, bending and chemical resistance tests respectively. The coating thickness of the films as measured by a Pentest coating-thickness gauge (Sheen Instrument Ltd., model 1117, UK) was found to be in the range of 60-70 μm . For the adhesion test, the plywood substrates were first washed with acetone to remove dirt and subsequently polished with sand paper of grit No. 60 (250 μm) according to the ASTM 906. The casted HBPU samples were cut by the manual sample cutter with dimension as per the ASTM D 412-51T for mechanical test.

2.3. Results and Discussions

2.3.1. Synthesis

A₂ + B₃ approach was adopted to synthesize the HBPU with four different percentages of hard segment contents through one pot pre-polymerization technique as shown in Scheme 2.1.



Scheme 2.1: Synthesis of HBPU

The pre-polymer was formed between isocyanate groups of the TDI with hydroxyl groups of monoglyceride and PCL, which was indicated by the increase of viscosity of the reaction medium. This isocyanate terminated pre-polymer along with unreacted TDI acted as the A₂ monomer in the second stage of PU synthesis. Gelation may be a problem for such type of reactions. In the present investigation, high dilution

and slow addition of monomers along with the controlling of other reaction parameters were employed to overcome the gelation problem. Very dilute solution of glycerol, B₃ monomer, (<10% in DMF) was added very slowly with the help of pressure equalizing funnel at temperature of (0-5) °C. This is because, the addition of glycerol at high temperature or high concentration leads to the gel formation. In the second stage, the chain extension with possible branched structure of PU occurs by the reaction of free and terminal isocyanate with hydroxyl groups of glycerol. The reactions were stopped when the viscosity was attained to a desired level in each case. In the synthesis of linear PU since multifunctional glycerol was absent, the possibility of the formation of branched structure can be ruled out.

2.3.2. Characterization

FTIR is an important tool to investigate the conformation, accessibility, extent of H-bonding and the interactions between hard-soft segments along with the confirmation of PUs.^{30,31} In this present study the extent of H-bonding has been examined by the changes in the mid-infrared region both in band intensity and frequency shift. Most of the inherent properties like viscosity, T_g, solubility etc. are strongly influenced by the degree of H-bonding present in the polymer. Therefore, the factors (like hard segment content), which influence the H-bonding is very vital to study. The FTIR spectra of the HBPU30 and the linear analog are shown in Fig. 2.4. The absorption bands of the HBPU30 with their corresponding functional groups are given in Table 2.2. The completion of the reaction was indicated by the absence of band at ~2250-2270 cm⁻¹ for -NCO group.³² Thus there is no free -NCO group present in the polymer structure. Shifts of -C=O and -NH bands to lower wavenumber regions with the increase of hard segment content in the HBPU30 were observed from FTIR spectra (Fig. 2.5). The magnitude of H-bonding can be measured from the position and intensity of these bands.³³ The hydrogen bonded -NH stretching vibration was observed at ~3409-3438 cm⁻¹. The H-bonding between -NH groups of PU with the urethane carbonyl, the PCL carbonyl or ether oxygen may form in these polymers. A continuous shift of the -NH band from 3438 cm⁻¹ to 3409 cm⁻¹ with the increase in amount of TDI from HBPU20 to HBPU47 was observed in the FTIR spectra (Fig. 2.5). Similarly, in case of -C=O stretching frequency a gradual shifting from 1710 to 1685 cm⁻¹ has been observed from HBPU20 to HBPU47 (Fig. 2.5). Hence, combining these two results it can be inferred that the increase of hard segment increases the extent of H-bonding.

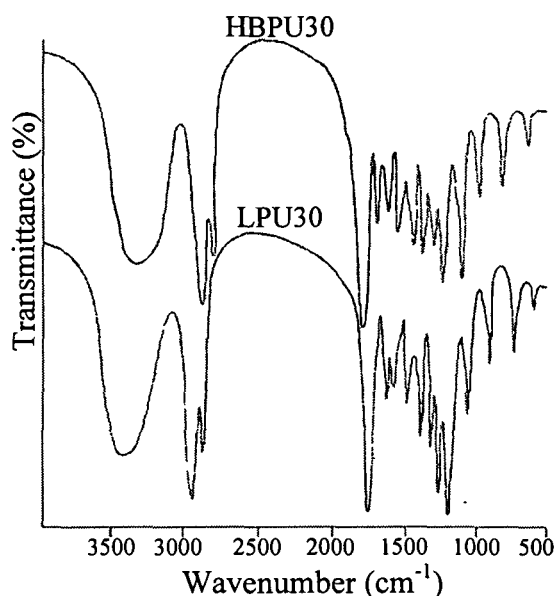


Fig. 2.4: FTIR spectra of HBPU30 and linear analog

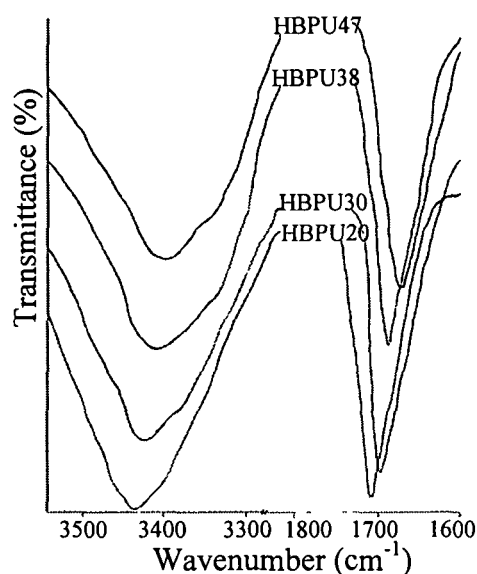


Fig. 2.5: FTIR spectra of all the HBPU's in the -NH and -CO stretching region

Table 2.2: FTIR spectral data of the hyperbranched and linear PUs

Band Position (cm ⁻¹)	Functional Groups
3409-3438	-NH stretching vibrations
2859-2950	-CH ₂ symmetric and anti-symmetric stretching vibrations
1669-1710	amide I, >C=O stretching vibrations
1557-1580	amide II, >C-N stretching and -NH bending
1469-1474	-CH ₂ scissoring, -CH ₃ deformation and -CH ₂ bending
1369	-C-H deformation
1243-1296	amide III, ν _{C-N} and in plane -NH deformation
1045-1050	-O-C=O stretching of urethane/ester group
872	>C-O stretching and CH ₂ rocking
703	amide IV

All HBPU's showed λ_{\max} value at 267 nm with low intensity, whereas the same was obtained at 274 nm with higher intensity for the linear analog. This is because of the fact that the effective overlap of the π -orbitals is possible in case of linear polymer because of the lesser hindrance structure and thus easier π - π^* transition than the hyperbranched polymer though both have similar conjugation. Same observation can be seen in case of stilbene. The literature value of cis-stilbene ($\lambda_{\max} = 280$ nm) and its *trans*-isomer ($\lambda_{\max} = 295$ nm) with a higher intensity.³⁴ This result might support the highly branched structure of the HBPU's. Further, as there was no absorption peak at

286 nm, which is characteristic λ_{\max} for TDI, thus the absence of free TDI can be confirmed¹⁸ (which is also supported by FTIR study).

¹HNMR study was also utilized to support the structure of HBPU30 (Fig. 2.6). The peaks at $\delta = 0.84$ ppm, $\delta = 1.28$ ppm and $\delta = 1.5$ ppm are due to the terminal methyl groups, all internal $-\text{CH}_2$ groups and the protons for $-\text{CH}_2$ groups attached next to the terminal methyl group of the fatty acid chains respectively.¹⁶ The protons of allylic $-\text{CH}_2$, $-\text{CH}_2$ adjacent to $-\text{NH}$ of urethane group and $-\text{CH}_3$ of TDI show peaks at $\delta = 1.97$ ppm, $\delta = 2.26$ ppm and $\delta = 2.5$ ppm respectively.^{17,18} The $-\text{CH}_2$ protons of glycerol moiety attached to the urethane linkages and $-\text{CH}_2$ protons adjacent to $-\text{OH}$ groups are found at $\delta = 3.34$ ppm and $\delta = 3.97$ ppm respectively.³⁴ The protons for $-\text{CH}$ of glycerol, unsaturation of fatty acid segment and $-\text{OH}$ groups may appear at $\delta = 5.30$ ppm, whereas the protons of aromatic moiety are found at $\delta = 7.0$ ppm.³² Thus the above spectral analyses confirmed the formation of vegetable oil based PUs.

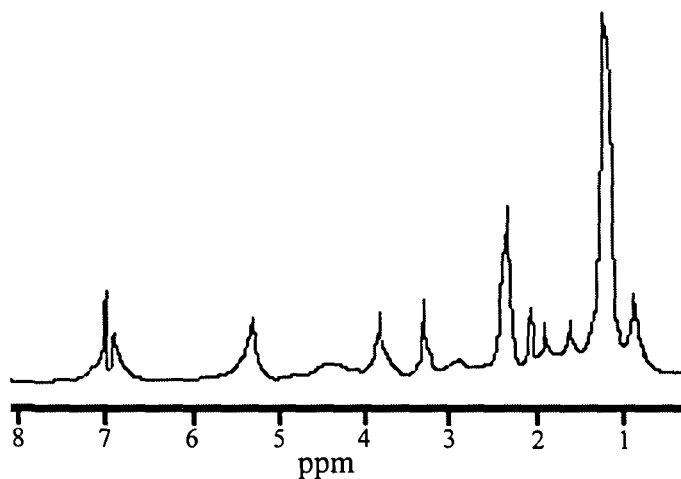


Fig. 2.6: ¹HNMR spectrum of HBPU30

2.3.3. Physical Properties

The hyperbranched polymers are known to be more soluble than their linear analogs. It was found that the synthesized HBPU30s were soluble in 1,4-dioxane, acetone, ethyl acetate where the linear analog was not soluble. However both the types of polymers were soluble in xylene, DMF, DMSO and THF. Again the linear analog was partly soluble in DMAc where the hyperbranched polymers were completely soluble. The branched backbone with large number of surface groups along with globular, non-entangled structure of the hyperbranched polymers offers rapid dissolution,⁵ which is the reason of the observed behavior. The synthesized HBPU30s possess relatively low polydispersity index compared to the linear analog, while the weight average

molecular weights (M_w) of both types of polymers were almost equivalent (Table 2.3). Further, the molecular weight of the hyperbranched polymers was determined by using linear polystyrene as the standard, so the exact value might be higher than the observed molecular weight for the hyperbranched polymers. The ratio of hydrodynamic diameter of hyperbranched polymer with respect to linear indicates that the former has lower diameter than the latter and the diameter increases with the increase of hard segment content in hyperbranched polymers (Table 2.3). The density of HBPU was found to be higher than the linear analog. This might be due to the compact structure of HBPU.¹ It was also observed that with the increase of ratio of hard segment the density increases as compactness increases through H-bonding, polar-polar interaction etc.

Table 2.3: Physical properties of the hyperbranched and linear PUs

Property	HBPU20	HBPU30	HBPU38	HBPU 47	LPU30
Color	Brown	Brown	Brown	Brown	Light Brown
Hydroxyl value (mgKOH/g)	44.82	37.35	21.31	12.23	14.21
Specific gravity (25 °C)	1.13	1.15	1.20	1.21	1.10
Inherent viscosity (dL/g)	0.29	0.31	0.32	0.32	0.34
M_w ($\times 10^4$ g/mol)	4.9	5.28	5.31	5.35	5.69
Polydispersity index	2.3	2.42	2.5	2.8	4.8
Extent of branching*	0.87	0.90	0.93	0.94	-

*This is the ratio of hydrodynamic diameter of hyperbranched polymer to linear polymer and calculated from their molecular weight and intrinsic viscosity by using Hester and Mitchell equation [19]

XRD analysis (Fig. 2.7) confirmed the presence of crystallinity in HBPU and linear analog. The two diffraction peaks observed at $2\theta = 21.2^\circ$ (4.19 Å) and 23.4° (3.81 Å) are due to (110) and (200) planes of PCL crystals. There was no effect on the position of PCL crystalline diffraction peaks after polymer formation though the intensity gradually decreases with the increase of hard segment content for hindering effect³⁵ (Fig. 2.7). The gloss property (Table 2.4) was found to be acceptable to industrial coating system and is comparable to the other polymers prepared from this oil.¹⁶⁻¹⁹

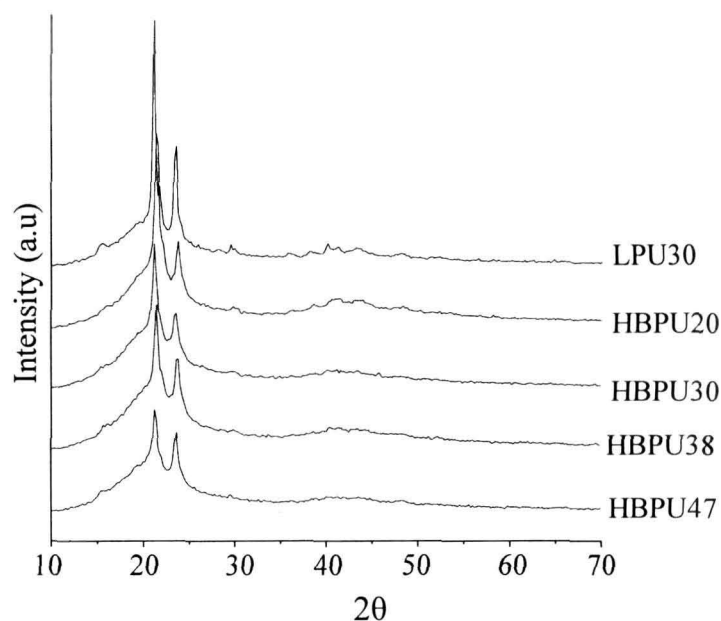


Fig. 2.7: WAXD patterns of all the HBPU_s and linear analog

2.3.4. Morphological Study

The morphological study was done with the help of SEM. The Fig. 2.8 shows the SEM micrographs of HBPU_s. However, from the SEM micrographs it is difficult to identify the hard and soft segments. The SEM micrographs confirmed the uniform phase distribution of the polymers at different hard segment contents.

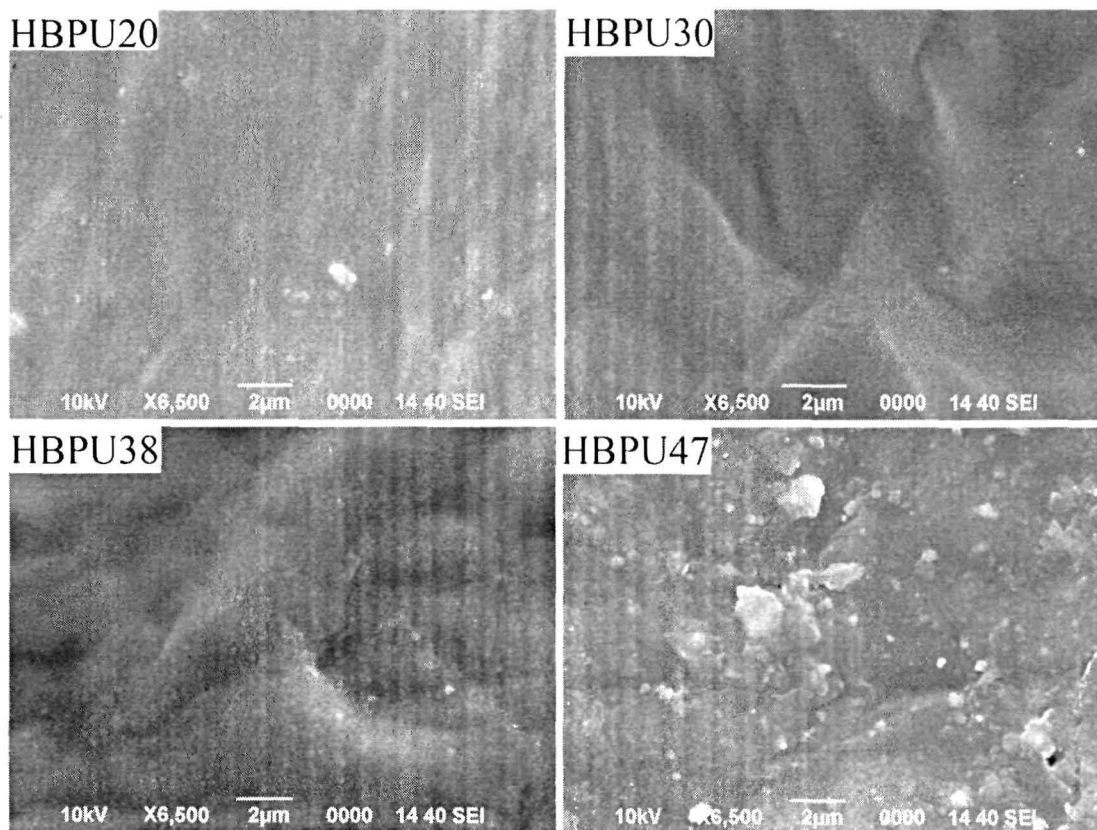


Fig. 2.8: SEM micrographs of HBPU_s

2.3.5. Mechanical Properties

The performance characteristics of the hyperbranched and linear PUs are given in Table 2.4. It was observed that the hardness (Shore A) increases with the increase of hard segment content of HBPU. This is because of the increase in inter and intra molecular interactions, degree of H-bonding and amount of aromatic moieties which increases with the hard segment content. All HBPU showed adequate flexibility as they can be bent in a cylindrical mandrel with diameter of 3 mm. This flexibility is attributed by the flexible PCL ether, ester linkages and the long aliphatic hydrocarbon chain of the oil. As the HBPU have good flexibility, so the impact resistance is also good except the HBPU47. This might be attributed to its maximal rigidity, which limits the studies of further increase in hard segment content in the polymer. The highest flexibility of the linear polymer resulted in its highest impact strength. The adhesion test was performed using plywood as substrate. The increase of adhesive strength values with the increase of hard segment content in the polymer is due to the increase of polar linkages such as urethane, ester and urea in the structure.³⁶ The linear polymer also showed good adhesive strength, which is comparable to 30% hard segment containing HBPU. The mechanical properties of PUs depend on molecular weight, chemical linkages, entanglement, crystallinity, size, shape and interaction of the hard segment present in the structure.³⁷ The stress-strain curves for all polymers are shown in Fig. 2.9. The presence of yield and necking points in all polymers except HBPU47 indicates the typical elastomeric nature.³⁸ The LPU30 exhibited tensile strength of 5.31 MPa and elongation at break of 779%, while the HBPU30 showed the highest elongation at 721% and HBPU47 had the highest tensile strength of 8.6 MPa among all HBPU (Table 2.4). It was also observed that with the increase of hard segment tensile strength increases at an expense of elongation at break value. This is because of the increase of rigid aromatic moiety, H-bonding and dipolar interactions that make HBPU hard to stretch.

Table 2.4: Mechanical properties of the hyperbranched and linear PUs

Property	HBPU20	HBPU30	HBPU38	HBPU47	LPU30
Tensile strength (MPa)	5.81	6.80	8.10	8.60	5.31
Elongation at break (%)	430.12	721.31	573.21	237.42	779.21
Hardness (Shore A)	70	72	74	77	68
Bending test (mm)	<3	<3	<3	<3	<3
Impact test (cm)	42	35	32	30	44
Adhesion (MPa)	4.08	4.67	5.12	5.32	4.21
Gloss (60°)	82.4	82.9	83.6	84.2	82.7

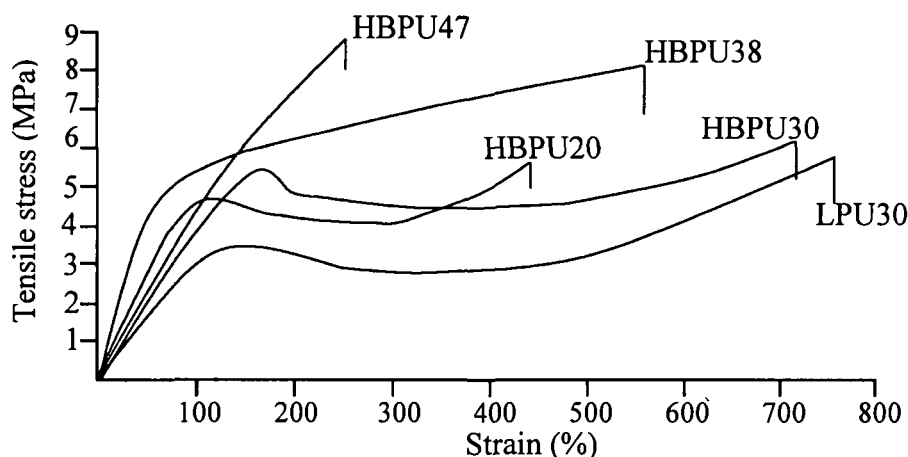


Fig. 2.9: Stress-strain profile of HBPU47, HBPU38, HBPU20, HBPU30, and LPU30

2.3.6. Thermal Properties

Several factors such as presence of aromatic moieties influence the thermo-stability of PUs, as they can withstand a considerable amount of heat. Also the existence of secondary interactions increases the thermo-stability of PUs. The studied hyperbranched polymers showed two-step degradation in the TGA thermograms (Fig. 2.10) which is supported by the reported literatures.³⁹ With the increase of the hard

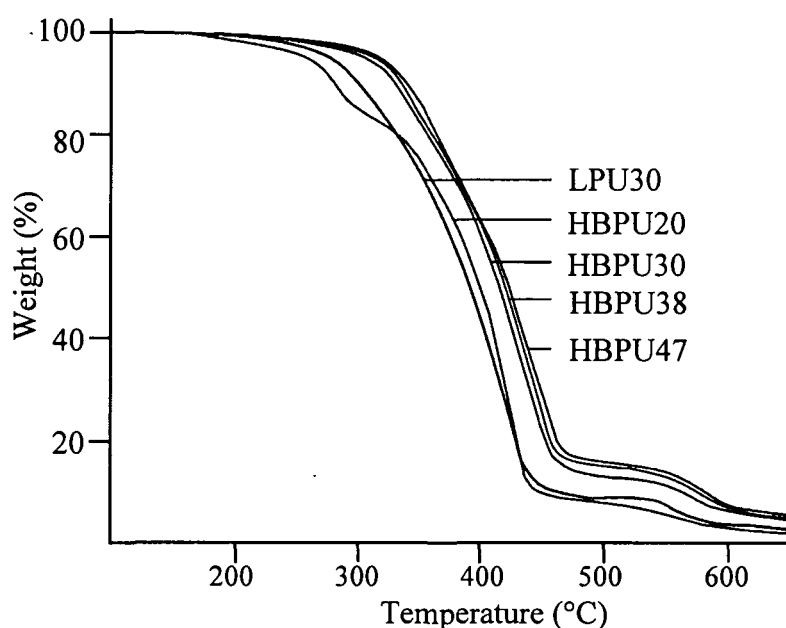


Fig. 2.10: TGA thermograms of HBPU47, HBPU38, HBPU30, HBPU20, and LPU30

segment the decomposition temperature was found to be increased. This is due to the increase of aromatic moiety of TDI and increase of intermolecular attractions between $-NH$ and $-C=O$ through H-bonding, polar-polar interaction etc., all of those also make the structure more compact. In addition, the segmental motion of the polymer chains decreases to certain extent for the increase of secondary interactions. The synergistic effect of the above factors leads the HBPU47s to be more thermo-stable with the

increase of hard segment. The thermo-stability of LPU30 was found to be lower than its hyperbranched analog. This might be due to the differences of secondary interactions, which is stronger in hyperbranched polymers for their compact structures than the linear analog. The onset decomposition temperature ($T_{1st\ ON}$), temperature corresponding to maximum rate of weight loss (T_{MAX}) and initiation of endset decomposition temperature ($T_{2nd\ ON}$) for the hyperbranched and linear PUs are shown in Table 2.5.

Table 2.5: The characteristic thermal decomposition temperatures

Code	$T_{1st\ ON}$ (°C)	T_{MAX} (°C)	$T_{2nd\ ON}$ (°C)
HBPU20	210	390	540
HBPU30	215	430	570
HBPU38	215	448	575
HBPU47	220	455	583
LPU30	212	400	528

2.3.7. Chemical Resistance Test

Chemical resistance of HBPU and linear analog was studied under various chemical media such as aqueous 10% NaCl, 20% EtOH, 5% HCl, 3% NaOH solutions and fresh water for 10 days. The polymers were stable under different chemical environments except in NaOH solution. The poor stability in alkaline medium is due to the presence of alkali hydrolyzable ester groups in PCL and monoglyceride segments.¹⁶ However, this qualitative test is unable to distinguish the effect of hard segment and degree of branching.

2.4. Conclusions

From this study it can be concluded that *Mesua ferrea* L. seed oil derived HBPU can be prepared successfully with varying segmental ratios. The segmental ratio has significant effect on physical, mechanical and thermal properties of the PUs. The increase of hard segment increases H-bonding and polarity in structure and hence the properties are influenced by the same. The compact globular hyperbranched structure with entanglement of oligomeric segment of the polymer resulted superior properties in most of the cases compared to the conventional linear analogous polymer. Since the synthesized polymers can be solution as well as melt casted, so this study confirmed the potentiality of the hyperbranched bio-based PU as thermoplastic materials for various applications.

References

1. Karak, N.; Maiti, S. *Dendrimers and Hyperbranched Polymers—Synthesis to Applications* (MD publication Pvt. Ltd., New Delhi, 2008)
2. Scholl, M.; Kadlecova, Z.; Klok, H.A. Dendritic and hyperbranched polyamides. *Prog. Polym. Sci.* **34**, 24-61 (2009)
3. Gao, C.; Yan, D. Hyperbranched polymers: From synthesis to applications. *Prog. Polym. Sci.* **29**, 183-275 (2004)
4. Bruchmann, B.; Schrepp, W. The AA* + B*B₂ approach- A simple and convenient synthetic strategy towards hyperbranched polyurea-urethanes. *e-Polymer* 014 (2003)
5. Fornof, A.R.; Glass, T.E.; Long, T.E. Degree of branching of highly branched polyurethanes synthesized via the oligomeric A₂ plus B₃ methodology. *Macromol. Chem. Phys.* **207**, 1197-1206 (2006)
6. Shao-Min, Z. et al. Synthesis and properties of hyperbranched polyurethane with a long chain between the branching points. *Des. Monomers Polym.* **12**, 221-231 (2009)
7. Sivakumar, C.; Nasar, A.S. Poly(ϵ -caprolactone)-based hyperbranched polyurethanes prepared via A₂+B₃ approach and its shape-memory behavior. *Eur. Polym. J.* **45**, 2329-2337 (2009)
8. Unal, S. A new generation of highly branched polymers: Hyperbranched, segmented poly(urethane urea) elastomers. *Macromolecules* **37**, 7081-7084 (2004)
9. Oprea, S. Synthesis and properties of polyurethane elastomers with castor oil as crosslinker. *J. Am. Oil. Chem. Soc.* **87**, 313-320 (2010)
10. Konwar, U.; Karak, N.; Mandal, M. *Mesua ferrea* L. seed oil based highly thermostable and biodegradable polyester/clay nanocomposites. *Polym. Degrad. Stab.* **94**, 2221-2230 (2009)
11. Gunera, F.S.; Yagcib, Y.; Erciyes, T. Polymers from triglyceride oils. *Prog. Polym. Sci.* **31**, 633-670 (2006)
12. Ramos, M.J.; Fernandez, C.M.; Casas, A.; Rodriguez, L.; Perez, A. Influence of fatty acid composition of raw materials on biodiesel properties. *Bioresour. Technol.* **100**, 261-268 (2009)
13. Chuang, P.H. Anti-fungal activity of crude extracts and essential oil of *Moringa oleifera* Lam. *Bioresour. Technol.* **98**, 232-236 (2007)

14. Bringi, N.V. (Ed.) *Non-Traditional Oil Seeds and Oils in India* (Oxford & IBH Publishing Co. Pvt. Ltd., New Delhi, 1987)
15. Erhan, S.Z.; Bagby, M.O. Vegetable-oil-based printing ink formulation and degradation. *Ind. Crop. Prod.* **3**, 237-246 (1995)
16. Dutta, N.; Karak, N.; Dolui, S.K. Synthesis and characterization of polyester resins based on Nahar seed oil. *Prog. Org. Coat.* **49**, 146-152 (2004)
17. Mahapatra, S.S.; Karak, N. Synthesis and characterization of polyestheramide resins from Nahar seed oil for surface coating applications. *Prog. Org. Coat.* **51**, 103-108 (2004)
18. Dutta, S.; Karak, N. Effect of the NCO/OH ratio on the properties of *Mesua Ferrea* L. seed oil-modified polyurethane resins. *Polym. Int.* **55**, 49-56 (2006)
19. Dutta, S.; Karak, N. Synthesis, characterization of poly(urethane amide) resins from Nahar seed oil for surface coating applications. *Prog. Org. Coat.* **53**, 147-152 (2005)
20. Woods, G. *The ICI Polyurethanes Book* (John Wiley, New York, 1990)
21. Yilgor, E.; Yilgor, I. Hydrogen bonding: A critical parameter in designing silicone copolymers. *Polymer* **42**, 7953-7959 (2001)
22. Aneja, A.; Wilkes, G.L. A systematic series of 'model' PTMO based segmented polyurethanes reinvestigated using atomic force microscopy. *Polymer* **44**, 7221-7228 (2003)
23. Huang, S.L.; Lai, J.Y. Structure-tensile properties of polyurethanes. *Eur. Polym. J.* **33**, 1563-1567 (1997)
24. Martin, D.J.; Meijjs, G.F.; Gunatillake, P.A.; McCarthy, S.J.; Renwick, G.M. The effect of average soft segment length on morphology and properties of a series of polyurethane elastomers. II. SAXS-DSC annealing study. *J. Appl. Polym. Sci.* **64**, 803-817 (1997)
25. Chu, B.; Gao, T.; Li, Y.; Wane, J.; Deeper, C.R.; Byrne, C.A. Microphase separation kinetics in segmented polyurethanes: Effects of soft segment length and structure. *Macromolecules* **25**, 5724-5729 (1992)
26. Konwer, D.; Taylor, S.E. Liquid fuels from *Mesua ferrea* L. seed oil. *J. Am. Oil. Chem. Soc.* **66**, 223-226 (1989)
27. Oil and Color Chemists Association of Australia, Surface Coatings, Vol. 1 (Chapman & Hall, London, UK, 1981)
28. Indian Standard, Methods of Sampling and Test for Paints, Varnishes and Related Products 101 (Part 5/Sec 2), (1988)

29. Annual Handbook of ASTM Standard, The American Society for Testing Materials, (USA, 1973)
30. Kumari, S.; Mishra, A.K.; Chattopadhyay, D.K.; Raju, K.V.S.N. Synthesis and characterization of hyperbranched polyesters and polyurethane coatings. *J. Polym. Sci., Part A: Polym. Chem.* **45**, 2673-2688 (2007)
31. Rubner, M.F. Synthesis and characterization of polyurethane-diacetylene segmented copolymers. *Macromolecules* **19**, 2114-2128 (1986)
32. Silverstein, R.M.; Webster, F.X. *Spectrometric Identification of Organic Compounds*, 6th edn. (John Wiley & Sons, India, 2007)
33. Mishra, A.K.; Chattopadhyay, D.K.; Sreedhar, B.; Raju, K.V.S.N. FT-IR and XPS studies of polyurethane-urea-imide coatings. *Prog. Org. Coat.* **55**, 231-243 (2006)
34. Kalsi, P.S. *Spectroscopy of Organic Compounds*, 6th edn. (New Age International Publication, New Delhi, 2005)
35. Blackwell, J.; Gardner, K.H. Structure of the hard segments in polyurethane elastomers. *Polymer* **20**, 13-17 (1979)
36. Chen, A.; Yao, C.; Zeng, S.; Yi, C.; Xu, Z. Preparation and properties of hyperbranched polyurethanes via oligomeric A_2+bB_2 approach. *Polym. Bull.* **61**, 363-371 (2008)
37. Szycher, M. *Szycher's Handbook of Polyurethanes* (CRC Press, Boca Ranton, 1999)
38. Cao, Q.; Cai, Y.; Jing, B.; Liu, P. Structure and mechanical properties of thermoplastic polyurethane based on hyperbranched polyesters. *J. Appl. Polym. Sci.* **102**, 5266-5273 (2006)
39. Javni, I.; Petrovic, Z.S.; Guo, A.; Fuller, R. Thermal stability of polyurethanes based on vegetable oils. *J. Appl. Polym. Sci.* **77**, 1723-1734 (2000)

CHAPTER 3

Modification of HBPU by epoxy resin

3.1. Introduction

PU is one of the most versatile polymers and this is further enhanced when it is synthesized from naturally renewable resources like vegetable oils. A lot of advantages associated with the vegetable oils have already been discussed in Chapter 2. Nowadays the vegetable oil based PUs are challenging to the PUs that are exclusively based on petroleum feedstock due to their sustainability, low price and bio-affable nature.^{1,2} However, vegetable oil based PUs bring forth few severe drawbacks such as low alkali resistance in case of polyester based PUs, low hardness, low dimension stability and low thermal stability etc.³⁻⁵ To overcome such shortcoming or to achieve the desired level of properties, PU can be modified by blending, interpenetrating network formation with other polymers etc.⁶ Several reports have been described various ways to eradicate the inadequacy of the vegetable oil based PUs. The improvement of mechanical properties, biodegradability etc. of castor oil based PUs by incorporation of chitosan,⁷ nitrocellulose,⁸ nitrokonjac glucomannan,⁹ soy dreg,¹⁰ poly(ethylene glycol),¹¹ polyricinoleate diol¹² etc. have been found in literature. Lenka and co-workers described the formation of a number of IPN systems with vegetable oil based PUs.¹³ Dutta and Karak reported the improvement of performance characteristics and thermal properties of *Mesua ferrea* L. seed oil based PUs after blending with commercially available resins such as epoxy and melamine formaldehyde.^{14,15} The PU is known to be compatible with a wide variety of polymers such as epoxy, amino, silicone, ketonic etc.¹⁶⁻¹⁸ This is due to the structure of PU that contains relatively polar and aromatic backbone as well as aliphatic side chains with low polarity.

Amongst the other polymers, epoxy resin is one of the best blend components for such PUs because of its ability to mix in any proportion and can cure PU by the crosslinking reactions between hydroxyl/epoxy groups of epoxy and hydroxyl/urethane groups of PU in the presence of a base like poly(amido amine) (hardener for epoxy resin).¹⁹ Epoxy is a thermosetting polymer available commercially for long time.²⁰ It possesses strained and reactive oxirane rings. The bisphenol-A and epichlorohydrin based epoxy resin is the oldest and is still the most widely used one.²¹ This is due to its

characteristic properties such as outstanding adhesion, excellent mechanical properties, alkali resistance, thermal resistance, dimensional stability, good dielectric behavior and low shrinkage during curing.²²⁻²³ However, the poor mechanical properties such as low fracture strength, inferior weathering resistance and brittle behavior restrict the applications of epoxy resins. Thus the right combination of PU with epoxy may results the synergistic effect of the properties such as strength, hardness, impact resistance etc. The epoxy modified linear PU systems are proven to be interesting because of their ease of modification, high flexibility in formulation and improvement of thermostability, mechanical and adhesion properties, weather resistance etc.²⁴ Therefore, it is expected that the epoxy modified HBPU can also result in significant enhancement of various properties. Specially, both PU and epoxy are constantly used as adhesive materials because of the presence of many polar groups, so the combined system may lead to the genesis of a high performance adhesive.

Again the use of hyperbranched structures may facilitate the better compatibility as well as homogenization due the presence of large number of surface functionality and their confined geometry.²⁵ Therefore it may be the right choice to utilize such materials to meet the highly diversified demands of modern technologies.

Again, due to the presence of phenomenal microphase inhomogeneities in PU structure, they are largely used as shape memory polymers in many avant-garde applications such as biomedical, aerospace automobile, smart textile etc.²⁶ These thermo-sensitive polymers can fix the deformation without external load by cooling and recover the original shape on heating[€] above their transition temperature.²⁷ HBPU have some added advantage over the conventional linear analogs.²⁸ So in the present study the shape memory property of epoxy modified HBPU has also been studied. As far as shape memory of epoxy modified vegetable oil based HBPU is concerned, it is the first study to the best of our knowledge.

Therefore in the present chapter the modification of the HBPU by commercial epoxy resin, characterization and properties of the resulted materials are discussed.

3.2. Experimental

3.2.1. Materials

The vegetable oil used in the present study is *Mesua ferrea* L. seeds oil. The isolation and purification of the oil was performed exactly the same ways as described in Chapter 2, section 2.2.1. Monoglyceride of *Mesua ferrea* L. seed oil was prepared by glycerolysis process as described in Chapter 2, section 2.2.2.1.

The *Mesua ferrea* L. seed oil based HBPU with 30% hard segment (NCO/OH = 0.96) was prepared by using the same methods as described in experimental section of Chapter 2, section 2.2.2.2. The required chemicals for HBPU preparation such as PCL, glycerol, TDI, DMF etc. are of same specifications as described in Chapter 2, section 2.2.1. It was observed from Chapter 2 that the HBPU containing 30% hard segment showed the best performance and hence this composition was chosen for further studies and denoted as **HBPU only instead of HBPU30**.

Bisphenol-A based epoxy resin (Araldite LY 250) and poly(amido amine) based hardener (HY 840) were purchased from Hindustan Ciba Geigy Ltd., India and specifications are given in Table 3.1. They were used as received.

Table 3.1: Technical specifications of epoxy resin and hardener

Properties	Araldite LY 250	Hardener HY 840
Viscosity at 25 °C (mPas)	450-650	10,000-25,000
Epoxy equivalent (g/eq)	182-192	-
Epoxy content (eq/kg)	5.2-5.5	-
Amine value (eq/kg)	-	6.6-7.5
Density	1.15	0.98

3.2.2. Instruments and Methods

The FTIR, XRD, SEM and TGA analyses were carried out using same instruments and methods as described in Chapter 2, section 2.2.2. The measurement of specific gravity, impact resistance, scratch hardness, flexibility (bending), mechanical properties and chemical resistance test were performed in the same way as mentioned in Chapter 2, section 2.2.2. The percent of swelling, sol fraction and curing time were evaluated according to the standard methods.¹⁴ DSC analysis was performed by Shimadzu, DSC 60, USA at heating rate of 3 °C /min from -50 to 200 °C under nitrogen flow rate of 30 mL/min. Ultrasonicator (Heishler, 200S, Germany) was used to mix the epoxy resin with HBPU at 45% of amplitude and continuous cycle for 10 min. Rheological behavior of the solution of epoxy modified HBPU [20% solid content (w/v) in DMF] was carried out with the help of Malvern, CVO100, UK with a parallel plate of 20 mm diameter (PP20). The study was done at controlled stress of 10 Pa under the variation of frequency from 1 to 100 s⁻¹ at 25 °C. The gap size was maintained at 150 micron for all the experiments.

The shape recovery of the samples was measured by following the method as described below. The samples were first heated at specified temperature (50, 60 and 70 °C) for 5 min and then they were stretched to twice the length of the original length (l_0).

The stretched length was denoted as l_1 . Immediately the stretched samples were immersed in the ice bath ($\sim 2\text{ }^\circ\text{C}$) for 5 min to fix the deformation and the length was measured as l_2 . The samples were then reheated to the same temperature for the same period of time and the length obtained was denoted as l_3 . The % retention and % recovery were calculated by the following equations (3.1) and (3.2) at different temperatures.

$$\text{Retention (\%)} = (l_2 - l_0) / l_0 \times 100 \quad (3.1)$$

$$\text{Recovery (\%)} = (l_1 - l_3) / l_0 \times 100 \quad (3.2)$$

3.2.2.1. Preparation of the HBPU and Its Modification with Epoxy Resin

Preparation

HBPU with 30% hard segment (NCO/OH = 0.96) was prepared as per the method described in Chapter 2, section 2.2.2.2.

Modification

A solution of prepared HBPU in DMF (25-30% solid content) was mixed with epoxy resin (100% solid content) and poly(amido amine) hardener (50% by weight with respect to the epoxy resin) in different ratios as given in Table 3.2. The systems were

Table 3.2: Composition and curing time of the modified systems at 120 °C

Code*	HBPU (g)	Epoxy resin (g)	Hardener (g)	Touch free time (min at 120 °C)	Drying time (min at 120 °C)
MHBPU5	100	5	2.5	25	60
MHBPU10	100	10	5	20	55
MHBPU20	100	20	10	15	45

*The digits in the code indicate the weight percent of the epoxy resin

thoroughly stirred by mechanical stirrer for about half an hour at room temperature ($\sim 27\text{ }^\circ\text{C}$) followed by ultrasonication for 10 min for proper homogenization of the components. The modified HBPU solutions were casted on different substrates followed by vacuum degassing, curing at specified time, temperature for further testing and analyses.

3.2.2.2. Sample Preparation for Performance Studies

The modified HBPU systems were casted on different substrates for various studies by the same way as mentioned in Chapter 2 section 2.2.2.3. The casted modified HBPU samples were cut by the manual sample cutter with dimension as per the ASTM D 412-51T for mechanical test.

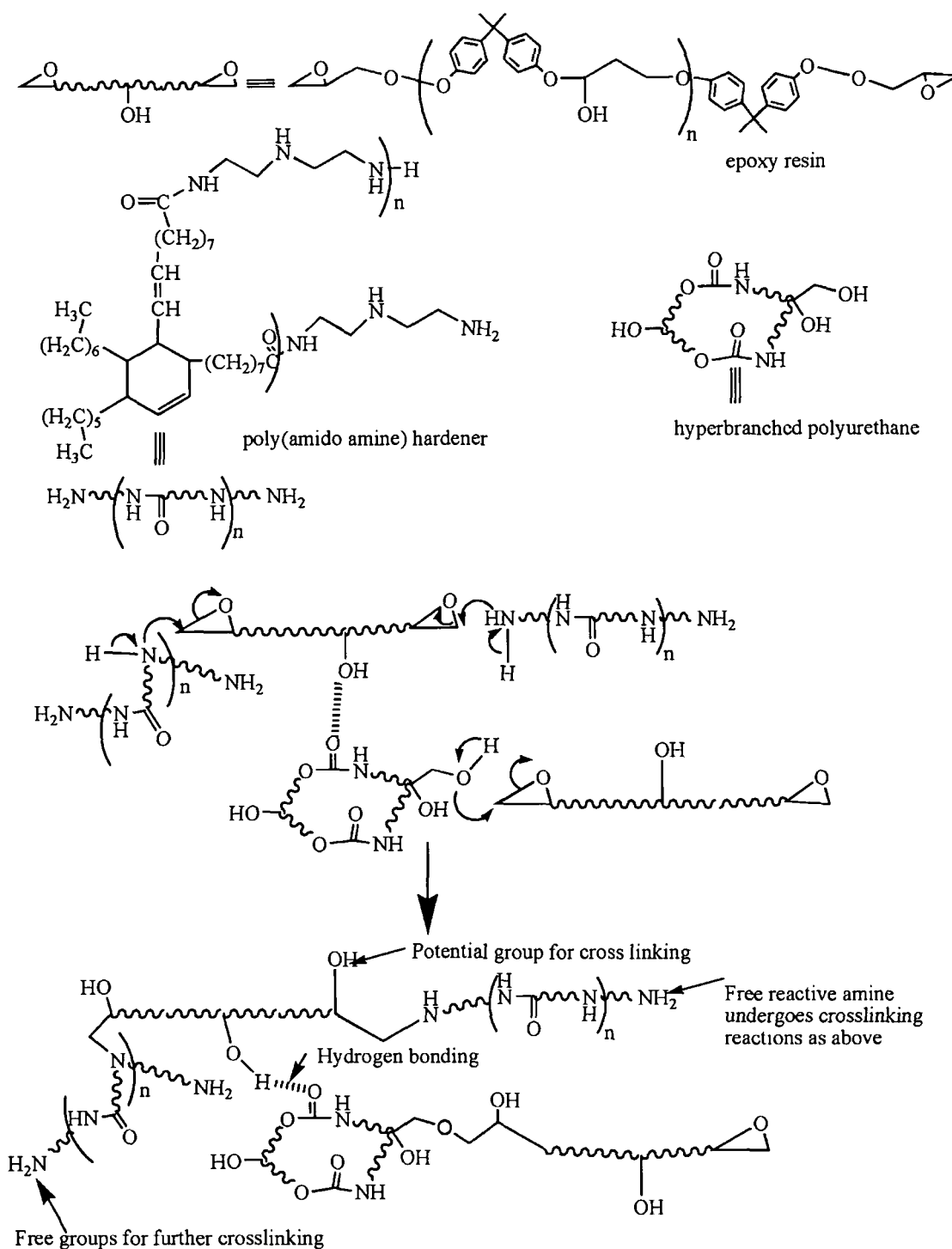
3.3. Results and Discussions

The utilized HBPU in the present investigation have the weight average molecular weight and polydispersity of 5.28×10^4 g/mol and 2.42 respectively as measured by GPC (Chapter 2, Table 2.3). The studied polymer is highly branched and possesses large numbers of functionalities as distinct from the structure shown in Chapter 2, Scheme 2.1. Therefore it is expected that these functional groups may take part in crosslinking reactions during the curing processes with epoxy resin in the presence of poly(amido amine) hardener.

3.3.1. Curing Study

The curing behavior of the modified systems was found to be improved after modification. The touch free time (minimum time required by the system to resist impression on touching its surface by thumb) as well as drying time (determined by indenting the cured film by an indenter) decreased with the increase of amount of epoxy resin and poly(amido amine) hardener at 120 °C (Table 3.2). The proposed crosslinking mechanism as shown in Scheme 3.1 reveals the fact. The surface –OH groups of HBPU were crosslinked by the epoxy groups of epoxy resin in the presence of poly(amido amine) hardener.²⁹ The increase of amount of epoxy resin and hardener resulted the increase of strained oxirane and reactive amino groups. This in turn, increased the rate of crosslinking reaction thereby forming a three dimensional network structure. This result is also supported by the other reports, where the conventional PU is cured by epoxy resins.³⁰ The process was accelerated by the presence of aromatic moiety of the HBPU forming active complexes with the epoxy/amino/urethane groups of the system.³¹

The crosslinking reactions between HBPU and epoxy resin were further supported by FTIR study. The FTIR spectra of epoxy modified HBPU before and after curing were shown in Fig. 3.1. The characteristic band for epoxy ring³² was found at around 908 cm^{-1} for the epoxy modified PUs before curing, whereas the same was absent after curing. The other characteristic bands were also observed in the FTIR spectra (Fig. 3.1). This further supports the crosslinking reactions as proposed in Scheme 3.1. In general free –OH (without H-bonding) and –NH groups show sharp band around 3500 cm^{-1} and $> 3420 \text{ cm}^{-1}$ respectively. But upon H-bond formation, these bands became broad and shifted to lower wavenumber.³⁰ In the present study the broad band in the region $3339\text{-}3407 \text{ cm}^{-1}$ revealed the overlapping of –OH and –NH stretching bands³³ as well as H-bonding between epoxy –OH and –NH groups of



Scheme 3.1: Proposed crosslinking reactions of HBPU with epoxy and hardener

HBPU. The -C=O stretching region also carries information about the intermolecular interactions. The shifting of -C=O absorption band from 1693 to 1620 cm^{-1} in the epoxy modified HBPU with the increase of amount of epoxy was observed in Fig. 3.1. This further proved the increase of interactions with the increase of amount of epoxy content through the formation of H-bonding, polar-polar interactions etc.³⁴

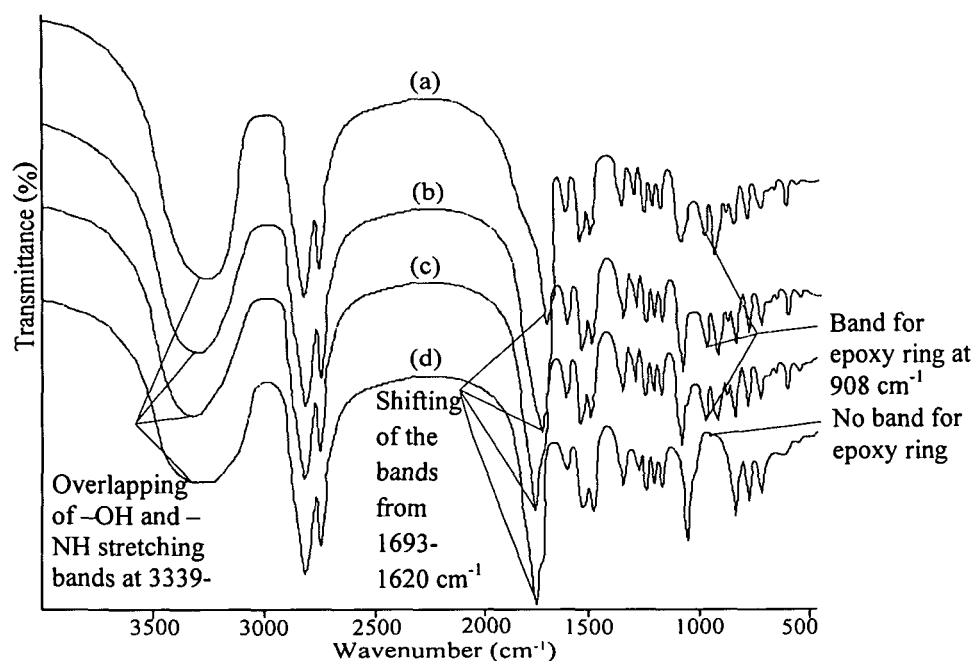


Fig. 3.1: FTIR spectra of (a) MHBPU20, (b) MHBPU10, (c) MHBPU5 before curing and (d) MHBPU10 after curing

3.3.2. Physical Properties

The modified HBPU possess higher density than the unmodified HBPU (Table 3.3). This is because of the compact structure of the cured HBPU. It was also noticed that with the increase of amount of epoxy resin, the density increases as the compactness increases through H-bonding, polar-polar interaction, in addition to crosslinking density. The decrease of percent swelling in the swelling test with the increase of epoxy content further confirmed the greater network formation (Table 3.3). The sol fraction at 60 °C was also calculated in support of swelling test and found in accord with the swelling test results (Table 3.3).

Table 3.3: Physical and mechanical properties of the MHBPU

Property	MHBPU5	MHBPU10	MHBPU20
Tensile strength (MPa)	16.14	22.05	30.20
Elongation at break (%)	550	538	510
Scratch hardness (kg)	2.5	3.1	4.2
Bending test (mm)	< 5	< 5	< 5
Impact test (cm)	57	79	92
Specific gravity	1.15	1.16	1.17
Swelling (at 25°C)	4.83	1.94	1.60
Swelling (at 60°C)	32.12	21.92	12.68
Sol fraction (% , at 60°C)	37.96	27.01	18.04

The XRD analysis proved the presence of crystallinity of the modified HBPU (Fig. 3.2). The two diffraction peaks at $2\theta = 21.2^\circ$ (4.19\AA) and 23.4° (3.81\AA) are due to

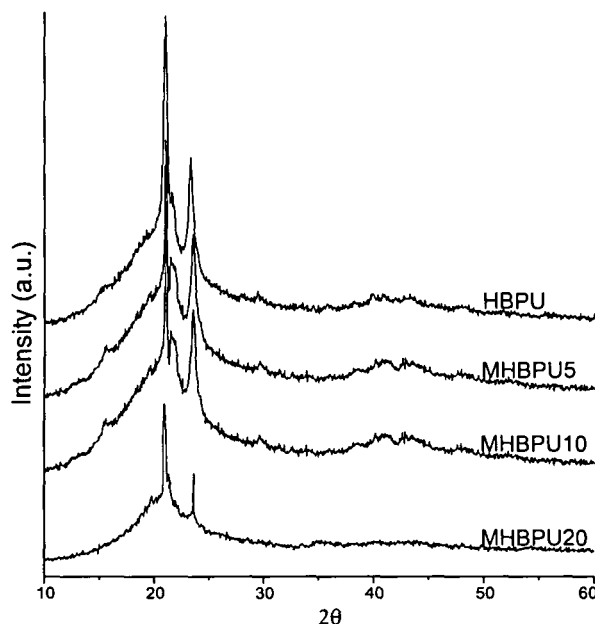


Fig. 3.2: XRD diffractograms of MHBPU

the crystalline PCL moiety in the structure.³⁵ The positions of these two peaks remain unchanged as that of pristine HBPU after modification, though the intensity gradually decreases with the increase of epoxy content. This may be due to the increase of molecular restriction through crosslinking reactions along with the decreased percent of PCL in the matrix.³⁶

3.3.3. Rheological Properties

The frequency dependence of the dynamic viscoelastic properties like G' , G'' and complex viscosity (η^*) were studied for the modified HBPU systems as a function of frequency and time sweep. G' and G'' were found to be increased monotonically with the increase of frequency as the amount of epoxy resin increases [Fig. 3.3 (a, b)]. This is because of the increase of moduli of the matrix after modification. These increments in the lower frequency ($< 10\text{ s}^{-1}$) region were more, especially for the G' values, which may be due to the pseudo-solid like nature of the materials.³⁷ The G'' values were independent for MHBPU5 and MHBPU10 at higher frequencies ($> 10\text{ s}^{-1}$). It was found that these curves can be well fitted to the Bingham equation for oscillation by the Bohlin curve fitting software ($\tau = \tau_0 + \mu\dot{\gamma}^n$ where τ is the shear stress applied to the material, $\dot{\gamma}$ is the shear strain rate, also called the strain gradient, τ_0 is the yield stress and μ is the plastic viscosity). The η^* as a function of frequency is shown in Fig. 3.3 (c). The viscosity values were increased with the increase of epoxy content as it is obvious. With the increase of epoxy content in the system, the interactions increases

and as a result viscosity of modified HBPU increased. It was found that the η^* value decreases with frequency and at the higher frequencies, the values were very low. Thus, shear thinning was observed for the materials.³⁸ The G' was also studied at constant frequency (1 s^{-1}) under controlled stress (50 Pa) as a function of time sweep [Fig. 3.3 (d)]. Slight decrease of the values was noticed, which are not so prominent. Thus it implies that, under the studied conditions the structures of the materials are not changed.

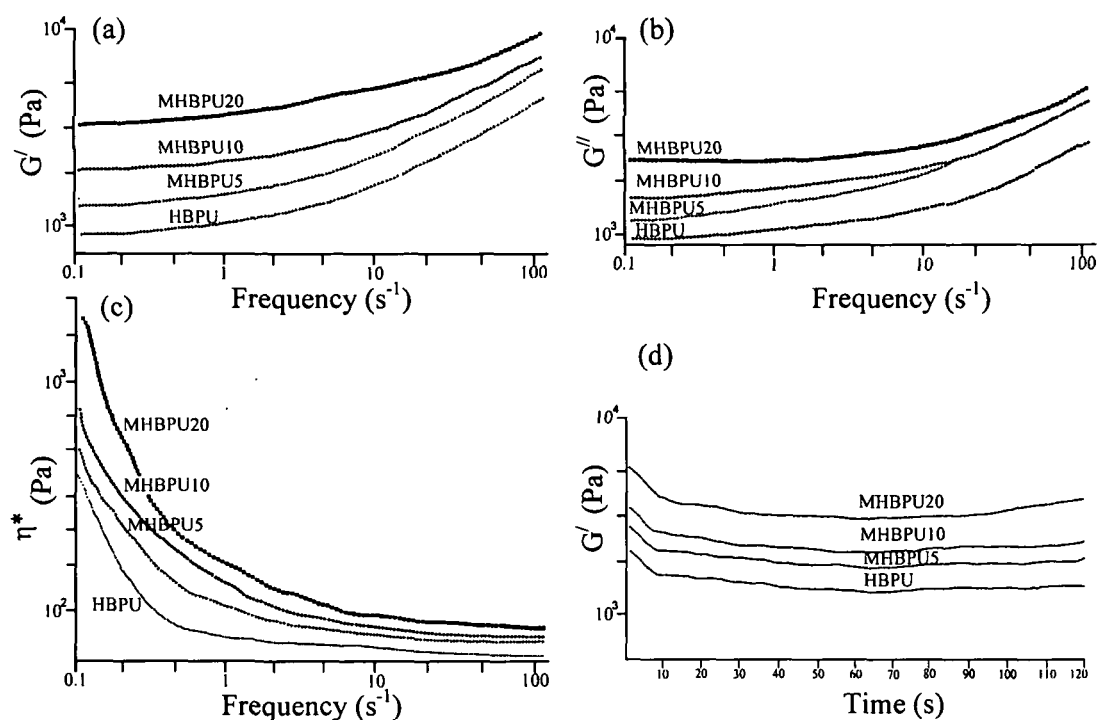


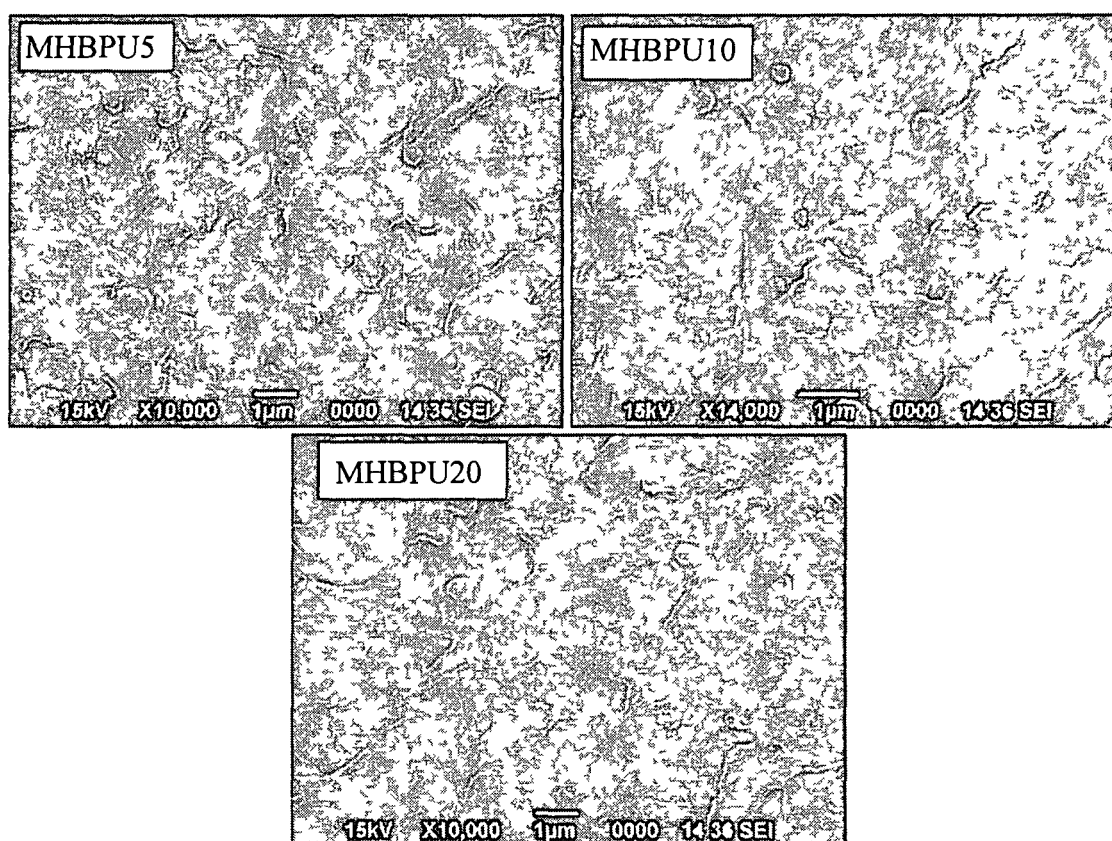
Fig. 3.3: Dependence of (a) G' , (b) G'' , (c) η^ with respect to frequency and (d) variation of G' as a function of time*

3.3.4. Morphological Study

In general PUs have good compatibility with epoxy resins.³⁹ Several factors such as chemical miscibility of the two components, method of mixing, interfacial interaction and crosslinking density etc. affect the morphology of a two-component system at a given composition.⁴⁰

The SEM micrographs of the modified HBPU are shown in Fig. 3.4. Among the SEM pictures, the MHBPU20 shows the best dispersion of epoxy resin in HBPU as no phase separation is observed in this blend. This is because of the good compatibility of aromatic moieties present in the system through polar-polar interaction between π -bonds of aromatic rings and with other polar groups such as hydroxyl, amino, urethane, carbonyl etc. in the polymers.^{29,30} In addition, the confined geometry of HBPU offers

improved compatibilizing ability with other components. It is well reported to form crosslinked product between hydroxyl/urethane groups of PU and epoxy groups of epoxy resin in the presence of amine hardener.²⁹ Thus the amine hardener also plays role as compatibilizing agent along with its normal crosslinking reactions.¹⁴ Further the homogenization is enhanced by the possibility of H-bonding between $-C=O$ of urethane groups of HBPU with $-OH$ of epoxy resin. Therefore, as the amount of epoxy with the hardener system increases in the matrix the interphasic interactions also increase, so the compatibility is improved with the same under the studied conditions



*Fig. 3.4: SEM micrographs of MHBPU*s

3.3.5 Mechanical Properties

The tensile strength of the crosslinked HBPU_s increased significantly with the epoxy content as seen from the Table 3.3. This is because of the fact that as the crosslink density increases and the bridges among the chain molecules also increase, which on the other way round demand for more stress value for their rupture. The increase of strength is also due to good compatibility and various intermolecular interactions as mentioned above. The scratch hardness was also found to be increased with the increase of the epoxy content, which is again caused by the increase of crosslinking density, H-bond formation etc. This is also supported by swelling test (Table 3.3) and FTIR study (Fig 3.1). The modified HBPU_s possess enough flexibility as found by the

bending test and elongation at break values though they had adequate scratch hardness (Table 3.3). All the films can be bent to 5 mm parallel mandrel without any difficulty and on average can be elongated about 500%. The long fatty acid chains of oil, ester and ether linkages of PCL render this high flexibility to the films. The impact resistance of all the films showed excellent result as expected from the tensile strength and flexibility test. The MHBPU20 exhibited the highest impact test, which may be due to the highest strength of the film.

3.3.6. Thermal Properties

A significant enhancement in thermal properties was achieved after modification of the HBPU with epoxy resins. The thermal-gravimetric analysis of HBPU with 30% hard segment content and modified HBPU elucidated the effect of the amount of epoxy loading on thermal stability of the systems (Fig. 3.5). For all the modified HBPU decomposition occurred at a range of 225-600 °C via a two step pattern of degradation. The first step degradation is for the reopening of allophanate and biuret linkages, which may form during the crosslinking reactions, decomposition of the aliphatic hydrocarbon chains of the oil and epoxy resin, as these bonds are quite thermolabile.⁴¹ On the other hand, the second step degradation corresponds to decomposition of the urethane linkages and aromatic moieties of TDI and epoxy resin.²⁹ An increment of the first initial onset decomposition temperature ($T_{1st ON}$), temperature corresponding to maximum rate of weight loss (T_{MAX}) and the second initial onset decomposition temperature ($T_{2nd ON}$) for the modified HBPU were observed (Table 3.4) compared to the pristine HBPU. This is because of the incorporation of epoxy resin that increases the crosslinking density and thereby bridging the polymer backbone together, which results a 'hard material'.¹⁴ Thus the molecular mobility is restricted to a certain extent that results the improvement of thermo-stability of the modified systems.⁴²

Table 3.4: Thermal properties of MHBPU

Code	$T_{1st ON}$ (°C)	T_{MAX} (°C)	$T_{2nd ON}$ (°C)	T_m (°C)	ΔH_m (J/g)
MHBPU5	225	430	574	48	48.6
MHBPU10	238	441	582	49	47.2
MHBPU20	243	456	593	52	45.1

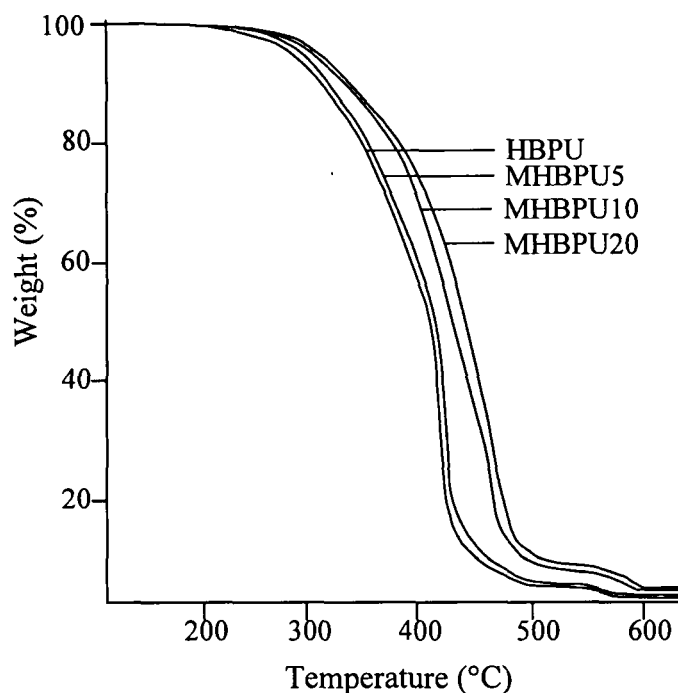


Fig. 3.5: TGA thermograms of MHBPU and HBPU

The melting temperature (T_m) and ΔH_m of the modified HBPU systems are given in Table 3.4. The DSC curves are shown in Fig. 3.6. The T_m was found to be

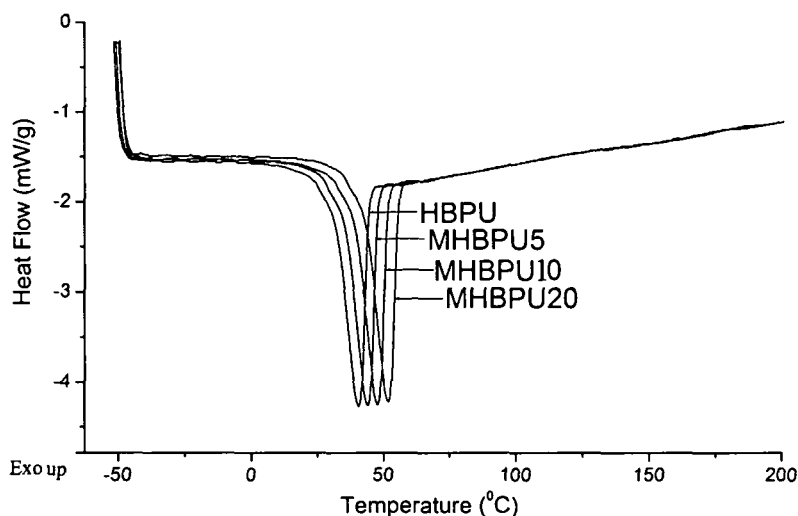


Fig. 3.6: DSC curves of MHBPU and HBPU

increased from 47 °C (T_m of pristine HBPU) to 52 °C with the increase of epoxy content. This may be due to the formation of compact crosslinked structure that is formed through different types of interactions as stated earlier.⁴³ From Table 3.4, it was observed that the values of ΔH_m decreased with the increase of epoxy content (ΔH_m of pristine HBPU was 51.8 J/g). This decrement is due to the diminution in the crystallinity which was also supported by the XRD results.

3.3.7 Shape Memory Study

A demonstrative experiment for the macroscopic shape memory effect of the modified HBPU is shown in the Fig. 3.7. The shape memory properties of crosslinked HBPU were measured at different temperatures and the values are tabulated in Table 3.5. All the samples exhibited very good shape recovery of 90-98%, though the influence of epoxy content was very small. The effect of temperature on the shape memory

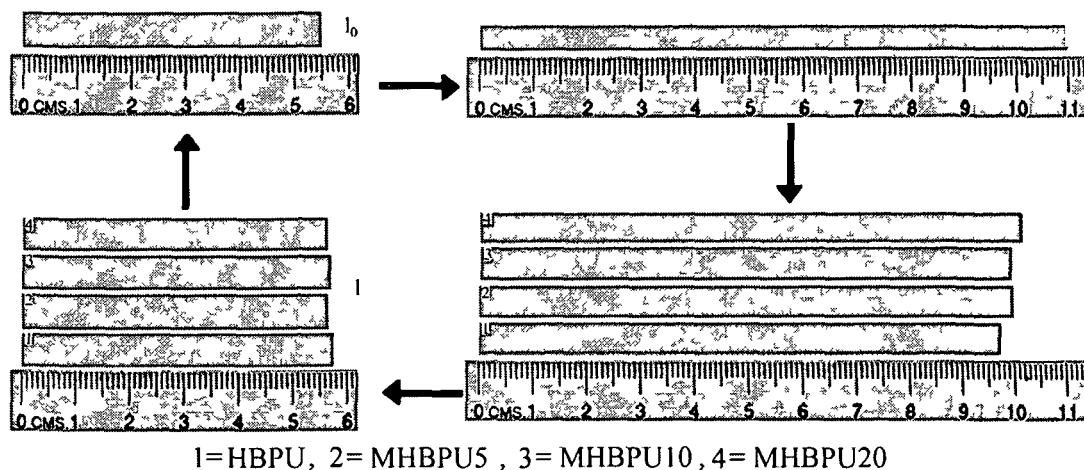


Fig. 3.7: Pictorial diagram of the shape memory behavior of MHBPU

Table 3.5: Shape memory data of MHBPU and HBPU at various temperatures

Code	At 50 °C		At 60 °C		At 70 °C	
	% Retention	% Recovery	% Retention	% Recovery	% Retention	% Recovery
HBPU	69	89	76	92	80	96
MHBPU5	74	90	81	95	85	97
MHBPU10	75	92	82	96	86	98
MHBPU20	77	93	84	96	87	98

property was also small, though the value increases slightly with temperature. The excellent shape recovery of the polymers may be ascribed to the increased stored energy of system due to an incorporation and uniform distribution of crosslinking in the hyperbranched polymer matrix.^{28,44} The small increase of shape recovery with the increase of epoxy content is due to increase of crosslinking density or in other word increase of stored elastic strain energy by crosslinking.⁴⁵ Thus while reheating the sample, it can obtain higher recovery stress due to the release of stored elastic strain.⁴⁶

3.3.8 Chemical Resistance Test

The chemical resistance test of the cured films was performed in different chemical environments for 10 days and subsequently the changes in the mass were determined. All the films showed excellent chemical resistance in all the test media. The good alkali

resistance of the cured films even in the presence of alkali hydrolysable ester linkages may be due to the formation of alkali stable crosslinking in between the chain molecules. This is also due the more compact structure of modified HBPU than unmodified one after crosslinking.⁴⁷ The excellent chemical resistance of the films may be due to the presence of intra- and inter-molecular secondary interactions, mutual crosslinking, presence of aromatic rings etc.

3.4. Conclusions

The present study reveals the successful modification of the HBPU by the commercially available epoxy resin with poly(amido amine) hardener. The notable enhancements in the tensile strength, scratch hardness, impact resistance and thermal stability were observed for modified HBPU from the pristine polymer. The amount of epoxy resin has prominent role in tuning many properties of the modified HBPU. The composition (ratio of HBPU to epoxy resin) dependence rheological behavior was observed for the materials. The excellent shape recovery and performance characteristics of the modified HBPU indicate the possibility of utilization of these materials as thermoresponsive smart polymers for different advanced applications.

References

1. Zlatanic, A.; Petrovic, Z.S.; Dusek, K. Structure and properties of triolein-based polyurethane networks. *Biomacromolecules* **3**, 1048-1056 (2002)
2. Lu, Y.; Tighzert, L.; Berzin, F.; Sebastien, R. Innovative plasticized starch films modified with waterborne polyurethane from renewable resources. *Carbohydr. Polym.* **61**, 174-182 (2005)
3. Petrovic, Z.S. Polyurethanes from vegetable oils. *Polym. Rev.* **48**, 109-155 (2008)
4. Lu, J.; Wool, R.P. Additive toughening effects on new bio-based thermosetting resins from plant oils. *Compos. Sci. Technol.* **68**, 1025-1033 (2008)
5. Dutta, S.; Karak, N. Effect of the NCO/OH ratio on the properties of *Mesua Ferrea* L. seed oil-modified polyurethane resins. *Polym. Int.* **55**, 49-56 (2006)
6. Jia, Q.M.; Zheng, M.; Chen, H.X.; Shen, R.J. Synthesis and characterization of polyurethane/epoxy interpenetrating network nanocomposites with organoclays. *Polym. Bull.* **54**, 65-73 (2005)
7. Gong, P.; Zhang, L. Properties and interfacial bonding of regenerated cellulose films coated with polyurethane-chitosan IPN coating. *J. Appl. Polym. Sci.* **68**, 1313-1319 (1998)

8. Zhang, L.; Zhou, Q.I. Effects of molecular weight of nitrocellulose on structure and properties of polyurethane/nitrocellulose IPNs. *J. Polym. Sci., Part B: Polym. Phys.* **37**, 1623-1631 (1999)
9. Gao, S.; Zhang, L. Semi-interpenetrating polymer networks from castor oil-based polyurethane and nitrokonjac glucomannan. *J. Appl. Polym. Sci.* **81**, 2076-2083 (2001)
10. Chen, Y.; Zhang, L.; Deng, R.; Cui, Y. A new network composite material based on soy dreg modified with polyurethane prepolymer. *Macromol. Mater. Eng.* **292**, 484-494 (2007)
11. Yeganeh, H.; Hojati-Talemi, P. Preparation and properties of novel biodegradable polyurethane networks based on castor oil and poly(ethylene glycol). *Polym. Degrad. Stab.* **92**, 480-489 (2007)
12. Xu, Y.; Petrovic, Z.S.; Das, S.; Wilkes, G.H. Morphology and properties of thermoplastic polyurethanes with dangling chains in ricinoleate-based soft segments. *Polymer* **49**, 4248-4258 (2008)
13. Nayak, R.R.; Ray, G.; Guru, B.; Lenka, S. Comparative studies of interpenetrating polymer networks derived from soybean oil-based polyurethane and cardanol m-aminophenol dye. *Polym.-Plast. Technol.* **43**, 261-272 (2004)
14. Dutta, S.; Karak, N. Blends of *Mesua ferrea* L. seed oil based polyurethane with epoxy resin. *Pigment Resin. Technol.* **36**, 74-82 (2007)
15. Dutta, S.; Karak, N. *Mesua ferrea* L. seed oil based polyurethane and melamine formaldehyde blends. *Euras. Chem. Tech. J.* **7**, 251-260 (2005)
16. Ong, S. et al. Polyurethane-modified epoxy resin: Solventless preparation and properties. *J. Appl. Polym. Sci.* **111**, 3094-3103 (2009)
17. Shi, Y.; Wu, Y.; Zhu, Z. Modification of aqueous acrylic-polyurethane via epoxy resin post crosslinking. *J. Appl. Polym. Sci.* **88**, 470-475 (2003)
18. Chen, S.; Tian, Y.; Chen, L.; Hu, T. Epoxy resin/polyurethane hybrid networks synthesized by frontal polymerization. *Chem. Mater.* **18**, 2159-2163 (2006)
19. Han, J.L.; Tseng, S.M.; Mai, J.H.; Hsieh, K.H. Polyurethane-crosslinked epoxy resins. II. Compatibility and morphology. *Macromol. Mater. Eng.* **184**, 89-97 (1991)
20. Swaraj, P. *Surface Coatings: Science and Technology*, 2nd edn. (Wiley, West Sussex, England, 1997)

21. Harani, H.; Fellahi, S.; Bakar, M. Toughening of epoxy resin using synthesized polyurethane prepolymer based on hydroxyl-terminated polyesters. *J. Appl. Polym. Sci.* **70**, 2603-2618 (1998)
22. Mahesh, K.P.; Alagar, M.; Kumar, S.A. Mechanical, thermal and morphological behavior of bismaleimide modified polyurethane-epoxy IPN matrices. *Polym. Adv. Technol.* **14**, 137-146 (2003)
23. Kumar, T.; Sivasankar, B. Poly(ether urethane) flexible cyanate ester resins: Synthesis, characterization and performance in commercial epoxy and polyurethane applications. *J. Appl. Polym. Sci.* **107**, 193-202 (2008)
24. Frisch, H.L.; Frisch, K.C. Polyurethane-epoxy interpenetrating polymer networks - barrier and surface properties. *Prog. Org. Coat.* **7**, 105-111 (1979)
25. Karak, N.; Maiti, S. *Dendrimers and Hyperbranched Polymers—Synthesis to Applications* (MD publication Pvt. Ltd., New Delhi, 2008)
26. Sokolowski, W.; Metcalfe, A.; Hayashi, S.; Yahia, L.H.; Raymond, J. Medical applications of shape memory polymers. *Biomed. Mater.* **2**, S23-S27 (2007)
27. Mather, P.T.; Luo, X. I.; Rousseau, A. Shape memory polymer research. *Annu. Rev. Mater. Res.* **39**, 445-471 (2009)
28. Rana, S.; Karak, N.; Cho, J.W.; Kim, Y.H. Enhanced dispersion of carbon nanotubes in hyperbranched polyurethane and properties of nanocomposites. *Nanotechnol.* **19**, 495707(pp8) (2008)
29. Hepburn, C. *Polyurethane Elastomers* (Elsevier Applied Science, London and New York, 1992)
30. Brydson, J.A. *Plastics Materials* (Butterworths Heinemann, London, 1982)
31. Han, J.L.; Hsieh, K.H.; Chiu, W.Y.; Chen, L.W. Effect of urethanes on base-catalyzed epoxy reaction. *J. Polym. Res.* **2**, 115-120 (1995)
32. Kalsi, P.S. *Spectroscopy of Organic Compounds*, 6th edn. (New Age International Publication, New Delhi, 2005)
33. Yi, Y.; Ye, F.; Huang, C.; Guan, J. Study on synthesis of polyurethane-epoxy composite emulsion. *J. Appl. Polym. Sci.* **115**, 451-459 (2010)
34. Ratna, D.; Banthia, A.K. Toughened epoxy adhesive modified with acrylate based liquid rubber. *Polym. Int.* **49**, 281-287 (2000)
35. Karak, N.; Rana, S.; Cho, J.W. Synthesis and characterization of castor-oil-modified hyperbranched polyurethanes. *J. Appl. Polym. Sci.* **112**, 736-743 (2009)
36. Han, C. Effect of peroxide crosslinking on thermal and mechanical properties of poly(ϵ -caprolactone). *Polym. Int.* **56**, 593-600 (2007)

37. James, M.I.; Hunt, B.J. *Polymer Characterization* (Blackie Academic & Professional, London, 1993)
38. Abraham, T.N.; Ratna, D.; Siengchin, S.; Kocsis, J.K. Rheological and thermal properties of poly(ethylene oxide)/multiwall carbon nanotube composites. *J. Appl. Polym. Sci.* **110**, 2094-2101 (2008)
39. Wang, H.H.; Chen, J.C. Modification and compatibility of epoxy resin with hydroxyl-terminated or amine-terminated polyurethanes. *Polym. Eng. Sci.* **35**, 1468-1475 (1995)
40. Xu, G.; Shi, W.F.; Gong, M.; Yu, F.; Feng, J.P. Photopolymerization and toughening performance in polypropylene of hyperbranched polyurethane acrylate. *Eur. Polym. J.* **40**, 483-491 (2004)
41. Szycher, M. *Szycher's Handbook of Polyurethanes* (CRC Press, Boca Raton, 1999)
42. Cascaval, C.N.; Rosu, D.; Rosu, L.; Ciobanu, C. Thermal degradation of semi-interpenetrating polymer networks based on polyurethane and epoxy maleate of bisphenol-A. *Polym. Test.* **22**, 45-49 (2003)
43. Nunez, E. et al. Crystal structure, melting behaviour and equilibrium melting point of star polyesters with crystallisable poly(ϵ -caprolactone) arms. *Polymer* **45**, 5251-5263 (2004)
44. Chun, B.C.; Cho, T.K.; Chung, Y.C. Blocking of soft segments with different chain lengths and its impact on the shape memory property of polyurethane copolymer. *J. Appl. Polym. Sci.* **103**, 1435-1441 (2007)
45. Petrovic, Z.S.; Ferguson, J. Polyurethane elastomers. *Prog. Polym. Sci.* **16**, 695-836 (1991)
46. Ni, Q.Q.; Zhang, C.S.; Fu, Y.; Dai, G.; Kimura, T. Shape memory effect and mechanical properties of carbon nanotube/shape memory polymer nanocomposites. *Compos. Struct.* **81**, 176-184 (2007)
47. Xu, G.; Shi, W.F.; Gong, M.; Yu, F.; Feng, J.P. Photopolymerization and toughening performance in polypropylene of hyperbranched polyurethane acrylate. *Eur. Polym. J.* **40**, 483-491 (2004)

CHAPTER 4

MHBPU/clay nanocomposites prepared by *ex-situ* technique

4.1. Introduction

From Chapter 3, it is cleared that the epoxy modified *Mesua ferrea* L. seed oil based HBPU showed improved properties, even though the improvement was not up to the desired levels for many advanced applications. There are common practices to remove these intricacies through the formation of conventional filled or composite systems. But in such cases a large amount of reinforcing agents are necessary to be incorporated to obtain acceptable range of mechanical properties, which may cause adverse effect in many other properties of the pristine polymers. In this context, the nanotechnology brings about a revolutionary era in material science. Nanocomposite is one of the avant-garde genres of the composite materials, which becomes multidisciplinary in contemporary times and is challenging to the extreme.¹ In this domain, the polymer/clay nanocomposites have been reported to be one of the best avenues to enhance the performance characteristics of the pristine polymers.²⁻⁷ The high aspect ratio, stiffness, in-plane strength and at the same time ease of dispersion of the nanoclay make it a choice as nanofillers for large numbers of polymer nanocomposite researches. The main incentive for the preparation of an exfoliated polymer nanocomposite is directed by the dramatic improvement of wide range of properties of the pristine polymers even at very low loading of organo modified nanoclay (≤ 5 weight%).⁸ This tremendous improvement is due to the significant change in size and shape of microphase domain of the polymeric structure that is occurred after incorporation of this nano-sized filler.⁹ The nanocomposites meet the desired properties without affecting the light weight and transparent characteristics of pristine polymers, unlike the conventional filled or composite systems. The efficacy of polymer nanocomposites is a direct scale of degree of dispersion of the nanofillers in the polymer matrix.¹⁰ The use of ultrasound may also result the better dispersion and homogenization of nanofillers in the polymer matrices.¹¹ Therefore the use of sonication in *ex-situ* technique may be a convenient and simple way to obtain suitable nanocomposites.¹²

Again among the various polymer matrices exploited, PU based nanocomposites have covered a lot of research interests.¹³⁻¹⁶ Further, the structural versatility of the PU can be diversified by synthesizing from bio-origins as stated in the previous chapters. The performance characteristics of the PU can also be enhanced to a significant extent by modifying with commercially available epoxy resins and poly(amido amine) as described in the Chapter 3. At the same time the structural confinement and the large number of surface functionality of the hyperbranched polymer may provide more site of interactions and better stabilization to the nano reinforcing agent than the conventional polymers.^{17,18} It is thereby expected that epoxy-cured vegetable oil based HBPU can bring about significant improvements in many desired properties coalescing the advantages of nanocomposites, structural beauty of hyperbranched polymers and environmentally benign vegetable oil based products by forming HBPU nanocomposites.

On the other hand, the rheological study of polymer nanocomposites provides the structural information about the materials, as it is highly susceptible to the dispersion state of nanofillers in the matrix and extent of interactions between filler and polymer.¹⁹ Furthermore the rheological properties help to decide the processing conditions of such systems. The rheological properties of polymer/clay nanocomposite melt are dependent on the molar mass, polydispersity index, amount of clay and their morphology.²⁰ Specially, the G' and G'' have attracted a remarkable attention for the close relation to the structural state of the nanocomposites.²¹ In so far, a plethora of reports described the rheological behavior of nanocomposites. But the appropriate study on the vegetable oil based clay nanocomposites is really scanty.

Thus in this chapter, the preparation, characterization and performance characteristics such as adhesive strength, physical, rheological, mechanical and thermal properties of *Mesua ferrea* L. seed oil based epoxy modified HBPU/clay nanocomposite prepared by *ex-situ* technique are discussed.

4.2. Experimental

4.2.1. Materials

The *Mesua ferrea* L. seed oil based HBPU was prepared by using the same methods as described in experimental section of Chapter 2, sections 2.2.2.2. The necessary chemicals and solvents such as PCL, glycerol, TDI, DMF, epoxy resin, hardener etc. are of same specifications and purified same ways as described in Chapter 2, section 2.2.1. and Chapter 3, section 3.2.1. Octadecylamine modified (25-30 weight%)

montmorillonite clay (OMMT), Nanomer[®] 1.30E was purchased from Sigma Aldrich, Germany and used without further purification. The plywood, polypropylene and aluminium rolled sheets for adhesion study were obtained from the local market.

4.2.2. Instruments and Methods

The FTIR, XRD, SEM, DSC and TGA analyses were carried out using the same instruments under the same conditions as mentioned in Chapter 3, section 3.2.2. The mechanical properties were tested by the same methods as stated in Chapter 2, section 2.2.2. The measurement of impact resistance, hardness and flexibility (bending) were determined according to the standard methods as mentioned earlier (Chapter 2, section 2.2.2.). Ultrasonicator of the same specification as mentioned in Chapter 3, section 3.2.2. was used at various amplitudes and continuous cycle for different time period. Thickness and distribution of the OMMT were studied using JEOL, JEM 2100, Japan transmission electron microscopy (TEM) at operating voltage of 200 kV.

The adhesive strength of the cured thin films was measured by lap-shear test as per the standard ASTM D3165-95 using plywood, aluminium and polypropylene sheets as the substrates. The plywood substrates were pre-treated by the same way as described in Chapter 2, section 2.2.2.3. The clean aluminium sheets were treated with hydrochloric acid (5% w/v) and then washed with distilled water and dried. The polypropylene sheets were treated with HNO₃ acid (6% w/v).

The rheological properties were studied with the help of the rheometer of same specification as mentioned in Chapter 3. All the experiments were performed at 120 °C using a parallel plate of 20 mm diameter with a gap of 150 micron. In the oscillatory shear mode the tests were carried out from 1-100 s⁻¹ under controlled stress value of 10 Pa. All the samples were placed at the preheated plate for 3 min prior to the measurements.

4.2.2.1. Preparation of HBPU and Its Modification by Epoxy Resin

The *Mesua ferrea* L. seed oil based HBPU was prepared following the same procedure as mentioned in Chapter 2, section 2.2.2.2. The modification of the prepared HBPU was done by the method described in Chapter 3, section 3.2.2.1. It was observed from the same chapter that the MHBPU20 showed the best performance characteristics amongst the various compositions and therefore this composition was chosen for further studies and **renamed as MHBPU only.**

4.2.2.2. *Preparation of Nanocomposites*

Requisite amounts of the OMMT (1, 2.5 and 5 weight%) were dispersed in 1-5 mL of DMF by magnetic stirring followed by ultrasonication for 5 min. It was then mixed with the epoxy/HBPU mixture with the help of mechanical stirrer for 2 h. Further the disruption as well as dispersion of the clay was assisted by ultrasonication for 0.5 h at amplitude of 65% and half cycle for each case. The films were obtained by solution casting, followed by vacuum degassing and curing at 120 °C for 45 min. The cured films were denoted as MHPUNCE1, MHPUNCE2.5 and MHPUNCE5 corresponding to the OMMT content of 1, 2.5 and 5 weight% respectively.

4.2.2.3. *Sample Preparation for Performance Studies*

The prepared nanocomposites were casted on different substrates for different studies by the same way as mentioned in Chapter 3 (section 3.2.2.2.). The cured casted nanocomposite samples were cut by the manual sample cutter with dimension as per the ASTM D 412-51T for mechanical test.

4.3. **Results and Discussions**

4.3.1. *Formation of Nanocomposites*

The performance characteristics of MHBPU are expected to be enhanced by formation of nanocomposites. MHBPU was used as the matrix for the nanocomposites as clay can interact strongly with this reactive matrix. Use of ultrasonication along with vigorous mechanical agitation enhances the dispersion and delamination of the clay layers in the polymer matrix.

4.3.2. *Characterization*

The Fig. 4.1 depicts the FTIR spectra of the cured MHBPU and its clay nanocomposite (MHPUNCE1). Interestingly in both systems the characteristic bands for the distinctive functional groups were observed (Fig. 4.1). As there was no noticeable change in band position, so it was expected that the affect of addition of OMMT on the structure of the polymer matrix was not significant.^{22,23} However, sharpening of the –NH vibration band was noticed with the addition of OMMT. This sharpening is due to the restricted interaction of the hard and soft segments imposed by the clay layers. Gorrasi et al.²⁴ explained such type of behaviors in the presence of clay layers in a similar matrix. The clay layers reduce the mobility of the hard segment than the soft segment resulting in reduction of H-bonding in the interfacial area. This further convinces to say that most of the –OH groups of the clay has not taken part in crosslinking reaction.²⁵

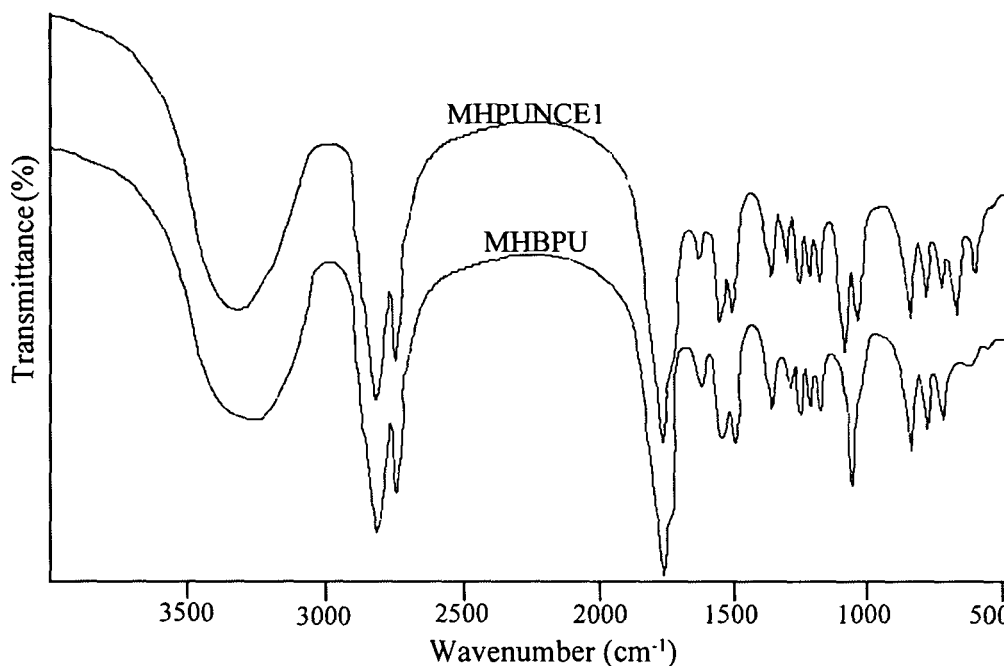


Fig. 4.1: FTIR spectra of MHBPU and MHPUNCE1

The H-bonding extensively influence the band position of urethane carbonyl and thus this region is the most important area for determination of the extent of H-bonding. The -C=O stretching vibration band of MHBPU appeared at 1742 cm^{-1} and shifted to 1718 cm^{-1} after nanocomposite formation (Fig. 4.1). This shifting predicts the formation of greater H-bonding of the clay with the matrix.²² However, in the clay nanocomposites the characteristic absorption bands at 522 and 1033 cm^{-1} corresponding to the Al-O stretching vibration and Si-O-Si stretching vibration of the OMMT were also observed.²⁶ In addition to the above, the bending vibration of -NH at 1490 cm^{-1} decreases in intensity due to interaction of -C=O group of the components and involvement in crosslinking reaction. Further, with the increase of clay loading, the reduction of molecular mobility of -NH group was occurred by the rigid clay layers.

XRD is a powerful tool to investigate the degree of dispersion and delamination of clay layers in polymer matrix. In general, the intercalated layers show intense peak in the range of 1° - 10° (2θ value) whereas exfoliated system does not show distinct peak in that range for their loss of structural integrity. The XRD diffraction patterns of the layered OMMT and all the nanocomposites are shown in Fig. 4.2. The interlayer spacing (d) was calculated on the basis of Bragg scattering equation (4.1) given as,

$$2d\sin\theta = n\lambda \quad (4.1)$$

where, λ is the wavelength (0.154 nm) of the X-ray radiation used in the diffraction experiment of the present study, d is the spacing between the diffractive lattice plane

also known as the basal spacing, n is the order of plane which is 1 in the present case and θ is the measured half diffraction angle or glancing angle. The d -spacing of the

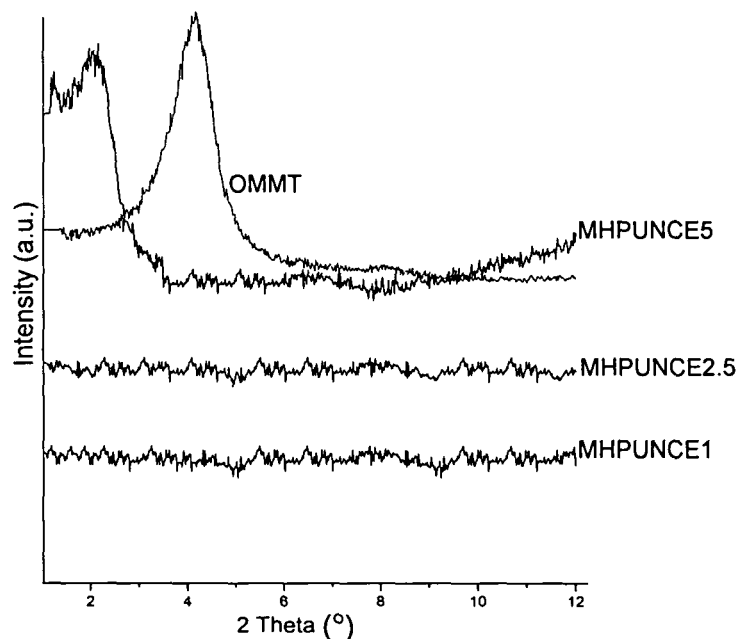


Fig. 4.2: WAXD of the nanocomposites and OMMT

OMMT was found to be 2.36 nm which increases to 4.95 nm for MHPUNCE5. This intercalation indicates the insertion of the HBPU chains in the gallery spacing of the OMMT and thereby forming an intercalated nanocomposite. On the other hand, exfoliated nanocomposites may form in the case of MHPUNCE1 and MHPUNCE2.5, as no diffraction peaks were observed in the 0-6° region (Fig. 4.2). At the same time, it is worth to note that the disappearance of the characteristic peak of OMMT is not due to the limitation of the instrument as the concentration of clay in the matrix is within the range of detection and also there is no heavy element present in the system.

Further SEM was employed to verify the distribution of the OMMT in the matrix. The SEM pictures of the fracture surfaces of the cured samples are shown in Fig. 4.3. The OMMT was appeared as the bright lines in the SEM pictures. The clay layers were dispersed homogeneously in the MHBPU matrix as revealed from the SEM micrographs. Again for confirmation of the distribution of OMMT in the matrix TEM analysis was performed for the nanocomposites (Fig. 4.4). The well dispersion of OMMT in polymer matrix as observed from the Fig. 4.4 is due to the combined actions of mechanical shearing and diffusion processes exerted by mechanical stirring and sonication.

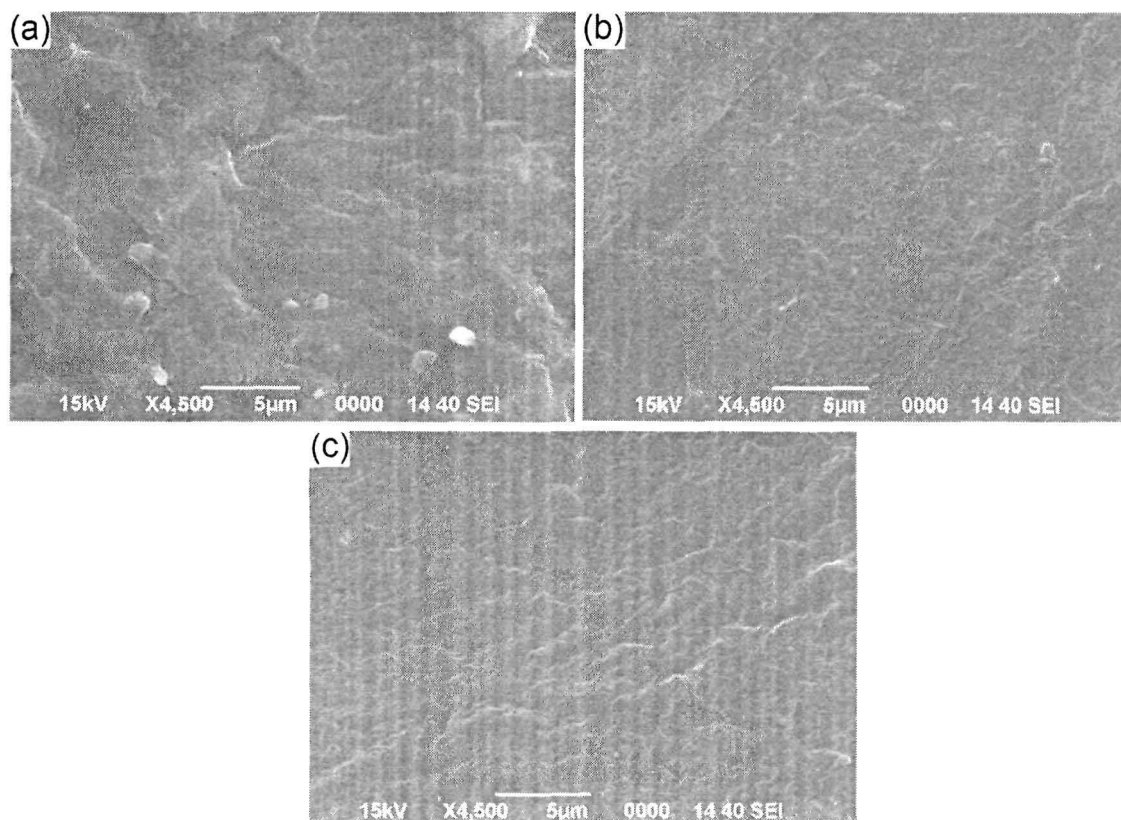


Fig. 4.3: SEM micrographs of (a) MHPUNCE1, (b) MHPUNCE2.5 and (c) MHPUNCE5

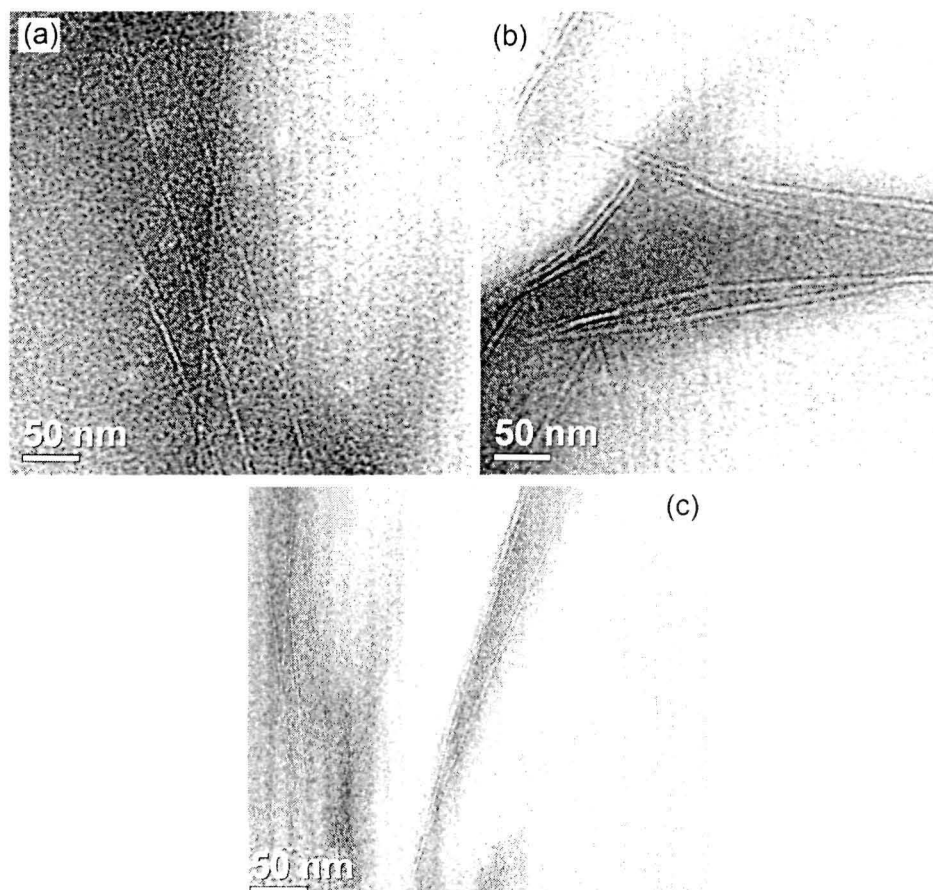


Fig. 4.4: TEM images of (a) MHPUNCE1, (b) MHPUNCE2.5 and (c) MHPUNCE5

4.3.3. Physical Properties

The specific gravity of the polymer nanocomposites are shown in Table 4.1. The density measurement revealed the retention of light weight characteristic of the prepared nanocomposites. The densities of all the nanocomposites approximately remained the same compared with the MHBPU. This is due to the addition of very little amount of clay (1-5 weight%), which may not influence the mass of the nanocomposites with respect to MHBPU.

4.3.4. Rheological Properties

The shear viscosity of the nanocomposites as a function of time at 120 °C under the shear rate of 50 s⁻¹ is shown in Fig. 4.5.

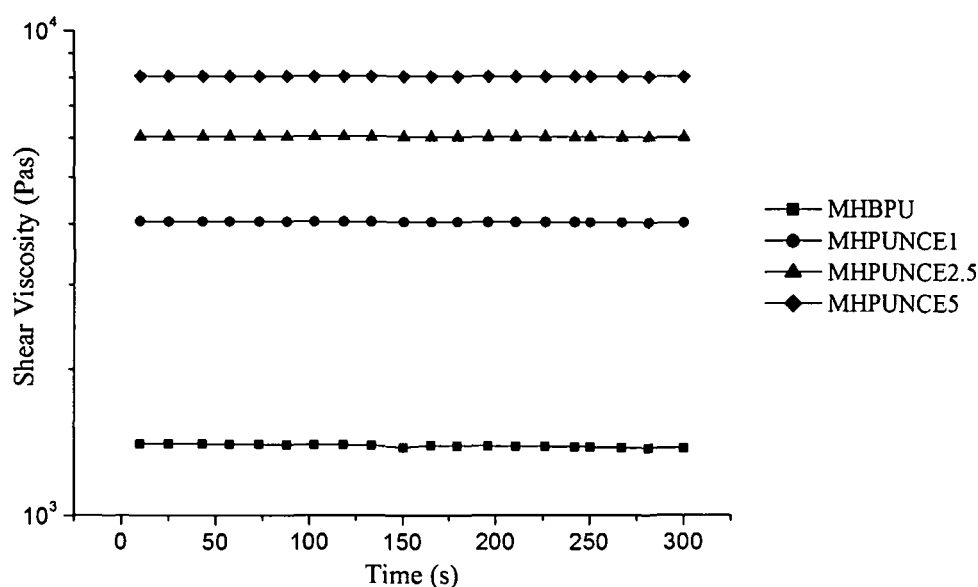


Fig. 4.5: Shear viscosity as a function of time

The shear viscosity showed Newtonian behavior with respect to time over a broad range. A substantial increase in the shear viscosity compared to the pristine MHBPU was observed. Also the viscosity increases with the increase of amount of clay loading in the matrix. This increment of viscosity is the result of interactions between polar groups of clay with polar hydroxyl, epoxy, urethane, ether and other polar groups of the matrix.²⁷ Xie et al.²⁸ described the ‘ball bearing’ effect of the spherical nanoparticles that resulted reduction in shear viscosity of the composite system. Here, the contrary result was found because the shape of the clay is not spherical and the exfoliated clay layers tightly bind the polymer segments through tail, loop and bridge interactions (Scheme 4.1). Thus viscosity was increased instead of decreased. The increase of clay concentration further increases these interactions and hence the viscosity. Dazhu et al. proved this fact experimentally for polystyrene/organo-MMT

nanocomposites varying the concentration of nanoclay from 0 to 10 phr.²⁹ The same was supported by Hyun et al.²¹ through the theoretical calculation, which clearly shown the increase of viscosity with the increase of clay concentration.

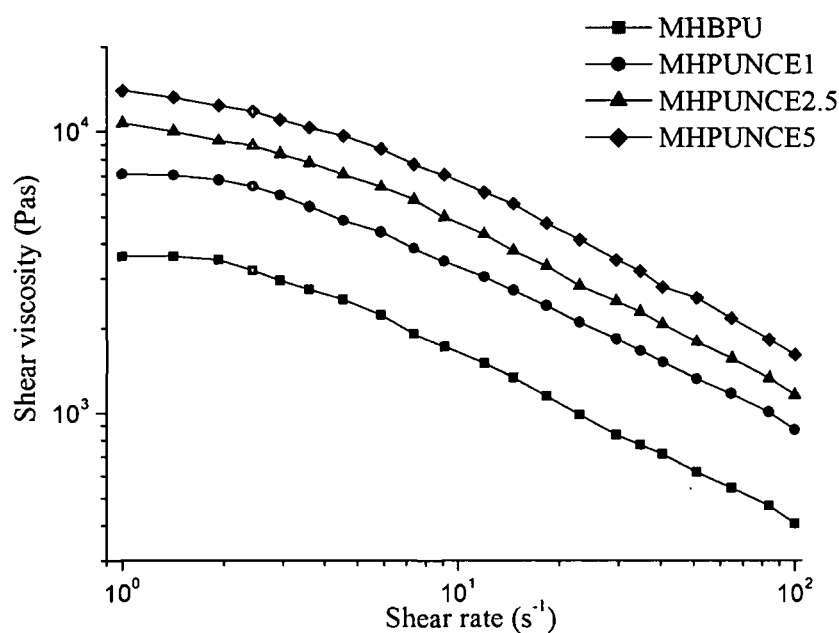


Fig. 4.6: Shear viscosity as a function of shear rate

The shear viscosity as a function of shear rate from 1-100 s⁻¹ was done at 120 °C as shown in Fig. 4.6. The flow and relaxation processes greatly influence the orientation of clay layers and the entanglement of the polymer chains, thereby the structure of the polymer matrix can be dislodged in the presence of clay layers.^{30,31} At low shear rate, MHPUNCE1 nanocomposite and the pristine MHBPU showed high shear viscosity and a Newtonian behavior. These shear values began to decrease at high shear rates and thus shear thinning behavior can be observed in that region (Fig. 4.6). It was noticeable that with the increase of clay content in the matrix (from 2.5 weight%), the Newtonian region disappeared and only shear thinning was occurred. This can be explained in terms of the increased particle-particle interactions that caused a physical network of the clay layers. The rheological percolation can account for such behavior. Further, the shear viscosity decreased to a much lower value at relatively high shear rate and comparable with the MHBPU system.^{32,33} A similar trend was reported by Krishnamoorti et al. for intercalated polystyrene-polyisoprene block copolymer/MMT nanocomposites.³¹ At higher shear rates they found more decrease of shear viscosity value with the increase of clay loading and the values were almost identical to the unfilled polymer. It is thought that the clay orientation at different shear rates plays important role for such behavior. With the increase of shear rates the intercalated/exfoliated clay layers are preferentially aligned parallel to the flow field.³⁴

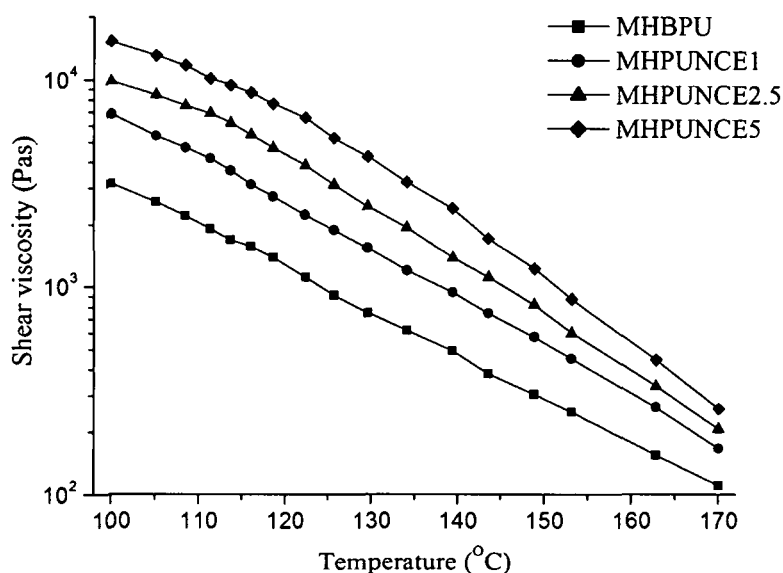


Fig. 4.7: Temperature dependence of shear viscosity

The temperature dependence of shear viscosity is elucidated in Fig. 4.7 for the nanocomposites and MHBPU. The study of temperature dependence of viscosity is important as it provides the basis for polymer flow processes in relation to the nature and composition of the materials. The exact processing conditions and the quality of the end product are decided from the temperature sensitivity of the shear viscosity of the materials. From Fig. 4.7 it is observed that with the increase of temperature the shear viscosity values decrease continuously and become almost identical to that of the MHBPU at higher temperature. This can be explained on the basis of free volume concept.³⁵ The high temperature causes more thermal motion to the polymer chain and this creates more free volume to the system. As a result of higher free volume, a significant decrease in the interactions corresponding to the decrease of viscosity takes place. Thus under the used conditions the extent of interactions has less significance to influence such behaviors and hence the results. The decreased shear values with temperature reveal the fact that the nanocomposites can be melt processed with the help of the available conventional equipment in the manufacturing unit.

The viscoelastic functions like G' and G'' can provide insight into the structural properties of polymer nanocomposites as they exhibit the largest changes between the unaligned and aligned states of the clay layers in the matrix.²⁰ The G' , G'' and η^* were monitored at constant frequency of 1 s^{-1} and temperature of $120\text{ }^\circ\text{C}$ (Fig. 4.8). The following observations are worth noting in the Fig. 4.8. Firstly, the addition of clay increases the moduli and viscosity of all the nanocomposites compared to the MHBPU. This indicates the presence of strong interactions among the components in the nanocomposites. Secondly, G' , G'' and η^* values are showing Newtonian behavior in

the time dependent curves, which state the structural stability of the nanocomposites. Thirdly, the concentration of the clay has a dramatic effect, which revealed the dose dependent characteristics of the nanocomposites. Krishnamoorti and his coworkers had elaborated the increase of moduli of disordered polystyrene-polyisoprene block copolymer on addition of organo MMT.³¹

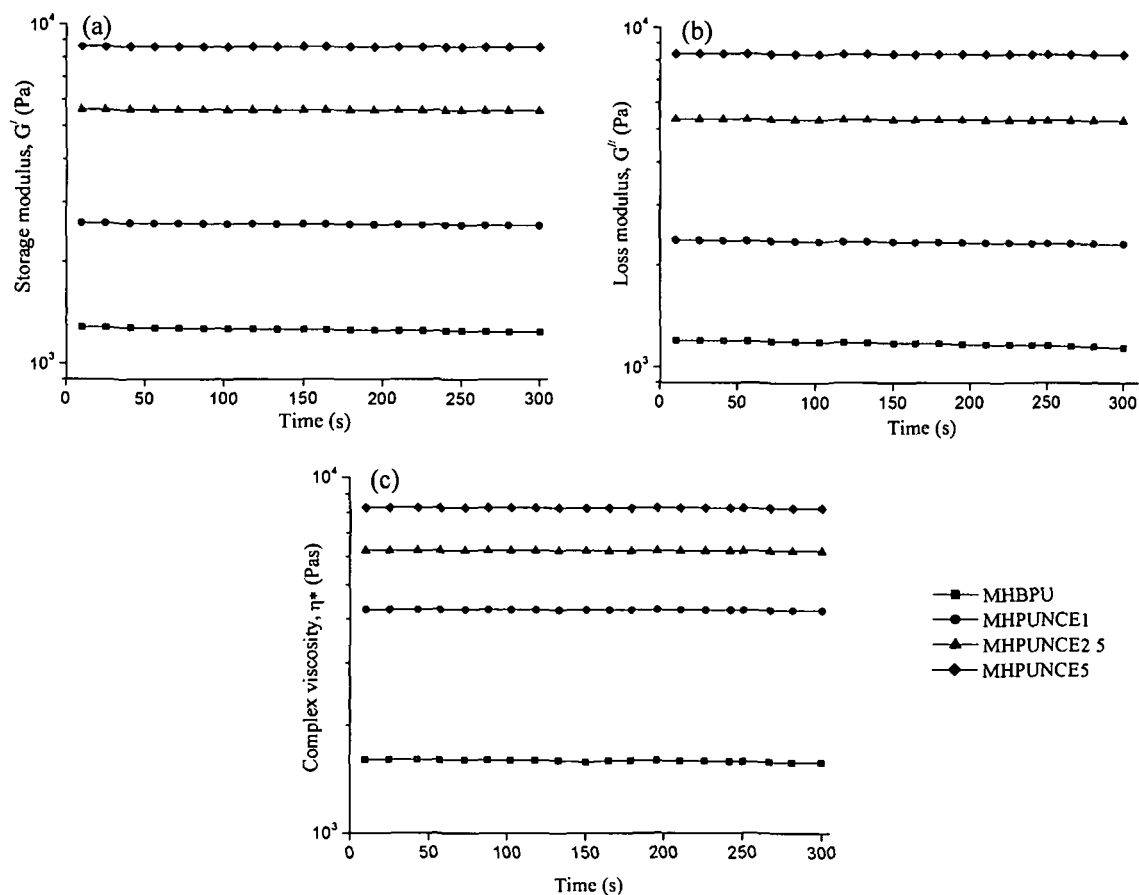


Fig. 4.8: Time dependence plot of (a) G' , (b) G'' and (c) η^*

The variation of the G' and G'' of the nanocomposites with frequency ranging from 1-100 s^{-1} at 120 °C are shown in Fig. 4.9. Both G' and G'' were increased

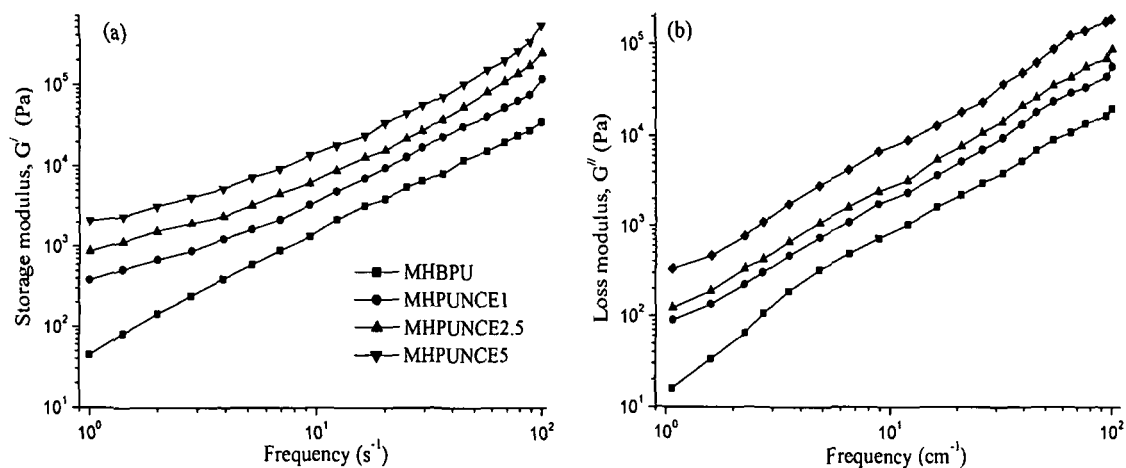


Fig. 4.9: Plot of (a) G' and (b) G'' against frequency

monotonically with the loading of clay for the whole frequency region.³⁶ The increment was prominent at lower frequencies and became almost linear at terminal. The low frequency dependence is indicative of a solid like behavior. For solid like behavior G' value should be higher than the G'' value. An illustrative description of the G' and G'' for solid like and liquid like materials was given by Larson.³⁷

The G' vs. G'' as a function of frequency was plotted for the nanocomposites in Fig. 4.10, which are analogous to Cole-Cole plots.³⁸ In all the nanocomposites the G' was higher than the G'' . Thus it conferred the elastic behavior of the nanocomposites over the whole tested frequency region. Agarwal et al. had observed solid like behavior for conventionally filled polymer system for the existence of strong interactions between polymer and fillers.³⁹ Here, the lower frequency increment is attributed by

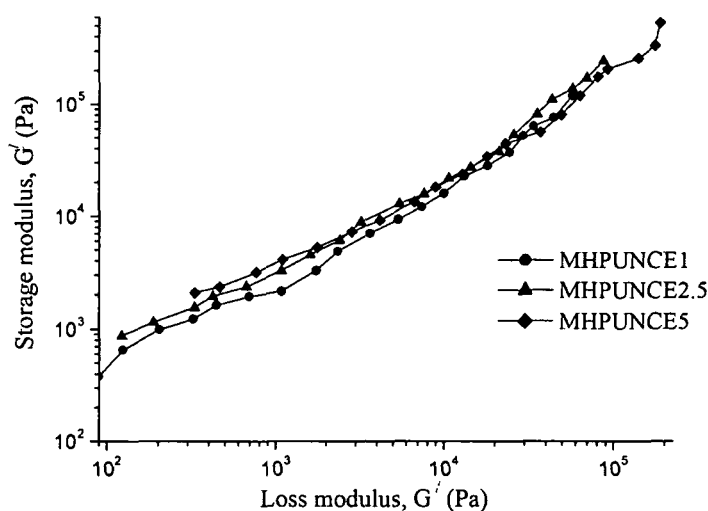


Fig. 4.10: Plot of G' against G'' for the nanocomposites

the presence of clay layers and the incomplete relaxation of polymer chains. The lower frequency dependence of G' and G'' are well described by Krishnamoorti et al.³¹ The clay layers form localized domains due to their highly anisotropic nature of the layered silicates and geometric constraints. The presence of these domains cause local correlations and enhances low frequency moduli. At minimum concentration of clay layers at critical volume fractions the tactoids and individual layers are failed to rotate freely. The applied small amplitudes are not sufficient for the complete relaxation. This is the physical jamming or percolation of the nanofillers that generate the incomplete relaxation resulting the pseudo-solid like behavior. The extent of clay to polymer interactions influences the relaxation processes of the polymers.²¹

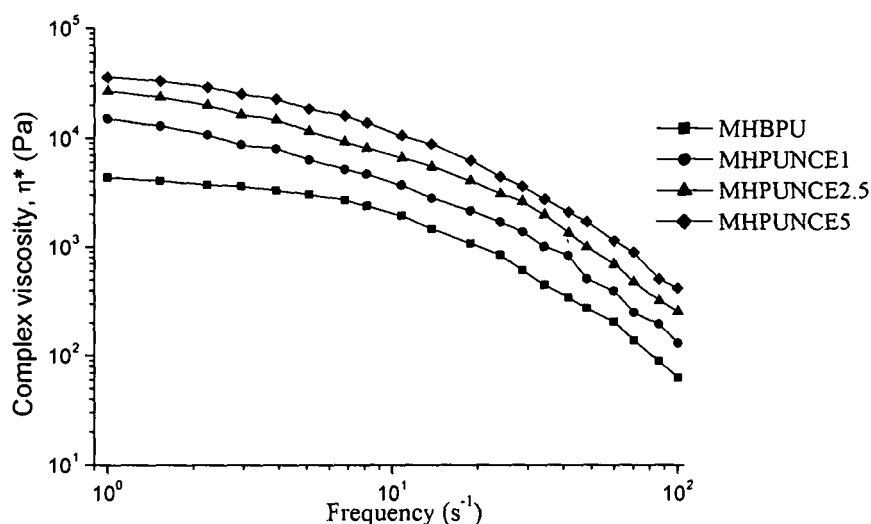


Fig. 4.11: Frequency dependence η^* of MHBPU and nanocomposites

Fig. 4.11 shows the plot of complex viscosity vs. frequency at 120 °C. The incorporation of the clay layers in the MHBPU matrix enhanced the viscosity of the system and it was dependent on the concentration of clay. This increase of the complex viscosity with the concentration of clay is mainly attributed to the increased of G' values. At low frequency region, the dependence of the clay concentration on η^* was more prominent than in the high frequency region. The oscillation thinning is responsible for such type of behavior.⁴⁰ Fig. 4.11 also shows that the η^* substantially increases with the increase of clay content from 1 to 5 weight% and the value is maximum for 5 weight% clay loading. Jana et al. also reported a clay dependent η^* increment for PU/silicate clay nanocomposites⁴¹ They proposed that, this enhancement is due to resistance to flow and the deformation of the molten polymer chains imparted by clay particles. Rodlert et al. had also found the increment of η^* and a noticeable oscillation thinning on incorporation of relatively small amount (~ 0.7 weight%) of Na^+ -MMT in the second pseudo-generation hyperbranched aliphatic polyester.⁴²

Both in steady state and oscillation mode similar type of viscosity behavior was noticed. Therefore it is justified to correlate the oscillatory viscoelastic properties with steady shear viscosity. In this regard, the Cox-Merz rule (equation 4.2) given by Cox and Merz are known to correlate complex viscosity with shear viscosity.⁴³ According to this rule the magnitude of complex viscosity ($|\eta^*|$) is equal to that of shear viscosity (η) at given values of frequency (ω) and shear rate ($\dot{\gamma}$) as

$$\eta(\dot{\gamma}) = |\eta^*|_{\omega = \dot{\gamma}} \quad (4.2)$$

The verification of this Cox-Merz rule was done in this present investigation. The obtained shear viscosity and the complex viscosity were compared for the systems.

But the results did not obey the rule. Thus the Cox-Merz rule does not hold for this vegetable oil based thermoset MHBPU/clay nanocomposites.

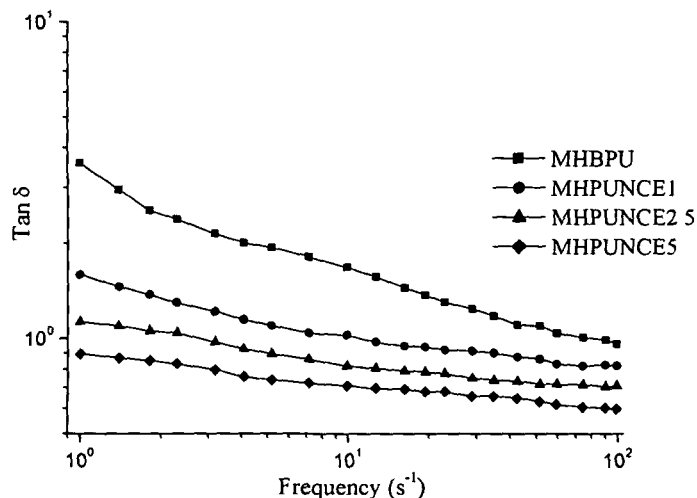


Fig. 4.12: Variation of $\tan\delta$ with frequency of the nanocomposites and MHBPU

The variations of $\tan\delta$ with frequency (1-100 s⁻¹) at different percentage of clay loading are shown in Fig. 4.12. The state of dispersion of the fillers is classified according to the $\tan\delta$ values. If $\tan\delta > 3$, particles are non-associated, when $1 < \tan\delta < 3$, fillers are weakly associated and if $\tan\delta < 1$, particles are strongly associated.⁴⁴ It was observed that the $\tan\delta$ values decreased with the increase of clay percentage. The nanocomposites showed strong interactions, which is supported by $\tan\delta$ values (Fig. 4.12).

The G' and G'' of the nanocomposites and the MHBPU as a function of temperature are demonstrated in Fig. 4.13. The tests were carried out in the temperature ranges from 100 to 170 °C at frequency of 1 s⁻¹. It was observed that with the increase of temperature the G' and G'' values decreased. In other words, the increment of the moduli at different temperature was different and at lower temperature (< 115 °C) the stiffness was more notable. It is a direct consequence of the clay layers in the matrix that act as crosslinkers.³⁶ The gradual drop of the G' and G'' values in the studied temperature range may be due to the reverse effect of the physical crosslinkages.⁴⁵ The decrease of interactions amongst the polar groups of the matrix with the clay layers at higher temperature upshot in reduction of G' and G'' . The haphazardly orientated clay layers, which were responsible for the enhanced values of G' and G'' , were forced to align at higher temperatures. This caused the decreased of G' and G'' . In other words, the clay layers “reset” themselves in the polymer matrix at higher temperatures (> 135 °C). The fatty acid chains of the monoglyceride may also help the process of alignment as they are more thermo-labile.

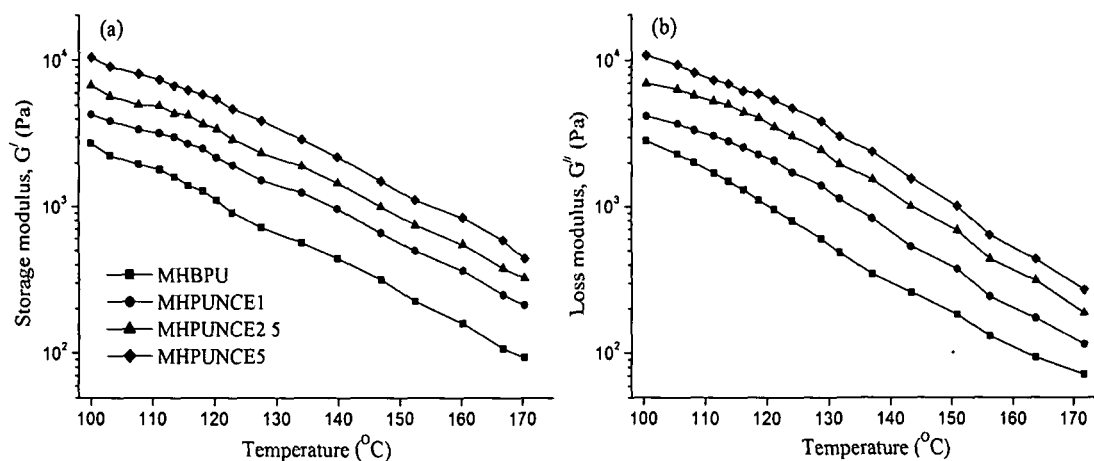


Fig. 4.13: Plot of (a) G' and (b) G'' as a function of temperature sweep

The temperature dependence of η^* was evaluated at 1 s^{-1} from 100 to 170 °C and are illustrated in Fig. 4.14. The temperature sweeps at fixed frequency showed a

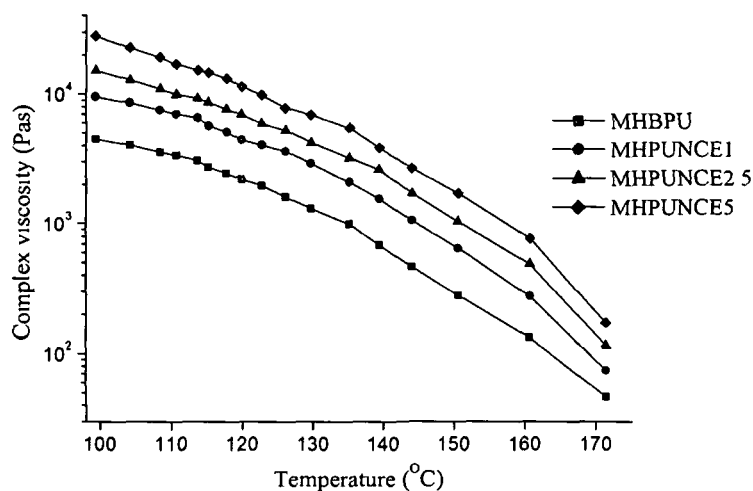


Fig. 4.14: Temperature dependence η^* of the nanocomposites and MHBPU

decrease of complex viscosity values. These prominent decreases were attributed to the large effect of physical contacts between the nanoparticles than the large changes in matrix mobility.⁴²

4.3.5. Mechanical Properties

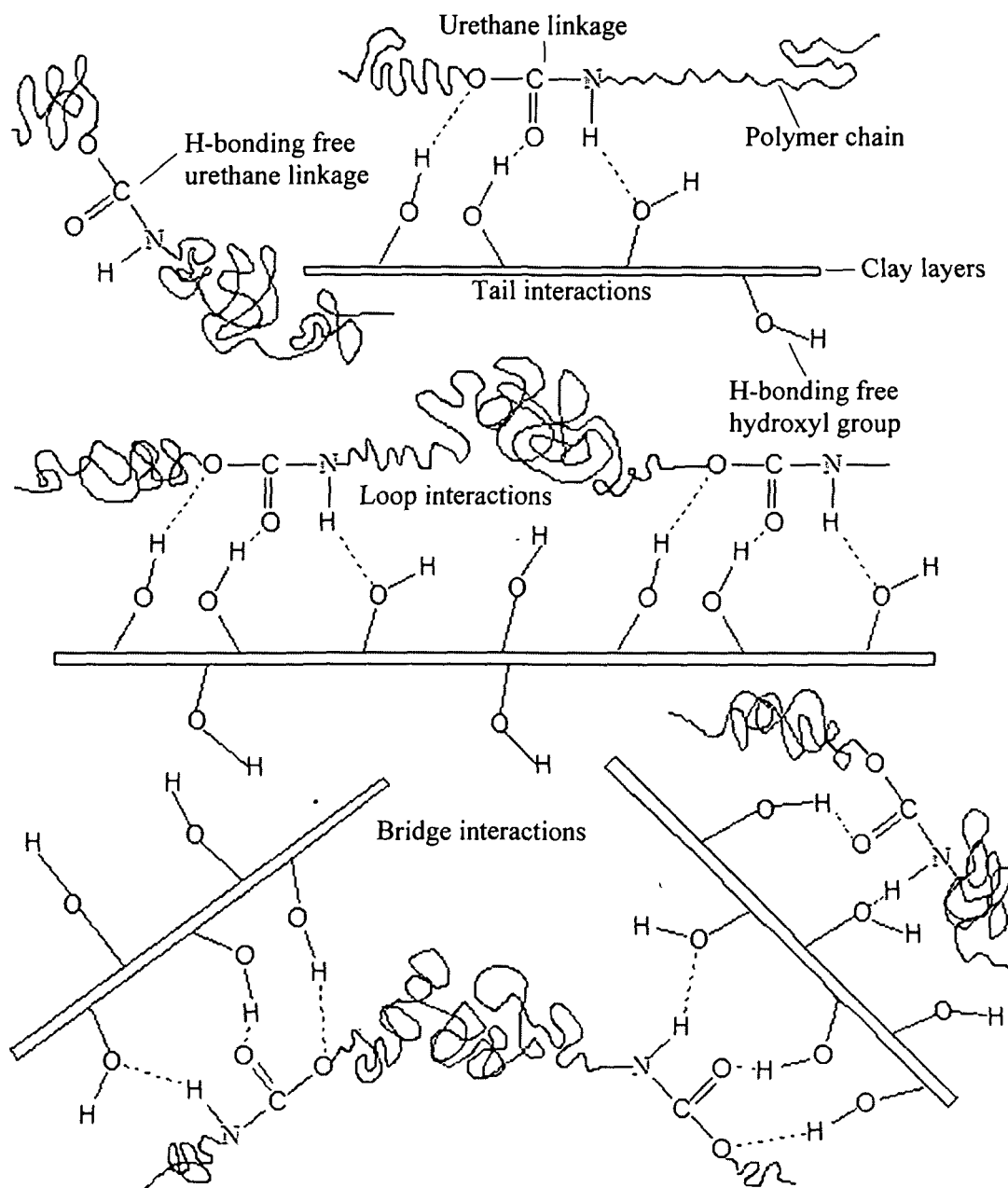
The mechanical properties such as tensile strength, elongation at break, impact resistance, flexibility and scratch hardness of the nanocomposites are given in the Table 4.1. The formation of nanocomposite resulted the improvement in tensile strength of the MHBPU up to 40 MPa. A non-linear increment of the tensile strength was observed with the clay content. Thus it can be stated that the clay content is not only the factor to influence the properties. The dispersion pattern of the clay in the matrix i.e. whether intercalated or exfoliated, also tells the story.⁴⁶ The increase of the tensile strength is the result of the well known reinforcing effect of the nano dimensional reinforcing

agents to the matrix.⁴⁷ In MHPUNCE2.5, the highest tensile strength of 40 MPa was obtained is due to partially exfoliated structure formation as supported by the XRD, SEM and TEM studies. The formation of such exfoliated clay structures enhances the

Table 4.1: *Physical and mechanical properties of the nanocomposites*

Properties	MHPUNCE1	MHPUNCE2.5	MHPUNCE5
Specific gravity	1.17	1.19	1.21
Tensile strength (MPa)	37.02	40.63	35.10
Elongation at break (%)	465	457	459
Impact resistance (cm)	98	99	97
Scratch hardness (kg)	7.7	9.1	9
Bending (dia. mm)	<5	<5	<5

interface interactions through bridge, loop and tail linkages of the polymer chains with the clay layers as shown in Scheme 4.1. In case of MHPUNCE1, the amount of clay content is not sufficient to get the optimum strength, even though low clay content results exfoliated structure and hence enhances the mechanical properties. However, at relatively high clay content, a low aggregation of the OMMT may take place instead of being completely intercalated or exfoliated, and thereby resulting poor mechanical properties.⁴⁶ Thus the strength of the MHPUNCE5 is the lowest in the studied systems. The elongation at break values were found to be decreased with the clay loading which is due to the imposed restricted mobility of the polymer chains by the increased interactions. However, the ductile PCL moiety of the HBPU assists the deformation and hence the decrement of the elongation at break value is not so high (Table 4.1). Retention of the flexibility of the prepared nanocomposites is an interesting achievement. The HBPU and MHBPU can be bent up to 5 mm diameter of a parallel mandrel. Similarly the nanocomposite films can also be bent to the same diameter without observing any damage in the films. The scratch hardness improved significantly with the increase of clay loading from 1 to 2.5 weight% though a slight decrease of the properties was observed for 5% loading (Table 4.1). However, the impact resistance remains almost unaffected. The overall increment of scratch hardness and almost no change of impact resistance compared to pristine polymer matrix are due to the combined effects of enhancement of tensile strength and good flexibility.



Scheme 4.1: Schematic representation of interface interactions of MHBPU with nanoclay

4.3.6. Adhesion Study

The adhesive strength of the nanocomposites was investigated by using different substrates namely plywood, aluminium and plastic (polypropylene) sheets in order to evaluate the performance and the influence of surface properties of the substrate on adhesion strength by lap-shear test (Fig. 4.15). The results showed that the adhesive strength for wood substrate is the highest and the strength increases with the loading of clay (14.5 MPa for MHPUNCE5). The adhesive strength of the systems is due to the presence of large numbers of end functionality of the hyperbranched polymer along with other polar groups in the systems. The adhesive performance on wood depends on

a wide range of variables such as surface smoothness of wood substrate, presence of wood extractives, pH etc.⁴⁸ The increment of adhesive strength is due to the strong interactions of polar hydroxyl, epoxy, urethane, ether and other polar groups of the cured MHBPU/clay system with the hydroxyl groups of the substrate.⁴⁹ The interactions are through H-bonding, polar-polar and polar-induced- polar interactions, or/and chemical bond formation. With the increase of the clay content the number of polar groups increases which increases the number of above interactions with the hydroxyl groups of the wood substrate, which is cellulosic substance. The result of such interactions enhances adhesive strength of the joint. The dose dependent adhesive strength was also observed by Rahman et al.⁵⁰ The partially exfoliated and intercalated clay layers may reduce the amount and size of voids during peeling, which can increase the length of the crack path in their vicinity enhancing adhesive properties.⁵¹ A similar trend was observed in case of aluminium surface which may be explained from the strong interactions of polar groups of the matrix on the substrate. The untreated surface of the plastic caused the poor adhesion with the nanocomposites adhesive as the surface polarity is low.⁵² However after HNO₃ acid treatment, the oxidation process may generate polar groups like hydroxyl, carbonyl etc. on the surface causing sufficient sites for interaction with the matrix.

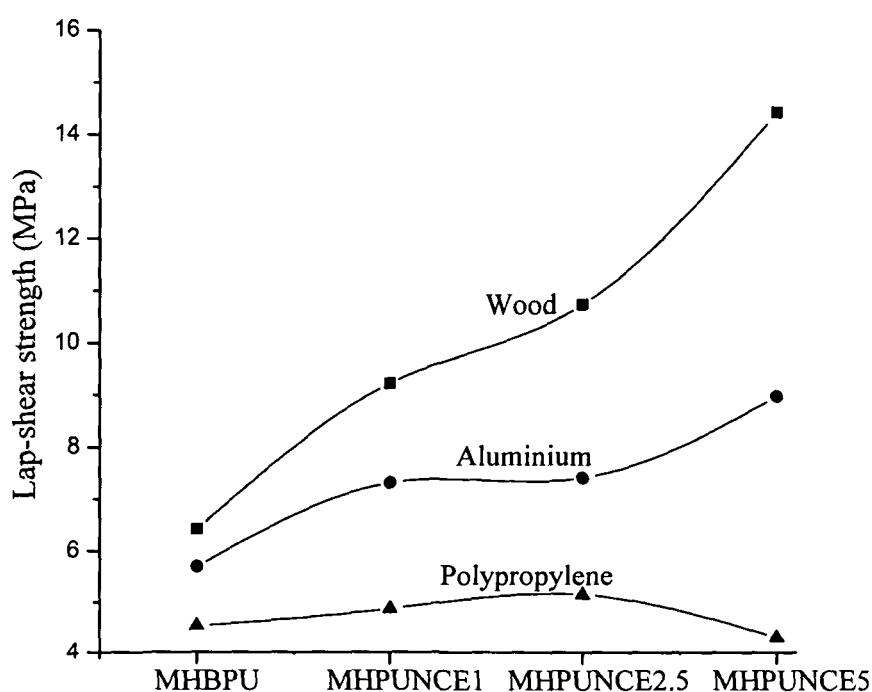


Fig. 4.15: Variation of adhesive strength for different substrates of the nanocomposites

4.3.7. Thermal Properties

The thermal properties of the nanocomposites were studied by DSC and TGA. The T_g , T_m , ΔH_m were shown in the Table 4.2.

Table 4.2: T_g , T_m and ΔH_m values of the nanocomposites

Code	T_g (°C)	T_m (°C)	ΔH_m (J/g)
MHPUNCE1	-33	52	56.1
MHPUNCE2.5	-31	54	55.4
MHPUNCE5	-35	55	54.7

It was observed that the T_g value increases from -41 °C (for MHBPU) to -35 °C (for MHPUNCE5) on addition of the clay. The restriction on the segmental chain movement imposed by clay particles is the cause of this behavior.⁵³ A slight increment of T_m values from 52 °C to 55 °C with increase of the clay content of the nanocomposites was observed compared to the MHBPU (50 °C). This may be due to the formation of compact structure that is formed through crosslinking and different types of molecular interactions as stated earlier with loading of nanoclay.⁵⁴ However, a miniature decrease of the ΔH_m value with the increase of the clay content were seen which may result from the small reduction of degree of crystallinity of the PCL moiety⁵⁵ and decrease of overall percentage of PCL content in the matrix.

Table 4.3: Thermal stability data of the nanocomposites

Code	$T_{1st\ ON}$ (°C)	$T_{1st\ MAX}$ (°C)	$T_{1st\ END}$ (°C)	$T_{2nd\ ON}$ (°C)	$T_{2nd\ MAX}$ (°C)	T_{2END} (°C)
MHPUNCE1	347	384	465	602	610	617
MHPUNCE2.5	351	402	463	611	620	627
MHPUNCE5	356	414	469	613	623	630

The relative thermal stability of the nanocomposites was examined by TGA. Two step degradation pattern (Fig. 4.16) with an enhanced thermal stability of the nanocomposites compared to pristine MHBPU was observed. The characteristic thermal degradation temperatures are reported in the Table 4.3. Shifts of 104 °C, 34 °C and 16 °C of the $T_{1st\ ON}$, $T_{1st\ MAX}$ and $T_{2nd\ ON}$ were observed with respect to the MHBPU respectively at 1 weight% of clay loading. This is due to the restricted motion of the polymer chain and the longer path of diffusion for volatiles offered by the clay layers.^{8,26} It is also noticeable that not only initial decomposition temperature increases but the weight residue also increases with the increase of the clay content (5-9%).

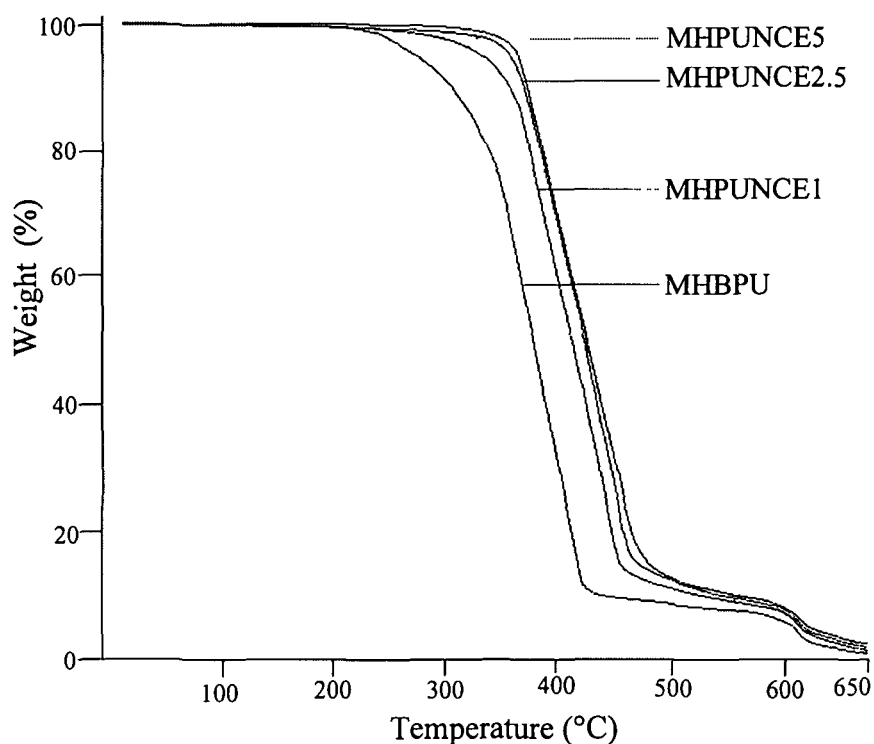


Fig. 4.16: TGA thermograms of the nanocomposites

4.4. Conclusions

From this study it can be concluded that *Mesua ferrea* L. seed oil based MHBPU/clay nanocomposites were prepared successfully by *ex-situ* technique with partial exfoliated structure of nanoclay. These nanocomposites can be used as excellent adhesives for cellulosic substrates. The formation of nanocomposites significantly improved the performance characteristics like adhesive strength, mechanical properties and thermostability without affecting impact resistance and flexibility. The study of rheological behaviors aids to the processing characteristics of the nanocomposites and to understand the state of dispersion of nanofiller in the matrix.

References

1. Pfaendner, R. Nanocomposites: Industrial opportunity or challenge? *Polym. Degrad. Stab.* **95**, 369-373 (2010)
2. Salahuddin, N.; Abo-El-Enein, S.A.; Selim, A.; Salah El-Dien, O. Synthesis and characterization of polyurethane/organo-montmorillonite nanocomposites. *Appl. Clay Sci.* **47**, 242-248 (2010)
3. Pavlidou, S.; Papaspyrides, C.D. A review on polymer-layered silicate nanocomposites. *Prog. Polym. Sci.* **33**, 1119-1198 (2008)
4. Zou, H.; Wu, S.; Shen, J. Polymer/silica nanocomposites: Preparation, characterization, properties and applications. *Chem. Rev.* **108**, 3893-3957 (2008)

5. Koerner, H. ZnO nanorod-thermoplastic polyurethane nanocomposites: Morphology and shape memory performance. *Macromolecules* **42**, 8933-8942 (2009)
6. Maji, P.K.; Das, N.K.; Bhowmick, A.K.; Preparation and properties of polyurethane nanocomposites of novel architecture as advanced barrier materials. *Polymer* **51**, 1100-1110 (2010)
7. Dutta, S.; Karak, N.; Saikia, J.P.; Konwar, B.K. Biocompatible epoxy modified bio-based polyurethane nanocomposites: Mechanical property, cytotoxicity and biodegradation. *Bioresour. Technol.* **100**, 6391-6397 (2009)
8. Karak, N. Polymer (epoxy) clay nanocomposites. *J. Polym. Mater.* **23**, 1-20 (2006)
9. Wang, Z.; Pinnavaia, T.J. Nanolayer reinforcement of elastomeric polyurethane. *Chem. Mater.* **10**, 3769-3771 (1998)
10. Rehab, A.; Salahuddin, N. Nanocomposite materials based on polyurethane intercalated into montmorillonite clay. *Mater. Sci. Eng. A* **399**, 368-376 (2005)
11. Finnigan, B.; Martin, D.; Halley, P.; Truss, R.; Campbell, K. Morphology and properties of thermoplastic polyurethane nanocomposites incorporating hydrophilic layered silicates. *Polymer* **42**, 2249-2260 (2004)
12. Seo, W.J. et al. Effects of ultrasound on the synthesis and properties of polyurethane foam/clay nanocomposites. *J. Appl. Polym. Sci.* **102**, 3764-3773 (2006)
13. Khudyakov, I.V.; Zopf, R.D.; Turro, N.J. Polyurethane nanocomposites. *Des. Monomers Polym.* **12**, 279-290 (2009)
14. Joulazadeh, M.; Navarchian, A.H. Effect of process variables on mechanical properties of polyurethane/clay nanocomposites. *Polym. Advan. Technol.* **21**, 263-271 (2010)
15. Silva, G.R. da; Silva-Cunha A. da Jr.; Behar-Cohen, F.; Ayres, E.; Orefice, R.L. Biodegradation of polyurethanes and nanocomposites to non-cytotoxic degradation products. *Polym. Degrad. Stab.* **95**, 491-499 (2010)
16. Wu, Q.; Henriksson, M.; Liu, X.; Berglund, L.A. A high strength nanocomposite based on microcrystalline cellulose and polyurethane. *Biomacromolecules* **8**, 3687-3692 (2007)
17. Karak, N.; Maiti, S. *Dendrimers and Hyperbranched Polymers-Synthesis to Applications* (MD Publication Pvt Ltd., New Delhi, 2008)
18. Irfan, M.; Seiler, M. Encapsulation using hyperbranched polymers: From research and technologies to emerging applications. *Ind. Eng. Chem. Res.* **49**, 1169-1196 (2010)

19. Susteric, Z.; Kos, T. Rheological idiosyncrasies of elastomer/clay nanocomposites. *Appl. Rheol.* **18**, 548941-5489410 (2008)
20. Ren, J.; Casanueva, B.F.; Mitchell, C.A.; Krishnamoorti, R. Disorientation kinetics of aligned polymer layered silicate nanocomposites. *Macromolecules* **36**, 4188-4194 (2003)
21. Hyun, Y.H.; Lim, S.T.; Choi, H.J.; Jhon, M.S. Rheology of poly(ethylene oxide)/organoclay nanocomposites. *Macromolecules* **34**, 8084-8093 (2001)
22. Chen, T.K.; Tien, Y.I.; Wei, K.H. Synthesis and characterization of novel segmented polyurethane/clay nanocomposites. *Polymer* **41**, 1345-1353 (2000)
23. Rihayat, T. et al. Synthesis and thermal characterization of polyurethane/clay nanocomposites based on palm oil polyol. *Polym.-Plastic. Technol.* **45**, 1323-1326 (2006)
24. Gorrasi, G.; Tortora, M.; Vittoria, V. Synthesis and physical properties of layered silicates/polyurethane nanocomposites. *J. Polym. Sci., Part B: Polym. Phys.* **43**, 2454-2467 (2005)
25. Osman, M.A.; Mittal, V.; Morbidelli, M.; Suter, U.W. Polyurethane adhesive nanocomposites as gas permeation barrier. *Macromolecules* **36**, 9851-9858 (2003)
26. Jia, Q.M.; Zheng, M.; Chen, H.X.; Shen, R.J. Synthesis and characterization of polyurethane/epoxy interpenetrating network nanocomposites with organoclays. *Polym. Bull.* **54**, 65-73 (2005)
27. Zhao, C.; Zhang, P.; Chen, G.; Wang, X. Rheological behavior of novel polyamide 6/silica nanocomposites containing epoxy resins. *J. Cent. South. Univ. Technol.* **15**, 76-79 (2008)
28. Xie, X.L. et al. Rheological and mechanical properties of PVC/CaCO₃ nanocomposites prepared by *in situ* polymerization. *Polymer* **45**, 6665-6673 (2004)
29. Dazhu, C.; Haiyang, Y.; Pingsheng, H.; Weian, Z. Rheological and extrusion behavior of intercalated high-impact polystyrene/organomontmorillonite nanocomposites. *Compos. Sci. Technol.* **65**, 1593-1600 (2005)
30. Kim, T.H.; Jang, L.W.; Lee, D.C.; Choi, H.J.; Jhon, M.S. Synthesis and rheology of intercalated polystyrene/Na⁺-montmorillonite nanocomposites. *Macromol. Rapid. Commun.* **23**, 191-195 (2002)
31. Ren, J.; Silva, A.S.; Krishnamoorti, R. Linear viscoelasticity of disordered polystyrene-polyisoprene block copolymer based layered-silicate nanocomposites. *Macromolecules* **33**, 3739-3746 (2000)

32. Choi, H.J.; Kim, S.G.; Hyun, Y.H.; Jhon, M.S. Preparation and rheological characteristics of solvent-cast poly(ethylene oxide)/montmorillonite nanocomposites. *Macromol. Rapid. Commun.* **22**, 320-325 (2001)
33. Choi, H.J.; Park, S.H.; Yoon, J.S.; Lee, H.S.; Choi, S.J. Rheological study on poly-D(-)(3-hydroxybutyrate) and its blends with poly(ethylene oxide). *Polym. Eng. Sci.* **35**, 1636-1642 (1995)
34. Schmidt, G.; Nakatani, A.I.; Butler, P.D.; Karim, A.; Han, C.C. Shear orientation of viscoelastic polymer-clay solutions probed by flow birefringence and SANS. *Macromolecules* **33**, 7219-7222 (2000)
35. Williams, M.L.; Landel, R.F.; Ferry, J.D. The temperature dependence of relaxation mechanisms in amorphous polymers and other glass-forming liquids. *J. Am. Chem. Soc.* **77**, 3701-3707 (1955)
36. Samakande, A.; Sanderson, R.D.; Hartmann, P.C. Rheological properties of RAFT-mediated poly(styrene-co-butyl acrylate)-clay nanocomposites [P(S-co-BA)-PCNs]: Emphasis on the effect of structural parameters on thermo-mechanical and melt flow behaviors. *Polymer* **50**, 42-49 (2009)
37. Larson, R.G. *The Structure and Rheology of Complex Fluids* (Oxford University Press, New York, 1999)
38. Cole, K.S.; Cole, R.H. Dispersion and absorption in dielectrics I. Alternating current characteristics. *J. Chem. Phys.* **9**, 341-351 (1941)
39. Agarwal, S.; Salovey, R. Model filled polymers: The effects of chemical interactions and matrix molecular weight on rheology. *Polym. Eng. Sci.* **35**, 1241-1251 (1995)
40. Rodlert, M.; Plummer, C.J.G.; Leterrier, Y.; Manson, J.A.E.; Grunbauer, H.J.M. Rheological behavior of hyperbranched polymer/montmorillonite clay nanocomposites. *J. Rheol.* **48**, 1049-1065 (2004)
41. Pattanayak, A.; Jana, S.C. Properties of bulk-polymerized thermoplastic polyurethane nanocomposites. *Polymer* **46**, 3394-3406 (2005)
42. Rodlert, M. et al. Hyperbranched polymer/montmorillonite clay nanocomposites. *Polymer* **45**, 949-960 (2004)
43. Cox, W.P.; Merz, E.H. Correlation of dynamic and steady flow viscosities. *J. Polym. Sci.* **28**, 619-622 (1958)
44. Rohn, C.L. *Analytical Polymer Rheology: Structural Processing Property Relationships* (Hanser Publisher, Munich, 1995)

45. Han, S.I.; Im, S.S.; Kim, D.K. Dynamic mechanical and melt rheological properties of sulfonated poly(butylene succinate) ionomers. *Polymer* **44**, 7165-7173 (2003)
46. Ray, S.S.; Okamoto, M. Polymer/layered silicate nanocomposites: A review from preparation to processing. *Prog. Polym. Sci.* **28**, 1539-1641 (2003)
47. Crosby, A.J.; Lee, J.Y. Polymer nanocomposites: The "nano" effect on mechanical properties. *Polym. Rev.* **47**, 217-229 (2007)
48. Desai, S.D.; Patel, J.V.; Sinha, V.K. Polyurethane adhesive system from biomaterial-based polyol for bonding wood. *Int. J. Adhes. Adhes.* **23**, 393-399 (2003)
49. Rahman, M.M.; Yoo, H.J.; Mi, C.J.; Kim, H.D. Synthesis and characterization of waterborne polyurethane/clay nanocomposite-effect on adhesive strength. *Macromol. Symp.* **249-250**, 251-258 (2007)
50. Rahman, M.M.; Kim, J.H.; Kim, H.D. Characterization of waterborne polyurethane/clay nanocomposite adhesives containing different amounts of ionic groups. *J. Adhes. Sci. Technol.* **21**, 1575-1588 (2007)
51. Wang, J.; Chen, Y.; Tang, Y.; Xu, M. Preparation, properties, and mechanism of novel polyurethane adhesive/organic montmorillonite nanocomposites. *High Perform. Polym.* **21**, 155-171 (2009)
52. Malucelli, G. et al. Polyurethane resin-based adhesives: Curing reaction and properties of cured systems. *Int. J. Adhes. Adhes.* **25**, 87-91 (2005)
53. Kim, M.S.; Jun, J.K.; Jeong, H.M. Shape memory and physical properties of poly(ethyl methacrylate)/Na-MMT nanocomposites prepared by macroazoinitiator intercalated in Na-MMT. *Compos. Sci. Technol.* **68**, 1919-1926 (2008)
54. Xiong, J.; Zheng, Z.; Jiang, H.; Ye, S.; Wang, X. Reinforcement of polyurethane composites with an organically modified montmorillonite. *Compos. Part A: Appl. Sci. Manufact.* **38**, 132-137 (2007)
55. Lepoittevin, B. et al. Poly (ϵ -caprolactone)/clay nanocomposites prepared by melt intercalation: Mechanical, thermal and rheological properties. *Polymer* **43**, 4017-4023 (2002)

CHAPTER 5

MHBPU/clay nanocomposites prepared by *in-situ* technique

5.1. Introduction

PU/clay nanocomposite has been offering a candidature as an advanced polymeric material for its unique properties. The extent of enhancement of the properties of these nanocomposites depends on the degree of exfoliation of the clay layers.^{1,2} Amongst the various ways for preparation of polymer nanocomposites, *in-situ* preparative technique is preferably chosen over the *ex-situ* by many researchers.³⁻⁵ In *ex-situ* technique the nanomaterials are incorporated into the prepared polymer matrix, while the *in-situ* approach involves the preparation of polymer matrix from its monomer(s) or pre-polymer in the presence of nanomaterial.⁶ In *ex-situ* technique as prepared polymers are mixed with the nanomaterials so the polymerization process remain unaltered, however in *in-situ* technique as polymerization occurs in the presence of nanomaterials so this may have strong impact on the polymerization kinetics and hence on the structure. Further, the uniform dispersion of the clay may be difficult in the highly viscous polymer matrix through *ex-situ* technique which can be overcome by the incorporation of nanomaterials in low viscous monomers or pre-polymers in *in-situ* technique.⁷ Again, the concomitant increase of viscosity during the polymerization contributes the stabilization of the nanomaterials. Therefore, *in-situ* techniques bestowed a wide spectrum of properties to the final nanocomposites through a fine tuning of the preparative conditions.⁸ Furthermore the *in-situ* techniques are simple and cost effective as they neither require the costly extra solvent as in solution technique nor extra energy as in melting technique. A lot of research addressing on the preparation of PU nanocomposites is directed through the *in-situ* preparative technique.⁹⁻¹¹ Thus it is worth thinking to utilize the *in-situ* technique for the formation of exfoliated MHBPU/clay nanocomposites in the present study.

In this chapter, therefore, the properties like mechanical, thermal, rheological, chemical, water vapor permeability etc. of *Mesua ferrea* L. seed oil based MHBPU/clay nanocomposites prepared by *in-situ* technique are reported. The shape memory behavior and biodegradation of the nanocomposites have also been studied.

5.2. Experimental

5.2.1. Materials

The chemicals used in this study such as PCL, glycerol, TDI, DMF, OMMT, epoxy resin, hardener etc. were of same specification as described in Chapter 4, section 4.2.1.

The minerals $(\text{NH}_4)_2\text{SO}_4$, Na_2HPO_4 , KH_2PO_4 , $\text{MgSO}_4 \cdot 7\text{H}_2\text{O}$, $\text{CaCl}_2 \cdot 2\text{H}_2\text{O}$, $\text{FeSO}_4 \cdot 7\text{H}_2\text{O}$, $\text{CuSO}_4 \cdot 7\text{H}_2\text{O}$, $\text{MnSO}_4 \cdot 5\text{H}_2\text{O}$, $\text{ZnSO}_4 \cdot 7\text{H}_2\text{O}$, $\text{H}_3\text{BO}_3 \cdot 5\text{H}_2\text{O}$ and MoO_3 used for the bacterial broth preparation were obtained from Merck, India. The *Pseudomonas aeruginosa* strains MTCC 7814 and MTCC 7815 and other ingredients required for biodegradation test were obtained from the Department of Molecular Biology and Biotechnology (Department of Biotechnology, DBT Centre, Government of India), Tezpur University.

5.2.2. Instruments and Methods

The FTIR, XRD, SEM, TEM, TGA and DSC analyses were carried out using the same instruments and conditions as mentioned in Chapter 4, section 4.2.2. The shape memory test of the prepared nanocomposites was evaluated by following the same method as given in Chapter 3, section 3.2.2. The measurements of impact resistance, hardness and flexibility (bending) were performed according to the standard methods as mentioned earlier (Chapter 2, section 2.2.2.). The mechanical properties, adhesive strength, rheological properties were evaluated as per the methods mentioned in the Chapter 4, section 4.2.2.

The water vapor barrier property was measured by taking 10 mL of water in the standard cup of 1cm^2 cut on the lid. The nanocomposite films of 60-70 μm thick were fixed in the open space of the lid and the systems were kept in the vacuum oven under reduced pressure of 760 mm of Hg and at 27 °C. The initial weight of the cup with water and film is W_0 . The percent weight loss through the films was calculated by weighing the weight of the cup (W_1) at specific interval during the test using the following equation (5.1)

$$(W_0 - W_1) / W_0 \times 100\% \quad (5.1)$$

5.2.2.1. Preparation of HBPU and Its Modification by Epoxy Resin

The *Mesua ferrea* L. seed oil based HBPU was prepared by the same procedure as mentioned in Chapter 2, section 2.2.2.2. The modification of the prepared HBPU was carried out by the method as described in Chapter 3, section 3.2.2.1.

5.2.2.2. Preparation of Nanocomposites

Solution containing different amounts of the OMMT (1, 2.5 and 5 weight%) were added into the pre-polymer solution of HBPU, separately. Before addition of the clay into the pre-polymer, it was dispersed in 1-5 mL of DMF by magnetic stirring followed by ultrasonication for 5 min at amplitude of 35% and half cycle. The remaining parts of the preparative method were same as elaborated in Chapter 4, section 4.2.2.2. Finally, the nanocomposite films were obtained by solution casting, followed by vacuum degassing and curing at 120 °C for 35 min for further testing and analyses. The cured films were denoted as MHPUNCI1, MHPUNCI2.5 and MHPUNCI5 correspond to the clay content of 1, 2.5 and 5 weight% respectively.

5.2.2.3. Sample Preparation for Performance Studies

The prepared nanocomposites were casted on different substrates for different studies by the same way as mentioned in Chapter 3, section 3.2.2.2. The cured casted nanocomposite samples were cut by the manual sample cutter with dimension as per the standard ASTM D 412-51T for mechanical testing.

5.2.2.4. Biodegradation by Broth Culture Technique

A nutrient broth medium for microbial culture was prepared by dissolving 2.0 g $(\text{NH}_4)_2\text{SO}_4$, 2.0 g Na_2HPO_4 , 3.61 g KH_2PO_4 , 1.75 g $\text{MgSO}_4 \cdot 7\text{H}_2\text{O}$, 0.2 g $\text{CaCl}_2 \cdot 2\text{H}_2\text{O}$, 50 mg $\text{FeSO}_4 \cdot 7\text{H}_2\text{O}$, 1 mg $\text{CuSO}_4 \cdot 7\text{H}_2\text{O}$, 50 μg $\text{MnSO}_4 \cdot 5\text{H}_2\text{O}$, 70 μg $\text{ZnSO}_4 \cdot 7\text{H}_2\text{O}$, 10 μg $\text{H}_3\text{BO}_3 \cdot 5\text{H}_2\text{O}$ and 10 μg MoO_3 in 1.0 L of demineralized water. An amount of 10 mL of this liquid culture medium was poured into 100 mL conical flasks and was sterilized by using autoclave at 121 °C and 15 lb pressure for 15 min. The autoclaved media were then allowed to cool down to room temperature and polymer films were applied to the media under sterile condition inside a laminar air hood. Media containing no polymer film was also cultured as negative control.

Microbe Selection

Two *Pseudomonas aeruginosa* strains were selected for the study with strain number MTCC 7814 and MTCC 7815. Pure culture of each bacterial strain was prepared using urea as carbon source along with mineral media that are mentioned above for a period of 48 h at 37 °C. 100 μL of the culture medium containing $10^8/\text{mL}$ microbes as calculated from McFarland turbidity method¹²⁻¹⁴ was inoculated to the conical flask containing 10 mL media for each test. The flasks were then incubated under sterile condition at 37 °C for the degradation study. The samples were collected

for spectrophotometric observation at 600 nm against blank culture media on weekly basis under sterile condition. Bacterial growth was calculated from the absorbance data using McFarland turbidity as the standard.

McFarland Standard Preparation

In microbiology, McFarland standards are taken as a reference to adjust the turbidity of bacterial suspensions to keep the number of bacteria in a given range. It was obtained by mixing specified amounts of 1% BaCl₂ and 1% H₂SO₄ solutions which creates turbidity due to the precipitation of BaSO₄ in the solution. Five McFarland standards were prepared by mixing solutions of BaCl₂ and H₂SO₄ in different proportions (Table 5.1). The plot of absorbance at the wavelength of 600 nm against known population gives a straight line of the following equation (5.2),

$$y = 18.96x - 1.629 \quad (5.2)$$

where 'y' is the bacterial population and 'x' is the absorbance of the cultured broth. The constants 18.96 and 1.629 are the slopes and intercepts of the straight line respectively.¹²⁻¹⁴

Table 5.1: McFarland Nephelometer standards

McFarland Standard Number	0.5	1	2	3	4
1% BaCl ₂ (mL)	0.05	0.1	0.2	0.3	0.4
1% H ₂ SO ₄ (mL)	9.95	9.9	9.8	9.7	9.6
Cell Density (approx. 1 X 10 ⁸ CFU/mL)*	1.5	3.0	6.0	9.0	12.0
Absorbance at 600 nm	0.132	0.257	0.451	0.582	0.669

*CFU stands for Collony Forming Unit

5.3. Results and Discussions

5.3.1. Formation of Nanocomposites

In the preparation of the nanocomposites the dispersed OMMT in DMF solvent was added in the pre-polymer state during the synthesis of HBPU. Therefore it was easy to disperse the OMMT in the low viscous and reactive matrix.

5.3.2. Characterization

The FTIR spectra of the nanocomposites and MHBPU (for comparison purpose) are shown in Fig. 5.1. The distinctive absorption bands for the functional groups in case of MHBPU were also observed in the nanocomposites (Fig. 5.1).

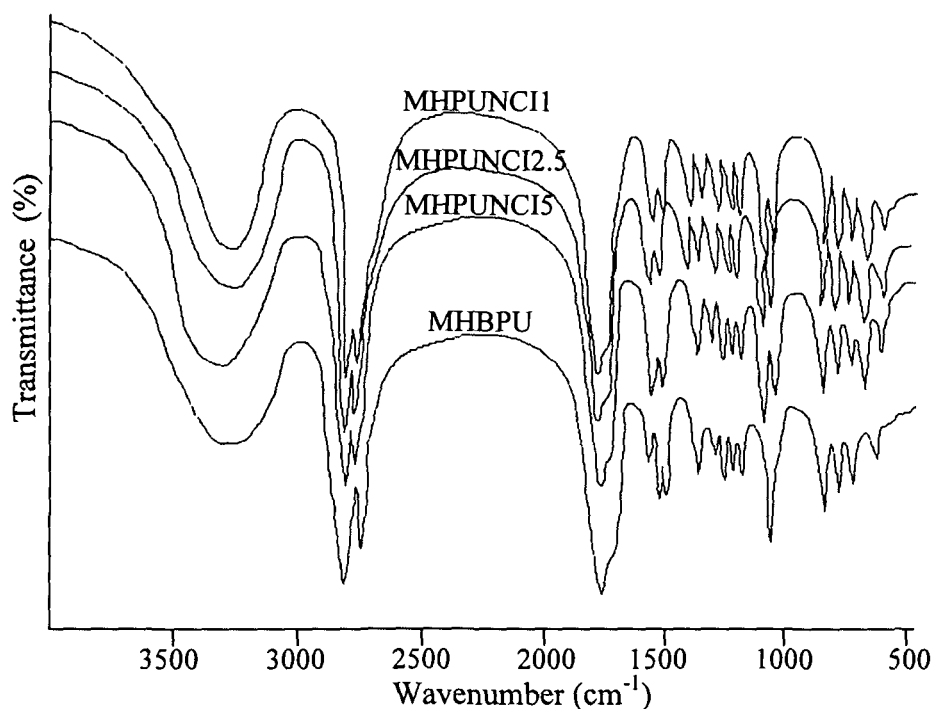


Fig. 5.1: FTIR spectra of the MHBPU and nanocomposites

The -NH stretching band was broadened after nanocomposite formation. This can be explained by the formation of H-bonding between the -NH of urethane with -OH groups of the OMMT in addition to other polar groups present in the matrix. The change of the band position near 1600 cm^{-1} may be due to the interaction of OMMT with the -C=O of the MHBPU through H-bonding. The band appeared in case of MHBPU, where the degree of H-bonding was less compared to the nanocomposites, but the delaminated clay provided more -OH groups for H-bonding between -OH/-NH and -C=O in nanocomposites and thus the band $\sim 1600\text{ cm}^{-1}$ was enveloped. Thus to an extent structural change was occurred in the HBPU in presence of the OMMT which was not observed in the nanocomposites prepared by *ex-situ* technique. The appearance of the absorption bands at ~ 522 and $\sim 1033\text{ cm}^{-1}$ corresponding to Al-O and Si-O-Si stretching vibration inferred the presence of OMMT in the nanocomposites.¹⁵ Although the dispersion state of the OMMT layers cannot be predicted directly from FTIR study but the identical FTIR spectra taken from random parts of the nanocomposites reveals the uniformly dispersed OMMTs in the polymer matrix.

Further the FTIR study was employed to evaluate the microphase structure of the nanocomposites. The urethane carbonyl region is the most helpful area to determine the H-bonding.¹⁶ The -C=O stretching vibration of urethane group was observed from $1740\text{-}1710\text{ cm}^{-1}$ for the nanocomposites. The hydrogen bonded and free -C=O group showed absorption band at 1710 cm^{-1} and 1740 cm^{-1} respectively. The band intensity

ratio of these two bands gives an estimate of the degree of H-bonding. Thus the H-bonding index, R, may be defined as the ratio of absorption A_{1710}/A_{1740} .¹⁷ The degree of phase separation (DPS) in the nanocomposites can be calculated from the band intensity of the two bands following the equation (5.3).

$$\text{DPS (\%)} = \frac{C_{\text{bonded}}}{(C_{\text{bonded}} + C_{\text{free}})} \times 100 \quad (5.3)$$

where C is the concentration of the bonded and free carbonyl groups.

With the increase of clay content (1-5 weight%) it was observed that the degree of phase separation increased as DPS values were found to be 47.2, 48.5 and 49.7 for MHPUNCI1, MHPUNCI2.5 and MHPUNCI5 respectively. This is due to the reaction of the -OH groups of the clay with the -NCO groups of the pre-polymer/TDI and the greater strength of the H-bonding between the -OH of clay and -C=O of urethane than intra molecular H-bonding.¹⁶

The XRD analysis was used to characterize the formation of nanocomposites. Fig. 5.2 shows the WAXD patterns for OMMT and nanocomposites. The diffraction

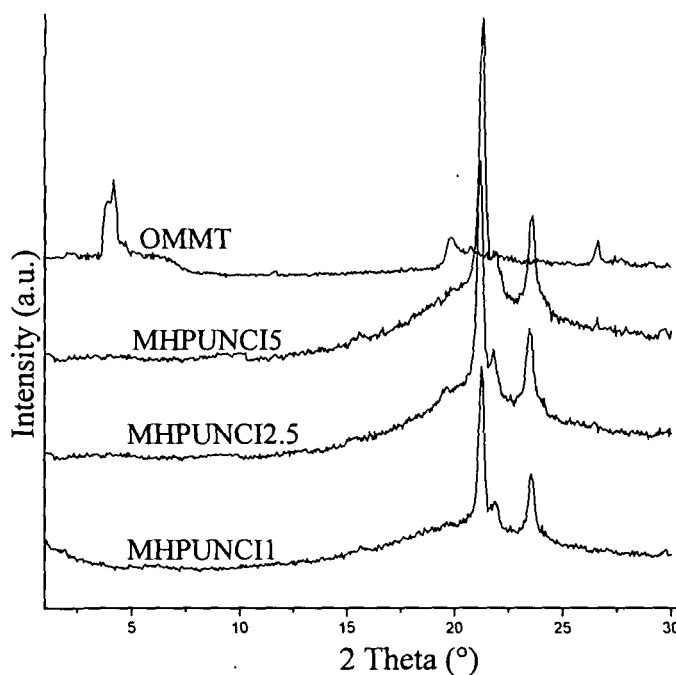


Fig. 5.2: WAXD of the OMMT and nanocomposites

peaks of the OMMT were observed at $2\theta = 4.17, 19.97$ and 26.63° corresponding to d-spacing of 2.36, 0.49 and 0.37 nm respectively as calculated on the basis of Bragg's equation. These peaks were completely disappeared in XRD diffractograms of the nanocomposites which may be due to the exfoliation (delamination) of clay layers by the polymer chains. While in the WAXD patterns of HPUNCE5 showed diffraction peaks at $2\theta = 1.98^\circ$ corresponding to d-spacing of 4.95 nm (Chapter 4, section 4.3.2.) but here the MHPUNCI5 showed no diffraction peak. This observation proves the

better efficiency of the *in-situ* technique over *ex-situ*. Again the characteristic two peaks of MHBPU at $2\theta = 21.2^\circ$ (4.19 Å) and 23.4° (3.81 Å) (Chapter 3, section 3.3.2) were also observed in the nanocomposites at the same position (Fig. 5.2). But a closer visual probing revealed a trifle increase of the intensity of the two peaks. This increment of intensity resulting from the enhancement of the crystallinity is explained later on with the DSC result.

Further TEM images proved the exfoliated structure of the OMMT layers in the nanometer range (Fig. 5.3). It provides a real picture what are happening inside the

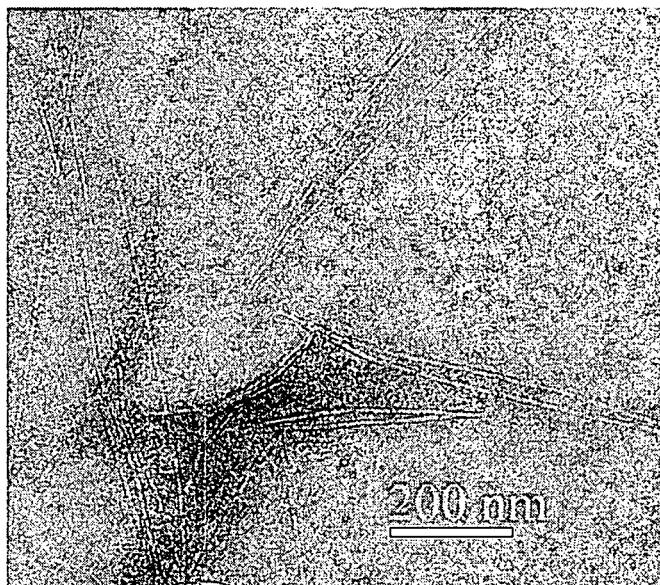


Fig. 5.3: TEM micrograph of MHPUNCI2.5 (representative one)

matrix. Observation of protruding lines indicates the well adhered clay layers to the polymer surface. The clay layers of approximately 10 nm thick were dispersed and disordered randomly in the matrix. Thus it can be said that the clay layers are almost exfoliated and dispersed in the MHBPU matrix.

5.3.3. Physical Properties

The specific gravity values of the nanocomposites were found to be almost similar to that of the MHBPU (Table 5.2). Thus the light weight characteristic of the pristine MHBPU was retained in the nanocomposites. The gloss of the nanocomposites was comparable with the similar type polymers prepared from the same vegetable oil.^{18,19} A decrease of gloss of nanocomposites from MHPUNCI1 to MHPUNCI5 was observed which may be due to the low gloss of clay. The decrease of gloss value on addition of clay was also reported by several literatures.^{20,21}

Table 5.2: Physical and mechanical properties of the nanocomposites

Properties	MHPUNCI1	MHPUNCI2.5	MHPUNCI5
Impact resistance (cm)	97	97.5	99
Bending (dia. mm)	<5	<5	<5
Gloss (60°)	78	77	77
Scratch hardness (kg)	8.5	9.2	9.8
Specific gravity	1.17	1.19	1.21
Tensile strength (MPa)	40.03	45.62	48.1
Elongation at break (%)	472.17	454.36	440.21
Lap-shear adhesion (MPa)	8.56	9.31	11.68

The retention of transparency of a transparent polymer is one of the characteristic properties of nanocomposites.²² The transparent character of the nanocomposites remains intact as seen from the Fig. 5.4.

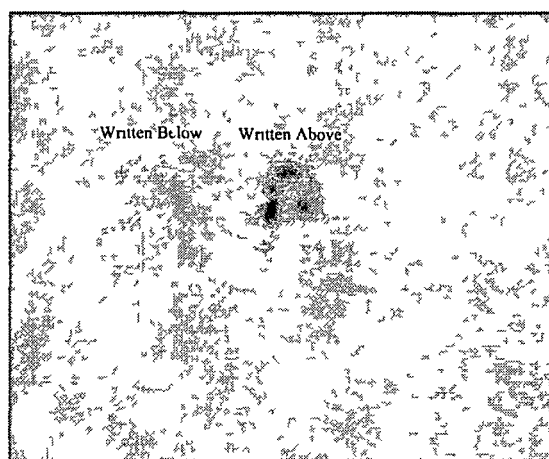


Fig. 5.4: A photograph showing the retention of transparency of the nanocomposites

5.3.4 Rheological Properties

The shear viscosity of the nanocomposites was investigated as function of time at 120 °C under the shear rate of 50 s⁻¹ (Fig. 5.5). The nanocomposites possess higher viscosity than the pristine MHBPU and they exhibited Newtonian behavior over the whole range of study. Also the viscosity increment was found to be dose dependent. It was observed that the nanocomposites prepared by *in-situ* technique showed higher shear viscosity than that of nanocomposites prepared by *ex-situ* as observed in Chapter 4, section 4.3.4. This may be due to the formation of more interactions between polar groups of OMMT with polar hydroxyl, epoxy, urethane, ether and other polar groups of the matrix caused by the exfoliated clay layers in *in-situ* prepared nanocomposites.

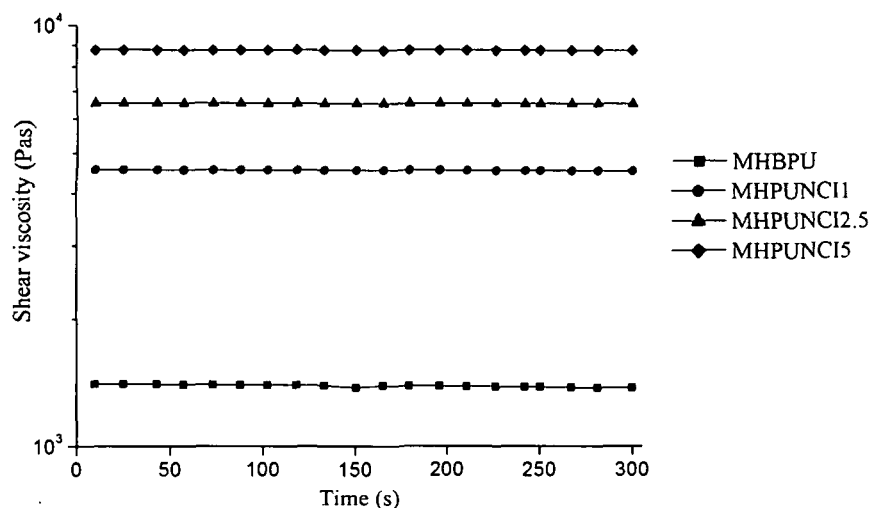


Fig. 5.5: Shear viscosity as a function of time

The shear viscosity as a function of shear rate for the nanocomposites is shown in Fig. 5.6. The test was done at 120 °C with varying shear rate from 1-100 s^{-1} . The MHPUNCI1 exhibited Newtonian behavior at low shear rates and shear thinning behavior at high shear rates. Interestingly, the MHPUNCI2.5 and MHPUNCI5 showed only shear thinning behavior over the whole tested region.

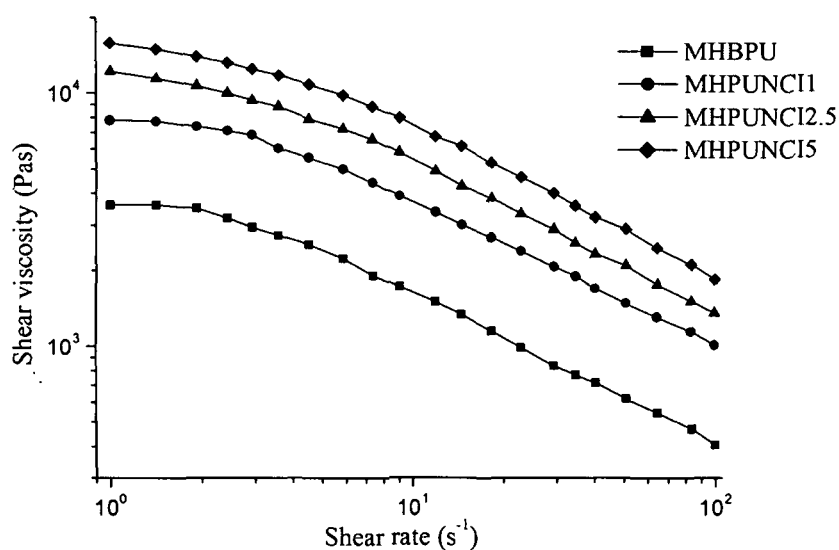


Fig. 5.6: Shear viscosity as a function of shear rate

The shear viscosity as a function of temperature is elucidated in Fig. 5.7 for all the nanocomposites. With the increase of temperature the shear viscosity values decreased continuously. At high temperatures the shear viscosity values became comparable to that of the pristine MHBPU. The nanocomposites prepared by the *in-situ* process initially showed higher shear values, but with the increase of temperature the values became identical to that of the nanocomposites prepared by the *ex-situ* technique.

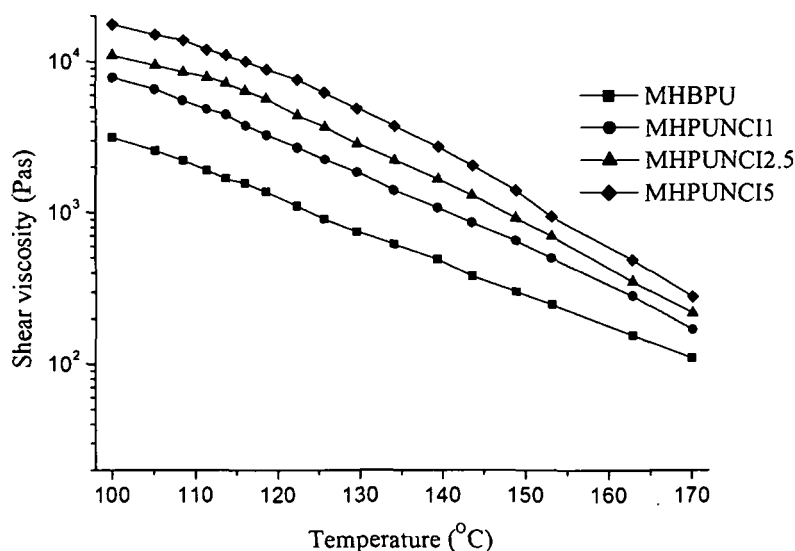


Fig. 5.7: Temperature dependence shear viscosity of the nanocomposites

The time dependence rheometric functions such as G' , G'' and η^* was monitored at constant frequency (1s^{-1}) and temperature of $120\text{ }^\circ\text{C}$ (Fig. 5.8). The enhanced moduli and η^* of the nanocomposites showed Newtonian behavior in the studied range. Also, the G' , G'' and η^* values were more for the nanocomposites prepared by *in-situ* technique, which confirmed the greater interactions among the components compared to the nanocomposites prepared by *ex-situ* technique.

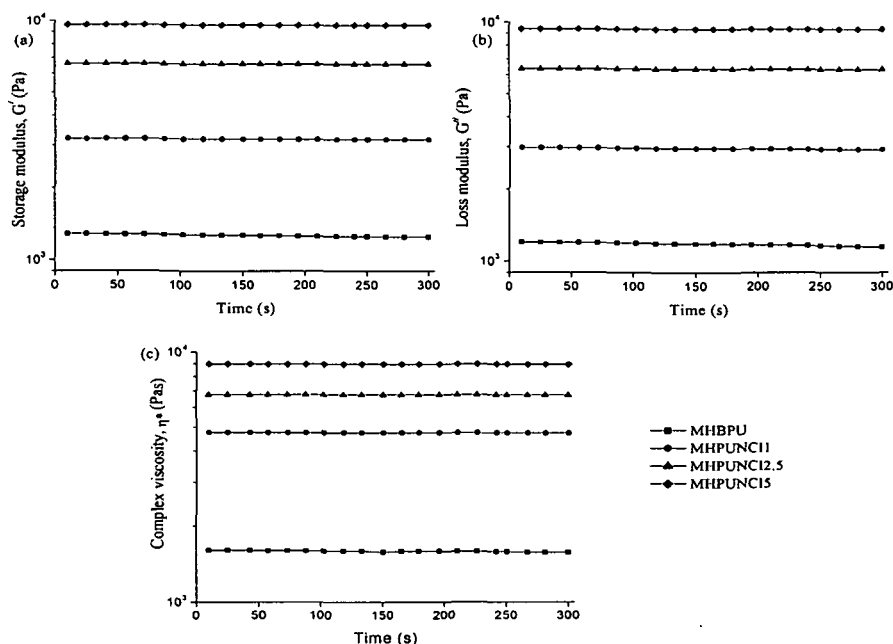


Fig. 5.8: Time dependence plot of (a) G' , (b) G'' and (c) η^* of the nanocomposites

Fig. 5.9 shows the change of the G' and G'' with respect to frequency ($1\text{-}100\text{ s}^{-1}$) at $120\text{ }^\circ\text{C}$ for the nanocomposites. A continuous increasing trend was observed for both the G' and G'' which was prominent at lower frequencies.

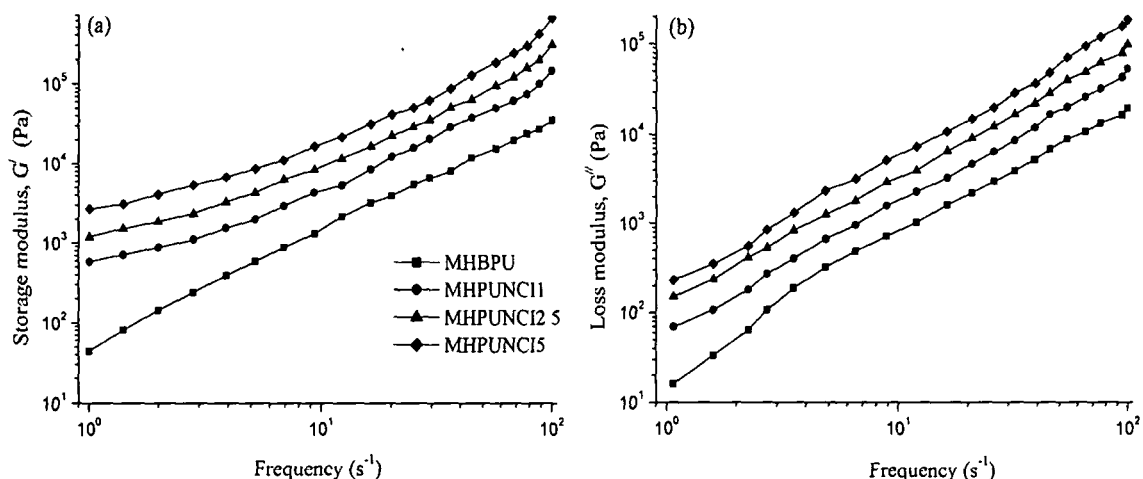


Fig. 5.9: Plot of (a) G' and (b) G'' against frequency

The plots of G' vs. G'' which are analogous to Cole-Cole plots²³ are given in Fig. 5.10 for all the nanocomposites. It was observed that for all nanocomposites $G' > G''$ over the whole tested frequency region. This indicates greater elastic nature of the nanocomposites than the viscous nature.

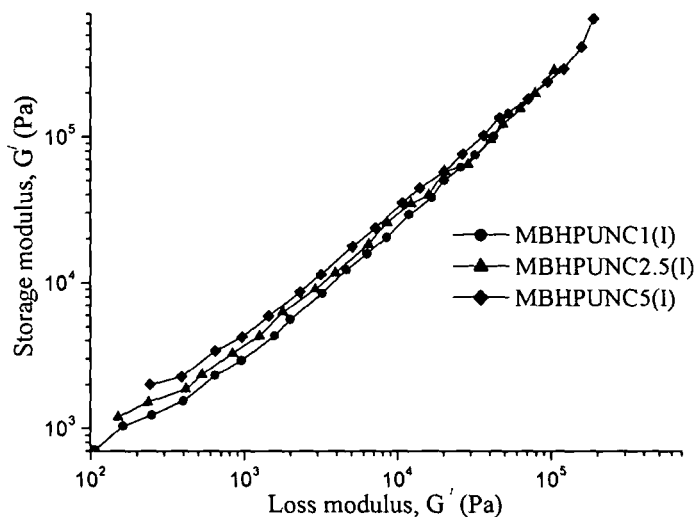


Fig. 5.10: Plot of G' against G'' of the nanocomposites

The variation of complex viscosity as a function of frequency (1-100 s^{-1}) at 120 $^{\circ}C$ is given in Fig. 5.11. At low frequency region, the dependence of the clay concentration on η^* was prominent than in the high frequency region. The values of η^* were increased continuously with the increase of clay content from 1 to 5 weight%. As the G' values are more in the nanocomposites prepared by *in-situ* process than the *ex-situ* nanocomposites, therefore the enhanced η^* value of the *in-situ* nanocomposites are obvious.

The applicability of Cox-Merz rule²⁴ was verified for the present studied systems. However, the results did match with the rule.

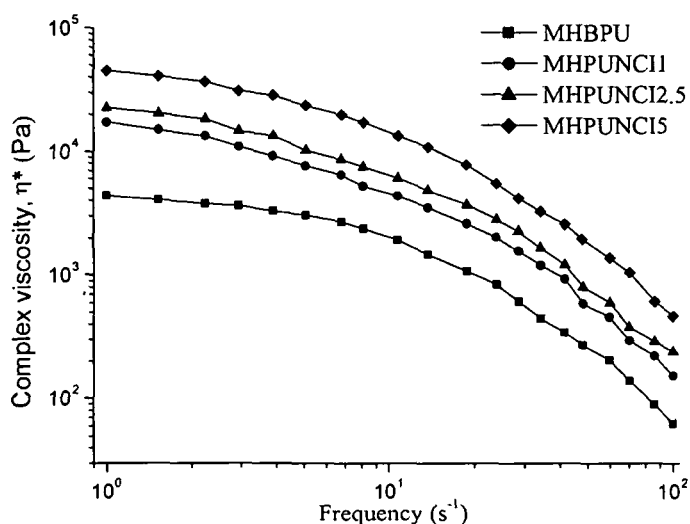


Fig. 5.11: Frequency dependence η^* of the nanocomposites

The variations of $\tan\delta$ with frequency ($1-100 \text{ s}^{-1}$) at different percentage of clay loading are shown in Fig. 5.12. It was observed that the $\tan\delta$ values decreased with the increase of clay percentage.

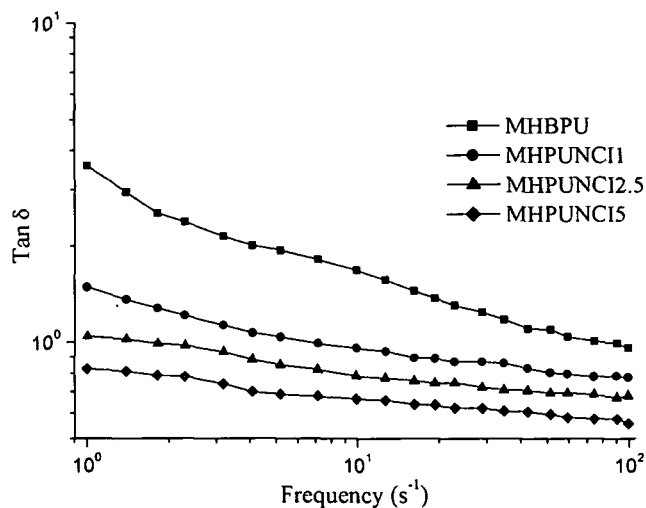


Fig. 5.12: Variation of $\tan\delta$ with frequency of the nanocomposites

The G' and G'' of the nanocomposites and the pristine MHBPU as a function of temperature are demonstrated in Fig. 5.13. The tests were carried out in the temperature ranges from 100 to $170 \text{ }^\circ\text{C}$ at frequency of 1 s^{-1} . It was observed that with the increase of temperature the G' and G'' values decreases.

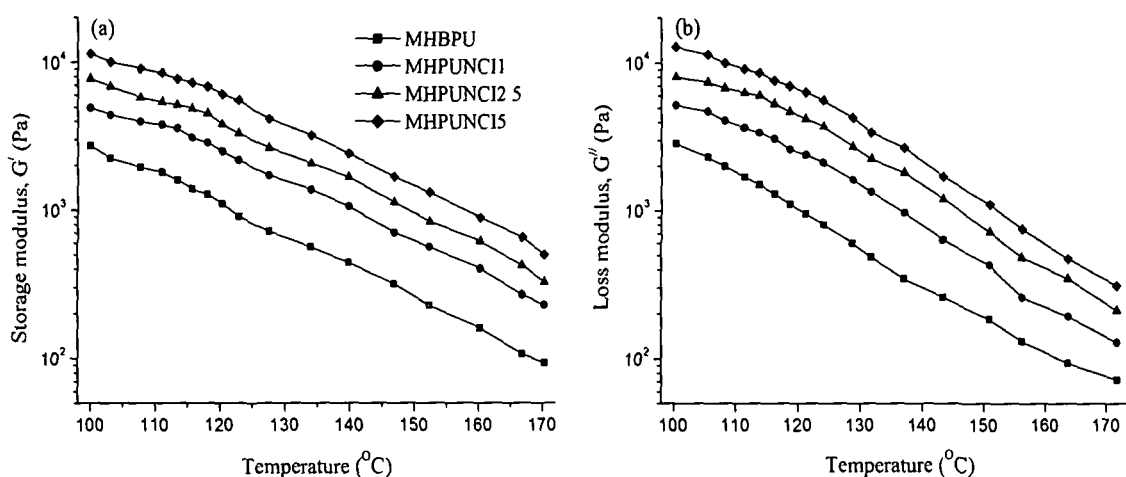


Fig. 5.13: Plot of (a) G' and (b) G'' as a function of temperature sweep

The temperature dependence of η^* was evaluated at 1 s^{-1} from 100 to 170 °C and are illustrated in Fig. 5.14. The temperature sweeps at fixed frequency showed a decrease of complex viscosity values.

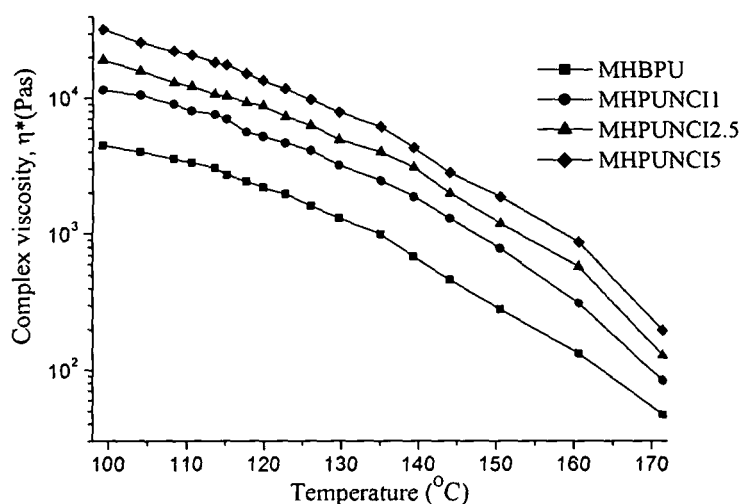


Fig. 5.14: Temperature dependence η^* of the nanocomposites

The same explanation as described in Chapter 4, section 4.3.4 can also put forwarded for the above mentioned rheometric behaviors of the nanocomposites.

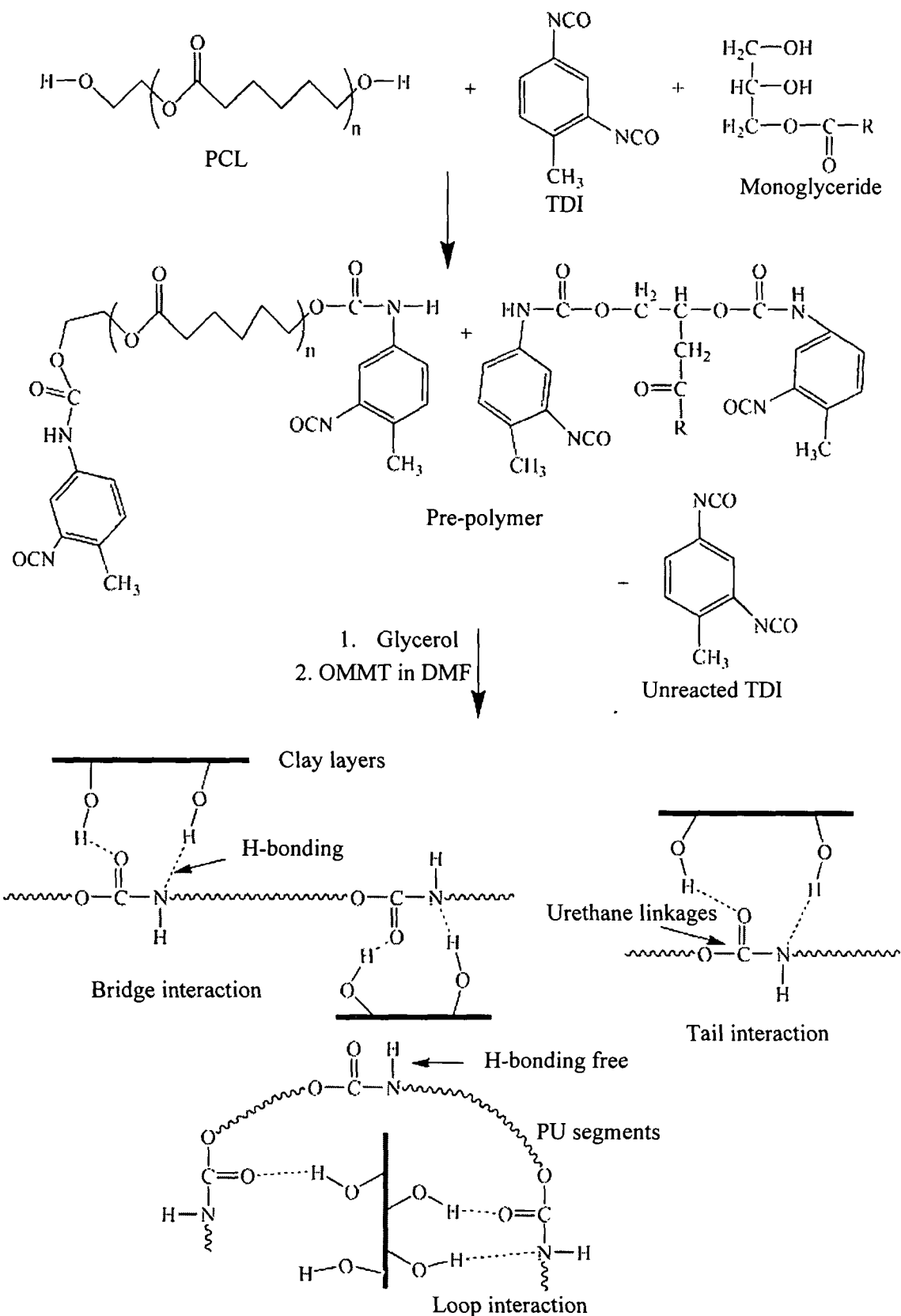
5.3.5. Mechanical Properties

The mechanical properties of the nanocomposites are tabulated in the Table 5.2. The tensile strength of the nanocomposites was found to be increased with the increase of OMMT content. This is because of the reinforcement of the matrix by the OMMT layers which increase the tensile strength.²⁵ In the nanocomposites the size of the nanofillers and the polymer chains are of similar length and develop unique interactions that give rise to optimal control of mechanical properties.²⁶ Further the crystallinity of semi-crystalline polymer matrix can be altered by the presence of nanofillers.^{27,28} In this

study the enhancement of crystallinity of the nanocomposites (as observed from the XRD and DSC study) in the presence of clay may also contribute to the improvement of mechanical properties. The highest tensile strength was obtained for MHPUNCI5 (48 MPa), may be due to high loading along with exfoliated structure formation as supported by the XRD and TEM results. The formation of exfoliated clay structure enhances the interface interactions through bridge, loop and tail linkages of the polymer chains with the clay layers via H-bonding and polar-polar interactions (Scheme 5.1). Thus the optimum strength was obtained for MHPUNCI5. Remarkably, the optimum tensile strength was observed for the nanocomposites MHPUNCE2.5 that prepared by *ex-situ* technique (Chapter 4, section 4.3.5) while this is MHPUNCI5 nanocomposite prepared by *in-situ* technique. The geometric confinement of the MHBPU matrix along with the presence of entanglement has also great impact on the development of mechanical properties in polymer nanocomposites.^{29,30} Generally the tensile strength of polymeric composites increases at an expense of its elongation at break value and it was observed in these nanocomposites also. This decrement is due to the restricted movement by clay layers in the matrixes by the above interactions. However, the decrement is not very high as the PCL moiety assists the deformation to a certain extent by its flexible chain.³¹

Another achievement observed in these nanocomposites was the retention of the flexibility (Table 5.2). The films can be easily bent up to 5 mm diameter of a parallel mandrel without any damage. The mechanical properties like impact and scratch hardness seen to be increased notably for all the nanocomposite films compared to the MHBPU. The same reason can also be implied in this case as described in Chapter 4, section 4.3.5.

The adhesive strength of the nanocomposites was investigated on wood substrate (Table 5.2). An increase of the strength with the loading of clay was observed. This may be due to the presence of large numbers of polar surface functionality of the hyperbranched polymer along with other polar groups in the systems. The increment of adhesive strength may be due to the strong interactions of polar hydroxyl, epoxy, urethane, ether and other polar groups of the MHBPU/clay system with the hydroxyl groups of the substrate.³²



Scheme 5.1: Proposed mechanism for interactions between clay and in-situ formed HBPU

5.3.6. Water Vapor Barrier Property

Many useful properties of PU systems are greatly influenced by water absorption phenomena by the PU films. Thus it is essential to study the water vapor loss of the closed system through the films. The barrier property of the clay nanocomposite films was enhanced due to the tortuous diffusion pathway offered by the matrix in the presence of nanoclay layers.³³ The Fig. 5.15 shows the significant decrease of water vapor loss with incorporation of clay compared to the MHBPU films. Along with the increase of path of penetration, the OMMT layers also increases the crosslinking density thereby reducing the free volume in MHBPU matrix. Further, OMMT also improved the phase morphology of the nanocomposites by forming a network structure, which in turn decreased the water absorption property.¹⁵

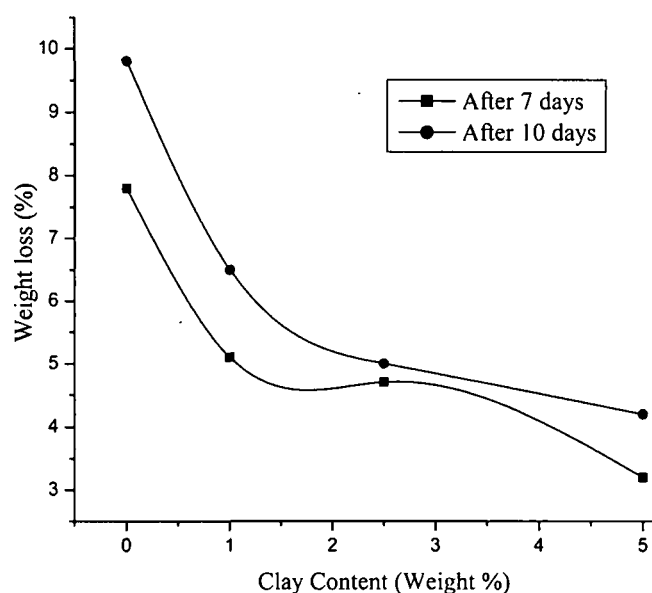


Fig. 5.15: Water vapor permeability of the MHBPU and nanocomposites

5.3.7. Thermal Properties

The thermal properties of the nanocomposites were studied by DSC and TGA. The T_g , T_m , ΔH_m for the nanocomposites are shown in the Table 5.3.

Table 5.3: Thermal properties and shape memory data of the nanocomposites

Code	T_g (°C)	T_m (°C)	ΔH_m (J/g)	Shape retention (%)	Shape recovery (%)
MHPUNCI1	-32	53	53.7	83.8	98.3
MHPUNCI2.5	-34	54	54.4	82.5	98.9
MHPUNCI5	-35	56	55.8	82.0	99.1

However, in case of T_g value, the distinct hump formation was not observed in the DSC curve and was taken after zooming the curve. Thus these T_g values give the

idea about the flexibility of the soft segment. It was observed that the T_g and T_m values were increased after nanocomposite formation. The T_g values increased from $-41\text{ }^\circ\text{C}$ (for pristine MHBPU) to $-32\text{ }^\circ\text{C}$ and the T_m values increased from $50\text{ }^\circ\text{C}$ (for pristine MHBPU) to $53\text{ }^\circ\text{C}$ with the addition of 1 weight% of clay. A miniature increase of the ΔH_m value with increase of the clay content are noticed (Table 5.3) which may result from the small enhancement of degree of crystallinity of the PCL moiety where the exfoliated clay are acting as a nucleating agent.³⁴ This result is in conformity with the observed XRD data.

The relative thermal stability of the nanocomposites was examined by TGA. Two step degradation pattern (Fig. 5.16) with an enhanced thermal stability of the nanocomposites compared to pristine polymer was observed.

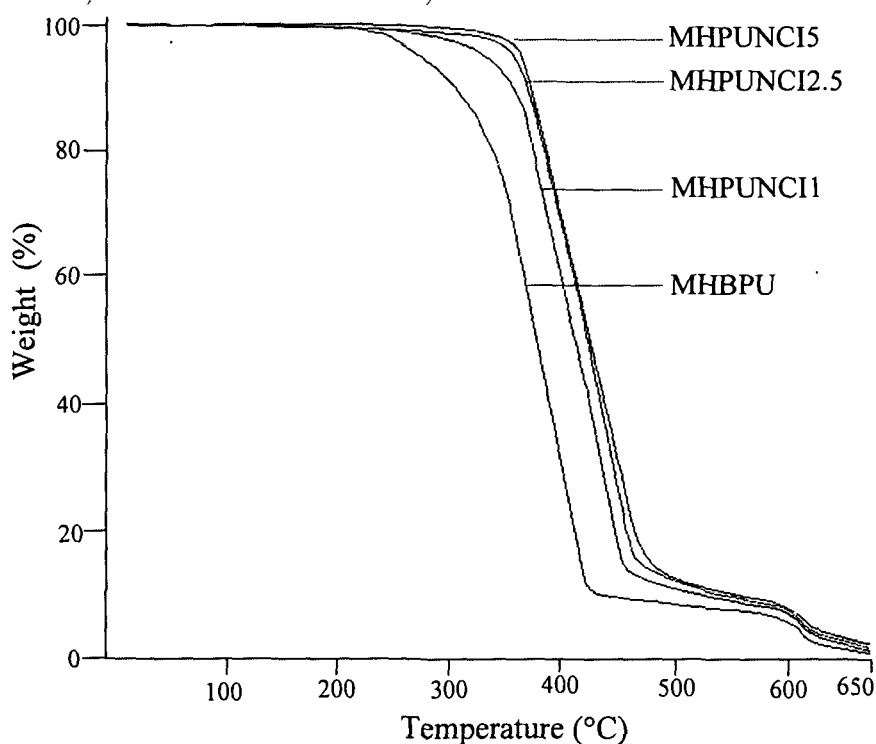


Fig. 5.16: Thermogravimetric curves of the nanocomposites

The characteristic thermal degradation temperatures are reported in the Table 5.4. $116\text{ }^\circ\text{C}$, $66\text{ }^\circ\text{C}$ and $33\text{ }^\circ\text{C}$ shifts of the $T_{1st\text{ ON}}$, $T_{1st\text{ MAX}}$ and $T_{2nd\text{ ON}}$ were observed with respect to the pristine polymer respectively at 5 weight% of clay loading. The same reason can also be put up here as described in Chapter 4, section 4.3.7. It is also noticeable that not only initial decomposition temperature increases but the weight residue (7-12 %) also increases (at $650\text{ }^\circ\text{C}$) with the increase of the clay content.

Table 5.4: Thermal stability data of the nanocomposites

Code	T _{1st ON} (°C)	T _{1st MAX} (°C)	T _{1st END} (°C)	T _{2nd ON} (°C)	T _{2nd MAX} (°C)	T _{2nd END} (°C)
MHPUNCI1	350	387	469	607	615	618
MHPUNCI2.5	354	407	465	612	625	629
MHPUNCI5	359	416	473	619	629	633

5.3.8. Shape Memory Study

The nanocomposites with different loading shows excellent shape recovery of 96-99%, out of which 90-95% is attained within about 2 min. The values of the shape memory properties of clay nanocomposites were given in Table 5.3. The increased stored energy due to the incorporation and uniform distribution of clay layers in the MHBPU matrix may be attributed to this excellent shape memory property.³⁵ The shape recovery increases with the increase of clay content which is due to increase of stored elastic strain energy by clay layers, so while reheating the samples, the film can obtain high recovery stress due to the release of stored elastic strain.³⁶

5.3.9. Chemical Resistance Test

Various chemical environments such as aqueous 10% NaCl, 20% EtOH, 5% HCl, 2% NaOH solutions and fresh water were used to investigate the effect of these chemical media on the nanocomposite films. An excellent chemical resistance was shown by all the nanocomposites compared to the pristine MHBPU for different media (Table 5.5). This may be due to the more compact structure and crosslinked structure of the matrix offered by the clay layers.¹⁷ The OMMT also created longer diffusion path way for the solvent molecules to penetrate the films.

Table 5.5: Chemical resistance in terms of percentage of weight loss in grams

Code	10% NaCl	20% EtOH	5% HCl	2% NaOH	Water
MHBPU	-0.022	-0.013	0.008	-0.035	0.016
MHPUNCI1	-0.012	-0.005	0.004	-0.021	0.009
MHPUNCI2.5	-0.007	-0.003	0.002	-0.023	0.011
MHPUNCI5	-0.004	-0.002	0.006	-0.022	0.014

5.3.10. Biodegradation Study

A noteworthy enhancement was found in the biodegradation pattern of the nanocomposites. The MHBPU and nanocomposite films were directly exposed to the bacterial degradation and the bacterial growth was monitored and evaluated with the help of McFarland Turbidity method. The *P. aeruginosa* of strain number MTCC 7814

and MTCC 7815 were used for biodegradation, as several member of the genus *Pseudomonas* have already been known for their ability to degrade polyester based PUs. The bacterial growth with respect to time is shown in the Fig. 5.17. The bacterial

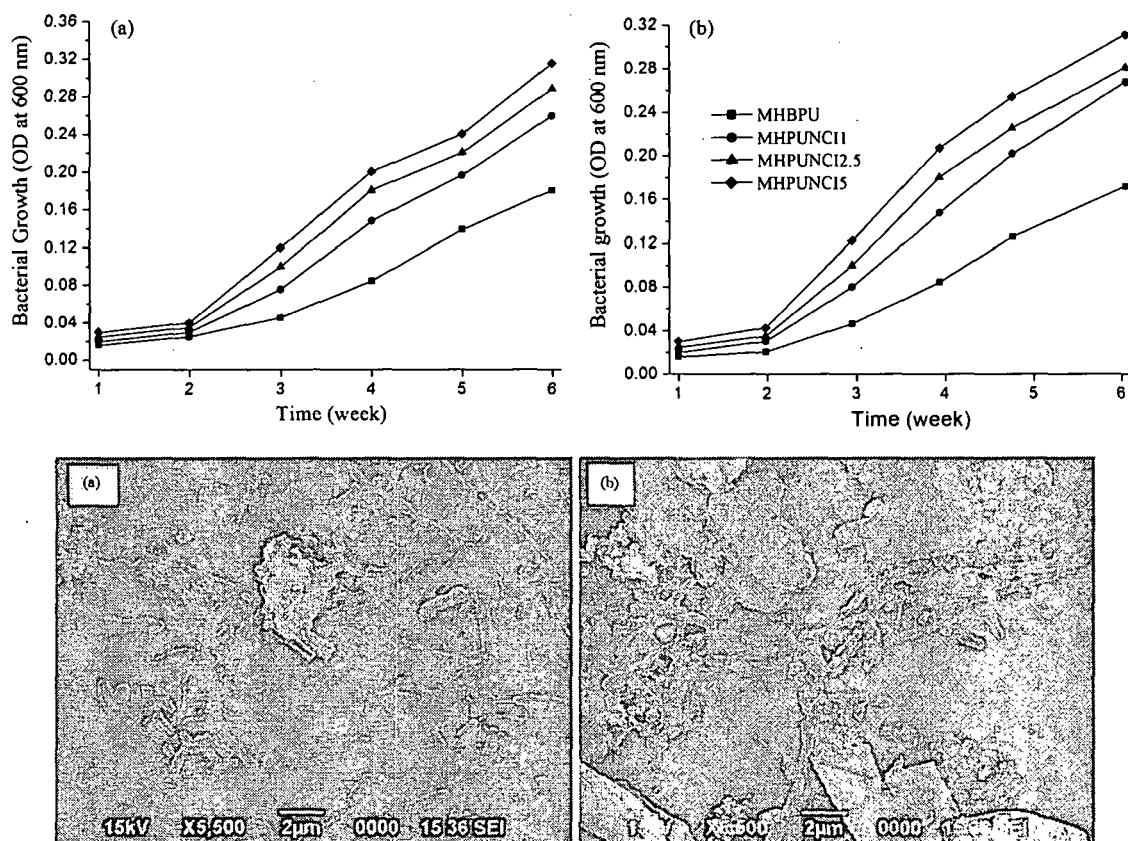


Fig. 5.17: Statistics for the growth of *P. aeruginosa* strain (a) MTCC 7815, (b) MTCC 7814 and SEM pictures of the degraded nanocomposite films: (a) MHPUNC11 and (b) MHPUNC15

growth was different for the nanocomposites than the pristine MHBPU. Several causes can be cited to account this biodegradation behavior of the nanocomposites. The biodegradation depends on the constituent of the PU, whether it is a polyether or polyester based, as polyester based PUs are more prompted to biodegradation.³⁷ Thus the vegetable oil based HBPU, which contains PCL as a constituent showed more degradation compared to the earlier report on conventional PU/clay nanocomposites from the same laboratory.³⁸ The effect of insertion of OMMT into the matrix can be seen from the bacterial growth pattern (Fig. 5.17). No significant improvement was noticed till two weeks. But after two weeks the nanocomposites showed tremendous biodegradability. This is attributed to the catalytic action of clay. The surface -OH groups of the clay layers take up water and cause heterogeneous hydrolysis which is aided by the microbes.³⁹ Further with the increase of clay content from 1 to 5 weight% the biodegradation rate was found to be increased, which implied the role of clay on

biodegradation. Jeong et al. also elucidated the higher biodegradation rate with the increase of MMT in the PCL based PU nanocomposites.⁴⁰ They ascribed, this biodegradation is due to the less phase separated morphology after nanocomposite formation. The extent of biodegradation as well as bacterial growth can be visualized from the SEM images (Fig. 5.17). Although there are many reports on biodegradation of clay nanocomposites still there is a lack of well documented consensus for the biodegradation mechanism. The biodegradation may involve the binding of bacterial cells to the nanocomposites and formation of floc and subsequently degradation of the films. Thus the esterase and/or protease activities of the bacteria govern the rate of biodegradation.⁴¹ The different types of growth rate for the two bacterial stains were observed, in Fig. 5.17, which account the fact.

5.4. Conclusions

The above study showed the successful way of preparing *Mesua ferrea* L. seed oil based MHBPU/clay nanocomposites through *in-situ* preparative technique. The formation of nanocomposites significantly improved the performance characteristics like mechanical properties, thermostability, adhesive strength, shape memory behavior, chemical resistance, etc. without much affecting the impact resistance and ductility. Most of the properties of the nanocomposites prepared by *in-situ* technique are superior to that of the nanocomposites prepared by *ex-situ* technique as described in the earlier chapter. The rheological study also patronized this observation. Thus the study indicates the potentiality of these materials as advanced materials in various fields of applications.

References

1. Meng, X. et al. A strategy of fabricating exfoliated thermoplastic polyurethane/clay nanocomposites via introducing maleated polypropylene. *Polymer* **50**, 3997-4006 (2009)
2. Xia, H.; Shaw, S.J.; Song, M. Relationship between mechanical properties and exfoliation degree of clay in polyurethane nanocomposites. *Polym. Int.* **54**, 1392-1400 (2005)
3. Ingrosso, C.; Panniello, A.M.; Comparelli, R.; Curri, M.L.; Striccoli, M. Colloidal inorganic nanocrystal based nanocomposites: Functional materials for micro and nanofabrication. *Materials* **3**, 1316-1352 (2010)

4. Rehab, A.; Akelah, A.; Agag, T.; Shalaby, N. Preparation and characterization of polyurethane-organoclay nanocomposites. *Polym. Compos.* **28**, 108-115 (2007)
5. Salahuddin, N.; Abo-El-Enein, S.A.; Selim, A.; Salah El-Dien, O. Synthesis and characterization of polyurethane/organo-montmorillonite nanocomposites. *Appl. Clay Sci.* **47**, 242-248 (2010)
6. Pavlidou, S.; Papaspyrides, C.D. A review on polymer-layered silicate nanocomposites. *Prog. Polym. Sci.* **33**, 1119-1198 (2008)
7. Ray, S.S.; Okamoto, M. Polymer/layered silicate nanocomposites: A review from preparation to processing. *Prog. Polym. Sci.* **28**, 1539-1641 (2003)
8. Ortega, D. et al. Maghemite-silica nanocomposites: Sol-gel processing enhancement of the magneto-optical response. *Nanotechnol.* **19**, 475706(pp7) (2008)
9. Choi, M.Y. et al. Synthesis and characterization of *in situ* polymerized segmented thermoplastic elastomeric polyurethane/layered silicate clay nanocomposites. *J. Appl. Polym. Sci.* **102**, 3048-3055 (2006)
10. Cao, X.; Lee, L.J.; Widy, T.; Macosko, C. Polyurethane/clay nanocomposites foams: Processing, structure and properties. *Polymer* **46**, 775-783 (2005)
11. Ding, Q. et al. Synthesis and characterization of polyurethane/montmorillonite nanocomposites by *in situ* polymerization. *Polym. Int.* **55**, 500-504 (2006)
12. http://en.wikipedia.org/wiki/McFarland_standards, (accessed on 15.02.2010).
13. Ash, R.J.; Mauck, B.; Morgan, M. Antibiotic resistance of gram-negative bacteria in rivers, United States. *Emerg. Infect. Dis.* **8**, 713-716 (2002)
14. Klugman, K.P.; Friedland, I.R.; Bradley, J.S. Bactericidal activity against cephalosporin-resistant *Streptococcus pneumoniae* in cerebrospinal fluid of children with acute bacterial meningitis. *Antimicrob. Agents Chemother.* **39**, 1988-1992 (1995)
15. Garrett, J.T.; Runt, J.; Lin, J.S. Microphase separation of segmented poly(urethane urea) block copolymers. *Macromolecules* **33**, 6353-6359 (2000)
16. Dai, X. et al. Study on structure and orientation action of polyurethane nanocomposites. *Macromolecules* **37**, 5615-5623 (2004)
17. Chen, T.K.; Tien, Y.I.; Wei, K.H. Synthesis and characterization of novel segmented polyurethane/clay nanocomposites. *Polymer* **41**, 1345-1353 (2000)
18. Dutta, S.; Karak, N. Effect of the NCO/OH ratio on the properties of *Mesua Ferrea* L. seed oil-modified polyurethane resins. *Polym. Int.* **55**, 49-56 (2006)

19. Dutta, S.; Karak, N. Synthesis, characterization of poly(urethane amide) resins from Nahar seed oil for surface coating applications. *Prog. Org. Coat.* **53**, 147-152 (2005)
20. Landry, V.; Blanchet, P.; Riedl, B. Mechanical and optical properties of clay-based nanocomposites coatings for wood flooring. *Prog. Org. Coat.* **67**, 381-388 (2010)
21. Decker, C.; Keller, L.; Zahouily, K.; Benharfi, S. Synthesis of nanocomposite polymers by UV-radiation curing. *Polymer* **46**, 6640-6648 (2005)
22. Karak, N. Polymer (epoxy) clay nanocomposites. *J. Polym. Mater.* **23**, 1-20 (2006)
23. Cole, K.S.; Cole, R.H. Dispersion and absorption in dielectrics I. Alternating current characteristics. *J. Chem. Phys.* **9**, 341-351 (1941)
24. Cox, W.P.; Merz, E.H. Correlation of dynamic and steady flow viscosities. *J. Polym. Sci.* **28**, 619-622 (1958)
25. Ganguly, A.; Bhowmick, A.K. Sulfonated styrene-(ethylene-co-butylene)-styrene/montmorillonite clay nanocomposites: Synthesis, morphology, and properties. *Nanoscale Res. Lett.* **3**, 36-44 (2008)
26. Crosby, A.J.; Lee, J.Y. Polymer nanocomposites: The "nano" effect on mechanical properties. *Polym. Rev.* **47**, 217-229 (2007)
27. Krikorian, V.; Pochan, D.J. Unusual crystallization behavior of organoclay reinforced poly(L-lactic acid) nanocomposites. *Macromolecules* **37**, 6480-6491 (2004)
28. Chen, T.K.; Tien, Y.I.; Wei, K.H. Synthesis and characterization of novel segmented polyurethane/clay nanocomposite via poly(ϵ -caprolactone)/clay. *J. Polym. Sci., Part A: Polym. Chem.* **37**, 2225-2233 (1999)
29. Bansal, A. et al. Quantitative equivalence between polymer nanocomposites and thin polymer films. *Nat. Mater.* **4**, 693-698 (2005)
30. Starr, F.W.; Schroder, T.B.; Glotzer, S.C. Molecular dynamics simulation of a polymer melt with a nanoscopic particle. *Macromolecules* **35**, 4481-4492 (2002)
31. Lepoittevin, B. et al. Poly (ϵ -caprolactone)/clay nanocomposites prepared by melt intercalation: Mechanical, thermal and rheological properties. *Polymer* **43**, 4017-4023 (2002)
32. Rahman, M.M.; Yoo, H.J.; Mi, C.J.; Kim, H.D. Synthesis and characterization of waterborne polyurethane/clay nanocomposite- Effect on adhesive strength. *Macromol. Symp.* **249-250**, 251-258 (2007)
33. Osman, M.A.; Mittal, V.; Morbidelli, M.; Suter, U.W. Polyurethane adhesive nanocomposites as gas permeation barrier. *Macromolecules* **36**, 9851-9858 (2003)

34. Chen, B.; Evans, J.R.G. Poly(ϵ -caprolactone) - clay nanocomposites: Structure and mechanical properties. *Macromolecules* **39**, 747-754 (2006)
35. Rana, S.; Karak, N.; Cho, J.W.; Kim, Y.H. Enhanced dispersion of carbon nanotubes in hyperbranched polyurethane and properties of nanocomposites. *Nanotechnol.* **19**, 495707(pp8) (2008)
36. Ni, Q.Q.; Zhang, C.S.; Fu, Y.; Dai, G.; Kimura, T. Shape memory effect and mechanical properties of carbon nanotube/shape memory polymer nanocomposites. *Compos. Struct.* **81**, 176-184 (2007)
37. Chandra, R.; Rustgi, R. Biodegradable polymers. *Prog. Polym. Sci.* **23**, 1273-1335 (1998)
38. Dutta, S.; Karak, N.; Saikia, J.P.; Konwar, B.K. Biocompatible epoxy modified bio-based polyurethane nanocomposites: Mechanical property, cytotoxicity and biodegradation. *Bioresour. Technol.* **100**, 6391-6397 (2009)
39. Bordes, P.; Pollet, E.; Averous, L. Nano-biocomposites: Biodegradable polyester/nanoclay systems. *Prog. Polym. Sci.* **34**, 125-155 (2009)
40. Jeong, E.H. et al. Effective preparation and characterization of montmorillonite/poly(ϵ -caprolactone)-based polyurethane nanocomposites. *J. Appl. Polym. Sci.* **107**, 803-809 (2008)
41. Howard, G.T. Biodegradation of polyurethane: A review. *Int. Biodeter. Biodegr.* **49**, 245-252 (2002)

CHAPTER 6

Highly branched poly(amido amine) modified clay/MHBPU nanocomposites

6.1. Introduction

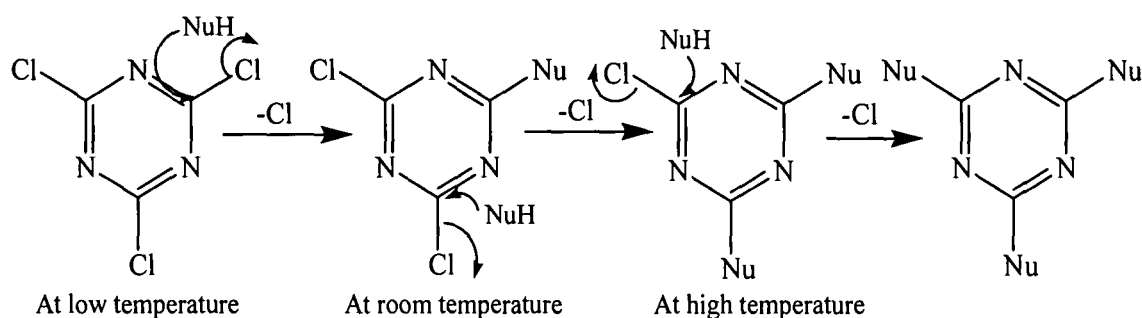
PU/clay nanocomposite is one of the hottest research topics in the domain of material science over the last two decades for their fascinating properties as described in Chapter 1. The restricted conformational degree of freedom of the polymer chains in the nanocomposites as imposed by the clay layers highly altered the chain dynamics. As a consequence, the polymer chains form a large volume fraction of the nanocomposite in the nano-confined environment and the overall properties behave in an unusual manner.¹ There has been considerable and rising interest in the study of PU/MMT nanocomposites, because of the high stiffness and high aspect ratio (100-1000) along with high swellability and ease of surface modification either by chemical or physical means of the MMT clay.^{2,3} The parameters such as state of dispersion of fillers, alignment and the ability to transfer the interfacial stress from polymer to filler etc. have great impact on the optimization of the properties of these nanocomposites.⁴ On the other hand, these factors depend on the ease of polymer chains insertion into the interlayer galleries of MMT and thus proper modification of the MMTs has crucial role in tuning the desired properties of PU/MMT nanocomposites. Therefore MMT is generally modified to render the hydrophobicity to the hydrophilic MMT before nanocomposite formation. In this regard, alkylammonium and alkylphosphonium are widely used to modify MMT in order to achieve the exfoliated structure of the nanocomposites.⁵ These organic cations lower the surface energy of the clay and enhance the wettability of clay with polymer.⁶ For further enhancement of the properties of the nanocomposites, the alternate functional modifiers are also being used.⁷ There have been lots of reports on PU/OMMT nanocomposites using different type of amine for modification of MMT.⁸⁻¹⁰ These include aliphatic primary, tertiary, quaternary amines and oligomeric amine derivatives. In all the modification processes, it has been observed that the nature of amine compounds, length of alkyl chain etc. also influence the ultimate properties of the nanocomposites.¹¹ Xiong et al. described the

Parts of this work have been published in *Mater. Chem. Phys.* 2010

(DOI:10.1016/j.matchemphys.2010.06.002)

improvement of thermal stability and modulus of the aromatic amine modified MMT/PU nanocomposites.¹² Bhowmick and co-workers had shown distinctive differences between the properties of PU/modified MMT nanocomposite and PU/unmodified MMT nanocomposites.⁴ They observed improvement in tensile strength, thermal stability, storage modulus and adhesive properties of the modified MMT nanocomposite over the pristine PU. Thus proper modified clay may lead to the polymer nanocomposites with desired level of property.

Interestingly it has been observed that in the case of aromatic nucleophilic substitution reaction of s-triazine based cyanuric chloride ($C_3N_3Cl_3$) (CYC), the chemoselectivity can be controlled with respect to parameters such as temperature and the nature of nucleophiles $[(Nu)_x, x = 1, 2 \text{ and } 3]$. Thus it may produce branched macromolecules by a single step process as given in Scheme 6.1. It is also significant to enlighten the fact that CYC is commercially available and a very inexpensive reagent, which make it's more attractive utilization. The s-triazazine based highly branched polymers are known for their interesting physical, chemical and thermal properties.^{13,14} Therefore it is expected that the insertion of such moiety into the MMT layers and their nanocomposites would lead to the genesis of high performance materials. It is to be worth noted here that though a plethora of reports described the effect of different type of amine modification of MMT, the effect of insertion of s-triazazine based highly branched amine into the MMT gallery is not studied till now.



Scheme 6.1: Chemoselective reactivity of cyanuric chloride

Therefore in this chapter effect of insertion of s-triazazine based highly branched poly(amido amine) (HBPA) in OMMT layers and on MHBPU/clay nanocomposites is reported. The characterization and properties of MHBPU/modified OMMT nanocomposites are also described here. Thus this chapter primarily focuses on the mode of modification and its effect on the properties of MHBPU/modified OMMT nanocomposites.

6.2. Experimental

6.2.1. Materials

CYC (Fig. 6.1) was purchased from Sigma Aldrich, Germany. It has m.p. 154-157 °C, purity $\geq 99.5\%$ and M_w 184.41 g/mol. It was recrystallized from chloroform before use. CYC is one of the important members of the triazine family. In this study it was used as a B_3 monomer.

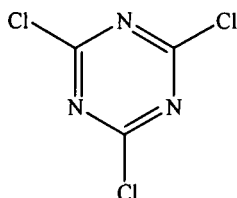


Fig. 6.1: Structure of cyanuric chloride

Urea (Fig. 6.2) was purchased from Merck, India. It has m.p. 132-135 °C, purity $\geq 99.5\%$ and M_w 60.06 g/mol. Interestingly, the urea was known to be the first natural compound to be synthesized artificially using inorganic compounds- a scientific breakthrough. Here, it was used as the A_2 monomer. Urea is very cheap and nontoxic chemical and therefore handling is very easy.

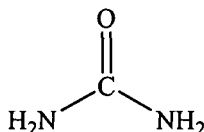


Fig. 6.2: Structure of urea

Diisopropylethylamine (DIPEA) (Fig. 6.3) was obtained from Merck, India. The compound has purity $\geq 98\%$ and M_w 410.52 g/mol. It was used as received. It is strong base and used as HCl scavenger.

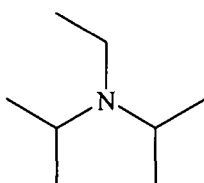


Fig. 6.3: Structure of diisopropylethylamine

N,N' -dimethylacetamide (DMAc) was purchased from Merck, India. Its purity is 99.7% with 0.1% water and 0.12% free acid as impurities. It has F_w 87.12 g/mol, density 0.940-0.942 g/mL and b.p. 164-166 °C. This was purified by the same procedure like DMF as described in the Chapter 2, section 2.2.1. and was kept in an amber bottle with 4A type molecular sieves. DMAc was used as the solvent.

Monoglyceride of *Mesua ferrea* L. seed oil was prepared as described in Chapter 2, section 2.2.2.1. Other chemicals like PCL, glycerol, TDI, DMF, epoxy resin, hardener and OMMT were of same specifications (as described in Chapter 4, section 4.2.1.) and were used without further purification.

6.2.2. Instruments and Methods

The FTIR, XRD, SEM, TEM, TGA and DSC analyses were carried out using the same instruments and conditions as mentioned in Chapter 4, section 4.2.2. The ¹HNMR and inherent viscosity of the HBPAAs were evaluated with the help of the same instruments and methods as mentioned in Chapter 2, section 2.2.2. The measurements of impact resistance, hardness and bending tests were performed according to the standard methods as reported earlier (Chapter 2, section 2.2.2.). The mechanical and rheological properties were evaluated as per the methods mentioned in the Chapter 4, section 4.2.2. The used ultrasonicator is of same specification as described in Chapter 3, section 3.2.2.

The flame retardancy was tested by the measurement of limiting oxygen index (LOI) value with the help of flammability tester as per the ASTM D 2863-77 method. UL 94 test method was also used to measure the flame retardancy of the nanocomposites.¹⁵ The samples were cut into pieces of size 25.4 x 7.6 x 0.1 cm³ and were mounted vertically in such a way that the gap between the specimen and the surgical cotton placed directly below the specimen was 30.5 cm. A flame was then applied to the center of the lower edge of each specimen at an angle of 45° for 10 s. A total of five tests were done for each specimen.

6.2.2.1. Synthesis of Highly Branched Poly(amido amine)

1.80 g (0.03 mol) of urea and 2.59 g (0.02 mol) of DIPEA in 40 mL DMAc were solubilized in a three neck round bottom flask equipped with a pressure equalizing funnel, a condenser along with a drying tube and a N₂ gas inlet. N₂ gas was purged before the addition of urea. An amount of 3.69 g (0.02 mol) of CYC solution in 35 mL DMAc at a 10% (w/v) concentration level was added dropwise by the pressure equalizing funnel for about 0.5 h at 0-5 °C with constant stirring. The reaction mixture was stirred for another 2 h under the same conditions, followed by the raise of temperature to 30-35 °C. At this temperature, again 2.59 g of DIPEA was added in the reaction mixture and stirring was continued for another 2 h. Then the temperature was again raised to 80-85 °C and 2.59 g of DIPEA was added. The reaction was continued

for 2 h under the same condition. Finally reaction was stopped after 2 h of stirring at 100 °C. Then it was cooled and poured slowly with constant stirring in dichloromethane. The precipitate formed was separated by filtration and washed several times with water, methanol followed by acetone to remove the unreacted reagents. The collected product was dried under vacuum at temperature 40 °C for 48 h to get the dry powder of HBPAAs.

6.2.2.2. Preparation of HBPU and Its Modification by Epoxy Resin

The *Mesua ferrea* L. seed oil based HBPU was prepared by the same procedure as mentioned in Chapter 2, section 2.2.2.2. The modification of the prepared HBPU was carried out by the method described in Chapter 3, section 3.2.2.1.

6.2.2.3. Modification of OMMT by HBPAAs

Two different methods were adopted to modify the OMMT. In one method, 1.0 g of the synthesized HBPAAs was dissolved in 5 mL of DMF and mixed with a solution of OMMT (2.0 g) in 10 mL of DMF. The mixture was vigorously stirred for 4 h and finally sonicated for 10 min at amplitude of 30% and half cycle. A part of the modified clay was then dried at 50 °C for further study. In another method, 1.0 g of HBPAAs was dissolved in 20 mL mixture of ethanol and HCl (10:1 v/v) and refluxed for 1 h. Then 2.0 g of OMMT was added to the above mixture and refluxed for another 6 h. Then, the mixture was filtered and washed repeatedly with hot water for complete removal of Cl⁻ ions (as no precipitate was observed on addition of the 0.1 M AgNO₃). The modified clay was then dried under vacuum at 50 °C.

6.2.2.4. Preparation of Nanocomposites

The MHBPU nanocomposites with the modified OMMT were prepared by *in-situ* technique following the same procedure as described in Chapter 5, section 5.2.2.2. The cured films were denoted as MHPUMNC1, MHPUMNC2.5 and MHPUMNC5 correspond to the modified OMMT content of 1, 2.5 and 5 weight% respectively by sonication method and MHPUMNC2.5(E) correspond to the modified OMMT of 2.5 weight% by exchange process.

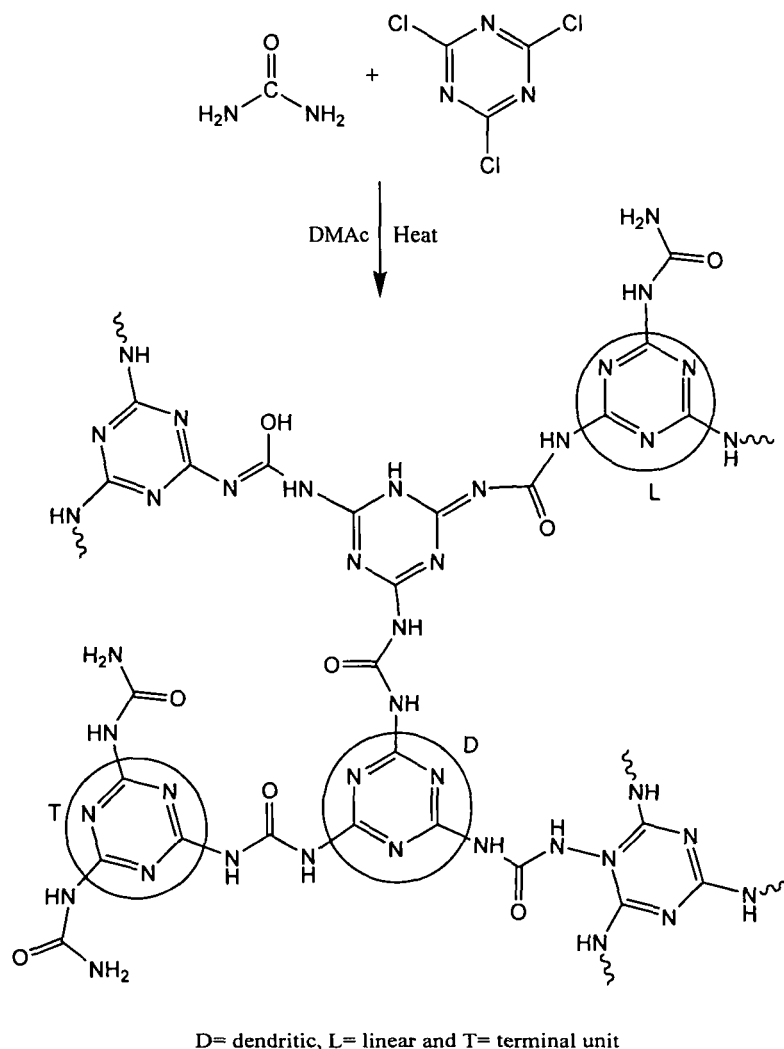
6.2.2.5. Sample Preparation for Performance Studies

The prepared nanocomposites were casted on different substrates for further studies by the same way as mentioned in Chapter 4 (section 4.2.2.3.).

6.3. Results and Discussions

6.3.1. Synthesis of HBPAA

The s-triazine based HBPAA was synthesized by $A_2 + B_3$ technique using urea (as A_2) and CYC (as B_3) for the first time as shown in Scheme 6.2. Both the CYC and urea are



Scheme 6.2: Synthesis of highly branched poly(amido amine)

very common and readily available chemicals. They undergo nucleophilic displacement polymerization reaction under appropriate conditions. The polycondensation reaction was carried out at three different temperature ranges as the reactivity of the three chlorine atoms of CYC was different.¹³ The highest reactivity is assigned to the first chlorine atom of the triazine moiety followed by the second chlorine atom, while the last one possesses the lowest reactivity for the passivation effect of amine substituent. Thus in this stage wise polycondensation reaction, the first chlorine atom was substituted at 0-5 °C, the second one substituted at 30-35 °C and the third at 80-100 °C. Further this stage wise fashion helped to prevent the gel formation. As it may be a problem in such synthesis. The 10% (w/v) CYC solution was slowly added to the urea solution of the same concentration in DMAc solvent and the mole ratio of $A_2 : B_3$ was

maintained at 3 : 2. The HCl gas, formed during the polymerization process, was trapped by using DIPEA as the scavenger. This promoted the reaction towards the forward direction.

6.3.2. Characterization of HBPA

The synthesized HBPA was characterized by various analytical as well as spectroscopic techniques. The HBPA is soluble in highly polar solvents like DMSO, DMF, NMP, DMAc and partially soluble in THF. Also it is soluble in acids like dilute aqueous HCl, acetic acid etc. The large number of surface amine groups and globular structure of the hyperbranched polymer render its high solubility. The density of the synthesized polymer was found to be 1.31 g/cc and it was light brown in color. The presence of rigid aromatic moiety and H-bonding (confirmed from FTIR) leads to this moderate density value. The XRD study revealed the amorphous nature of the polymer. This is the highly branched structure of the polymer that prevent from compactness. The inherent viscosity of HBPA was 0.18 dL/g. The globular like shape of the polymer renders its low solution viscosity.

The λ_{\max} of the HBPA in DMAc solvent was found to be 340 nm. This indicates the presence of aromatic structure with conjugation. The FTIR spectrum of the HBPA is given in the Fig. 6.4(a). The bands at 3452 and 3219 cm^{-1} are the

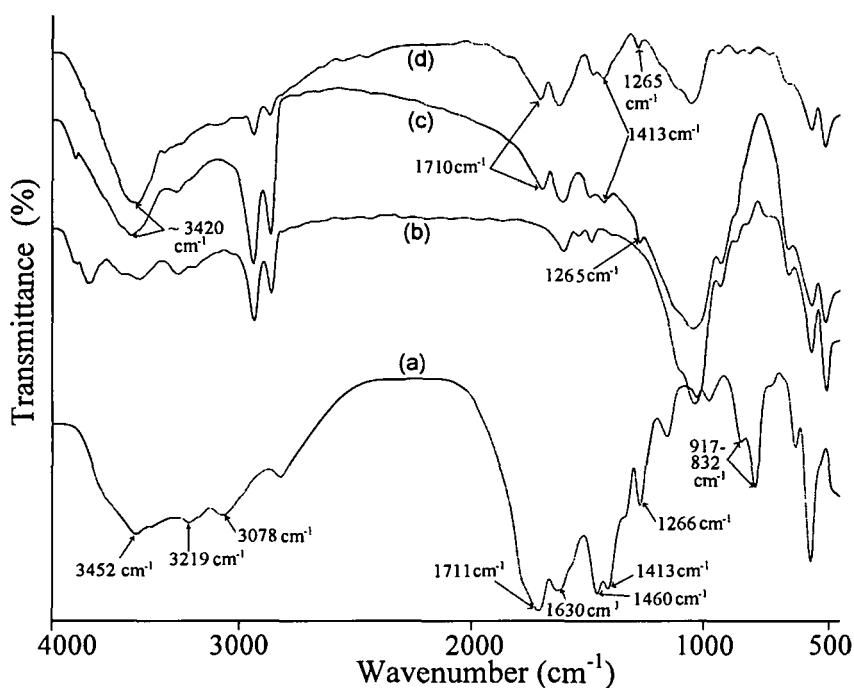


Fig. 6.4: FTIR spectra of (a) HBPA, (b) OMMT, (c) modified OMMT (sonicated) and (d) modified OMMT (exchanged)

coupling –NH stretching vibration of the primary amine. The band at 3078 cm^{-1} corresponds to the –NH stretching vibration of the secondary amine.¹⁶ The bands at 1711 and 1630 cm^{-1} are for –C=N (Amide III band) and –C=O stretching frequency of amide respectively. The –NH bending vibration for primary amine was observed at 1460 cm^{-1} while this band for secondary amine was enveloped by the –C=O stretching frequency. The –NH wagging bands for both the primary and secondary amine were seen at $917\text{--}832\text{ cm}^{-1}$ region.¹⁶ The presence of the triazine moiety in the hyperbranched structure can be confirmed from the bands at 1413 cm^{-1} (–C=N stretching vibration) and 1266 cm^{-1} (aromatic –C=N stretching vibration). The ^1H NMR study (Fig. 6.5) further confirmed the formation of hyperbranched structure as indicated by the

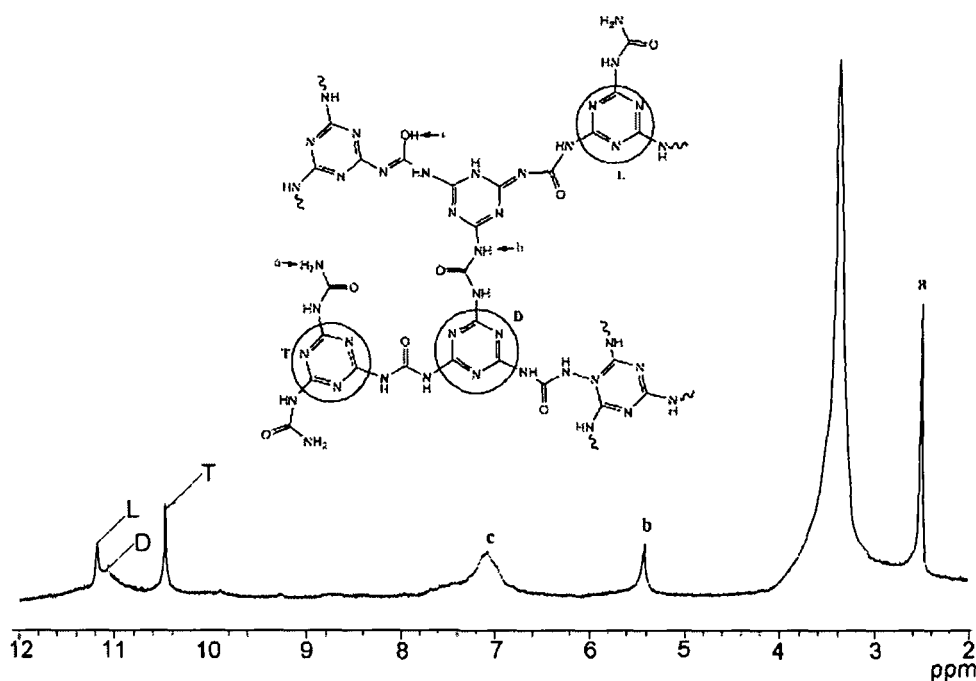


Fig.6.5: ^1H NMR spectrum of HBPAAs (*T*=terminal, *L*=linear and *D*=dendritic unit)

presence of different types of protons. The occurrence of three different units viz. dendritic, terminal and linear was confirmed from the three peaks of the secondary –NH protons of the hyperbranched polymer. The peak at $\delta = 10.5$ ppm is due to the –NH protons attached with the terminal unit. While the peak at $\delta = 11.3$ ppm corresponds to the –NH protons attached with the linear unit and the peak at $\delta = 11.1$ ppm appears for the –NH of the dendritic unit. The –NH₂ protons were observed at $\delta = 2.5$ ppm. The signal around $\delta = 5.2$ ppm corresponds to the amide –NH proton. The peak around $\delta = 3.6$ ppm is due to the DMSO solvent.¹⁷

Degree of branching (DB) of hyperbranched polymers is the scale of structural perfection and it is often determined by the Fréchet's equation¹⁸ equation (6.1) as-

$$\text{DB} = (D+T) / (D+T+L) \quad (6.1)$$

where D, T and L are the number of dendritic, terminal and linear units in the structure of the hyperbranched polymer respectively. Here, the DB was experimentally determined from the integration of the peak of the respective units in the ^1H NMR spectroscopy. The DB of the HBPAAs was found to be 0.52. The DB for linear polymer is close to zero, for hyperbranched polymer it is 0.5 and for dendrimers this value is 1.0. Thus the obtained value indicated the highly branched structure of the prepared polymer.

6.3.3. Modification of OMMT

The XRD diffraction patterns of OMMT and modified OMMT (both by sonicated and exchange processes) are shown in Fig. 6.6. The characteristic diffraction peak appeared at $2\theta = 4.17^\circ$, 3.01° and 3.31° for OMMT, modified OMMT (sonicated) and modified OMMT (exchanged) respectively. Thus the basal spacing increases from 2.11 nm to 2.93 nm in modified OMMT (sonicated) and 2.66 nm in modified OMMT (exchanged) as calculated by Bragg's equation. The sonication has a prominent effect on

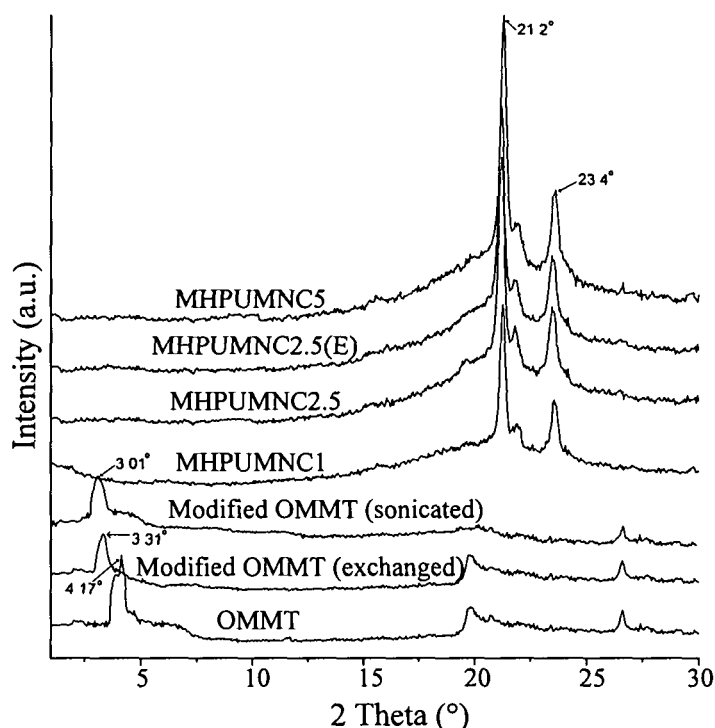


Fig. 6.6: XRD diffractograms of OMMT, modified OMMT and nanocomposites modification of the clay through forming efficient acoustic cavitations.^{19,20} It was observed that the peaks were broaden and less intense than the original peak. This reveals the increase of disordering of the clay layers.²¹ This is due to the non-entangled structure of HBPAAs that failed to open up the layers to a greater extent compared to the oligomeric diamine. But at the same time due to their globular shape, the ease of insertion into the clay galleries increases and the high surface functionality provides

sites for interactions with clay and matrix. Several literatures described the insertion of polymer chain with molecular weight higher than 2000 g/mol and resulted an increment of gallery distance up to 8 Å.^[8] Here in this investigation this value is 8.2 Å. Helical conformation or double layer planar zig-zag disposition models are used to explain such phenomena.²² This opening up of clay layers helped in ease of insertion of HBPU chain into the galleries. Also the surface end groups may provide more wetting capacity of HBPU to the clay through formation of physical interactions such as H-bonding, polar-polar interactions etc. as well as chemical bond formation compared to the conventional system. From the XRD analysis the sonication based modification was found to be more effective than the modified clay obtained by exchanged process and hence concentration dependence study was carried out by taking sonication modified OMMT.

The FTIR spectra of the OMMT and modified OMMT (both sonicated and exchanged) are shown in the Fig. 6.4(b, c and d). The broadening of the bands around 3420 cm⁻¹ is the results of the overlapping of the –OH band with the –NH vibration bands of primary and secondary amines.²³ The appearance of the new bands at 1701, 1413 and 1265 cm⁻¹ in the modified OMMT spectra correspond to the presence of –C=O of amide, –C=N stretching vibration of triazine moiety and aromatic –C=N stretching vibration in the clay layers. The marginal shift of the bands in comparison with the pure HBPA spectrum [Fig. 6.4(a)] is due to the formation of H-bonding between the surface amines to the –OH groups of the clay.

6.3.4. Characterization of the Nanocomposites

One of the interesting results was observed in curing study for the nanocomposites. While the nanocomposite with commercially modified MMT prepared by the *in-situ* technique discussed in Chapter 5, MHPUNCI2.5 needed 45 min, here MHPUMNC2.5 took only 30 min for curing. It was also noticed that with the increase of clay content the time required for curing was reduced. This may be due to the surface amine groups of the HBPA that took part in the crosslinking reaction and thus accelerated the process.

The formation of nanocomposites was first investigated by XRD analysis (Fig. 6.6). The diffraction peak for d₀₀₁ plane of the clay that appeared at 2θ = 3.01°, was diminished in the nanocomposites. This absence of Bragg scattering is an indication of delamination of the clay tactoids. The squeezing tendency²³ of the clay in the nanocomposites that resulted the intercalated structure was prevented by the HBPA.

Also the incorporation of the HBPA facilitates the compatibilizing ability of the MHBPU matrix to the clay by formation of different types of interactions such as H-bonding, polar-polar interactions etc. These interactions through bridge, loop and tail linkages of the polymer chains with the clay layers contributed to the formation of well dispersed clay layers. It is worth to note that the position of the two characteristic diffraction peaks of PCL moiety remain unaltered after nanocomposite formation with a trifle increment in the intensity. This enhancement can be explained in the same way as described in Chapter 5, section 5.3.7.

The FTIR spectra of the nanocomposites are given in Fig. 6.7. The increase of H-bonding with the incorporation of the polar bonds like urethane, epoxy etc. was the reason of shifting the band from 3420 cm^{-1} to 3430 cm^{-1} . With the increase of clay content this shifting was more as observed from the Fig. 6.7. Such behavior is also supported by other literatures.²⁴ The increase of intensity of the band $\sim 1666\text{ cm}^{-1}$ is due to the increase of $-\text{C}=\text{O}$ of amide linkages with the increase of clay content. The appearance of the characteristic bands at 525 and 1036 cm^{-1} corresponding Al–O and Si–O–Si stretching vibration that confirms the presence of clay in the systems as stated in the previous chapters. The indistinguishable spectra that were taken haphazardly from the nanocomposites convinced to state the uniform dispersion of modified OMMTs in MHBPU matrix.

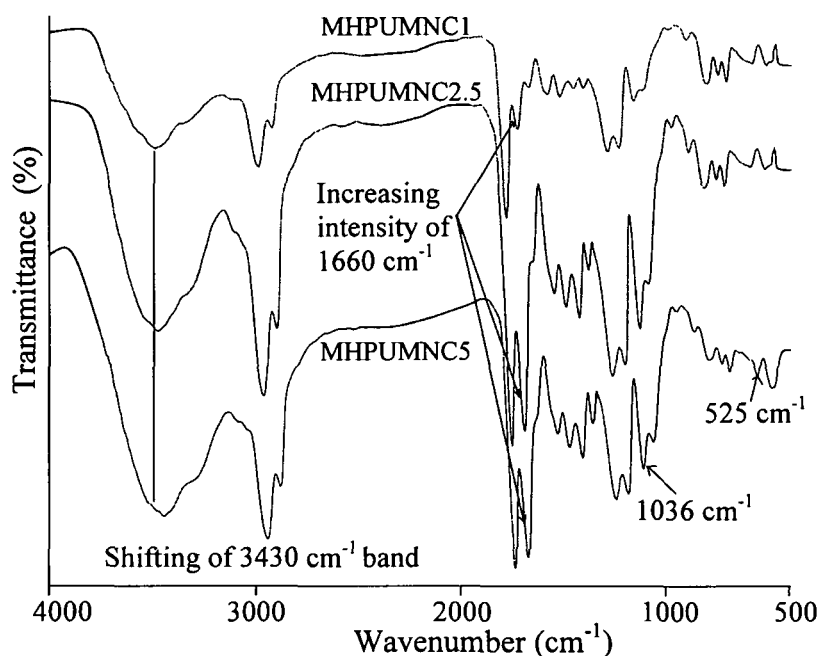


Fig. 6.7: FTIR spectra of the nanocomposites

To support the XRD results and to visualize the dispersion state of the clay in the matrix, the representative TEM micrographs of MHPUMNC1 and MHPUMNC5 are given in Fig. 6.8. The dark lines indicated by the arrow marks are the clay layers.

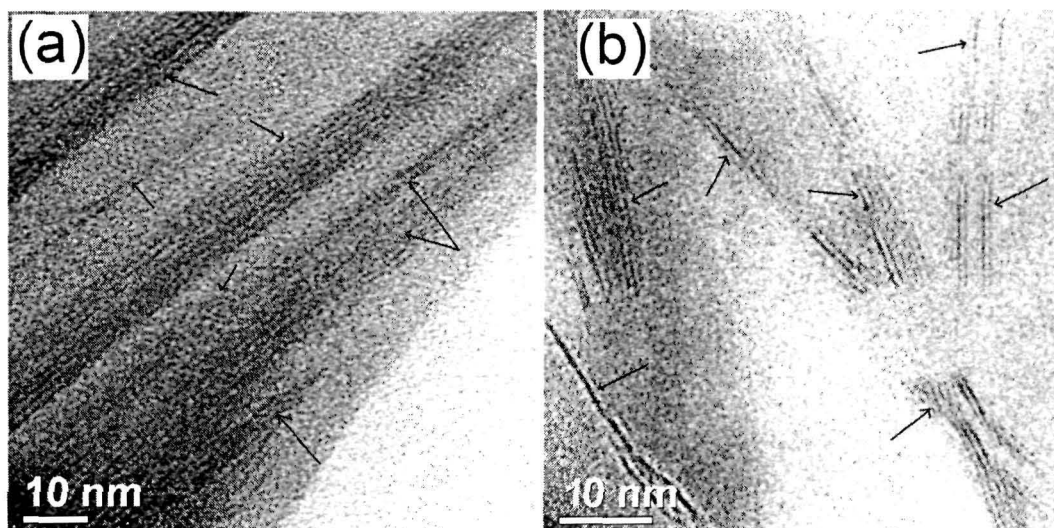


Fig. 6.8: Representative TEM images of (a) MHPUMNC1 and (b) MHPUMNC5

The micrographs proved the exfoliated structure of the clay in MHBPU matrix. This uniform dispersion of the clay layers is the reason for the disappearance of the diffraction peak at $2\theta = 3.01^\circ$ in the XRD diffractograms. Nonetheless it is appropriate to state here that, while the TEM images give local microscopic information the XRD analysis provides the macroscopic facts.

SEM is a valuable technique for examining the morphology of the systems. The SEM images of the fractured surface of the nanocomposites are given in the Fig. 6.9.

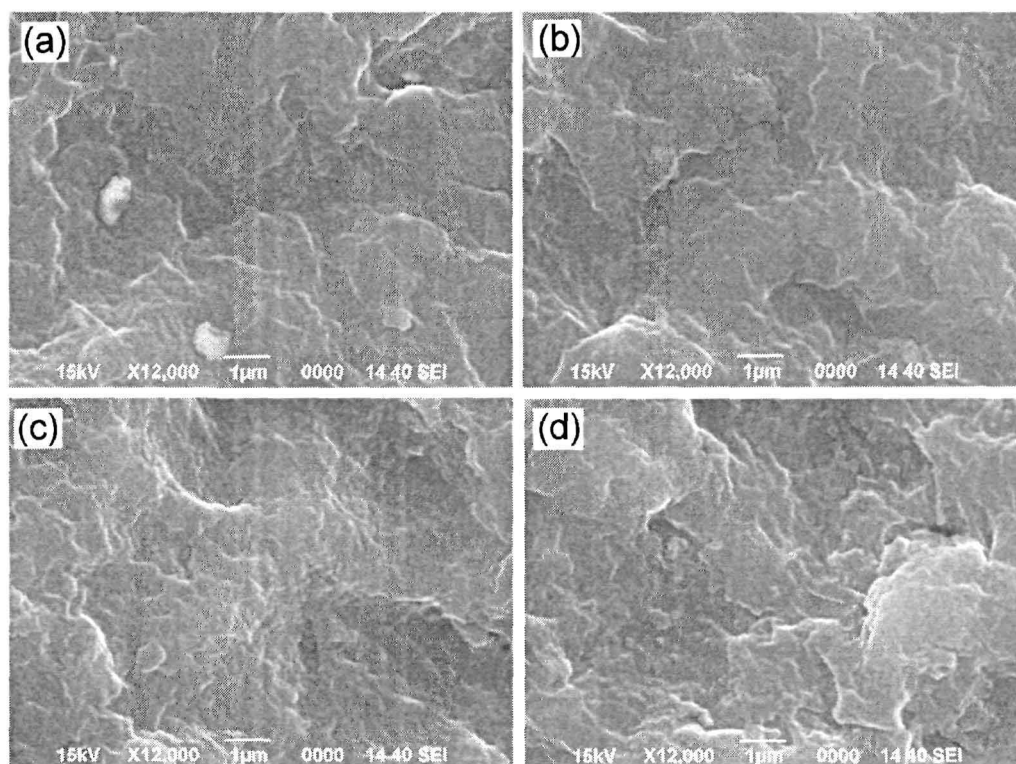


Fig. 6.9: SEM images of (a) MHPUMNC1, (b) MHPUMNC2.5, (c) MHPUMNC2.5(E) and (d) MHPUMNC5

The bumpy surface showed the uniform distribution of the clay layers. No agglomeration was observed in the micrographs which supports the TEM observations.

6.3.5. Rheological Properties of the Nanocomposites

The rheological properties of polymer/clay nanocomposites depend on the dispersion of clay in the matrix and the strength of the polymer clay interactions.²⁵ The G' , G'' and η^* of the nanocomposites in their melt state are shown in Fig. 6.10. The test was carried

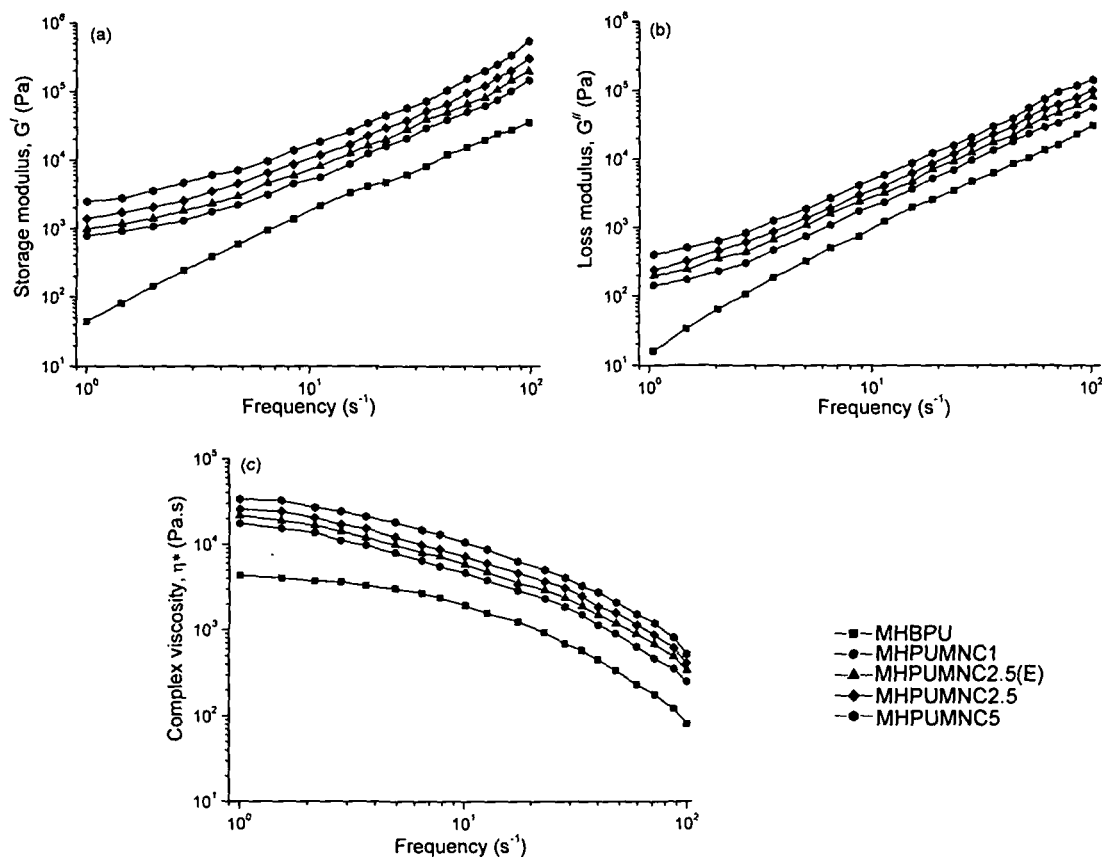


Fig. 6.10: Variation of (a) G' , (b) G'' and (c) η^* with frequency

out at 120 °C with varying frequency from 1-100 s^{-1} . All the nanocomposites showed apparent plateau for both G' and G'' at low frequencies [Fig. 6.10(a and b)]. The formation of the percolated structure of the anisotropic tactoids of clay platelets in the sluggish state or the intra frictional interactions amongst the anisotropic clay tactoids might be the cause of this pseudo solid-like behavior of the nanocomposites at low frequencies.²⁶ The η^* values were high in the low frequency region [Fig. 6.10(c)] and decreased in high frequency region. Thus oscillation-thinning behavior was observed for all the nanocomposites. The homogeneous dispersion of the clay patronized the retarded relaxation in terms of the frictional interactions between the clay tactoids and increased the complex viscosity at low frequencies. However, at high frequency region

the frictional interactions fail to resist the flow of the molten nanocomposites due to the large changes in the matrix mobility. This enhanced mobility in high frequency attributed to the effect of physical contacts between the nanoparticles and the matrix and hence decreases the complex viscosity. It was noticeable that the values of G' , G'' and η^* of the prepared nanocomposites were higher than that of the nanocomposites prepared by *in-situ* technique (Chapter 5, section 5.3.4.).

6.3.6. Mechanical Properties of the Nanocomposites

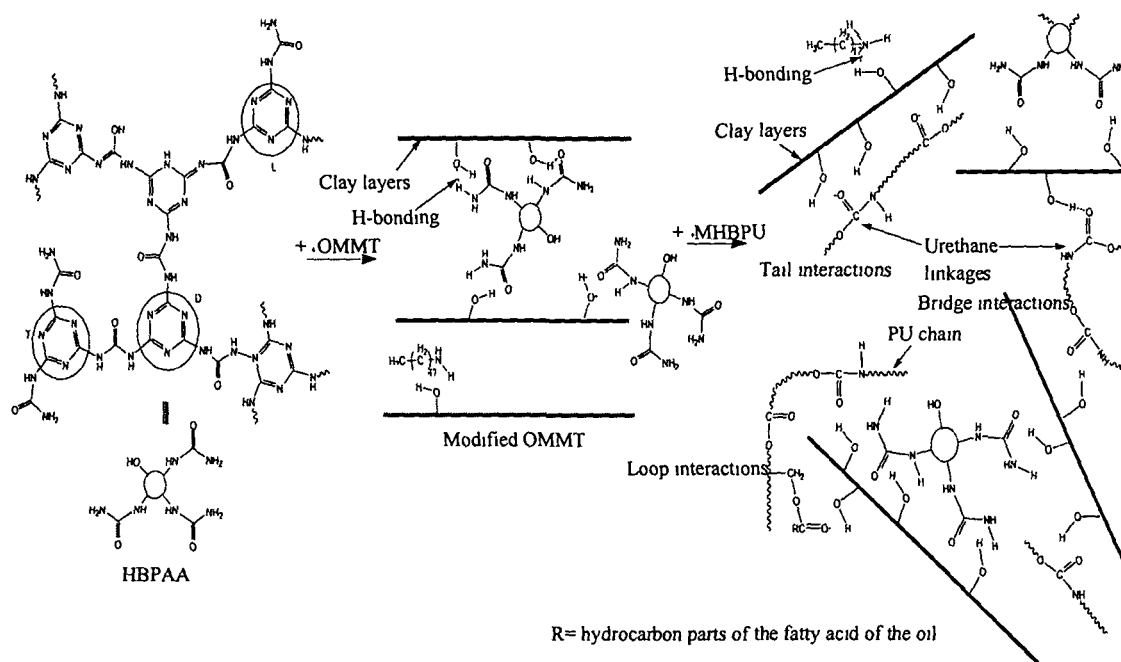
The effect of clay modification and concentration of the modified OMMT on the mechanical properties can be seen from the Table 6.1. It was observed that with the increased of modified OMMT the tensile strength increases and a maximum up to 1.7 times increment was achieved at 5 weight% loading compared to the MHBPU matrix. The improvement of tensile strength of the modified OMMT nanocomposites is well supported by various reports.²⁷ Due to the high aspect ratio and large surface area, the clay nanocomposites showed improved modulus of elasticity.¹² The inter layer distance of the OMMT increases due to the modification of clay by the HBPA. This helps in incorporation of more amount of HBPU chain into the clay tactoids. The degree of enlargement of clay layers consequently increases the effective filler volume fraction and hence polymer stiffness.²⁸ Also, the interface interactions in between clay and polymer matrix increased due to the presence of more functional groups after modification. These enhanced physico-chemical interactions result more wetting

Table 6.1: Mechanical properties, LOI values and UL 94 rating of the nanocomposites

Properties	MHPUMN C1	MHPUMN C2.5 (E)	MHPUMN C2.5	MHPUMN C5
Tensile strength (MPa)	42.0	46.1	48.2	51.4
Elongation at break (%)	460	432	430	422
Impact resistance (cm)	>100	97	>100	>100
Bending (dia. mm)	<5	<5	<5	<5
Scratch hardness (Kg)	8.7	9.4	9.1	9.8
UL94	V1	V1	V1	V1
LOI value	30	32	33	36

capability of the matrix (Scheme 6.3). Thus the applied stress can be effectively transferred to the OMMT. On the other hand, the increased stiffness reduces the elongation at break value of the nanocomposites (Table 6.1). Nonetheless the decrement was not so high due to presence of flexible PCL and long fatty acid chain of the *Mesua ferrea* L. seed oil as described in Chapter 4, section 4.3.5. These

nanocomposites showed enhanced impact resistance and scratch hardness compared to the pristine MHBPU and also to the nanocomposites prepared by *in-situ* technique (Chapter 3, Table 3.3 and Chapter 5, Table 5.2 respectively). The uniform distribution of the modified OMMT helped to absorb the applied energy throughout the matrix. The overall enhancement of the tensile strength of these flexible films is one of the factors attributed to these increments. The nanocomposite films were found to be flexible enough to bend the films up to 5 mm diameter of a parallel mandrel without any damage.



Scheme 6.3: Possible interactions of modified OMMT with the matrix

6.3.7. Thermal Properties of the Nanocomposites

The thermostability of the nanocomposites was determined by TGA (Fig. 6.11). It is evident that the degradation temperature of the matrix increased after nanocomposite formation. The well dispersed modified OMMT layers are acting as the physical barrier to the decomposed products for escaping from the matrix. The volatile products have to come across a torturous path way during the thermal decomposition. Further the thermal motion of the polymer chains was quite reduced by the increasing interfacial interactions between the clay and the matrix. This also helped in the improvement of thermal stability as stated in the previous chapters. The characteristic thermal decomposition temperatures are shown in the Table 6.2. The decomposition temperature was improved by 128 °C for MHPUMNC5 compared to pristine MHBPU (Chapter 3, Table 3.4). With the increase of clay content the thermal stability had also increased. The formation of more residual weight after thermal decomposition may also

lead to the enhancement of overall thermal stability of the nanocomposites. The 15 °C more increment of the decomposition temperature for MHPUMNC2.5 was achieved compared to the MHPUNCI2.5, nanocomposite prepared by *in-situ* technique (Chapter 5, Table 5.4). This was attributed to the high thermostability of the s-triazine ring and

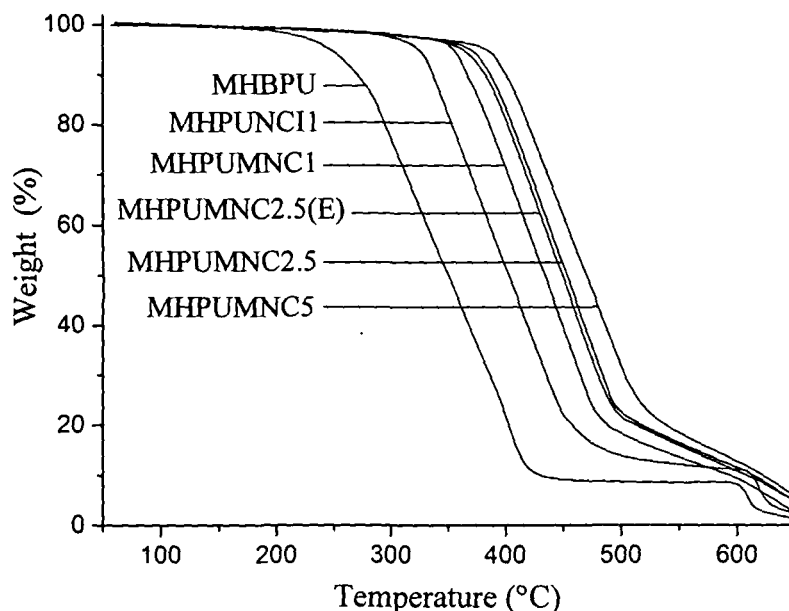


Fig. 6.11: TGA thermograms of the MHBPU and nanocomposites

the presence of nitrogen elements in the HBPAAs.¹⁴ Interestingly, while the MHBPU and the nanocomposites prepared by both *in-situ* and *ex-situ* techniques showed two step degradation patterns, the studied nanocomposites showed only one step degradation pattern (Fig. 6.11). This may be due to the incorporation of the s-triazine based HBPAAs modified OMMT into the matrix system. The formation of more interactions between the modified OMMT and matrix (as obtained from FTIR study) increases the crosslinking density and thereby bridging the polymer backbones together (as shown in Scheme 6.3). This results in the development of a “hard material” with restricted molecular mobility.

Table 6.2: Thermal properties of the nanocomposites

	MHPUMNC1	MHPUMNC2.5 (E)	MHPUMNC2.5	MHPUMNC5
T_{ON} (°C)	357	359	363	371
T_{MAX} (°C)	417	418	423	428
T_m (°C)	54	55	56	58
ΔH_m (J/g)	56.2	57.0	58.2	61.2

The thermal properties of the nanocomposites were also studied by DSC. The DSC thermograms of the nanocomposites are shown in the Fig. 6.12. The T_m of the nanocomposites was found to be increased from 53 °C to 58 °C for MHPUMNC5 (Table 6.2). Further the increase value of the ΔH_m with the increase of clay content

indicates the enhancement in the degree of crystallinity of the PCL moiety (Table 6.2). This result is also well agreement with the observed XRD data.

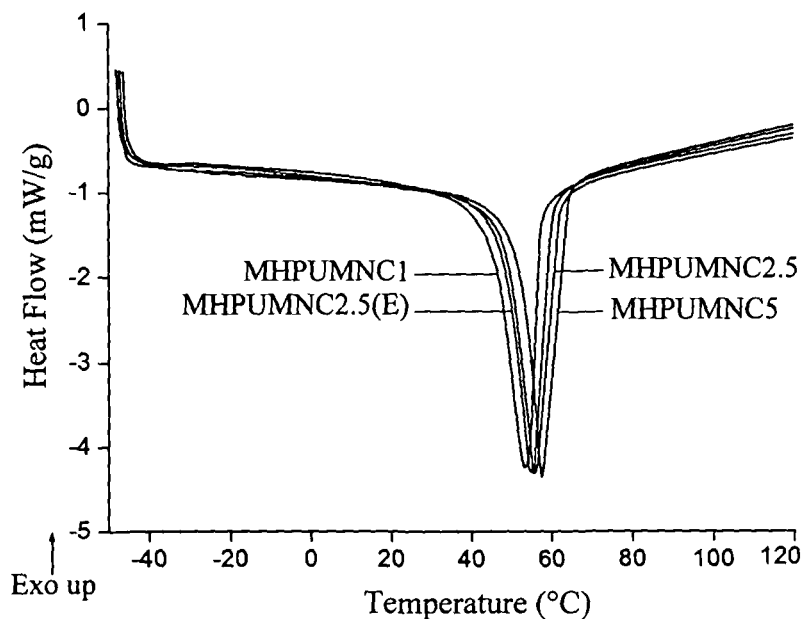


Fig. 6.12: DSC thermograms of the nanocomposites

6.3.8. Flame Retardancy of the Nanocomposites

The flame retardancy of the prepared nanocomposites was examined by UL94 and LOI tests. According to the UL94 rating the MHBPU matrix and the nanocomposites can be categorized as V2 and V1 rating respectively (Table 6.1). The LOI test results are also given in Table 6.1. The LOI value was also evaluated for the pristine MHBPU and found to be 27. The improvement of the flame retardancy of polymer/clay nanocomposites was explained in several literatures.^{29,30} During the combustion of the systems the organo-modified clay forms a barrier layer. Upon heating the clay layers can migrate and accumulate on the surface of the nanocomposites as the viscosity of the systems decreases with temperature. The protective layers prevent the diffusion of heat and oxygen to the material. Further, the migration of the clay layers are instigated by the formation of gas bubbles, initiated by the decomposition of both organo modifiers and the polymer chains. Moreover, the formed strong protonic catalytic sites on the surface of the nanocomposites on heating, can be catalyzed the formation of stable char residue. The char formation during the thermal degradation of the nanocomposites plays an important role in the improvement of the flame retardant behavior. The importance of modification of clay in improving the flame retardancy by formation of char residue was elucidated by Song et al.³¹ They explained the mechanism on the basis of Bronsted acid site on the modified MMT surface. The insulating layers of char residue retards the heat and oxygen transfer to the

nanocomposites to sustain the flame.³² The dispersion state of the clay layers is also crucial factor in determining the improvement of the flame retardancy.³³ The HBPA modified OMMT can disperse homogeneously due to the strong interactions (as discussed earlier). This explained higher flame retardancy of MHPUMNC2.5 than MHPUNCI2.5, nanocomposite prepared by *in-situ* technique (LOI value = 28 and UL94 rating is V2). Thus the formation of continuous OMMT-rich carbonaceous surface is more capable of preventing combustion.³⁰ With the increase of clay content the effect was more, as obvious.

6.4. Conclusions

The present chapter shows the successful way of preparing MHBPU/modified OMMT nanocomposites with varying clay content. The s-triazine ring containing HBPA was synthesized successfully by the A₂ + B₃ technique. The polymer was well characterized with the help of different spectroscopic and analytical techniques. The XRD analysis showed that the sonication based modification was more effective than the exchanged process. The well dispersed modified OMMT in the matrix can be observed from the FTIR, XRD, SEM and TEM analyses. The effect of modification of OMMT on the properties like physical, mechanical, thermal and flame retardancy of the nanocomposites was elucidated extensively. As the modification helps in distribution of clay layers in the matrix hence most of the properties of the nanocomposites are improved significantly.

References

1. Kaynak, C.; Nakas, G.I.; Isitman, N.A. Mechanical properties, flammability and char morphology of epoxy resin/montmorillonite nanocomposites. *Appl. Clay Sci.* 2009, **46**, 319-324
2. Huskic, M. et al. Modification of montmorillonite by cationic polyesters. *Appl. Clay Sci.* **43**, 420-424 (2009)
3. Tiwari, R.R.; Natarajan, U. Influence of organic modification on mechanical properties of melt processed intercalated poly(methyl methacrylate)-organoclay nanocomposites. *J. Appl. Polym. Sci.* **105**, 2433-2443 (2007)
4. Maji, P.K.; Guchhait, P.K.; Bhowmick, A.K. Effect of nanoclays on physico-mechanical properties and adhesion of polyester-based polyurethane nanocomposite, structure-property correlation. *J. Mater. Sci.* **44**, 5861-5871 (2009)

5. Paiva, L.B.de; Morales, A.R.; Diaz, F.R.V. Organoclays: Properties, preparation and applications. *Appl. Clay Sci.* **42**, 8-24 (2008)
6. Karak, N. Polymer (epoxy) clay nanocomposites. *J. Polym. Mater.* **23**, 1-20 (2006)
7. Herrera, N.N.; Letoffe, J.M.; Putaux, J.L.; David, L.; Bourgeat-Lami, E. Aqueous dispersions of silane-functionalized laponite clay platelets. A first step toward the elaboration of water-based polymer/clay nanocomposites. *Langmuir* **20**, 1564-1571 (2004)
8. Yoon, K.; Sung, H.; Hwang, Y.; Noh, S.K.; Lee, D. Modification of montmorillonite with oligomeric amine derivatives for polymer nanocomposite preparation. *Appl. Clay Sci.* **38**, 1-8 (2007)
9. Fornes, T.D.; Yoon, P.J.; Hunter, D.L.; Keskkula, H.; Paul, D.R. Effect of organoclay structure on nylon 6 nanocomposite morphology and properties. *Polymer* **43**, 5915-5933 (2002)
10. Salahuddin, N.; Abo-El-Enein, S.A.; Selim, A.; Salah El-Dien, O. Synthesis and characterization of polyurethane/organo-montmorillonite nanocomposites. *Appl. Clay Sci.* **47**, 242-248 (2010)
11. Kim, W.; Chung, D.; Kim, J.H. Effect of length of hydroxyalkyl groups in the clay modifier on the properties of thermoplastic polyurethane/clay nanocomposites. *J. Appl. Polym. Sci.* **110**, 3209-3216 (2008)
12. Xiong, J.; Zheng, Z.; Jiang, H.; Ye, S.; Wang, X. Reinforcement of polyurethane composites with an organically modified montmorillonite. *Compos. Part A: Appl. Sci. Manufact.* **38**, 132 (2007)
13. Mahapatra, S.S.; Karak, N. Hyperbranched aromatic polyamines with s-triazine rings. *J. Appl. Polym. Sci.* **106**, 95-102 (2007)
14. Mahapatra, S.S.; Karak, N. s-Triazine containing flame retardant hyperbranched polyamines: Synthesis, characterization and properties evaluation. *Polym. Degrad. Stab.* **92**, 947-955 (2007)
15. Gilman, J.W. Flammability and thermal stability studies of polymer layered-silicate (clay) nanocomposites. *Appl. Clay Sci.* **15**, 31-49 (1999)
16. Kalsi, P.S. *Spectroscopy of Organic Compounds*, 6th edn. (New Age International Publishers, New Delhi, 2004)
17. Bor ah, J.; Kar ak, N. Synthesis and characterization of a novel hyperbranched polyether. *Polym. Int.* **53**, 2026-2030 (2004)
18. Hawker, C.J.; Lee, R.; Frechet, J.M.J. One-step synthesis of hyperbranched dendritic polyesters. *J. Am. Chem. Soc.* **113**, 4583-4588 (1991)

19. Uchida, T.; Hamano, A.; Kawashima, N.; Takeuchi, S. Disaggregation and surface modification of nano-size diamond by ultrasound exposure: Relationships among acoustic intensity, disaggregation, and surface modification. *Electron. Commun. Japan* **90**, 10-18 (2007)
20. Seo, W.J. et al. Effects of ultrasound on the synthesis and properties of polyurethane foam/clay nanocomposites. *J. Appl. Polym. Sci.* **102**, 3764-3773 (2006)
21. Modesti, M.; Lorenzetti, A.; Bon, D.; Besco, S. Effect of processing conditions on morphology and mechanical properties of compatibilized polypropylene nanocomposites. *Polymer* **46**, 10237-10245 (2005)
22. Kim, M.S.; Jun, J.K.; Jeong, H.M. Shape memory and physical properties of poly(ethyl methacrylate)/Na-MMT nanocomposites prepared by macroazoinitiator intercalated in Na-MMT. *Compos. Sci. Technol.* **68**, 1919-1926 (2008)
23. Lee, H.T.; Lin, L.H.; Waterborne polyurethane/clay nanocomposites: Novel effects of the clay and its interlayer ions on the morphology and physical and electrical properties. *Macromolecules* **39**, 6133-6141 (2006)
24. Sreedhar, B.; Chattopadhyay, D.K.; Swapna, V. Thermal and surface characterization of polyurethane-urea clay nanocomposite coatings. *J. Appl. Polym. Sci.* **100**, 2393-2401 (2006)
25. Ren, J.; Casanueva, B.F.; Mitchell, C.A.; Krishnamoorti, R. Disorientation kinetics of aligned polymer layered silicate nanocomposites. *Macromolecules* **36**, 4188-4194 (2003)
26. Galgali, G.; Ramesh, C.; Lele, A. Rheological study on the kinetics of hybrid formation in polypropylene nanocomposites. *Macromolecules* **34**, 852-858 (2001)
27. Ha, S.R.; Ryu, S.H.; Park, S.J.; Rhee, K.Y. Effect of clay surface modification and concentration on the tensile performance of clay/epoxy nanocomposites. *Mat. Sci. Eng. A* **448**, 264-268 (2007)
28. Kornmann, X.; Thomann, R.; Mulhaupt, R.; Finter, J.; Berglund, L. Synthesis of amine-cured, epoxy-layered silicate nanocomposites: The influence of the silicate surface modification on the properties. *J. Appl. Polym. Sci.* **86**, 2643-2652 (2002)
29. Lewin, M. Reflections on migration of clay and structural changes in nanocomposites. *Polym. Adv. Technol.* **17**, 758-763 (2006)
30. Xiong, J.; Liu, Y.; Yang, X.; Wang, X. Thermal and mechanical properties of polyurethane/montmorillonite nanocomposites based on a novel reactive modifier. *Polym. Degrad. Stab.* **86**, 549-555 (2004)

31. Song, R.; Wang, Z.; Meng, X.; Zhang, B.; Tang, T. Influences of catalysis and dispersion of organically modified montmorillonite on flame retardancy of polypropylene nanocomposites. *J. Appl. Polym. Sci.* **106**, 3488-3494 (2007)
32. Zanetti, M.; Kashiwagi, T.; Falqui, L.; Camino, G. Cone calorimeter combustion and gasification studies of polymer layered silicate nanocomposites. *Chem. Mater.* **14**, 881-887 (2002)
33. Pastore, H.O.; Franche, A.; Boccaleri, E.; Marchese, L.; Camino, G. Heat induced structure modifications in polymer-layered silicate nanocomposites. *Macromol. Mater. Eng.* **289**, 783-786 (2004)

CHAPTER 7

HBPU/metal nanocomposites

7.1. Introduction

The expanding horizon of the nanotechnology has opened new alleys for application oriented utilities in many niches. In this context, metal nanoparticles have attracted considerable interest in recent years for their tremendous potential in the area of biomedical, catalysis, optoelectronics etc.¹⁻³ due to the unique size dependent properties. Among the different nanoparticles silver and iron nanoparticles have been occupying their own recesses especially in biomedical field.

The rising interest in the silver based medical products has endowed a myriad of new materials ranging from topical ointments to coated stents including bandages.⁴ A wide range of microorganisms are affected by the toxicity of silver nanoparticles though it is not at all harmful to higher animals. But a well documented consensus on the toxicity of silver nanoparticles is yet to clear. It may be the inadequacy of physical barrier to the nanoparticles of overdose diffusion into the cell or interactions of silver with sulphhydryl or thiol groups (-SH) of bacterial membranes lead to death of the same.⁵ The burgeoning medical devices containing silver nanoparticles such as silver impregnated catheters, wound dressings, contraceptive devices, surgical instruments, bone prostheses etc. have ample contribution to the healthcare sector. On the contrary, this facilitates the easy entry of the nanoparticles into the cells which was often overwhelmed by most of the literatures. Of course late, the adverse affect of the prolonged exposure of the nanoparticles towards human health is becoming the order of the day.⁶ Recently, AshaRani et al. unravelled the effect of silver nanoparticles on the cellular events.⁷ It was found that the metallic silver has a minimal health risk, but it becomes imperative once reaching at nanoscale.⁸ This can be minimized by embedding the silver nanoparticles in polymer matrix. On the other hand, for an ideal biomaterial, biodegradability is another important facet along with the biocompatibility as there is a continuous driving force to replace bio-stable biomaterials to biodegradable biomaterial in contemporary time.

Parts of this work have been published in

J. Macromol. Sci., Part A **46**, 1128-1135 (2009)

Polym. degrad. Stab. 2010 (DOI: 10.1016/j.polymdegradstab.2010.06.017)

Again, the iron is one of the most widely used noble metals that find applications in its colloidal or nanocrystalline form. The iron nanoparticles have attracted much attention⁹ because of their potential applications in many industrial and biological fields, such as mineral separation,¹⁰ heat transfer,¹¹ electro-photography,¹² radical scavenging¹³ etc. But the foremost challenge of the nanocrystalline superparamagnetic metals is to protect them from rapid environmental degradation.

Thus the above mentioned shortcoming can be minimized by incorporation of the nanoparticles in polymer matrices. The polymer metal nanocomposites have drawn special attention due to their (i) differences in physical and chemical properties, (ii) enhanced stability, (iii) film forming ability of polymer etc. In so far as the polymer matrices are concerned, hyperbranched polymer matrices have received considerable attention in recent times as they have better control over size, shape and structure of metal nanoparticles than that of conventional polymers.¹⁴ The highly functionalized three dimensional globular non-entangled structures of hyperbranched polymers can regulate the size, shape and stability of metal nanoparticles.¹⁵ Although, a number of reports described the utility of hyperbranched polymer as the matrix for metal nanoparticles but the vegetable oil derived matrices are really in scanty.

Again, a great deal of interest is being paid in the studies of polyaniline (PANI)/iron nanocomposites, because they possess excellent electric and magnetic properties which inclined them towards various applications such as in battery, microwave absorbing material etc.¹⁶ But it is difficult to prepare homogeneous and stable PANI/nanoparticle composites by conventional method as PANI is not easy to melt and also insoluble in most of the solvents.¹⁷ Owing to aforesaid intricacy, an *in-situ* chemical oxidative polymerization approach is adopted to synthesize PANI/iron based nanocomposites in presence of HBPU matrix.

Furthermore, it is worthwhile to note that the oxidizability and the antioxidant properties of polymer nanocomposite and polyphenolic compounds as found in a number of food items bear considerable similarity.¹⁸ The antioxidant characteristic of a molecule is commonly tested by using 2,2-diphenyl-1-picrylhydrazyl (DPPH) in methanol.

Therefore in this chapter, the preparation and characterization of HBPU/ silver and iron based nanocomposites are reported. The suitability of HBPU matrix for silver nanocomposites compared to the LPU as antimicrobial, biodegradable, biocompatible and thermostable material was also studied. The performance characteristics such as mechanical properties, antimicrobial activity, cytocompatibility and biodegradability of

the silver nanocomposites were investigated. Similarly, the thermal and magnetic properties of the iron based nanocomposite were also studied. In addition, the free radical scavenging capacity of this nanocomposite was too investigated against DPPH.

7.2. Experimental

7.2.1. Materials

Silver nitrate (AgNO_3) was purchased from Merck, India. It has m.p. 212 °C, minimum assay 99.8% and M_w 169.6 g/mol. It was used as received and utilized for preparation of silver nanoparticles.

Anhydrous iron (III) chloride (FeCl_3) was obtained from Merck, India. It has m.p. 300 °C, M_w 162.2 g/mol and minimum assay is 98%. Here it was used for the preparation of iron based nanoparticles. Due to its high moisture sensitivity the handling demands precaution.

Aniline was purchased from Merck, India. It has density 1.02 g/mol, M_w 93.13 g/mol, b.p. 181-185 °C and purity > 99.5%. Aniline was vacuum distilled prior to use and kept in amber bottle in dark place.

2,2-Diphenyl-1-picrylhydrazyl (DPPH) was purchased from HIMEDIA, India. It has M_w 394.33 g/mol. Here it was used for the free radical scavenging test.

Hydrochloric acid (HCl) was obtained from Merck, India and was used as received. It has F_w 36.45 g/mol, assay \geq 36.5-38% and the impurities present generally are sulfate (0.0005%), sulfite (0.001%), free chlorine (0.0001%) and heavy metals as lead (0.0005%), iron (0.0002%) and arsenic (0.0001%).

The bacterial strain *Staphylococcus aureus* (MTCC96), *Escherichia coli* (MG1655) and the yeast *Candida albicans* (clinical isolate) for antimicrobial test and the *P. aeruginosa* strains, MTCC 7814 and MTCC 7815 and other items used for the RBC hemolysis protection assay were taken from the Department of Molecular Biology and Biotechnology (Department of Biotechnology, DBT Centre, Government of India), Tezpur University.

Monoglyceride of *Mesua ferrea* L. seed oil was prepared as illustrated in Chapter 2, section 2.2.2.1. Other chemicals required in this study such as PCL, glycerol, TDI, DMF and methanol are of same specifications as described in the previous chapters. The necessary minerals for bacterial broth preparation in biodegradation study were obtained from Merck, India.

7.2.2. *Instruments and Methods*

The FTIR, UV, XRD, SEM, TEM, TGA and DSC analyses were carried out using the same instruments and conditions as mentioned in Chapter 4, section 4.2.2. The measurement of impact resistance, Shore A hardness, flexibility (bending) and mechanical properties were performed according to the standard methods as described in Chapter 2, section 2.2.2.

Magnetic properties were studied by vibrating sample magnetometer (VSM) Lakeshore 7410, Ohio, in the range of +20,000 G to -20,000 G at room temperature.

7.2.2.1. *Preparation of HBPU, LPU*

The *Mesua ferrea* L. seed oil based HBPU and LPU were prepared by the same procedure as described in Chapter 2, section 2.2.2.2.

7.2.2.2. *Preparation of Silver Nanocomposites*

Required amount of AgNO_3 solutions in DMF were prepared and added to the HBPU matrix at room temperature. The system was vigorously stirred for 2.5 h and UV-visible absorption spectra were taken time to time to observe the complete formation of silver nanoparticles. Finally, the nanocomposites were solution casted on inert substrates, followed by vacuum degassing and drying at 45 °C for 24 h for further testing and analyses. The nanocomposites were denoted as HBPUAg1, HBPUAg2.5 and HBPUAg5 corresponding to the AgNO_3 content of 1, 2.5 and 5 weight% respectively. Similarly the LPU based nanocomposite was denoted as LPUAg2.5 for 2.5 weight% of AgNO_3 content.

7.2.2.3. *Preparation of Iron Based Nanocomposite*

0.5 weight% of FeCl_3 (with respect to HBPU) was added in DMF solution of the HBPU matrix. 1 mL of distilled aniline (molar ratio of FeCl_3 : aniline was 1: 1.2) was dissolved in 4 mL water in the presence of dilute HCl and the solution was added dropwise in the above mixture. The yellowish mixture turned to black within 10 min of addition of aniline. The formation of the iron based nanoparticles was immediately confirmed from the UV-visible absorption spectrum. The solution was then casted on teflon sheet, followed by vacuum degassing and drying at 45 °C for 24 h for further testing and analyses. The nanocomposite was denoted as iron-HBPU-PANI.

7.2.2.4. *Antimicrobial Assay*

The antimicrobial tests of the silver nanocomposites were performed by the agar-well diffusion method according to Turkoglu et al. after some modifications.¹⁹ In this study the used bacterial strains were *Staphylococcus aureus* (MTCC96) and *Escherichia coli* (MG1655) and the yeast was *Candida albicans*. The bacteria were incubated at 37 °C for 24 h by inoculation into Mueller Hinton broth while *C. albican* was incubated at 30 °C for 48 h in Sabouraud dextrose broth. The culture suspensions were prepared by adjusting turbidity against 0.4-0.5 McFarland turbidity standard tubes. 100 µL of the cultured bacteria and yeast were injected into 20 mL of both the broth and mixed homogeneously in sterilized petri dishes (10 x 90 mm²). For the investigation of the antibacterial and antifungal activities, the samples were filtered through a 0.22 µm membrane filter. The above prepared samples at various concentrations were introduced directly into the wells (6 mm) in agar plates. Plates injected with the yeast cultures were incubated at 30 °C for 48 h and the bacteria were incubated at 37 °C for 24 h. At the end of the incubated period, minimum inhibitory concentration (MIC) for the respective samples was determined. The antimicrobial activities were performed in triplicates with positive control of Ampicillin (50 µg) for bacteria and Nystatin (10 µg) for *Candida*.

7.2.2.5. *Biodegradation of Silver Nanocomposites by Broth Culture Technique*

The biodegradation study of the silver nanocomposites was carried out by the same method as described in Chapter 5, section 5.2.2.4.

7.2.2.6. *RBC Hemolysis Protection Assay of Silver Nanocomposites for Cytocompatibility*

The RBC were separated from the blood and washed four times with 5 volume of phosphate buffer saline (PBS, pH 7.4). Centrifugation was done to collect the RBC at 3000g for 10 min at 25 °C. And a suspension of RBC with four volume of PBS was prepared. The nanocomposite films were sterilized by UV light for 1h in a sterile laminar air flow hood.

According to the Zhu et al.²⁰ with modifications, the RBC protection assay was carried out. In brief, 10 mg of nanocomposite was put into 2 mL of RBC suspension and a total concentration was kept 100 µM by adding H₂O₂. The system was incubated at 37 °C. About 200 µL of the suspension was taken out at an interval of 2 h and diluted to eight times by PBS. The monitoring was continued up to 6 h. The absorption was

measured at a wavelength of 540 nm taking the supernatant liquids obtained after centrifuging the collected samples at 3000g for 10 min at 25 °C. The PBS blank solution was taken as reference. The percentage of inhibition was measured using the equation (7.1).

$$\% \text{ RBC hemolysis inhibition} = \left[\frac{(A_{\text{H}_2\text{O}_2} - A_{\text{sample}})}{A_{\text{H}_2\text{O}_2}} \right] \times 100 \quad (7.1)$$

7.2.2.7. *Free Radical Scavenging Activity of Iron based Nanocomposite*

The free radical scavenging test of the iron based nanocomposite was performed according to the modified DPPH method for insoluble materials as reported by Serpen et al.²¹ The materials were washed with water to obtain neutral filtrate. 8×10^{-5} M of DPPH solution in methanol was prepared for this test. In a 3 mL quartz cuvette, 2.5 mL of DPPH solution and 50 mg of the test sample were combined and vortexed for 3 min to facilitate the surface reactions. The mixture was decanted and absorbance at 517 nm was monitored after 30 min of the total period. Analysis was carried out in triplicates and percent scavenging was calculated using the equation (7.2).

$$\text{Scavenging (\%)} = [1 - (A_{\text{DPPH after reacting with the sample}} / A_{\text{free DPPH}})] \times 100 \quad (7.2)$$

7.2.2.8. *Sample Preparation for Performance Studies*

The prepared silver nanocomposites were casted on different substrates for different studies in similar ways as mentioned in Chapter 3, section 3.2.2.2.

7.3. **Results and Discussions**

7.3.1. *Formation of Nanocomposites*

Nanoparticles have very high aspect ratio and possess very high surface energy, therefore have a great tendency to agglomerate.²² Polymers have the ability to prevent the agglomeration and precipitation of nanoparticles and thus they are being used as stabilizer for the nanoparticles in chemical synthetic route. The polymer nanocomposites can be easily processed and fabricated which expand their fields of utility. In this present study, the large number of surface hydroxyl groups along with the other polar groups like urethane, ether etc. of HBPU form stable complexes with the metal ions. This phenomena helps in uniform dispersion and better stability compared to non-polymeric system. Further the peculiar geometry and structural confinement of the hyperbranched polymer matrix provide more stabilization than the conventional polymers.¹⁵ Thus the HBPU metal nanocomposites may lead to the genesis of advanced materials with various utilities.

The silver nanoparticles were prepared by a simple and one pot *in-situ* polymerization technique. Here the same reaction medium, DMF is acting as a diluent as well as a reducing agent for silver ions. It was found that there was no effect on nature of atmosphere i.e., under open atmosphere or blanket of inert atmosphere on the nanocomposite formation.

The iron based nanoparticles were also formed by *in-situ* reduction of FeCl_3 in the HBPU matrix by aniline. The Fe^{3+} ions were reduced to Fe^0 while aniline simultaneously polymerized to polyaniline in the presence of matrix. The HBPU chains protected the surface of the Fe^0 nanoparticles from being agglomeration and at the same time reduced the oxidation of the metal nanoparticles by the oxygen in air and water after reduction. However, the complete preservation was not possible as observed from the XRD study (discussed later). The present stable iron/iron oxide decorated nanocomposite had the film forming ability along with other useful properties.

In both the cases, there was no need of any external reducing agent, which follows one of the principles of green chemistry.

7.3.2. Characterization of Silver Nanocomposites

Metal nanoparticles at a very finer dimension exhibit absorption bands or broad region of absorption in the UV-visible range. These bands are due to the excitation of plasmon resonance or inter band transition. So each type of metal nanoparticle has their characteristic absorption band at a particular wave length. The formation of silver nanoparticles was first observed by the change of color and UV-visible absorption spectra of the reaction medium. The color of the polymer solution changed from brown to black as the nanoparticle formation progressed. The UV absorption spectra of pristine and HBPU nanocomposites with varying amounts of silver are shown in Fig. 7.1(a). Increase of intensity with the increase of amount of silver salt was observed at 410-415 nm (λ_{max}) indicating formation of more Ag nanoparticles.²³ The peak at 400-420 nm (λ_{max}) is characteristic of silver surface plasmon resonance. Further, nature of peaks indicates size distribution of the nanocomposites in polymer matrix which can also be revealed from TEM micrographs (discussed later). A time evolution UV absorption study [Fig. 7.1(b)] showed that the peak at 410 nm started to appear after 30 min of addition of silver salt in the matrix. Similar type of observation was also explained by Cocca et al.²⁴ The intensity gradually increases and attained a steady state after 2.5 h. This indicates that the time for maximum conversion of silver nanoparticles need 2.5 h. From Fig. 7.1(a), a red shift of 4-5 nm in wavelength (λ_{max}) for LPU

nanocomposite compared to the HBPU nanocomposite was observed. This may be due to larger size of silver nanoparticles in LPU compared to HBPU matrix for the unique structural characteristic of the latter. This also may be due to greater interaction of silver particles with latter matrix (which is supported by IR data). The stability of the

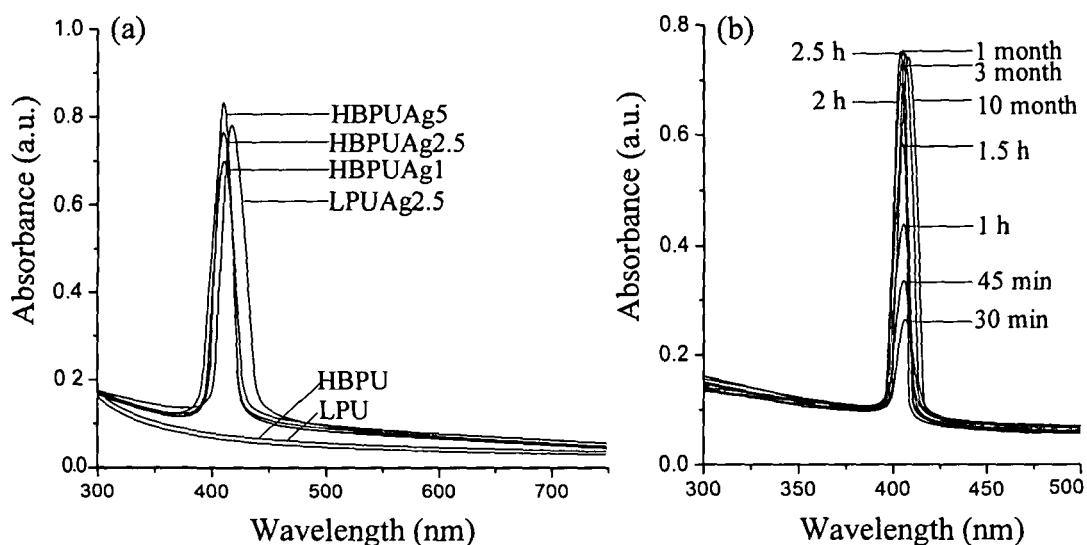


Fig. 7.1: UV-visible absorption spectra of (a) nanocomposites and pristine polymers, (b) time evolution curves starting from formation to the maximum stability period

silver nanoparticles in the nanocomposites was studied from the time profile UV absorption spectra [Fig. 7.1(b)]. Noticeably the shifting of wavelength occurs after 10 months due to initiation of agglomeration. This excellent stability is offered by the HBPU matrix for their inimitable confined structures.

The FTIR spectra of the nanocomposites are shown in Fig. 7.2. A noticeable

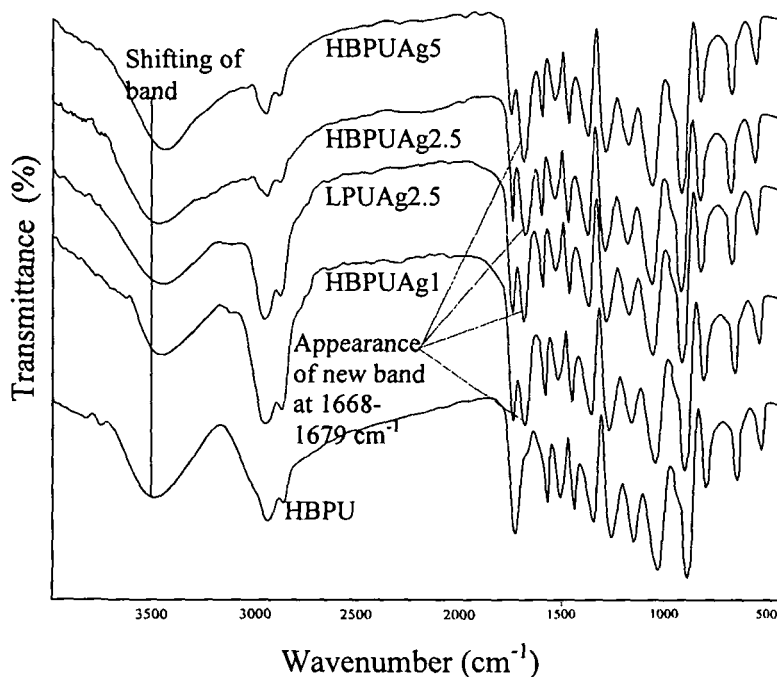


Fig. 7.2: FTIR spectra of the silver nanocomposites

change was observed in the region $1729\text{--}1679\text{ cm}^{-1}$ where the pristine HBPU showed only one band at 1729 cm^{-1} , but splits to two bands in the nanocomposites. The appearance of the bands at $1668\text{--}1679\text{ cm}^{-1}$ is due to the interactions (mainly H-bonding) of the silver nanoparticles with the --C=O , --NH and --CN stretching modes.²⁵ Further it was observed that the band intensity at 1730 cm^{-1} for HBPUAg5 was less than the others. This is due to the reduction of the extent of H-bonding between the hard and soft segment of the HBPU matrix by the more number of nanoparticles.²⁶ The shifting of the --NH absorption band from 3469 to 3454 cm^{-1} also supports this fact.

The XRD diffractograms of the nanocomposites are shown in Fig. 7.3. All the nanocomposites showed crystalline peaks for PCL at $2\theta = 21.2^\circ$ and 23.4° . The observed diffraction peaks at 38.5° , 44.9° and 64.8° imply the (110), (200) and (220) Bragg reflections of “fcc” structure of silver.²⁷ Thus the formation of silver nanoparticles can be confirmed from XRD study. An attempt was also taken to evaluate the average crystalline size using Debye-Scherrer’s equation and found in the range of 10.6 to 12.2 nm for HBPU matrix while 15.3 nm for LPUAg2.5. From the calculation it can be conferred that smaller size nanoparticles can be regulated in HBPU matrix than LPU system. This result was further confirmed by the TEM analysis.

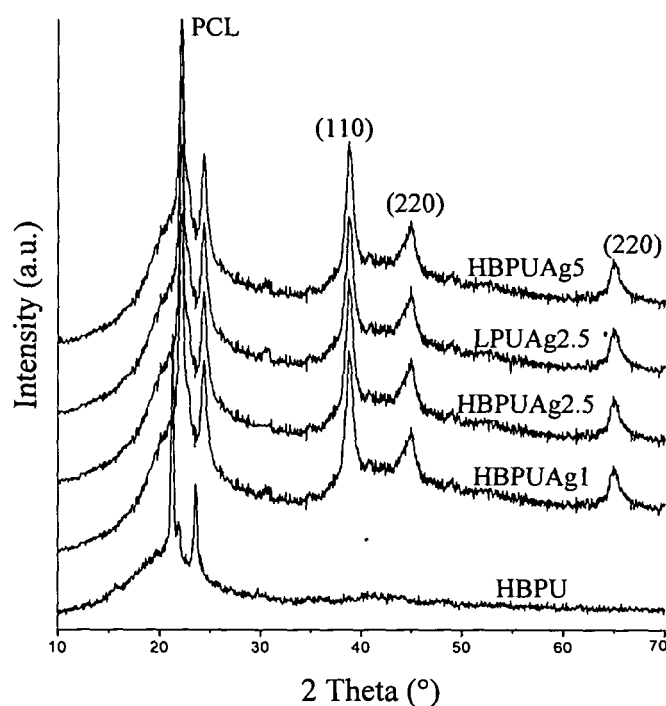


Fig. 7.3: XRD patterns of the silver nanocomposites

The representative TEM micrographs along with the histograms (Fig. 7.4) for HBPUAg2.5 and LPUAg2.5 enlighten the well dispersed and narrow size distribution of the nanoparticles. The sizes of the smaller particles were in range of 9-10 nm while

the bigger were 11-15 nm with average particle size of 11 nm for HBPU matrix. On the other hand for the linear matrix these two ranges were 5-10 nm and 11-22 nm respectively with an average particle size of 15 nm. Again, the histograms (Fig. 7.4) show that the distribution of nanoparticles is narrower in HBPU than the LPU matrix.

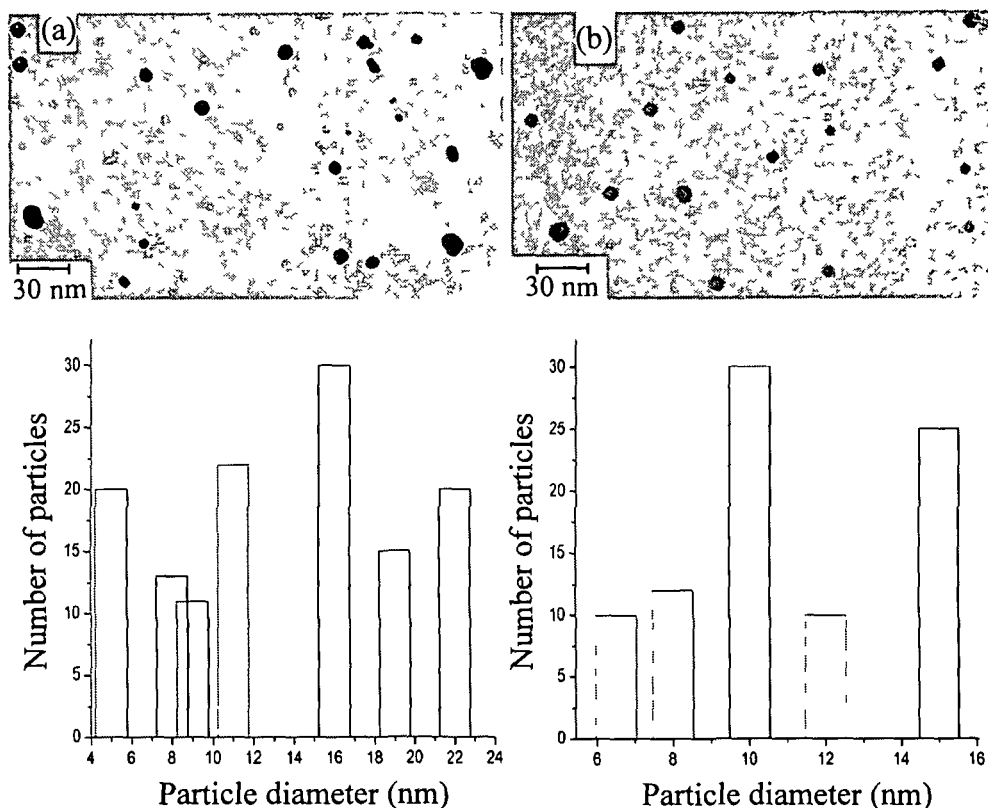


Fig. 7.4: Typical TEM micrographs of (a) LPUAg2.5 and (b) HBPUAg2.5 and corresponding histograms for distribution of particle size

7.3.3 Characterization of Iron based Nanocomposite

The UV-visible absorption spectrum was employed to characterize the iron based nanoparticles embedded in polymer matrix. The iron based nanoparticles dispersed in the polymer matrix showed maximum absorption at around 320 nm which is characteristic of iron/iron oxide nanoparticles surface plasmon resonance (Fig. 7.5). However, the pristine HBPU does not show any band in the aforesaid region. The plasmon absorption peak shifts to a higher wavelength with the increase of aggregation of the nanoparticles.²⁸ The stability of the iron-HBPU-PANI nanocomposite was observed with the help of UV spectrophotometer. Absorbance of the nanocomposite was taken after 24 h and one month. A red shift with respect to time was observed from 320 to 330 nm for the nanocomposite which indicates the increase of size of the nanoparticles is not significant (Fig. 7.5). Thus the UV study predicts the good stability offered by the HBPU matrix.

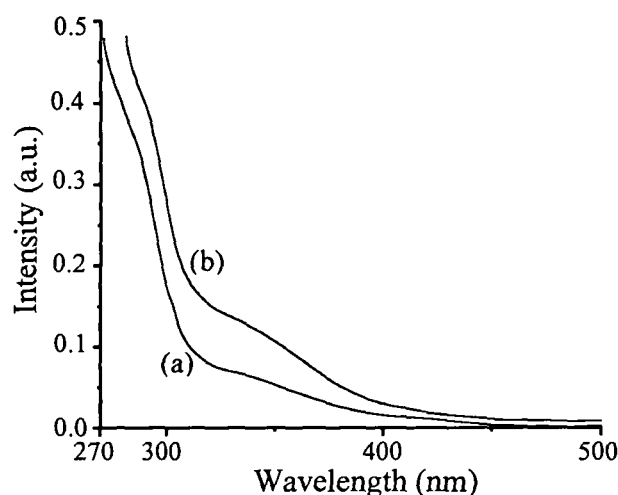


Fig. 7.5: UV spectra of iron-HBPU-PANI nanocomposite after (a) 0.5 h and (b) 24 h

FTIR analysis was performed to characterize the interactions of the iron based nanoparticles with the matrix as shown in Fig. 7.6. The FTIR band for iron oxide

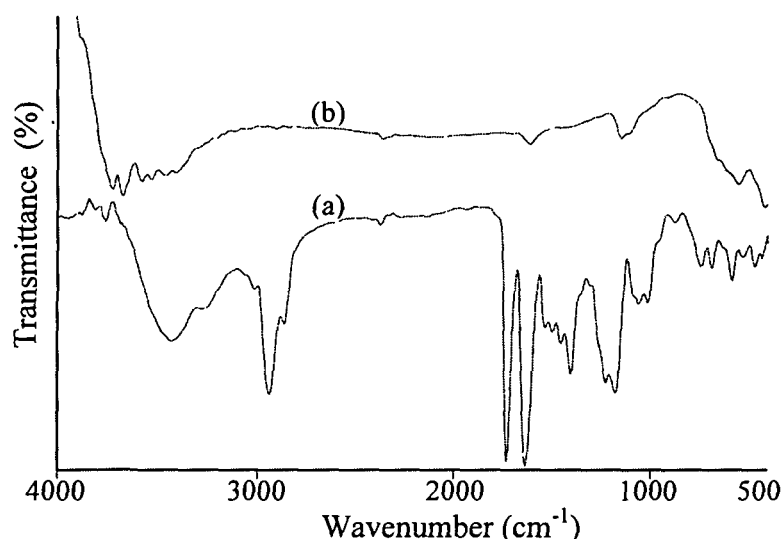


Fig. 7.6: FTIR spectra of (a) iron-HBPU-PANI nanocomposite and (b) annealed iron-HBPU-PANI nanocomposite

appears at 590-550 cm^{-1} correspond to the vibration of Fe-O bonds in the tetrahedral and octahedral sites.²⁹ After annealing the nanocomposite lost most of the bands other than the bands at 2370, 1630, 1160 and 565 cm^{-1} which is attributed to the formation of oxides of iron with carbonaceous coating.³⁰ The band at 1650-1670 cm^{-1} is due to the overlapping of $-\text{C}=\text{O}$ stretching, $-\text{NH}_2$ bending and coupling modes between $-\text{CN}$ stretching and $-\text{NH}$ bending. It is also due to the interaction between amide group or urethane group and iron based nanoparticles. The characteristic FTIR bands for the presence of PANI in the nanocomposites are found at 1450 cm^{-1} ($\text{N}=\text{C}_{\text{ar}}=\text{N}$) and 1100 cm^{-1} ($-\text{CN}$). The intensity of the above bands decreases or disappears after annealing, due to the burning of the polymer phase.

The XRD patterns of the nanocomposite are shown in the Fig. 7.7. In Fig. 7.7(a), the XRD pattern of the pure HBPU-PANI shows sharp peaks at $2\theta = 21.2^\circ$ and 23.4° is due to crystallinity of PCL moiety. Whereas, the XRD pattern of the iron/iron oxide HBPU-PANI nanocomposite does not show any distinct peak besides the peaks present in HBPU-PANI system [Fig 7.7(b)]. The absence of any distinct diffraction pattern corresponding to iron/iron oxide predicts the amorphous nature of the nanoparticles^{31,32} in the polymer matrix. This can also be attributed to the formation of

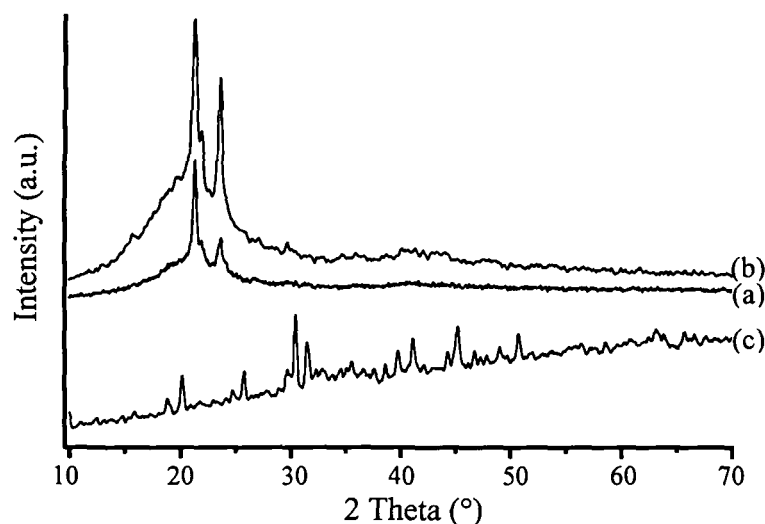


Fig. 7.7: XRD patterns of (a) HBPU-PANI, (b) iron-HBPU-PANI nanocomposite and (c) annealed iron-HBPU-PANI nanocomposite

very small particles of iron/iron oxide in hyperbranched matrix. The XRD pattern of the nanocomposite after annealed³¹ at 600°C for 5 h is shown in Fig 7.7(c). The strong and sharp peaks of different crystallographic phases of iron oxides were appeared in the XRD diffractogram of the annealed sample. During the burning process of the matrix the size of the nanoparticles increased due to oxidation. The peak at the $2\theta = 44.5^\circ$ indicates the presence of the zero valent iron and the other peaks are for the iron oxides. This is due to the partial transformation of Fe^0 to Fe^{2+} or Fe^{3+} (iron oxide) state during annealing under open atmosphere.³³

The morphology, size and size distribution of the iron based nanoparticles are shown in Fig. 7.8. The spherical and homogenously dispersed iron based nanoparticles with an average particle size of diameter 10 nm within a size window of 5-15 nm can be visualized in the HBPU-PANI matrix. The histograms for the particle size distribution clearly indicate that the size distribution of the nanoparticles is narrow (Fig. 7.8). Interestingly, it was noticed that no clear oxide layer was formed over the nanoparticles in HBPU matrix as it is frequently found in most of the conventional polymer iron nanocomposites.³⁴ Thus it can be stated that HBPU provides enhanced

dispersibility and stability of the nanoparticles due to the unique architectural feature of channel and cavity in its structure.³⁵

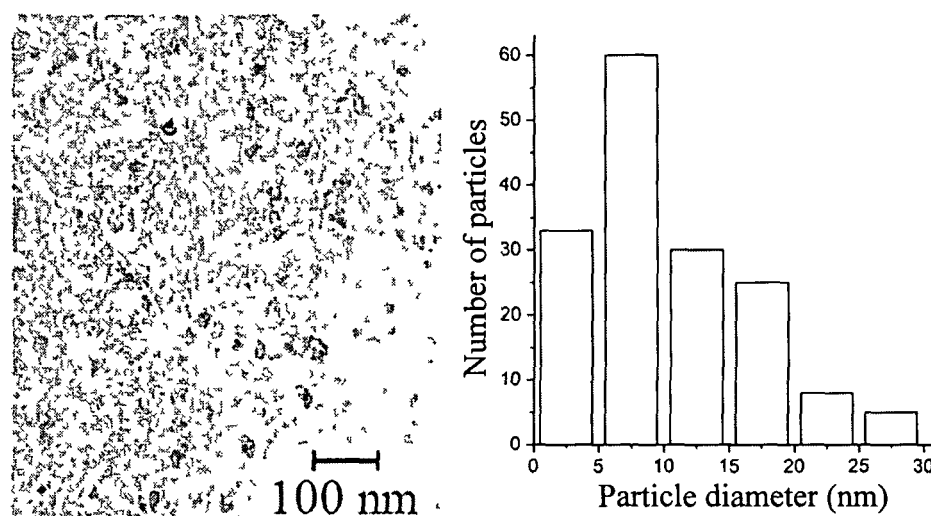


Fig. 7.8: TEM micrograph and histogram of the iron-HBPU-PANI nanocomposite

The surface morphology of the polymer iron based nanocomposite was characterized by SEM micrograph. The SEM image of the iron-HBPU-PANI nanocomposite shows very few nanoparticles on the surface conforming that the nanoparticles tend to dispersed towards the bulk of the polymer matrix (Fig. 7.9)

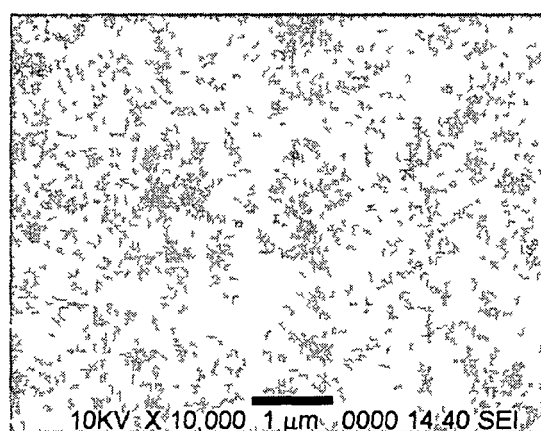


Fig. 7.9: SEM image of iron-HBPU-PANI nanocomposite

7.3.4 Antimicrobial Activity of Silver Nanocomposites

The antimicrobial activities of the nanocomposites were tested against different bacteria such as Gram positive (*Staphylococcus aureus*), Gram negative (*Escherichia coli*) and yeast such as *Candida albicans* by disc diffusion assay. The comparative bar-graphs of antimicrobial efficiency of the prepared discs with standard antibiotics and antifungal are shown in Fig. 7.10. It is clear that the antimicrobial properties of the nanocomposites are due to the incorporation of the silver nanoparticles in the matrix as the pristine HBPU matrix does not show any antimicrobial activity. Further, the

response towards the Gram positive and Gram negative bacteria was not the same. *Staphylococcus aureus* being Gram positive bacteria has a much stronger defense system compared to *E. coli*, a Gram negative bacteria, as the former possesses a thicker

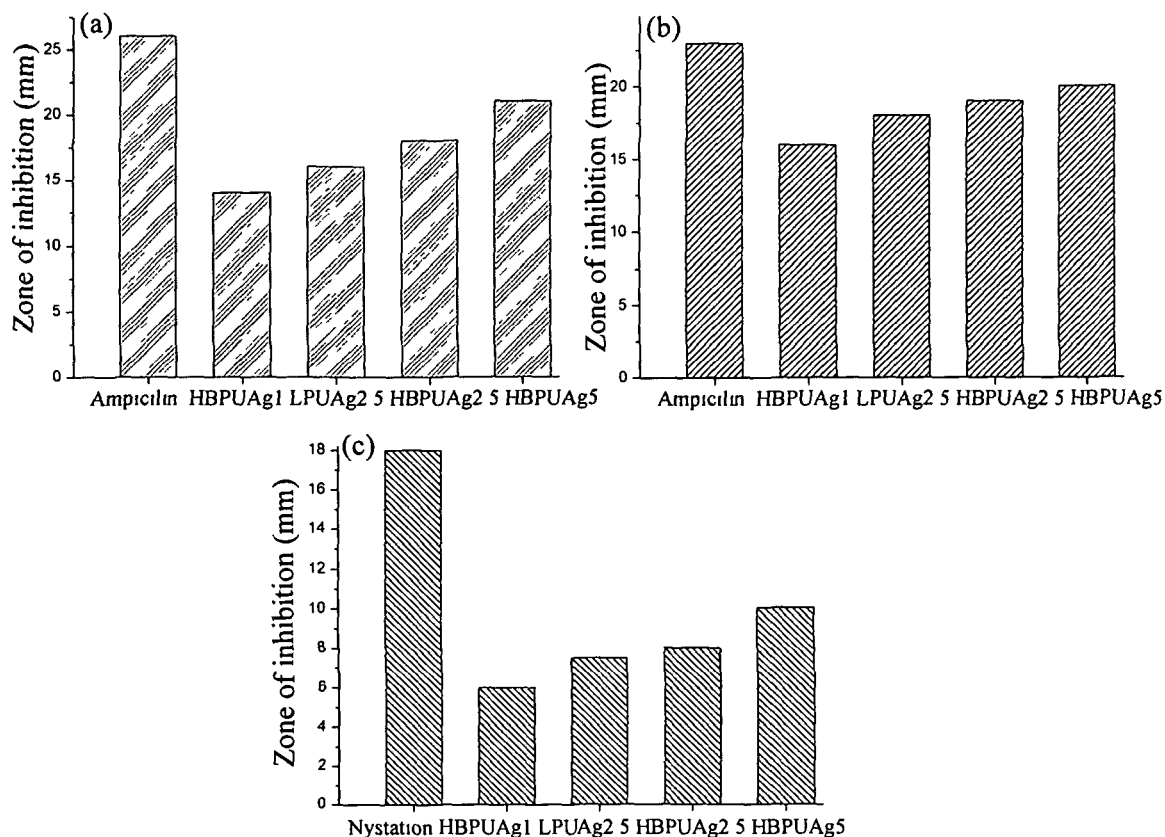


Fig. 7.10: The comparative bar-graphs of antimicrobial efficiency of the silver nanocomposites against (a) *Staphylococcus aureus*, (b) *Escherichia coli*, and (c) *Candida albicans* with standard antibiotics and antifungal

peptidoglycan cell wall.³⁶ This thicker wall prevents the silver ions from penetrating into the cytoplasm of the organism. It has been suggested that Ag^+ ions enter into the bacterial cells by penetrating through the cell wall and consequently turn the DNA into condense form which reacts with the thiol group of the proteins. Thus it ultimately causes death of the cell.³⁶ Though it is suggested that the antimicrobial mechanism of silver nanoparticles follows the same manner as that of its ions, but it is still not confirmed. A redox imbalance may be caused by the nanoparticles resulting death of a large number of bacteria. This effect is further enhanced by the large surface area of the nanoparticles.³⁷ The antimicrobial activity of the nanocomposites was increased with the increase of silver nanoparticles. This present study also supports the observation of Shahverdi et al.³⁸ that dose dependent silver nanoparticles have marked activity against Gram positive than Gram negative bacteria. Rosenberg and co-workers extensively described the toxicity of the Ag^+ ions on *E. coli*.³⁹ The ions inhibit phosphate uptake

and exchange in *E. coli*, which causes efflux of accumulated phosphate. *E. coli* contains two types of NADH dehydrogenase both contains cysteine residue. This cysteine residue has high affinity for silver.⁷ The Ag⁺ ions bind with the enzymes of the bacterial respiratory chain causing an inefficient passage of electrons to oxygen at the terminal oxidase. This produces large quantities of reactive oxygen species and thus toxicity to *E. coli*. It is expected that the silver nanoparticles also act as the same way as the Ag⁺ ions for *E. coli*. The nanocomposites also showed antifungal activity against *Candida albicans* [Fig. 7.10(c)]. The nanocomposites showed comparable results with the studied antibiotics. Wright et al. proved the antifungal properties of silver against a broad spectrum of common fungi.⁴⁰

7.3.5. Mechanical Properties of Silver Nanocomposites

The results of mechanical properties of the silver nanocomposites are tabulated in the Table 7.1. An improvement in tensile strength was observed whereas the elongation at break remains almost same compared to the pristine polymer matrices as stated in Chapter 2, Table 2.4. The increase of the interactions of silver nanoparticles with the hard segment of HBPU matrix and enhanced crystallinity (higher enthalpy value, discussed in DSC study) may promote its strength. The highest strength was found for HBPUAg5 (11.5 MPa). Although the silver nanoparticles restrict the segmental motions of the polymer chains, still it is not sufficient to decrease the elongation at break value to a noticeable extent. Other significant achievements observed in these nanocomposites were the retention of the flexibility and enhancement of impact resistance (Table 7.1). The films can be easily bent to 3 mm diameter of a parallel mandrel without any damage. An increase of impact resistance and marginal increase, of Shore A hardness were found for all the nanocomposites with increased amount of silver nanoparticles compared to the HBPU. Misjak et al.⁴¹ had also found dose dependent mechanical properties of thin films of silver nanocomposites.

Table 7.1: Mechanical properties of the silver nanocomposites

Property	HBPUAg1	HBPUAg2.5	HBPUAg5	LPUGAg2.5
Tensile strength (MPa)	8.13	9.42	11.51	9.60
Elongation at break (%)	719	712	710	730
Bending (mm)	3	3	3	3
Hardness (Shore A)	74	75	76	74
Impact resistance (cm)	56	60	65	59

7.3.6. RBC Hemolysis Protection Assay for Cytocompatibility of Silver Nanocomposites

The peculiar properties of metal nanocomposites lead to execute novel activities. At the same time the possible harmful interactions of nanoparticles with the biological systems are of prime concern. Thus there is an urgent need of approach to access the safety of such materials. The toxicity of nanoparticles depends on several factors like rate of cellular uptake of nanoparticles, intracellular distribution, exocytosis, size, shape, aspect ratio, surface functionality of nanoparticles etc.⁴² One of the known mechanisms for cellular damages is oxidative stress that is induced by the nano and ultrafine particles.⁴³ The presence of silver nanoparticles accelerates the production of reactive oxygen species (ROS) and subsequent oxidative stress. This also accounts the metabolic disturbances as well as other toxicological outcomes in the existence of such nanoparticles. The highly reactive oxygen species result in oxidative damages to the cells, proteins, DNA, RNA etc. In the present study, RBC hemolysis protection assay was carried out to check the cytocompatibility of the nanocomposites. The hemolysis inhibition data were recorded in the time intervals of 0, 30, 60 and 90 min. From the Fig. 7.11, it can be conferred that the nanocomposites are non-cytotoxic. The HBPUAg5 showed the highest hemolysis prevention capacity, revealing the dose dependency. The free radicals may be stabilized by the silver nanoparticles through

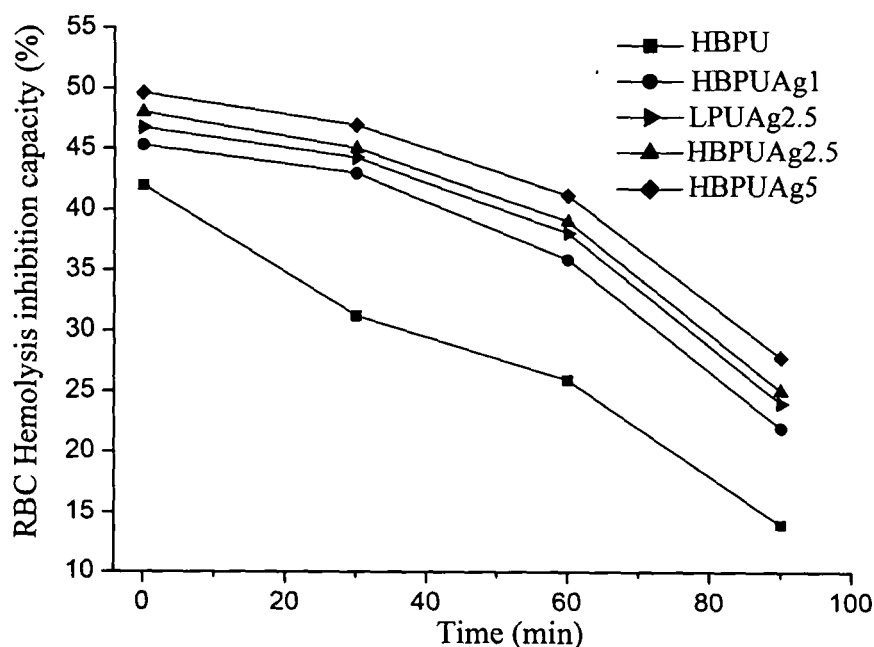


Fig. 7.11: The RBC hemolysis inhibition assay of the silver nanocomposites

sharing of unpaired electron of the free radicals with the conduction band electrons of the metal nanoparticles⁷ and ultimately it is deposited on the surface of the

nanocomposite films. Further a declination in inhibition of hemolysis of RBC was observed after 90 min may be due to the saturation after reacting with free radicals.²⁰ The pristine polymer showed very less hemolysis inhibition capacity compared to the nanocomposites. Such observations signify the critical role of the silver nanoparticles in the matrix in RBC hemolysis inhibition. This also supports the aforesaid interactions of the silver nanoparticles with the free radicals. Thus, although the free silver nanoparticles cause toxicity to the living cells, the polymer bound silver nanoparticles are non-toxic at cellular level.

7.3.7. Free Radical Scavenging Activity of Iron Based Nanocomposite

The free radical scavenging ability of the pristine HBPU, HBPU-PANI system and the nanocomposite are shown in Fig. 7.12. The HBPU and HBPU-PANI showed 23% and 45% radical scavenging capacity respectively whereas the iron-HBPU-PANI nanocomposite showed about 67% scavenging. The radical scavenging capability of the HBPU matrix can be attributed to the scavenging ability of the urethane and other polar groups such as ether, ester etc. present in the HBPU. This property is improved by the presence of PANI in the matrix. The polar amine group may attribute to this radical scavenging ability. The incorporation of the iron based nanoparticles in the system further enhances this free radical scavenging ability to a significant extent as observed from the Fig 7.12.

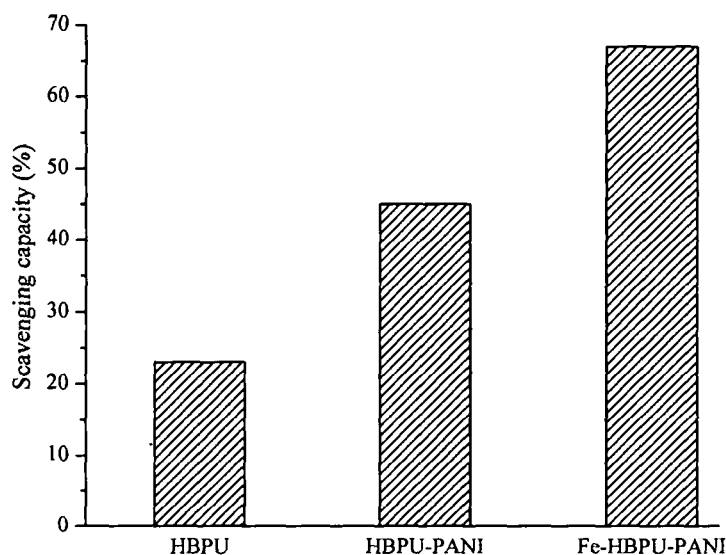


Fig. 7.12: Scavenging capacity (%) of different systems

7.3.8. Magnetic Behavior of Iron Based Nanocomposite

The ferromagnetic behavior of the iron based nanocomposite is demonstrated by the hysteresis loop measurement using VSM. Fig. 7.13(a) shows the magnetization curve

of the nanocomposite at room temperature. From the figure, it is cleared that the magnetization of the nanocomposite did not reach the saturation value even at the maximum applicable magnetic field of the instrument. However it is obvious that the magnetic particles present in the polymer matrix were of almost single domain superparamagnetic in nature due to the very small size of the iron based nanoparticles which can be explained by very low coercivity and retentivity of the hysteresis loop⁴⁴ [(Fig. 7.13(a)]. But the polymer being diamagnetic in nature, supporting the iron based nanoparticles decreases the magnetic nature of the nanocomposites to a very effective extent, and it is further decreased by the non-magnetic phase of the oxide layer formed over the iron based nanoparticles.^{44,45} The retentivity value [as found from the Fig. 7.13(a)] was 0.0005 emu/g for iron-HBPU-PANI nanocomposite, whereas the coercivity was 220 G.

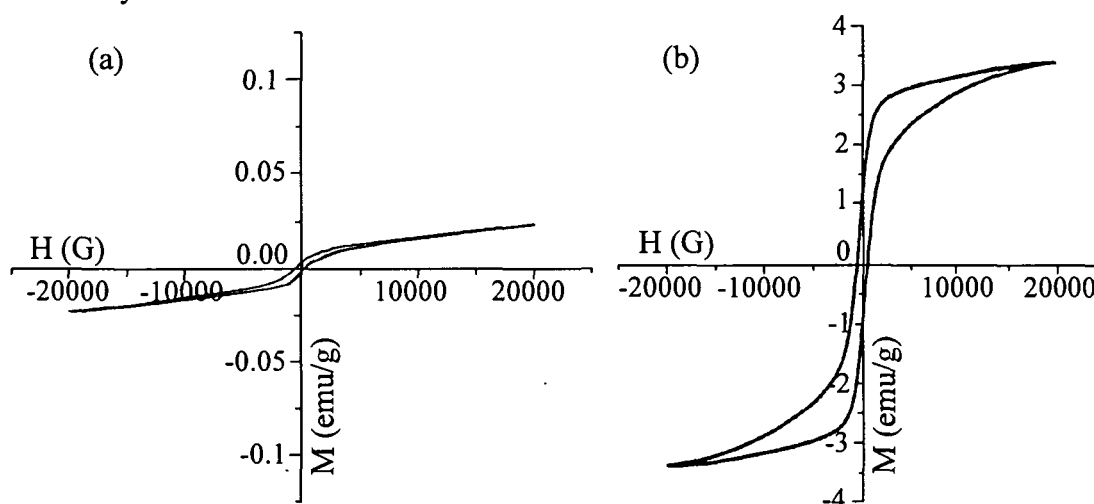


Fig. 7.13: Magnetization curve of the nanocomposites (a) iron-HBPU-PANI and (b) annealed iron-HBPU-PANI

Fig. 7.13(b) depicts the hysteresis loop of the annealed sample. The loop width in this case slightly broaden due to the increase in size of the nanoparticles by the oxidation during annealing in air, which results in the increase of the coercivity.^{19,44} Also the saturation magnetization increased here due to the burning of the polymer leaving a carbon-complexed coating. The retentivity and coercivity values for the annealed sample as found from the Fig. 7.13(b) were 1.02 emu/g and 470 G respectively.

7.3.9. Thermal Properties of the Nanocomposites

The thermal properties of the nanocomposites were studied by TGA and DSC studies. An excellent achievement in thermal stability was noticed for the silver nanocomposites (Fig. 7.14). One step degradation was observed for the

nanocomposites, whereas the pristine HBPU showed two step degradation. It is quite obvious that the incorporation of the silver nanoparticles have enhanced the thermal stability of the HBPU matrix. The characteristic thermal degradation temperatures are reported in the Table 7.2. A shift of 46-53 °C of the T_{ON} was observed for HBPU silver nanocomposites whereas for LPUAg2.5, it was 42 °C compared to their respective pristine polymers. Again the T_{MAX} of pristine HBPU is 370 °C, while the T_{MAX} for the HBPU nanocomposites were 402-413 °C. Thus the T_{MAX} is shifted by 32-43 °C for HBPU based silver nanocomposites. Similarly for LPUAg2.5, this enhancement was 48 °C (T_{MAX} of pristine LPU was 362 °C and for LPU nanocomposite 400 °C) (Table 7.2). The silver nanoparticles acted as the nucleating agent for enhancing the crystallization which restricts the movement of the polymer chains.²⁶ Thus fantastic improvements in thermal stability were observed.

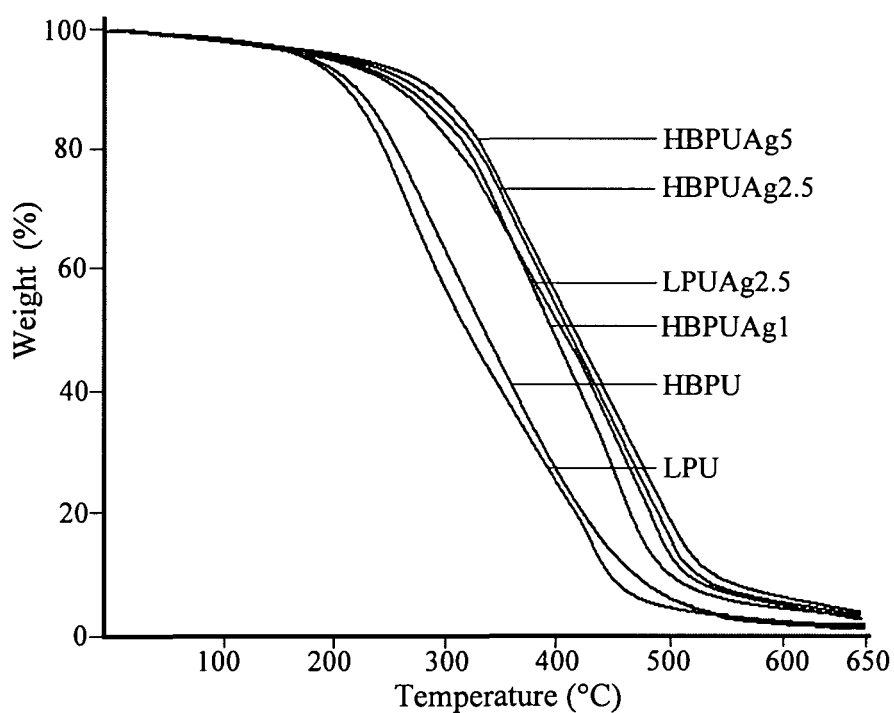


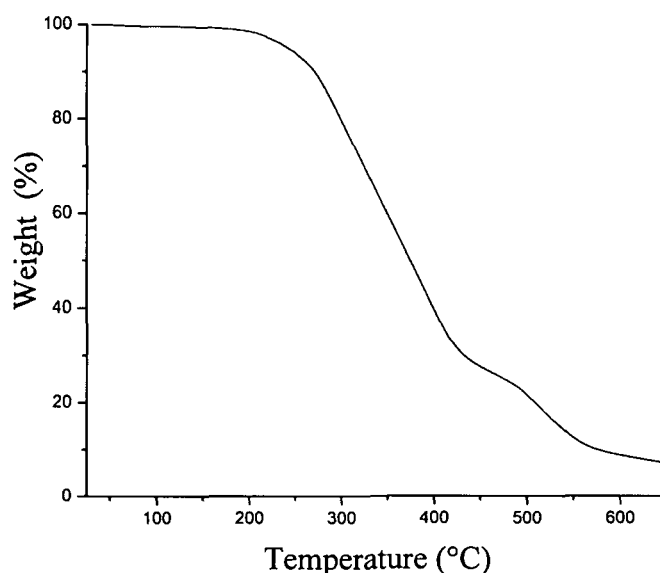
Fig. 7.14: Thermogravimetric curves of the silver nanocomposites

The T_g , T_m and ΔH_m are shown in the Table 7.2. A slight increment in T_g in the HBPU nanocomposites (from -44 to -40 °C) and LPU nanocomposite (from -46 to -42 °C) were observed which is due to the restriction on the segmental chain movement imposed by silver nanoparticles.⁴⁶ With the increase of amount of nanoparticles this restriction increases considerably. The T_m of the nanocomposites was found to be increased with the increase of silver nanoparticles due to the increase of interactions of silver nanoparticles with the HBPU matrix. An enhancement in crystallinity can also be predicted from the ΔH_m value (Table 7.2) due to the aforesaid fact.

Table 7.2: Thermal properties of the silver nanocomposites

Code	T _g (°C)	T _m (°C)	ΔH _m (J/g)	T _{ON} (°C)	T _{MAX} (°C)	T _{END} (°C)
HBPUAg1	-42	50	53.6	261	402	487
HBPUAg2.5	-41	52	54.2	264	409	493
HBPUAg5	-40	55	56.3	268	413	498
LPUAg2.5	-43	50	51.5	256	400	490

The relative thermal stability of the iron based nanocomposites was also investigated by TGA. Two step degradation pattern (Fig. 7.15) with an enhanced thermal stability of the iron-HBPU-PANI than the pristine HBPU matrix was observed. The characteristic thermal degradation temperatures T_{1st ON}, T_{1st MAX} and T_{2nd ON} are 236 °C, 450 °C and 580 °C respectively. Thus 21, 20 and 10 °C shifts of the T_{1st ON}, T_{1st MAX} and T_{2nd ON} were observed for iron-HBPU-PANI nanocomposite with respect to the HBPU matrix respectively.

**Fig. 7.15:** TGA curve of iron-HBPU-PANI nanocomposite

7.3.10. Biodegradation of Silver Nanocomposites

From the antimicrobial test results it is expected, in general, that the materials may not be biodegradable. However, it was noticed that the antimicrobial polymeric nanocomposites exhibited biodegradation under the studied conditions. This noteworthy observation was achieved due to right choice of bacterial strains, which are treated as hydrocarbon degrading bacteria and expected to be utilized for bioremediation of petroleum contaminated areas. The pristine HBPU and the nanocomposite films were directly exposed to the bacterial strains and the bacterial growth was monitored and evaluated with the help of McFarland Turbidity method. The bacterial growth with respect to time for the studied systems is shown in the Fig.

7.16. The bacterial growth was higher for the nanocomposites than their respective pristine systems. Several causes can be cited to account this biodegradation behavior of

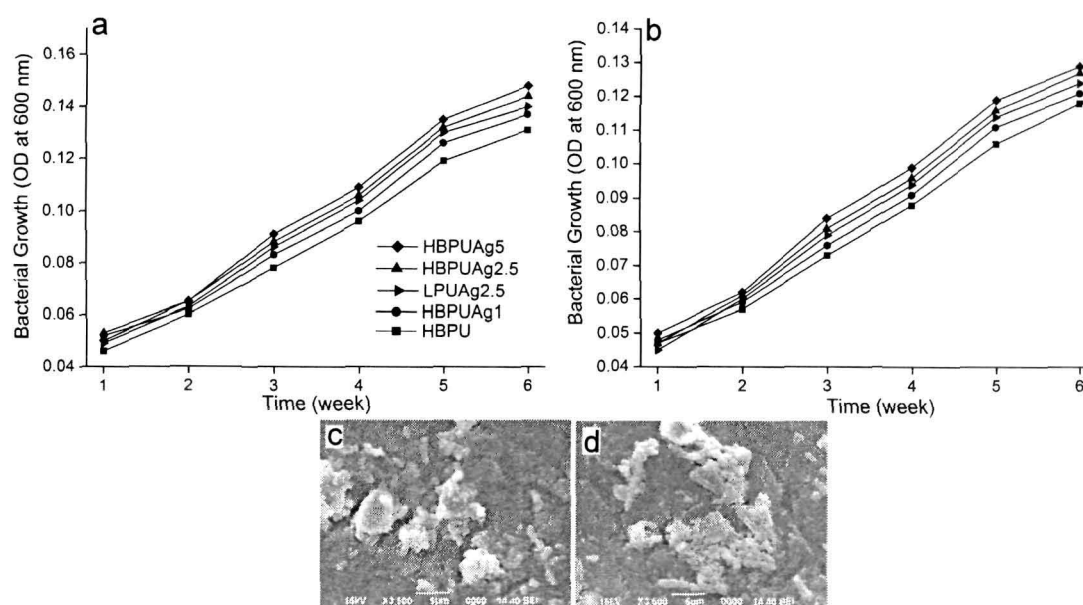


Fig. 7.16: Statistics for the growth of *P. aeruginosa* strain (a) MTCC 7814, (b) MTCC 7815 and SEM pictures of the degraded films: (c) LPUAg2.5, (d) HBPUAg2.5

HBPU and the nanocomposites. No significant improvement in biodegradation was noticed till two weeks for all the systems. But after two weeks the nanocomposites showed comparatively good biodegradability. Further, with the increase of silver nanoparticles content the biodegradation rate was found to be increased which may be due to ease of access of polymer surface by the degrading bacterial strains as they can be accommodated by the favorable geometry of the polymer chains. This is again due to decrease of H-bonding among the chain molecules due to incorporation of silver nanoparticles in the matrix (as described in the FTIR analysis). The decreased phase separated morphology after nanocomposite formation is due to the increase of interfacial interactions between silver nanoparticles and polymer chains may also attribute to this enhancement of the biodegradation. However, the correct understanding on the mechanism of biodegradation of such antimicrobial materials requires much details study. The extent of biodegradation as well as bacterial growth can be visualized from the SEM images (Fig. 7.16). The growth rate of the two bacterial strains was also found to be different, which indicates that this biodegradation is even dependent on the strain of the same bacteria.

7.4. Conclusions

Thus the present study describes the simple and state forward processes for the preparation of various metal/HBPU nanocomposites. The silver nanocomposites

showed the potentiality as antimicrobial biodegradable biocompatible biomaterials. *Mesua ferrea* L. seed oil based hyperbranched matrix based nanocomposites proved their superiority over the linear analog. The well-dispersed and stable silver nanoparticles improved the mechanical properties like tensile strength and impact resistance without affecting the flexibility and elongation at break value of the pristine polymer in both the cases. Thermal properties were also found to be well-improved in the prepared nanocomposites. The silver incorporated PU nanocomposite films exhibited excellent antimicrobial activities against *Staphylococcus aureus*, *Escherichia coli* and *Candida albicans*, even though they also exhibited adequate bacterial biodegradation by the right strain of *P. aeruginosa* (MTCC 7814 and MTCC 7815). The RBC hemolysis inhibition assay indicates the cytocompatibility of the materials but before use these materials in actual field they need to verify by *in vivo* test.

The well-dispersed iron based nanoparticles in HBPU matrix was characterized by different techniques. The nanocomposite exhibits remarkable free radical scavenging capability towards DPPH. The iron based nanoparticles exhibited super-paramagnetic behavior and the magnetization increases on annealing. Thus the observed results implied the high potential of the HBPU/metal nanocomposites in various niches.

References

1. Pinchuk, A.; Hilger, A.; von-Plessen, G.; Kreibitz, U. Substrate effect on the optical response of silver nanoparticles. *Nanotechnol.* **15**, 1890(pp6) (2005)
2. Chan, W.C.W.; Nie, S. Quantum dot bioconjugates for ultrasensitive nonisotopic detection. *Science* **281**, 2016-2018 (1998)
3. Kim, Y.; Johnson, R.C.; Hump, J.T. Gold nanoparticle-based sensing of "spectroscopically silent" heavy metal ions. *Nano Lett.* **1**, 165-167 (2001)
4. Chen, X.; Schluesener, H.J. Nanosilver: A nanoparticle in medical application. *Toxicol. Lett.* **176**, 1-12 (2008)
5. Lee, D.; Cohen, R.E.; Rubner, M.F. Antibacterial properties of Ag nanoparticle loaded multilayers and formation of magnetically directed antibacterial microparticles. *Langmuir* **21**, 9651-9659 (2005)
6. Wijnhoven, S.W.P. et al. Nano-silver - A review of available data and knowledge gaps in human and environmental risk assessment. *Nanotoxicol.* **3**, 109-138 (2009)
7. AshaRani, P.V.; Mun, G.L.K.; Hande, M.P.; Valiyaveetil, S. Cytotoxicity and genotoxicity of silver nanoparticles in human cells. *ACS Nano* **3**, 279-290 (2009)

8. Drake, P.L.; Hazelwood, K.J. Exposure-related health effects of silver and silver compounds: A review. *Ann. Occup. Hyg.* **49**, 575-585 (2005)
9. Alivisatos, A.P. Semiconductor clusters, nanocrystals, and quantum dots. *Science* **271**, 933-937 (1996)
10. Uzum, C. et al. Application of zero-valent iron nanoparticles for the removal of aqueous Co^{2+} ions under various experimental conditions. *Chem. Eng. J.* **144**, 213-220 (2008)
11. Ponder, S.; Darbab, J.; Mallouk, T. Remediation of Cr(VI) and Pb(II) aqueous solutions using supported, nanoscale zero-valent iron. *Environ. Sci. Technol.* **34**, 2564-2569 (2000)
12. Sandhu, A.; Handa, H. Practical hall sensors for biomedical instrumentation. *IEEE Trans. Magn.* **41**, 4123-4127 (2005)
13. Senyei, A.; Widder, K.; Czerlinski, G. Magnetic guidance of drug-carrying microspheres. *J. Appl. Phys.* **49**, 3578-3583 (1978)
14. Y. Zhang et al. Hyperbranched poly(amidoamine) as the stabilizer and reductant to prepare colloid silver nanoparticles *in situ* and their antibacterial activity. *J. Phys. Chem. C* **112**, 2330-2336 (2008)
15. Karak, N.; Maiti, S. *Dendrimers and Hyperbranched Polymers—Synthesis to Applications* (MD publication Pvt. Ltd., New Delhi, 2008)
16. Long, Y.; Chen, Z.; Duvail, J.L.; Zhang, Z.; Wan, M. Electrical and magnetic properties of polyaniline/ Fe_3O_4 nanostructures. *Physica. B* **370**, 121-130 (2005)
17. Henglein, A. Physicochemical properties of small metal particles in solution: "Microelectrode" reactions, chemisorption, composite metal particles, and the atom-to-metal transition. *J. Phys. Chem.* **97**, 5457-5471 (1993)
18. Gizdavic-Nikolaidis, M. et al. The antioxidant activity of conducting polymers in biomedical applications. *Curr. Appl. Phys.* **4**, 347-350 (2004)
19. Turkoglu, A.; Duru, E.M.; Mercan, N.; Kivrak, I.; Gezer, K. Antioxidant and antimicrobial activities of *Laetiporus sulphureus* (Bull.) Murrill. *Food Chem.* **101**, 267-273 (2007)
20. Zhu, Q.Y.; Holt, R.R.; Lazarus, S.A.; Orozco, T.J.; Keen, C.L. Inhibitory effects of cocoa flavanols and procyanidin oligomers on free radical-induced erythrocyte hemolysis. *Exp. Biol. Med.* **227**, 321-329 (2002)
21. Serpen, A.; Capuano, E.; Fogliano, V.; Gokmen, V. A new procedure to measure the antioxidant activity of insoluble food components. *J. Agr. Food Chem.* **55**, 7676-7681 (2007)

22. Turkevich, J.; Stevenson, P.C.; Hillier, J. A study of the nucleation and growth processes in the synthesis of colloidal gold. *Discuss Faraday Soc.* **11**, 55-75 (1951)
23. Slistan-Grijalva, A. et al. Assessment of growth of silver nanoparticles synthesized from an ethylene glycol-silver nitrate-polyvinylpyrrolidone solution. *Physica. E* **25**, 438-448 (2005)
24. Cocca, M.; D'Orazio, L. Novel silver/polyurethane nanocomposite by *in situ* reduction: Effects of the silver nanoparticles on phase and viscoelastic behavior. *J. Polym. Sci., Part B: Polym. Phys.* **46**, 344-350 (2007)
25. Mukherjee, S.; Mukherjee, M. Nitrogen-mediated interaction in polyacrylamide-silver nanocomposites. *J. Phys. Condens Matter.* **18**, 11233-11242 (2006)
26. Chou, C.W.; Hsu, S.H.; Chang, H.; Tseng, S.M.; Lin, H.R. Enhanced thermal and mechanical properties and biostability of polyurethane containing silver nanoparticles. *Polym. Degrad. Stab.* **91**, 1017-1024 (2006)
27. Zhang, Z.; Han, M. One-step preparation of size-selected and well-dispersed silver nanocrystals in polyacrylonitrile by simultaneous reduction and polymerization. *J. Mater. Chem.* **13**, 641-643 (2003)
28. Cha, H.G.; Kim, Y.H.; Kim, C.W.; Kwon, H.W.; Kang, Y.S. Preparation for exchange-coupled permanent magnetic composite between α -Fe (soft) and $\text{Nd}_2\text{Fe}_{14}\text{B}$ (hard). *Curr. Appl. Phys.* **7**, 400-403 (2007)
29. Barrado, E.; Prieto, F.; Medina, J.; Lopez, F.A. Characterisation of solid residues obtained on removal of Cr from waste water. *J. Alloy Compd.* **335**, 203-209 (2002)
30. Predoi, D. A study on iron oxide nanoparticles coated with dextrin obtained by coprecipitation. *Digest. J. Nanomater. Biostruct.* **2**, 169-173 (2007)
31. Li, Q. Sonochemical synthesis, structural and magnetic properties of air-stable Fe/Co alloy nanoparticles. *New J. Chem.* **27**, 1194-1199 (2003)
32. Oh, S.J. et al. Mössbauer analysis on the magnetic properties of Fe-Co nanoparticles synthesized by chemical vapor condensation process. *J. Magn. Magn. Mater.* **280**, 147-157 (2004)
33. Guo, L.; Huang, Q.; Li, X.Y.; Yang, S. Iron nanoparticles: Synthesis and applications in surface enhanced Raman scattering and electrocatalysis. *Phys. Chem. Chem. Phys.* **3**, 1661-1665 (2001)
34. Li, X.Q.; Zhang, W.X. Iron nanoparticles: The core-shell structure and unique properties for Ni(II) sequestration. *Langmuir* **22**, 4638-4642 (2006)

35. Lu, H.W. et al. Silver nanocrystals by hyperbranched polyurethane-assisted photochemical reduction of Ag⁺. *Mater. Chem. Phys.* **81**, 104-107 (2003)
36. Feng, Q.L. et al. A mechanistic study of the antibacterial effect of silver ions on *Escherichia coli* and *Staphylococcus aureus*. *J. Biomed. Mater. Res.* **52**, 662-668 (2000)
37. Morones, J.R. The bactericidal effect of silver nanoparticles. *Nanotechnol.* **16**, 2346(pp8) (2005)
38. Shahverdi, A.R.; Fakhimi, A.; Shahverdi, H.R.; Minaian, S. Synthesis and effect of silver nanoparticles on the antibacterial activity of different antibiotics against *Staphylococcus aureus* and *Escherichia coli*. *Nanomed. Nanotechnol. Biol. Med.* **3**, 168-171 (2007)
39. Schreurs, W.J.; Rosenberg, H. Effect of silver ions on transport and retention of phosphate by *Escherichia coli*. *J. Bacteriol.* **152**, 7-13 (1982)
40. Wright, J.B.; Lam, K.; Hansen, D.; Burrell, R.E. Efficacy of topical silver against fungal burn wound pathogens. *Am. J. Infect. Control.* **27**, 344-350 (1999)
41. Misjak, F. et al. Structure and mechanical properties of Cu-Ag nanocomposite films. *Thin Solid Films* **516**, 3931-3934 (2008)
42. Singh, S.; Nalwa, H.S. Nanotechnology and health safety-Toxicity and risk assessments of nanostructured materials on human health. *J. Nanosci. Nanotechnol.* **7**, 3048-3070 (2007)
43. Xia, T. et al. Comparison of the abilities of ambient and manufactured nanoparticles to induce cellular toxicity according to an oxidative stress paradigm. *Nano Lett.* **6**, 1794-1807 (2006)
44. Cha, H.G.; Kim, Y.H.; Kim, C.W.; Kang, Y.S. Preparation of aqueous dispersion of colloidal α -Fe nanoparticle by phase transfer. *Sensor Actuat. B Chem.* **126**, 221-225 (2007)
45. Wilson, J.L. et al. Synthesis and magnetic properties of polymer nanocomposites with embedded iron nanoparticles. *J. Appl. Phys.* **95**, 1439-1443 (2004)
46. Mahapatra, S.S.; Karak, N. Silver nanoparticle in hyperbranched polyamine: Synthesis, characterization and antibacterial activity. *Mater. Chem. Phys.* **112**, 1114-1119 (2008)

CHAPTER 8

HBPU/MWCNT nanocomposites

8.1. Introduction

The CNT based polymer nanocomposites are drawing a great deal of interest in recent times due to their outstanding mechanical, thermal and electrical properties.^{1,2} On the other hand, the homogeneous dispersion of the CNT in polymer matrix and to generate sufficient interfacial adhesion in between CNT and matrix is of foremost challenging task to achieve the desirable properties of the nanocomposites.¹ The lack of interactions resulted in failure of load transferring from the host polymer as the nanotubes slip on each other forming bundles or rope like aggregates.³ In this context the modification of the CNTs plays an important role to enhance the interphasic interactions. Several reports described the improvements of modulus, thermal and mechanical properties of PU/modified CNT nanocomposites.^{4,5} The contemporary technology also employs hyperbranched structure to improve the dispersion of modified CNT in the matrix⁶ in much better way than the conventional linear polymer. The large number of surface functionality of the hyperbranched polymer increases the physico-chemical interactions with nanofillers.⁷ There has been much interest in the hyperbranched polymers in view of the comparative ease with which these can be synthesized *vis-a-vis* the dendrimers as described in Chapter 1.

Again, the shape memory materials (SMMs) respond to external stimuli such as thermal heating, electric field, light energy or magnetic field and can also fix the consequent deformation.^{8,9} Amongst the SMMs, the shape memory polymers (SMPs) are receiving increased attention because of their easy processibility, low cost, appreciable shape recovery, low density, high deformation and a broad range of shape recovery temperature.¹⁰ SMPs are emerging as prominent potential candidates for the applied fields like smart actuators, textile engineering, aerospace engineering and biomedical applications, etc.^{11,12} SMPs are generally phase segregated multi block copolymers wherein the soft or the reversible phase becomes flexible which can be deformed elastically while the hard phase memorizes the original shape.¹³ The PUs are being focused, in this regard, for their high strain recovery, high control on the softening and retraction temperatures, and good physical properties.¹⁴

The biomaterials are biodegradable materials used in medical devices that are intended to interact with the biological systems.¹⁵ Biomaterials therefore must be biocompatible entailing the feature of biodegradability and non-toxicity.¹⁶ Good blood and tissue compatibility have been proved for PU based vascular prostheses, endotracheal tubes, catheters and artificial hearts.¹⁷ On the other hand, CNT is known for the adverse affect on human health and environment because of its toxicity.¹⁸ polymer/CNT nanocomposites may be designed which would offset these adverse affects without losing the fascinating property of CNT. The toxicity level, in general, is measured by the direct contact method and the MTT [3-(4,5-dimethylthiazol-2-yl)-2,5-diphenyltetrazolium bromide] assay.¹⁹ Besides these, the RBC hemolysis protection assay is also a direct indication for cytocompatibility.¹⁶ The biodegradability of nanocomposite materials is also an important aspect of many advanced biocompatible materials.

Again, the rheometry is an imperative investigation technique to know the dispersion state of nanofillers in the matrix and extent of interactions between nanofillers and host polymer as described in Chapter 4, section 4.1. The rheological properties of polymer/CNT nanocomposite melt are dependent on several factors such as amount of CNT, state of dispersion, interactions with the polymer matrix etc.²⁰ In general, G' and G'' show pseudo solid-like behavior at low frequencies due to the presence of the more interactions between CNT and polymers.²¹

Therefore, in this chapter the preparation, characterization and properties of the *Mesua ferrea* L. seed oil based HBPU/MWCNT nanocomposites are described. The potential of HBPU/MWCNT nanocomposites as shape memory biomaterial is primarily focused here. The effect of MWCNT on various properties like mechanical, thermal, shape recovery, biodegradation and cytocompatibility of the hyperbranched matrix have been investigated. The dose dependent property has also been addressed in the present study. Further the rheological characteristics have been studied in details to interpret the structure property relationship for such systems.

8.2. Experimental

8.2.1. Materials

MWCNTs with 10-20 nm diameter and about 20 μm of length were purchased from Iiljin Nanotech, Korea. The details about the MWCNTs were described in Chapter 1, section 1.4.1.2. The MWCNTs were treated by a mixture of concentrated $\text{H}_2\text{SO}_4/\text{HNO}_3$

(3:1 v/v) at 100 °C for 90 min. They were dried in vacuum at 80 °C for two days after proper washing with distilled water.

Monoglyceride of *Mesua ferrea* L. seed oil was prepared as described in Chapter 2 (section 2.2.2.1.). Other required chemicals such as PCL, TDI, glycerol, DMF, minerals for bacterial broth preparation in the biodegradation study and RBC hemolysis protection assay are of same specification and used without further purification unless otherwise as stated in the previous chapters. The *P. aeruginosa* strains MTCC 7814 and MTCC 7815 were taken from the Department of Molecular Biology and Biotechnology (Department of Biotechnology, DBT Centre, Government of India), Tezpur University.

8.2.2. Instruments and Methods

The FTIR, XRD, SEM, TEM, TGA and DSC analyses were carried out using the same instruments and conditions as mentioned in Chapter 4, section 4.2.2. The mechanical and rheological properties were evaluated as per the methods mentioned in the Chapter 4, section 4.2.2. The used ultrasonicator has same specifications as described in Chapter 3, section 3.2.2.

There are various methods to evaluate the shape memory property. In this investigation the used method was different than the earlier method (Chapter 3, section 3.2.2). While the earlier one calculates the shape memory on the basis of change in the length of the samples, the present one calculates on the change in the shape in terms of angle. Here, the shape memory property was observed by folding the sample in ring form at 60 °C followed by quenching into an ice water bath and finally reheating it. While heating, the shape recovery by the samples was recorded by using a video camera.

The shape recovery and shape fixity were calculated using equation (8.1) and (8.2).

$$\text{Shape recovery (\%)} = (90 - \theta)/90 \times 100 \quad (8.1)$$

where θ in degree denotes the angle between the tangential line at the midpoint of the sample and the line connecting the midpoint and end of the curved samples.

$$\text{Shape fixity (\%)} = \epsilon_u/\epsilon_m \times 100 \quad (8.2)$$

where the ϵ_u and ϵ_m are the maximum strain (100%) and residual strain after unloading the stress at 0 °C.²²

8.2.2.1. Preparation of HBPU

The *Mesua ferrea* L. seed oil based HBPU was prepared by the same procedure as mentioned in Chapter 2, section 2.2.2.2.

8.2.2.2. Preparation of HBPU/MWCNT Nanocomposites

The nanocomposites were prepared by *in-situ* technique. The required amount of modified MWCNT was dispersed in DMF by sonication for 15 min and added in to the HBPU reaction mixture 1 h before completion of the reaction. The HBPU/MWCNT nanocomposites were finally obtained in DMF as a solution of 25-30% solid content (w/v) after the completion of HBPU synthesis. The solutions were casted on teflon sheets, followed by vacuum degassing and drying at 50 °C for 24 h for different testing and analyses. The nanocomposites were denoted as HBPUMWCNT1, HBPUMWCNT2.5 and HBPUMWCNT5 corresponding to the MWCNT content of 1, 2.5 and 5 weight% respectively.

8.2.2.3. Biodegradation Study by Broth Culture Technique

The biodegradation study of the HBPU/MWCNT nanocomposites was carried out by broth culture technique as the same way as described in Chapter 5, section 5.2.2.4.

8.2.2.4. RBC Hemolysis Protection Assay for Cytocompatibility

The cytocompatibility of the prepared nanocomposites was tested through RBC hemolysis protection assay as described in Chapter 7, section 7.2.2.6.

8.3. Results and Discussions

8.3.1. Formation of Nanocomposites

The HBPU/MWCNT nanocomposites were prepared through *in-situ* preparative technique. The modified MWCNTs were first dispersed in DMF solvent with the help of ultrasonication. It was then added in the pre-polymer state during the synthesis of HBPU which facilitated the ease of dispersion of the MWCNT in the low viscous and reactive matrix.

8.3.2. Characterization

The linkages between modified MWCNT and HBPU were revealed from the FTIR analysis. In Fig. 8.1(a), the bands at ~ 3430 and 1720 cm^{-1} correspond to the $-\text{OH}$ and $-\text{C}=\text{O}$ stretching of carboxylic acid group.²³ The band at 1498 cm^{-1} is assigned to the IR photon mode of MWCNT.²⁴ These induced carboxylic groups on the surface of the

MWCNT are responsible for the enhanced interactions between HBPU and MWCNT. The FTIR spectra for the nanocomposites are shown in Fig. 8.1(b, c and d). The broad band at $\sim 3458\text{ cm}^{-1}$ are the overlapping of $-\text{NH}$ stretching of urethane and $-\text{OH}$ stretching of modified MWCNT. Further, the shifting of $-\text{C}=\text{O}$ band from 1698 to 1667 cm^{-1} with the increase of MWCNT loading is cleared from the Fig. 8.1. It can be inferred that with the increase of MWCNT content the interactions between the HBPU and nanofillers increases.²⁴

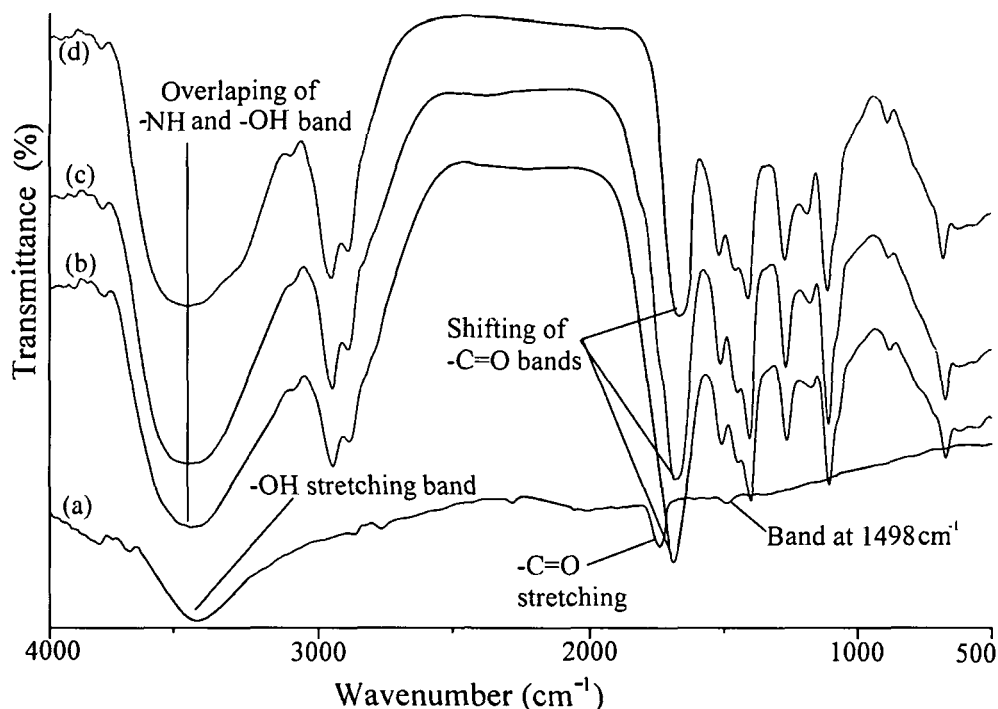


Fig. 8.1: FTIR spectra of (a) acid modified MWCNT, (b) HBPUMWCNT1, (c) HBPUMWCNT2.5 and (d) HBPUMWCNT5

The XRD diffractograms of MWCNT and nanocomposites are given in the Fig. 8.2. The XRD pattern of MWCNT showed two peaks at 2θ value of 25.7° and 42.8° . These can be assigned to (002) and (100) planes of carbon atoms corresponding to the interlayer spacing of 0.34 and 0.21 nm respectively.³ On the contrary, the nanocomposites only showed two peaks at $2\theta = 21.1^\circ$ and 23.4° (Fig. 8.2) for PCL crystals but no peak was observed for MWCNT. The positions of the PCL crystals remain constant in the nanocomposites compared to the pristine HBPU though the intensity of the peaks increased. This is due to the strong nucleating effect of the MWCNT. Other reported literatures also support this observation.^{3,14,25} With the increase of MWCNT concentration the intensity became more and more prominent. The crystallinity obtained from the XRD data are 24.5%, 26.4% and 28.5% for HBPUMWCNT1, HBPUMWCNT2.5 and HBPUMWCNT5 respectively (21.3% for

pure HBPU). The enhancement in the crystallinity of the nanocomposites influences the properties like shape memory (discussed later).

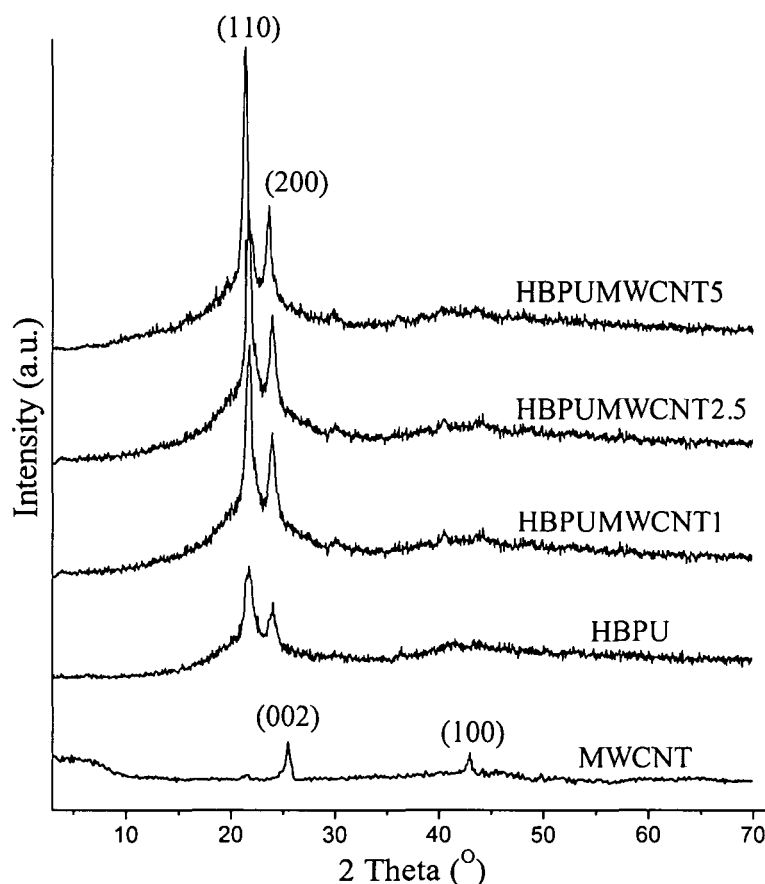


Fig. 8.2: XRD diffractograms of MWCNT, HBPU and the nanocomposites

The SEM and TEM analyses were employed to examine the morphology and distribution of the nanotubes in the HBPU matrix. The SEM micrograph was taken for the fractured surface of the sample after tensile test. The random distribution of the MWCNTs in the polymer matrix can be distinctly seen from Fig. 8.3. The polymer embedded nanotubes were appeared as bright lines in the micrographs. The bright lines increased with the increase of MWCNTs loading. Remarkably, no aggregate was observed from the lowest to the highest loading of MWCNT containing nanocomposites. This is the effect of chemical modification of the MWCNT that facilitates the high degree of wetting by the HBPU and phase adhesion between them.²⁶ It also tempts us to claim the easy way to disperse the MWCNTs in the vegetable oil based hyperbranched matrix. The absence of aggregation of the nanofillers in the matrix, which deteriorates the properties like mechanical, thermal, etc.²⁶ indicates the possibility of significant improvement of the properties in the studied nanocomposites.

Further the distribution pattern of the individual MWCNT was scrutinized with the help of TEM. The representative TEM micrograph of HBPUMWCNT2.5 is given

in the Fig. 8.4. The individual nanotube proves the debundling of the MWCNTs as the diameter was found to be 15 nm (outer) [Fig. 8.4(a)].

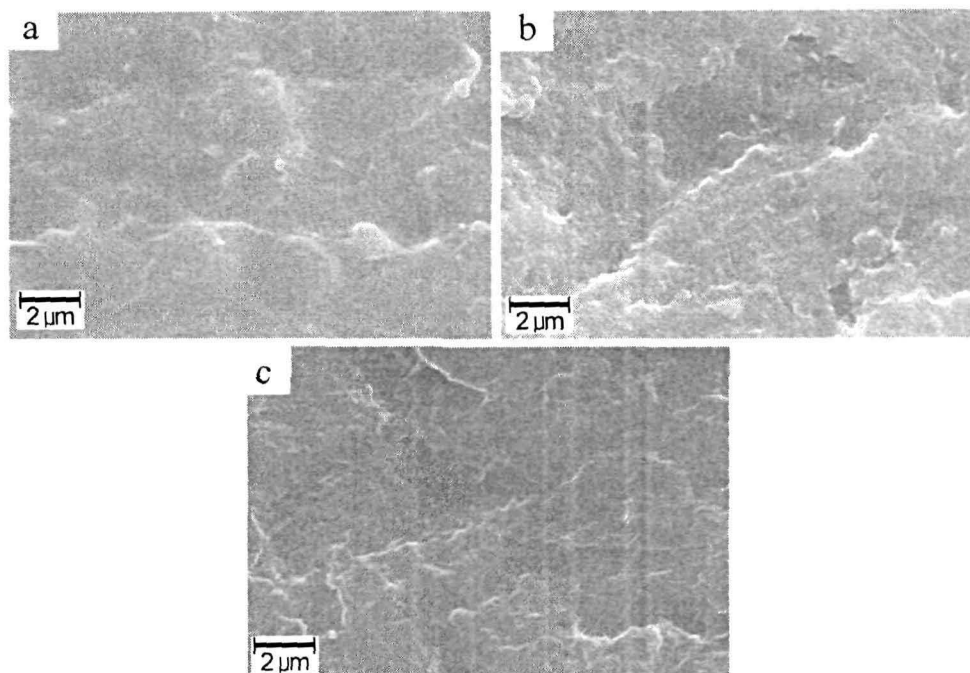


Fig. 8.3: SEM micrographs of (a) HBPUMWCNT1, (b) HBPUMWCNT2.5 and (c) HBPUMWCNT5

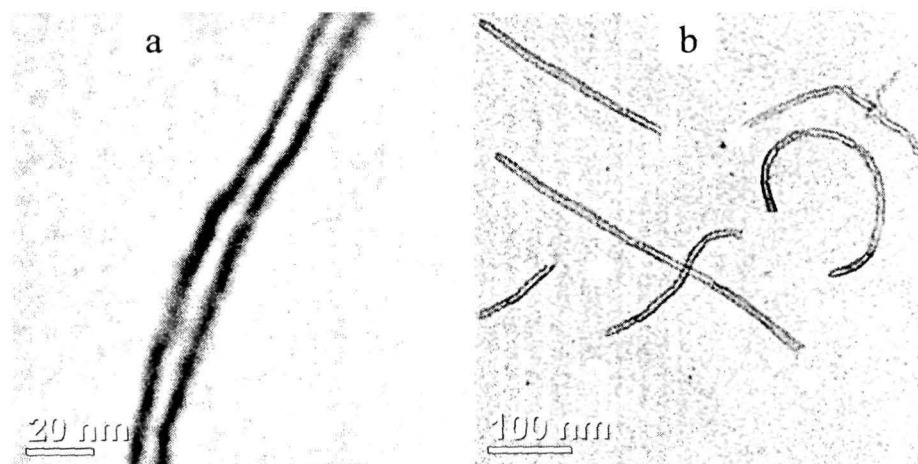


Fig. 8.4: TEM images of (a) magnified single MWCNT and (b) HBPUMWCNT2.5

Thus the SEM and TEM analyses proved the compatibility of the MWCNTs with HBPU matrix and well distribution of the nanotubes without any aggregation.

The use of hyperbranched polymer matrix aids in the uniform dispersion of the nanotubes. The pictorial diagram shown in Fig. 8.5 reflects the fact. The MWCNTs in DMF was settled down completely after one week from the date of sonication. On the other hand, the MWCNTs remain stable and well dispersed in HBPU solution even after seven months. This is possible for the structural confinement of HBPU, where the MWCNTs can easily stabilized by it.⁷

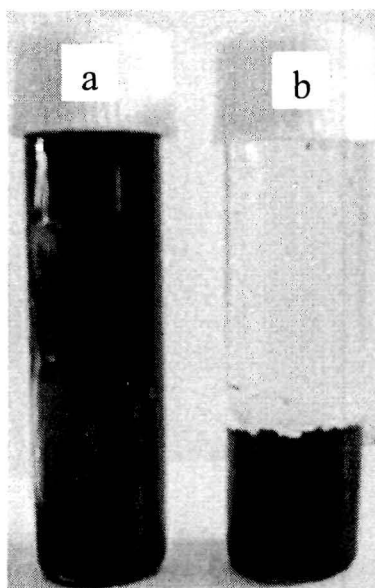


Fig. 8.5: Stability of dispersed MWCNT in (a) HBPU matrix after seven months and (b) DMF after one week

8.3.3. Rheological Properties

The rheological properties of polymer nanocomposites offer some insight about the dispersion state of the fillers in the matrix and hence their properties.

Kuan et al.²⁷ observed aggregation of carbon nanotubes in the linear PU matrix at melting state. They proposed that due to the breakage of the ionic bonds at that processing temperature the interface between the CNT and PU diminished and lead to phase separation. But in this present investigation there was no phase separation occurred by melting the nanocomposites at 120 °C. The structural confinement of the hyperbranched matrix contributed significantly to form stable nanocomposite. This leads us to state the superiority of the hyperbranched matrix for preparation of such nanocomposites.

The shear viscosities of the nanocomposites were determined under controlled rate and constant strain of 10 Pa at 120 °C (Fig. 8.6). The enhancement of the dose dependent shear viscosity of the nanocomposites was observed. The better compatibilizing ability of the HBPU matrix to the modified MWCNT (as observed from SEM and TEM analyses) resulted more interactions. Thus with the increase of amount of MWCNT the imprisonment of segmental movement also increases and hence the viscosity. These interactions may include H-bonding, polar-polar interactions, van der Waals interactions through loop, tail and bridge linkages as shown in Scheme 8.1.

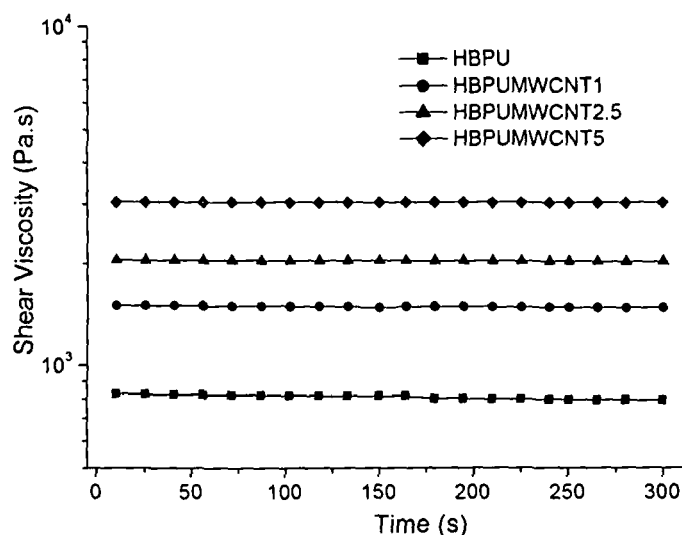


Fig. 8.6: Shear viscosity as a function of time

The effect of shear rate on the shear viscosity of the nanocomposites is shown in Fig. 8.7. The effect of MWCNT loading on the shear viscosity was also examined in the shear rate sweep from 1-100 s^{-1} . It was observed that after incorporation of the modified MWCNT into the pristine HBPU, the shear viscosity increases especially at the low shear rates. The increase of the viscosity also indicated the better dispersion of the nanotubes.^{28,29} The nanocomposites showed shear thinning behavior at relatively high shear rates. It has already been reported that due to the high aspect ratio and strong

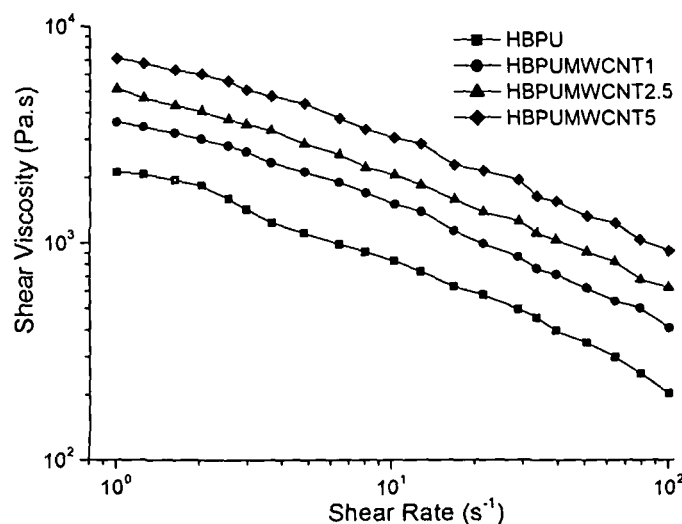


Fig. 8.7: Shear viscosity as a function of shear rate

tube-tube interactions, the dispersed carbon nanotube may form a superstructure network.³⁰ This results a solid-like behavior particularly at low shear rates. The shear thinning behavior at relative high shear rates has been observed. This can be explained by rheological percolation theory as mentioned in Chapter 4, section 4.3.4. Such shear thinning behavior was also reported by different nano fillers containing

nanocomposites.^{31,32} In the present study the observed shear thinning behavior can be fitted by the Ostwald-de Waele power law (equation 8.3) model as follows

$$\eta = K (dy/dt)^{n-1} \quad (8.3)$$

where η is apparent or effective viscosity, K is a constant and n is the flow behavior index ($0 < n < 1$) which indicates the deviation from Newtonian behavior. The prominent decrease of viscosity at relatively high shear rates implies the diminished of processing difficulties associated with the nanotube nanocomposites.

The temperature dependence shear viscosity of the nanocomposites is shown in Fig. 8.8. The experiment was carried out at controlled rate, constant shear (10 s^{-1}) with varying temperature from 100 to 170 °C. It was observed that the shear viscosity decreases with the increase of temperature. The underlying reasons of such dependence are mostly described by two models using William-Landel-Ferry (WLF) and Arrhenius type equations. The WLF equation is based on the concept of free volume fraction.³³ The molecular motions increase with the increase of temperature and result in decrease of intra or inter molecular interactions related to the viscosity as stated in Chapter 4, section 4.3.4. The later equation is purely based on absolute theory of rate process.³⁴ The decrement of viscosity of the nanocomposites with temperature reveals the fact that the nanocomposites can be melt processed with the help of the available conventional equipment in the manufacturing unit. This results further supports the presence of strong secondary interactions amongst the HBPU chain molecules as well as virtual inter phasic interactions between filler-polymer, which were weakened with the increase of temperature.

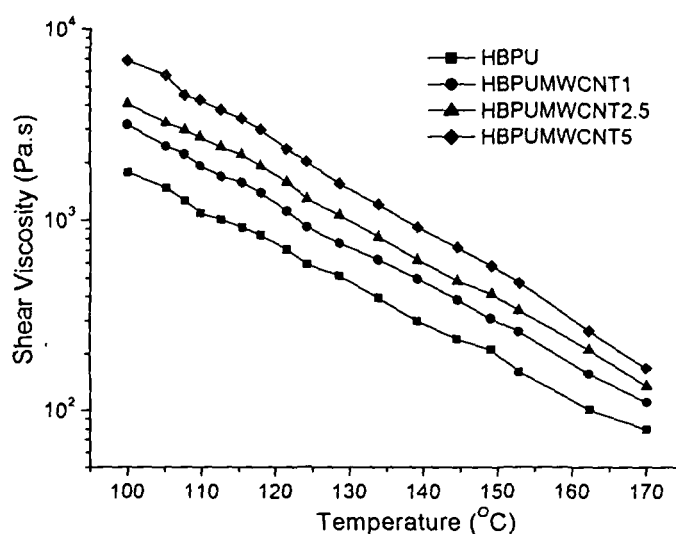


Fig. 8.8: Temperature dependence shear viscosity of the nanocomposites and HBPU

The viscoelastic properties of the nanocomposites were explored by the frequency sweep experiment. The G' , G'' , $\tan\delta$ and η^* of the nanocomposites and pure

HBPU were measured as a function of frequency from 10^0 - 10^2 s^{-1} at 120 °C. The oscillatory stress was kept constant at 10 Pa. It was cleared that the G' and G'' monotonically increased with the increase of frequency [Fig. 8.9(a, b)]. The increments were pronounced at lower frequency region (1 - 5 s^{-1}) than the higher frequencies. Also the G' and G'' values increased with the increased of MWCNT loading. The low frequency dependence of G' and G'' values indicate the solid like behavior of the nanocomposites. The solid like behavior is a sign of the presence of strong interactions

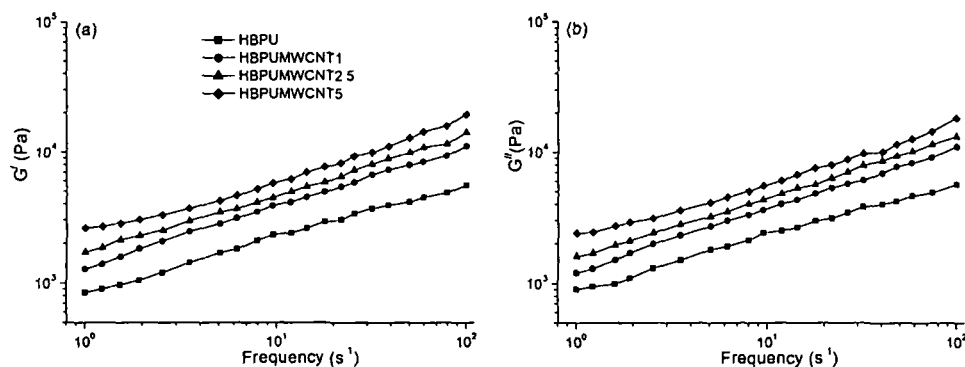


Fig. 8.9: Frequency dependence of (a) G' and (b) G'' of the nanocomposites and HBPU between matrix and reinforcing agents.³² This may be due to the unique structural features of hyperbranched polymers and presence of different polar functionalities in vegetable oil based PU structure and modified MWCNTs. These strong interactions caused incomplete relaxation of the polymer chains contributing the solid like behavior at low frequencies.³⁵ This pseudo solid like response of polymer/CNT nanocomposites has been reported in several literatures.^{36,37} Due to the high aspect ratio, high surface area and modification of surface functionality of the MWCNT, they formed percolated structures and hence the G' and G'' values increased. Moreover the enhancements of the G' and G'' values on incorporation of the nanofillers such as clay, MWCNT etc. were found in other literatures also.^{38,39} The dramatic increment of interfacial area between nanofillers and the matrix is pointed as the main reasons for such enhancement. As the concentration of nanofillers increases, indeed the interactions between the nanofillers become prominent and eventually lead to percolation and forms some interconnected structures. The structural confinement of HBPU along with the dangling chain of the monoglyceride moiety may have contributions to stabilize these superstructures. Hoffman et al.⁴⁰ suggested how the end tethered polymer chain stabilized the superstructures. Noteworthy that, over the whole frequency region the G' was higher than the G'' indicating an enhanced elastic behavior of the nanocomposites. The oscillatory experiments were carried out at oscillatory stress of 10 Pa, because the

nanocomposites showed Newtonian behavior over a period of time up to this stress value as shown in Fig. 8.10.

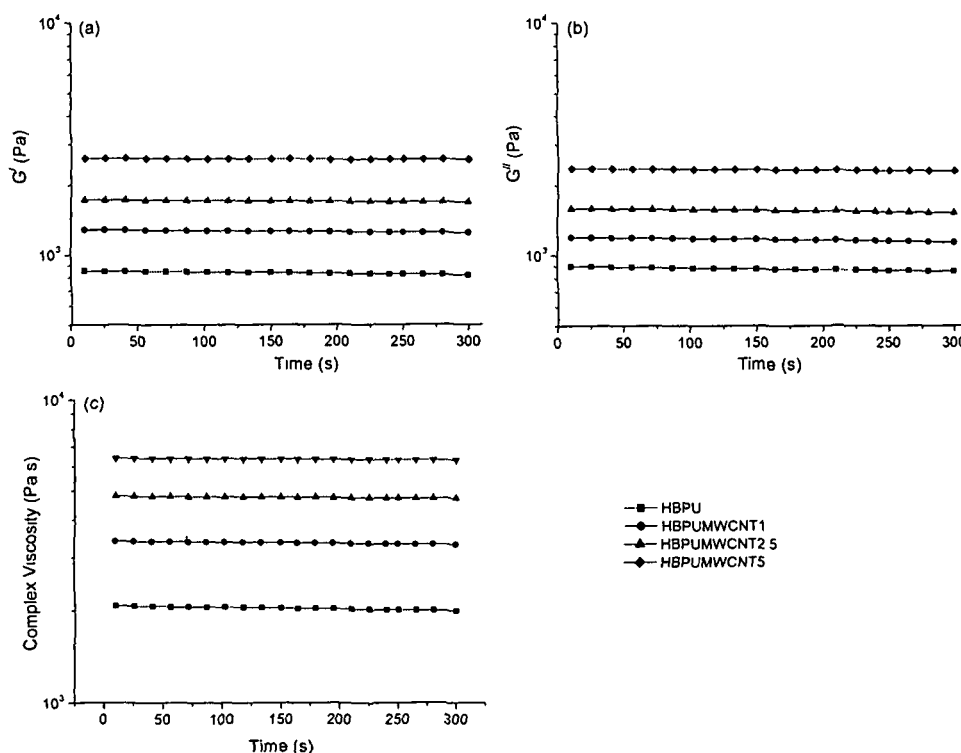


Fig. 8.10: Time dependence plot of (a) G' , (b) G'' and (c) η^* of the nanocomposites and HBPUM

Fig. 8.11(a) depicts the frequency dependence η^* values. The incorporation of the MWCNT in the HBPUM matrix eventually enhances the viscosity of the matrix and it was dependent on MWCNT concentration. This increment of the η^* with loading of MWCNTs is mainly attributed to the increased modulus of the nanocomposites. The effect was more in the low frequency and decreased with the increased of frequency. Thus a frequency thinning character was privilege in the lower frequency range. The η^* of the nanocomposites also followed a similar trend like shear viscosity (Fig. 8.7). Efforts have been made to correlate the oscillatory viscoelastic properties with steady shear viscosity in the literatures.⁴¹ In this regard the applicability of Cox-Merz rule as mentioned in the Chapter 4, section 4.3.4. was investigated. The shear viscosity and the η^* which were obtained at 120 °C were compared for HBPUMWCNT2.5 as given in Fig. 8.11(b).

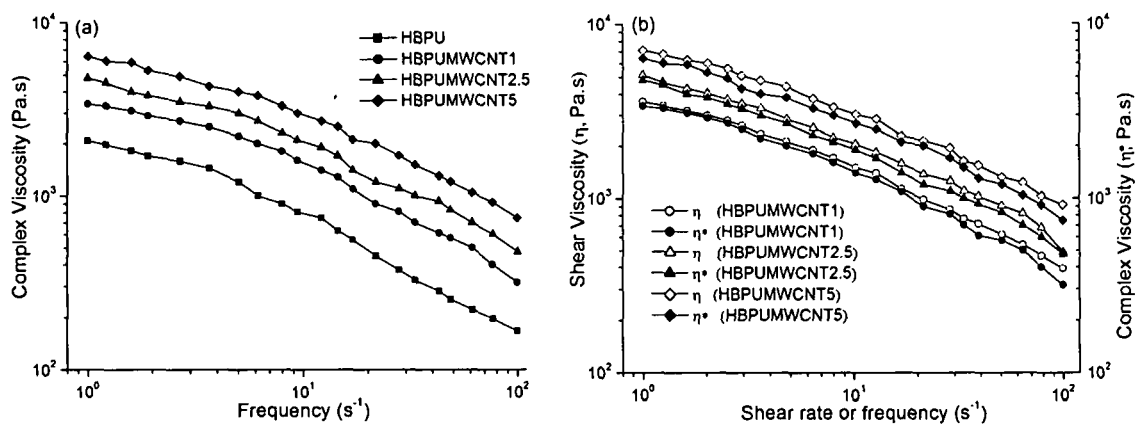


Fig. 8.11: Plot of (a) η^* against frequency of the nanocomposites and HBPUC, (b) shear and η^* against shear rate or frequency

The variation of the $\tan\delta$ with frequency ($1-100\text{ s}^{-1}$) for different loading of MWCNT is shown in Fig. 8.12. It was observed that the $\tan\delta$ values decreased with the increase of MWCNT loading. The $\tan\delta$ values revealed the strong interactions between the HBPUC and nanotubes.

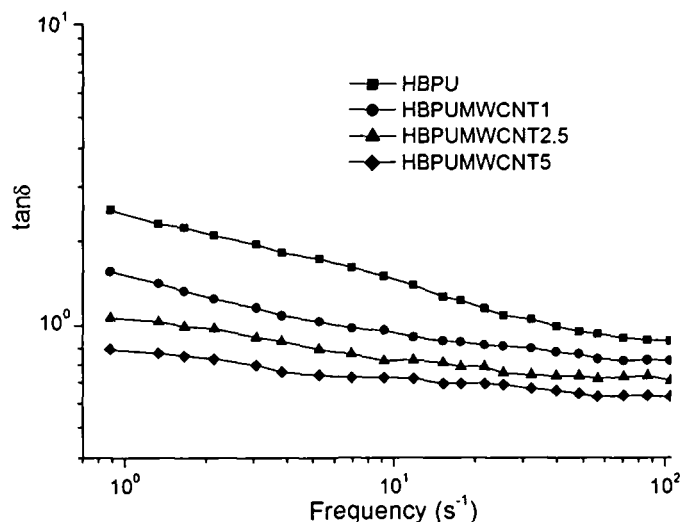


Fig. 8.12: Variation of $\tan\delta$ with frequency

G' and G'' were also studied as a function of temperature sweep (100 to $170\text{ }^\circ\text{C}$) at controlled stress of 10 Pa and constant frequency of 1 s^{-1} in shown Fig. 8.13. The values of G' and G'' were found to be decreased with the increased of temperature. The randomly orientated MWCNTs, which are responsible for the enhanced values of G' and G'' , were forced to align at higher temperatures. This caused the decreased of G' and G'' . The elastic nanotubes “reset” themselves in the polymer matrix at high temperatures.⁴² The more thermo-labile fatty acid chains of the monoglyceride may help the process of alignment of the MWCNT. The highest values of G' and G'' of the

HBPUMWCNT5 at relatively high temperature are attributed to the formation of more afore-stated interactions with the increased of MWCNT loading.

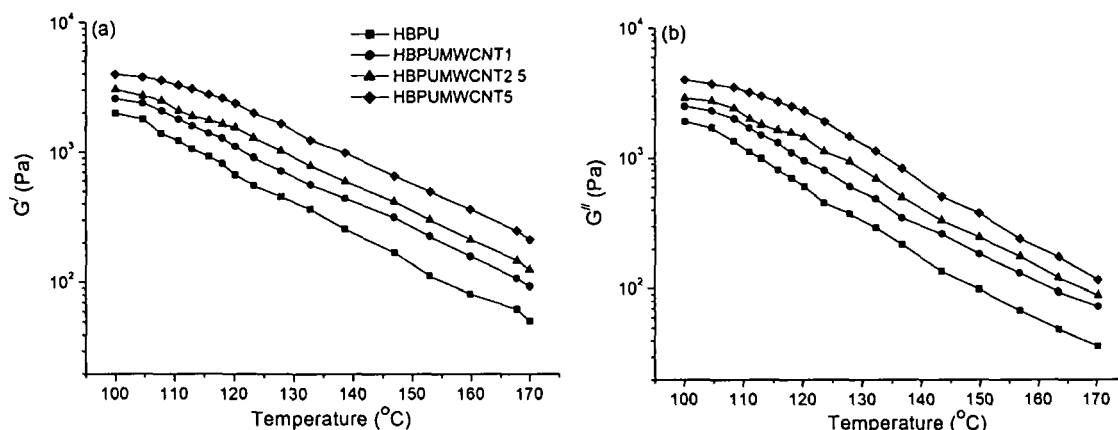


Fig. 8.13: Plot of (a) G' and (b) G'' as a function of temperature sweep

The temperature dependence of η^* was evaluated at 1 s^{-1} from 100 to 170 °C, illustrated in Fig. 8.14. The decreased of η^* values with temperature was observed. These prominent decreases are attributed to the large effect of physical contacts between the nanotubes than the large changes in matrix mobility.⁴³ The two models WLF equation and the Arrhenius type equation as cited above can also be used to explain the decreased of the η^* with temperatures.

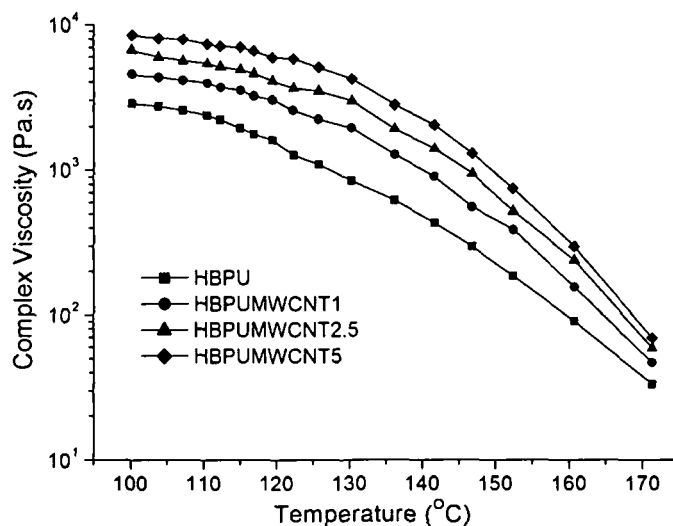


Fig. 8.14: Temperature dependence η^* of the nanocomposites and HBPUM

8.3.4. Mechanical Properties

Several factors such as distribution and orientation, aspect ratio of the nanofillers, domain size and shape, degree of compatibility etc. affect the mechanical properties of polymer nanocomposites.⁴⁴ The efficiency of transferring of stress between the MWCNTs and matrix is the scale for improvement of the mechanical properties. The mechanical properties of the nanocomposites are shown in Table 8.1.

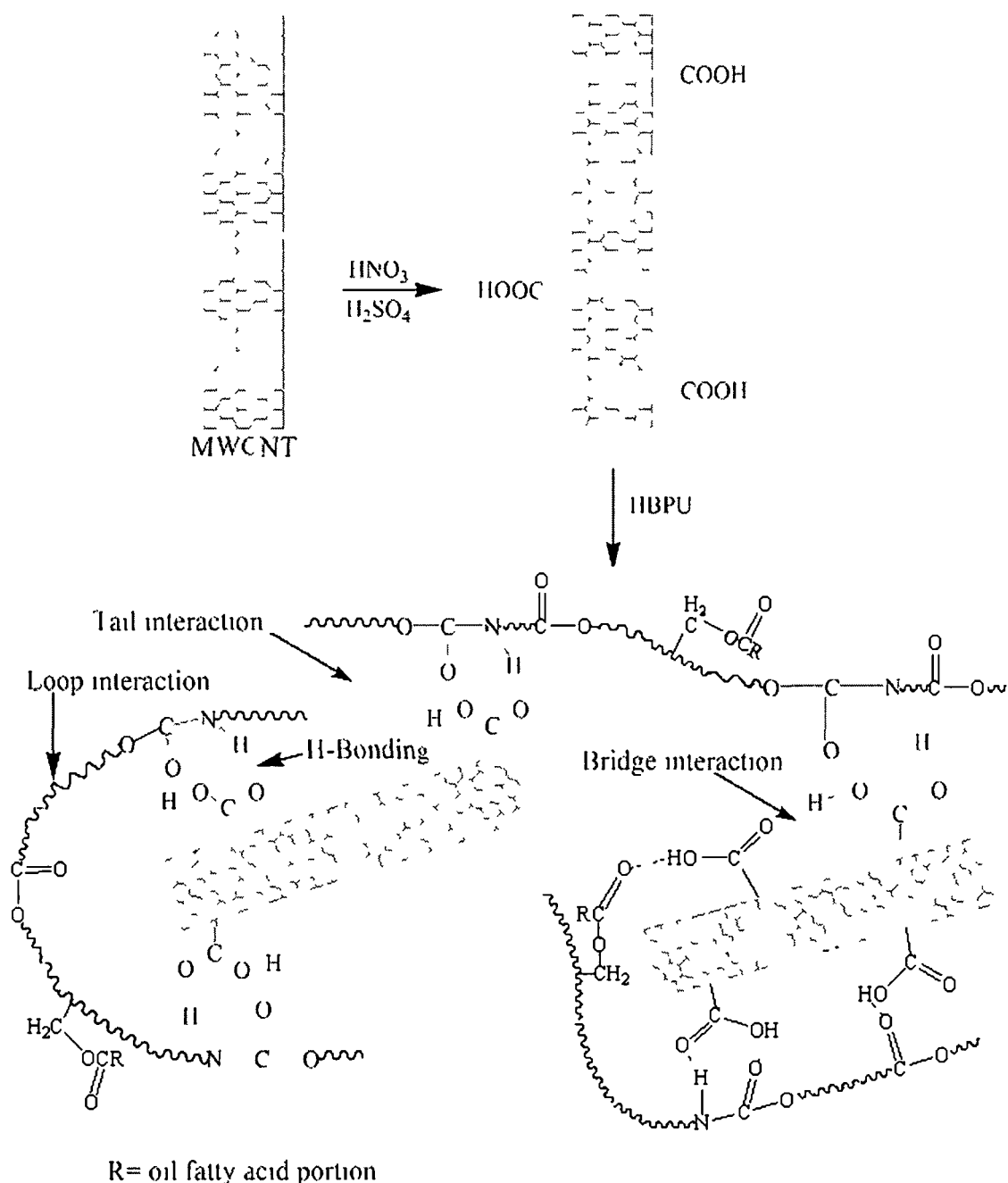
Table 8.1: Mechanical properties and characteristic thermal decomposition temperatures

Code	Tensile strength (MPa)	Elongation at break (%)	T _{ON} (°C)	T _{MAX} (°C)
HBPUMWCNT1	25.2	611	275	410
HBPUMWCNT2.5	37.5	590	288	422
HBPUMWCNT5	46.4	540	296	437

The inclusion of the nanotubes into the HBPU matrix dramatically improves the mechanical properties due to the well known nano-reinforcing effect of the CNTs.^{3,4,6} While the pristine HBPU shows the tensile strength of 6 MPa (Chapter 2, Table 2.4), the nanocomposite comprising of 1 weight% MWCNTs has the strength of 25 MPa. With the increase of MWCNTs dose from 1 to 5 weight%, the strength also increases up to 46 MPa (Table 8.1). Kim et al. described the improvement of mechanical strength of similar type of acid modified MWCNT/polyester nanocomposites, where the predicted theoretical values by modified Halpin-Tsai equation are in agreement with the experimental results.²⁴ Here, about 3 fold increase in the tensile strength has been achieved by formation of nanocomposites even at very low loading of MWCNTs (1 weight%). The better interfacial bonding (as confirmed from SEM and TEM micrographs) between HBPU and modified MWCNTs is attributed to this improvement. The introduction of –COOH groups on the surface wall of MWCNTs facilitates the H-bonding amongst the urethane, ester groups of HBPU as shown in Scheme 8.1. This increase of molecular restrictions of the polymer chains manifested by the decrease of elongation at break of the nanocomposites compared to the pristine HBPU (Table 8.1). However, the final elongation at break value even at 5 weight% MWCNT is sufficient for any biomedical application. Thus the optimum mechanical property was obtained for HBPUMWCNT5.

8.3.5. Thermal Properties

The thermal stability of the prepared nanocomposites was tested by TGA analysis (Fig. 8.15). The eminent feature of MWCNTs is their excellent thermal stability.² Insertion of these MWCNTs into the hyperbranched matrix increases its thermal stability as evident from the Fig. 8.15. The pristine HBPU was stable up to 215 °C (Chapter 2, Table 2.5), whereas with the incorporation of 1 weight% MWCNTs into



Scheme 8.1: Possible interactions of MWCNTs with HBPU matrix

the matrix the thermal stability increases up to 275 °C. Further, the nanocomposites showed one step degradation pattern, while the pristine HBPU exhibited two step degradation patterns. Thus it signified uniform dispersion and high interactions of MWCNTs with HBPU matrix. The T_{ON} and T_{MAX} for the nanocomposites are shown in Table 8.1. The reason behind the steady enhancement of such parameters is due to the fact that MWCNTs act as the physical crosslinking points (as shown in Scheme 8.1), which restrict the movements of the polymer chains.⁴⁵ Thus volatile products formed during heating process have to cross a longer path to escape from the matrix⁴⁶ Also the MWCNTs act as thermal insulator. Further the dose dependent increment of thermo-

stability was also noticed from the Fig. 8.15. The delay of thermal degradation is mainly due to the presence of well dispersed thermo-insulating MWCNTs in the

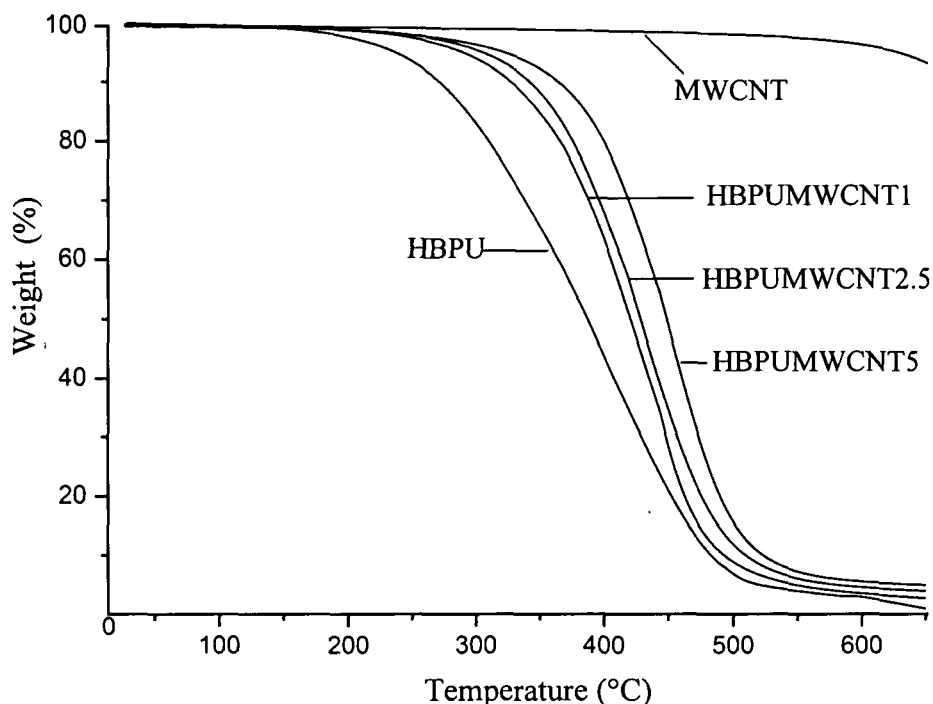


Fig. 8.15: TGA thermograms of MWCNT and nanocomposites

polymer matrix. The improved interfacial adhesion between the modified MWCNT and HBPU (as explained earlier) retarded the segmental motions of the polymer chains. The increase of residual yield with the increase of MWCNT loading from 1 to 5 weight% further proves the thermo-insulating nature of the nanofillers.

The thermal properties such as T_m and ΔH_m were studied by DSC (Table 8.2). The T_m of the soft segments was found to be increased for the nanocomposites from 47 to 56 °C compared to the pristine HBPU (T_m value for HBPU is 47 °C). The increase in amount of MWCNT also raises the T_m . The well dispersion of the nanotubes as well as formation of rigid structure through different molecular interactions (as affirmed earlier) is responsible for this increment. The increase of the ΔH_m value with the increase of MWCNT amount further confirmed the enhancement of degree of crystallinity of the PCL. This indicates the nucleating effect of the MWCNT.^{3,14} The obtained results from DSC are in agreement with the result of the XRD study. The storage elastic energy increases with the increase of crystallinity in the system. This is reflected in shape recovery values of the nanocomposites (Table 8.2).

Table 8.2: T_m , ΔH_m and shape recovery of the nanocomposites

Code	T_m (°C)	ΔH_m (J/g)	Shape recovery (%)	Shape fixity (%)
HBPUMWCNT1	49	53.8	96.5	92.2
HBPUMWCNT2.5	52	56.7	97.3	91.5
HBPUMWCNT5	56	59.1	98.5	90.7

8.3.6. Shape Memory Study

The shape memory behavior of the HBPU/MWCNT is shown in Fig. 8.16. The nanocomposites exhibited well shape memory property on addition of MWCNT as shown in Table 8.2. All the nanocomposites recovered their shape (shape recovery time) within 30 s after release of stress. The shape memory property of material depends on two crucial factors. Firstly, the presence of quantitative amount of unlocked orientated polymer chains. When an external force is applied to stretch the samples, the produced deformation is memorized by crystallization of the soft segment. A few numbers of chains retain the mobility and can generate an instantaneous retractive force upon elimination of the load because of the entropic elasticity. However, this small fraction is not enough to cause instantaneous recovery of shape. Second imperative factor is the value of room temperature modulus. If the modulus of the material at room temperature is low, then one can expect a rapid instantaneous recovery strain.⁴⁷

The shape recovery was estimated after the nanocomposites were fixed for 5 min at (0-5) °C (below the transition temperature of PCL crystal). The shape recovery and shape fixity values for the HBPU were 93% and 93.3% respectively. Thus nanocomposites showed better shape recovery than the pristine HBPU (Table 8.2). This can be attributed to the increased stored energy as a result of homogeneously distributed nanotubes in the polymer matrix.³ The MWCNT produced higher stored elastic strain energy which in turn helped the nanocomposites to gain higher recovery stress due to release of stored elastic strain.⁴⁸ With the increase of amount of MWCNT in the matrix the shape recovery was also found to be increased. It may be justified to correlate the increased degree of crystallinity to this increasing trend of shape memory property. The increased crystallinity on incorporation of MWCNTs (as obtained from DSC and XRD results) resulted increase in amount of unlocked oriented chains, which in turn enhanced the shape recovery.⁴⁷ The importance of crystallinity in determining shape memory property of HBPU is described by Sivakumar et al.⁴⁹ The factors that affect the crystallinity also influence the shape memory property. Further, the acid

modification of MWCNT layers attributed to this enhancement of the soft segments crystallinity. Gunes et al. observed higher soft segments crystallinity for the oxidized-CNT/PU nanocomposites than the unmodified CNT/PU nanocomposites.⁵⁰ Rana et al.³ observed shape recovery of 84% for vegetable oil based HBPU/MWCNT nanocomposites having 2 weight% MWCNT loading, while this value is 97.3% for HBPUMWCNT2.5 in the present study.

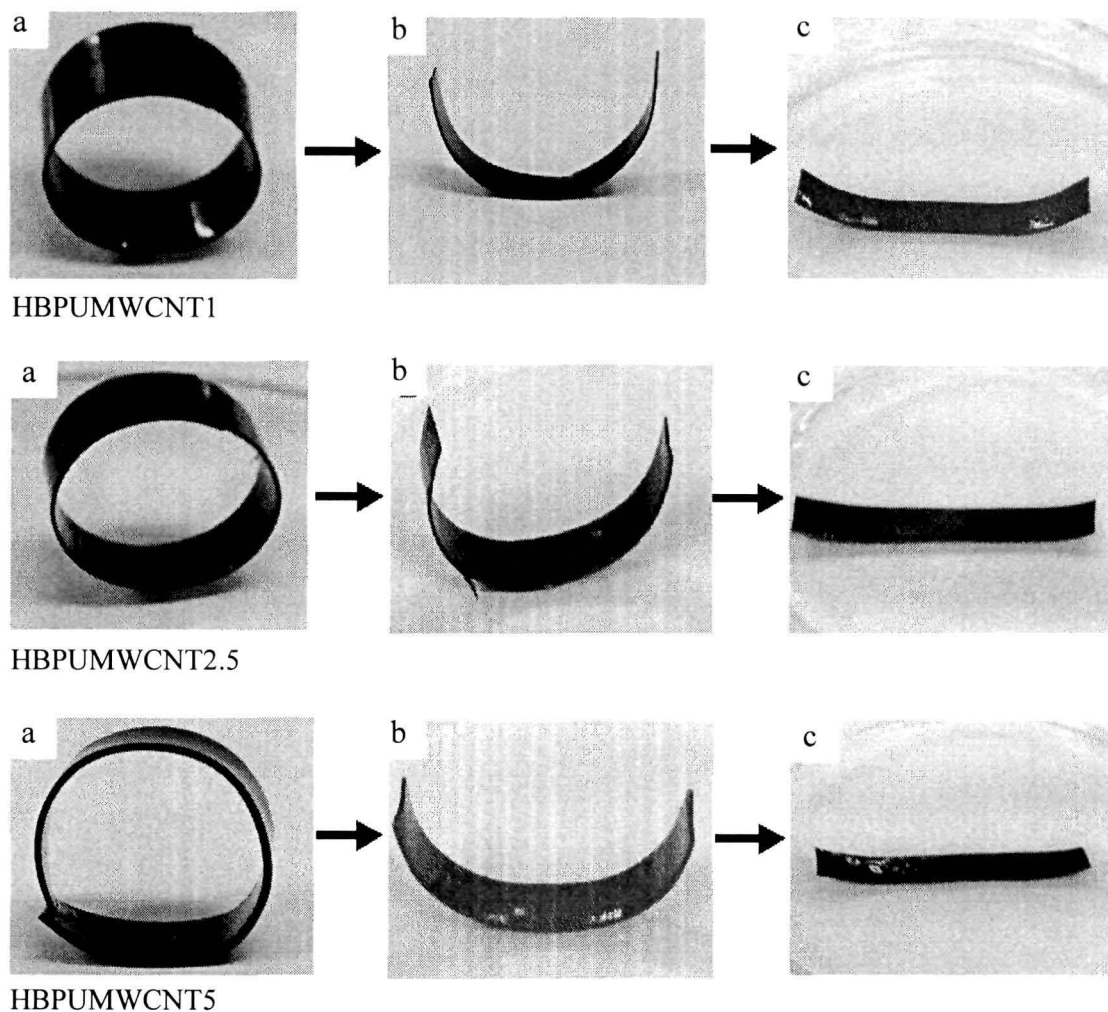


Fig. 8.16: Shape recovery behavior of the nanocomposites measured at 60 °C: (a) initial shape, (b) intermediate shape and (c) permanent shape after recovery

8.3.7. RBC Hemolysis Protection Assay

The emergence of nanotechnology also raises the question of safety from any possible toxic effect of nano structures.¹⁸ Thus it is imperative to investigate the adverse effect of MWCNT based biomaterials before they may be forwarded for widespread acceptance and use. Here, the cytocompatibility for the HBPU and nanocomposites was investigated by RBC hemolysis protection assay and the results are shown in Fig. 8.17. The films are non-cytotoxic as implied by the assessment. The nanocomposites

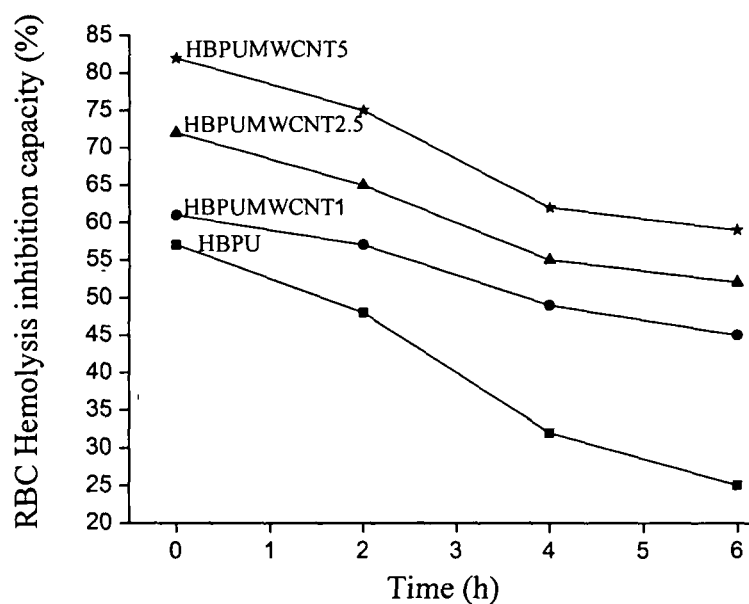


Fig. 8.17: The RBC hemolysis protection assay of the nanocomposites

prominently prevented the damage to the cell by the free radicals. This is due to the high free radical scavenging property of HBPU/MWCNT nanocomposites that react with free radicals, by two mechanisms, viz., electron transfer process and adduct formation.⁵¹ The assay was continued for 6 h with monitoring at 2 h interval. A decline in the inhibition of hemolysis was observed after 2 h of the assay period. The increasing saturation of MWCNTs may be responsible for this retardation.⁵² However, up to 6 h the nanocomposites retained sufficient inhibition capacity. The hemolysis inhibition value increased with the increase of MWCNT concentration from 1 to 5 weight%. This dose dependent inhibition behavior is a direct consequence of MWCNT. The high tendency of agglomeration of the MWCNT due to their strong intertubular forces raises question about their toxicity.⁵³ The modification of MWCNT enhanced the interaction with HBPU matrix. The architectural beauty of HBPU has ample contribution to the stabilized composite formation. Thus the study reveals the cytocompatibility of the nanocomposites as well as capacity to protect the cell from harmful free radical activity. Hence, the fixed MWCNTs are proved to be non-toxic, even though the free MWCNT may be toxic.⁵³

8.3.8. Biodegradation

The study of the effect of MWCNT on degradation behavior was one of the prime objects in this experiment. The nanocomposite films were directly exposed to the microbial attack and their growth was monitored. Finally, the quantitative degradation of the nanocomposites was estimated. Two different strains of *P. aeruginosa*, MTCC

7814 and MTCC7815 were employed. The growth of the bacterial strains as obtained from McFarland turbidity method, are shown in Fig. 8.18. Substrate specificity in

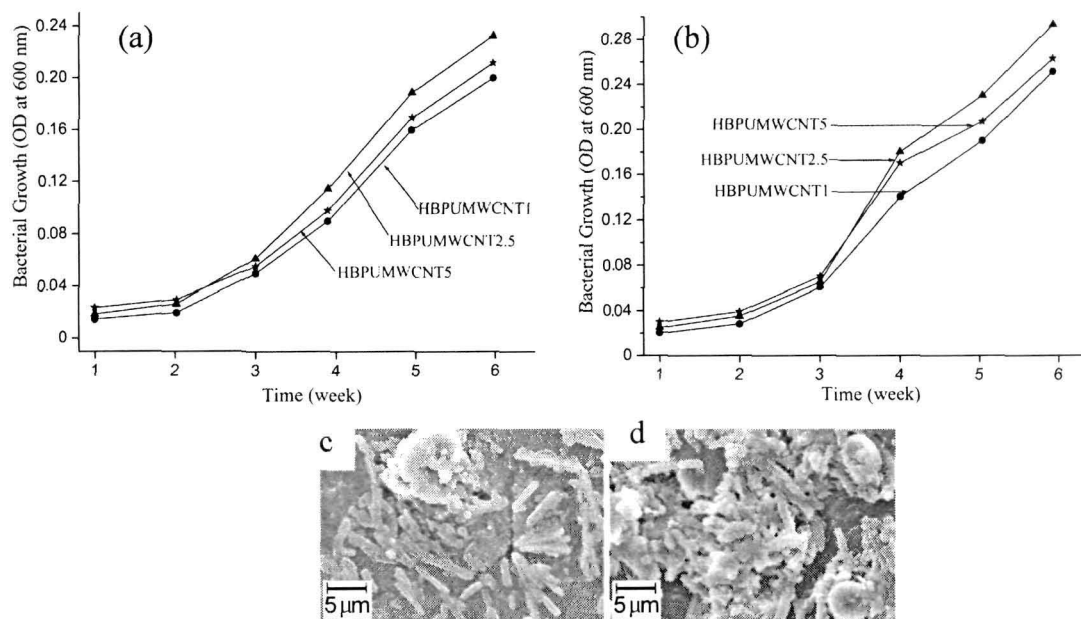


Fig. 8.18: Statistics for the growth of *P. aeruginosa* strain (a) MTCC 7814, (b) MTCC 7815 and SEM images of degraded nanocomposites: (c) HBPUMWCNT1 and (d) HBPUMWCNT5

degradation pattern is cleared from the figure. The effect of MWCNT on degradation of HBPU is seen after 3 weeks of exposure as the bacterial population is higher in nanocomposites than in the pristine HBPU. The bacterial growth was continuously increasing up to 6 weeks. Generally the microbial degradation takes place in two steps. The higher molecular weight polymers are initially hydrolyzed to lower molecular weight oligomers, where acids, base or water accelerate this step followed by the consumptions of the oligomeric products to produce CO_2 , humus etc.⁵⁴ The polar groups of the matrix along with the acid groups of the MWCNTs absorb water which accelerates the first step and thus became the determining step for biodegradation. The composite comprising of 5 weight% MWCNT showed sluggish degradation than the other two. This is because of the two opposite factors controlling the rate of degradation. While the water absorption capacity enhances the rate of degradation, the increasing crystallinity slows down the rate. With the increase of MWCNT, both these aspects become prominent and the negative factor is the strongest in case of HBPUMWCNT5.

8.4. Conclusions

Thus the study revealed good dispersion of MWCNT in the *Mesua ferrea* L. seed oil based HBPU matrix as evident from the FTIR, XRD, SEM and TEM analyses. It was observed that the MWCNT had prolific influence on the rheological properties of the nanocomposites. The nanocomposites showed improved mechanical and thermal properties. The shape memory property of the nanocomposites was found to be enhanced with the increase of concentration of MWCNTs with reference to the pristine HBPU. It may be pointed out that the overall shape recovery of the composite, to the extent of 98.5%, is quite significant. The nanocomposite displayed biocompatibility in terms of non-toxicity at the cellular level, and biodegradability. In view of the above features, the HBPU/MWCNT nanocomposites may be considered as strong candidates for further exploration in biomedical applications.

References

1. Kim, K.H.; Jo, W.H. A strategy for enhancement of mechanical and electrical properties of polycarbonate/multi-walled carbon nanotube composites. *Carbon* **47**, 1126-1134 (2009)
2. Moniruzzaman, M.; Winey, K.I. Polymer nanocomposites containing carbon nanotubes. *Macromolecules* **39**, 5194-5205 (2006)
3. Rana, S.; Karak, N.; Cho, J.W.; Kim, Y.H. Enhanced dispersion of carbon nanotubes in hyperbranched polyurethane and properties of nanocomposites. *Nanotechnol.* **19**, 495707(pp8) (2008)
4. Zhao, C.X.; Zhang, W.D.; Sun, D.C. Preparation and mechanical properties of waterborne polyurethane/carbon nanotube composites. *Polym. Compos.* **30**, 649-654 (2009)
5. Kuan, H.C. et al. Synthesis, thermal, mechanical and rheological properties of multiwall carbon nanotube/waterborne polyurethane nanocomposites. *Compos. Sci. Technol.* **65**, 1703-1710 (2005)
6. Xu, Y.; Gao, C.; Kong, H.; Zheng, Y.Z.; Watts, P.C.P. Growing multihydroxyl hyperbranched polymers on the surfaces of carbon nanotubes by *in situ* ring-opening polymerization. *Macromolecules* **37**, 8846-8853 (2004)
7. Karak, N.; Maiti, S. *Dendrimers and Hyperbranched Polymers-Synthesis to Applications* (MD Publication Pvt Ltd., New Delhi, 2008)
8. Liu, C.; Qin, H.; Mather, P.T. Review of progress in shape-memory polymers. *J. Mater. Chem.* **17**, 1543-1558 (2007)

9. Ratna, D.; Karger-Kocsis, J. Recent advances in shape memory polymers and composites: A review. *J. Mater. Sci.* **43**, 254-269 (2008)
10. Behl, M.; Lendlein, A. Shape-memory polymers. *Mater. Today* **10**, 20-28 (2007)
11. Feninat, F.El; Laroche, G.; Fiset, M.; Mantovani, D. Shape memory materials for biomedical applications. *Adv. Eng. Mater.* **4**, 91-104 (2002)
12. Meng, Q.; Hu, J.; Zhu, Y. Shape-memory polyurethane/multiwalled carbon nanotube fibers. *J. Appl. Polym. Sci.* **106**, 837-848 (2007)
13. Kim, B.K.; Lee, J.S.; Lee, Y.M.; Shin, J.H. Shape memory behavior of amorphous polyurethanes. *J. Macromol. Sci. Phys. B* **40**, 1179-1191 (2001)
14. Sahoo, N.G.; Jung, Y.C.; Yoo, H.J.; Cho, J.W. Influence of carbon nanotubes and polypyrrole on the thermal, mechanical and electroactive shape-memory properties of polyurethane nanocomposites. *Compos. Sci. Technol.* **67**, 1920-1929 (2007)
15. Chandra, R.; Rusti, G. Biodegradable polymers. *Prog. Polym. Sci.* **23**, 1273-1335 (1998)
16. Dutta, S.; Karak, N.; Saikia, J.P.; Konwar, B.K. Biocompatible epoxy modified bio-based polyurethane nanocomposites: Mechanical property, cytotoxicity and biodegradation. *Bioresour. Technol.* **100**, 6391-6397 (2009)
17. Planck, H.; Syre, I.; Dauner, M.; Egbers, G. *Polyurethane in Biomedical Engineering II, Progress in Biomedical Engineering* (Elsevier, Amsterdam, 1987)
18. Smart, S.K.; Cassady, A.I.; Lu, G.Q.; Martin, D.J. The biocompatibility of carbon nanotubes. *Carbon* **44**, 1034-1047 (2006)
19. Gultekin, G. et al. Fatty acid-based polyurethane films for wound dressing applications. *J. Mater. Sci. Mater. Med.* **20**, 421-431 (2009)
20. Zhang, Q. et al. Use of dynamic rheological behavior to estimate the dispersion of carbon nanotubes in carbon nanotube/polymer composites. *J. Phys. Chem. B* **112**, 12606-12611 (2008)
21. Song, Y.S. Rheological characterization of carbon nanotubes/poly(ethylene oxide) composites. *Rheol. Acta.* **46**, 231-238 (2006)
22. Ji, F.L.; Hu, J.L.; Li, T.C.; Wong, Y.W. Morphology and shape memory effect of segmented polyurethanes. Part I {cyrillic, ukrainian}: With crystalline reversible phase. *Polymer* **48**, 5133-5145 (2007)
23. Xiong, J. et al. The thermal and mechanical properties of a polyurethane/multi-walled carbon nanotube composite. *Carbon* **44**, 2701-2707 (2006)
24. Kim, J.Y.; Han, S.I.; Hong, S. Effect of modified carbon nanotube on the properties of aromatic polyester nanocomposites. *Polymer* **49**, 3335-3345 (2008)

25. Xu, D.; Wang, Z. Role of multi-wall carbon nanotube network in composites to crystallization of isotactic polypropylene matrix. *Polymer* **49**, 330-338 (2008)
26. Chen, W.; Tao, X.; Liu, Y. Carbon nanotube-reinforced polyurethane composite fibers. *Compos. Sci. Technol.* **66**, 3029-3034 (2006)
27. Kuan, H.C. et al. Synthesis, thermal, mechanical and rheological properties of multiwall carbon nanotube/waterborne polyurethane nanocomposites. *Compos. Sci. Technol.* **65**, 1703-1710 (2005)
28. Mitchell, C.A.; Bahr, J.L.; Arepalli, S.; Tour, J.M.; Krishnamoorti, R. Dispersion of functionalized carbon nanotubes in polystyrene. *Macromolecules* **35**, 8825-8830 (2002)
29. Song, Y.S. Effect of surface treatment for carbon nanotubes on morphological and rheological properties of poly(ethylene oxide) nanocomposites. *Polym. Eng. Sci.* **46**, 1350-1357 (2006)
30. Chatterjee, T.; Yurekli, K.; Hadjiev, V.G.; Krishnamoorti, R. Single-walled carbon nanotube dispersions in poly(ethylene oxide). *Adv. Funct. Mater.* **15**, 1832-1838 (2005)
31. Hyun, Y.H.; Lim, S.T.; Choi, H.J.; Jhon, M.S. Rheology of poly(ethylene oxide)/organoclay nanocomposites. *Macromolecules* **34**, 8084-8093 (2001)
32. Valentini, L.; Biagiotti, J.; Kenny, J.M.; Santucci, S. Morphological characterization of single-walled carbon nanotubes-PP composites. *Compos. Sci. Technol.* **63**, 1149-1153 (2003)
33. Williams, M.L.; Landel, R.F.; Ferry, J.D. The temperature dependence of relaxation mechanisms in amorphous polymers and other glass-forming liquids. *J. Am. Chem. Soc.* **77**, 3701-3707 (1955)
34. Eyring, H. Viscosity, plasticity, and diffusion as examples of absolute reaction rates. *J. Chem. Phys.* **4**, 283-291 (1936)
35. Zhang, Q.; Lippits, D.R.; Rastogi, S. Dispersion and rheological aspects of SWNTs in ultrahigh molecular weight polyethylene. *Macromolecules* **39**, 658-666 (2006)
36. Lee, S.H.; Kim, M.W.; Kim, S.H.; Youn, J.R. Rheological and electrical properties of polypropylene/MWCNT composites prepared with MWCNT masterbatch chips. *Eur. Polym. J.* **44**, 1620-1630 (2008)
37. Abdel-Goad, M.; Potschke, P. Rheological characterization of melt processed polycarbonate-multiwalled carbon nanotube composites. *J. Non. Newtonian Fluid Mech.* **128**, 2-6 (2005)

38. Lim, S.T.; Hyun, Y.H.; Choi, H. Synthetic biodegradable aliphatic polyester/montmorillonite nanocomposites. *Chem. Mater.* **14**, 1839-1844 (2002)
39. Jin, S.H.; Park, Y.B.; Yoon, K.H. Rheological and mechanical properties of surface modified multi-walled carbon nanotube-filled PET composite. *Compos. Sci. Technol.* **67**, 3434-3441 (2007)
40. Hoffmann, B.; Kressler, J.; Stoppelmann, G.; Friedrich, Chr.; Kim, G.M. Rheology of nanocomposites based on layered silicates and polyamide-12. *Colloid. Polym. Sci.* **278**, 629-636 (2000)
41. Laun, H.M. Prediction of elastic strains of polymer melts in shear and elongation. *J. Rheol.* **30**, 459-501 (1986)
42. Schoch, A.B.; Shull, K.R.; Brinson, L.C. Junction-controlled elasticity of single-walled carbon nanotube dispersions in acrylic copolymer gels and solutions. *Macromolecules* **41**, 4340-4346 (2008)
43. Rodlert, M. et al. Hyperbranched polymer/montmorillonite clay nanocomposites. *Polymer* **45**, 949-960 (2004)
44. Crosby, A.J.; Lee, J.Y. Polymer nanocomposites: The "nano" effect on mechanical properties. *Polym. Rev.* **47**, 217-229 (2007)
45. Jin, S.H.; Park, Y.B.; Yoon, K.H. Rheological and mechanical properties of surface modified multi-walled carbon nanotube-filled PET composite. *Compos. Sci. Technol.* **67**, 3434-3441 (2007)
46. Jeong, E.H. et al. Effective preparation and characterization of montmorillonite/poly(ϵ -caprolactone)-based polyurethane nanocomposites. *J. Appl. Polym. Sci.* **107**, 803-809 (2008)
47. Gunes, S.; Cao, F.; Jana, S.C. Evaluation of nanoparticulate fillers for development of shape memory polyurethane nanocomposites. *Polymer* **49**, 2223-2234 (2008)
48. Ni, Q.Q.; Zhang, C.S.; Fu, Y.; Dai, G.; Kimura, T. Shape memory effect and mechanical properties of carbon nanotube/shape memory polymer nanocomposites. *Compos. Struct.* **81**, 176-184 (2007)
49. Sivakumar, C.; Nasar, A.S. Poly(ϵ -caprolactone)-based hyperbranched polyurethanes prepared via $A_2 + B_3$ approach and its shape-memory behavior. *Eur. Polym. J.* **45**, 2329-2337 (2009)
50. Gunes, I.S.; Jimenez, G.A.; Jana, S.C. Carbonaceous fillers for shape memory actuation of polyurethane composites by resistive heating. *Carbon* **47**, 981-997 (2009)

51. Galano, A. Carbon nanotubes as free-radical scavengers. *J. Phys. Chem. C* **112**, 8922-8927 (2008)
52. Zhu, Q.Y.; Holt, R.R.; Lazarus, S.A.; Orozco, T.J.; Keen, C.L. Inhibitory effects of cocoa flavanols and procyanidin oligomers on free radical-induced erythrocyte hemolysis. *Exp. Biol. Med.* **227**, 321-329 (2002)
53. Tagmatarchis, N.; Prato, M. Functionalization of carbon nanotubes via 1,3-dipolar cycloadditions. *J. Mater. Chem.* **14**, 437-439 (2004)
54. Maiti, P.; Batt, C.A.; Giannelis, E.P. New biodegradable polyhydroxybutyrate/layered silicate nanocomposites. *Biomacromolecules* **8**, 3393-3400 (2007)

CHAPTER 9

Conclusions and future directions

9.1. Summary and Conclusions

The thesis highlights the synthesis, characterization, properties evaluation and application of *Mesua ferrea* L. seed oil based HBPU and their various nanocomposites. The first chapter of this thesis describes a brief review on the vegetable oil based PU nanocomposites emphasizing the importance, general techniques of preparation, characterization, properties and applications. The scopes, objectives and plans of work for the present investigation are also focused here. The entire technical work of the present investigation is divided into seven different parts.

In the first part, the synthesis, characterization and properties evaluation of *Mesua ferrea* L. seed oil based HBPU with varying hard and soft segment ratio were described. The linear analog was also synthesized for comparison purpose. The HBPU were prepared by an $A_2 + B_3$ approach through one pot pre-polymerization technique.

In the second part, enhancement of various performance characteristics of the HBPU with 30% hard segment content was reported through the modification by commercial bisphenol-A based epoxy resin and poly(amido amine) hardener system.

The third and fourth parts of the technical work dealt with the preparation, characterization and performance characteristics of epoxy modified HBPU nanocomposites reinforced with organically modified montmorillonite, OMMT, by *ex-situ* and *in-situ* techniques respectively. The rheological characterization also provides some insights about the dispersion state of the nanofillers in the matrices. Further the nanocomposites prepared by *in-situ* technique showed biodegradation behavior as tested by laboratory broth culture technique.

In the fifth part, the effect of modification of OMMT by s-triazine based highly branched poly(amido amine), HBPA, and consequent nanocomposites with the epoxy modified HBPU were reported. The HBPA was synthesized by a simple nucleophilic displacement polymerization technique by using relatively low cost materials via an $A_2 + B_3$ approach. This part primarily focuses on the mode of modification and its effect on the properties of the nanocomposites. The nanocomposites exhibited high thermal stability and flame retardancy.

The preparation, characterization, properties evaluation and applications of different metal nanocomposites using the aforementioned HBPU as the matrix with

silver, and with iron based nanoparticles were reported in the sixth part of the technical work. While the silver based nanocomposites showed the high potential as a biodegradable biomaterial, the iron based nanocomposite can be utilized as free radical scavenging material.

The final part of the technical work described the preparation, characterization and properties of the HBPU/MWCNT nanocomposites as shape memory biomaterials. Along with the physical, mechanical, thermal etc. properties, rheological characteristics, biodegradability etc. were studied in details to interpret the structure property relationship for the nanocomposite systems.

The summary and conclusions along with the future directions of the whole thesis is described in the last chapter that is the present chapter of the thesis.

From the present investigation following conclusions have been drawn.

- (i) A highly potential non-edible vegetable oil, *Mesua ferrea* L. seed oil was successfully utilized for the first time to prepare HBPU by an $A_2 + B_3$ approach without gel formation. The linear analog of the HBPU was also synthesized for comparison purpose. Among the various ratios of hard and soft segments, 30% hard segment containing HBPU showed the optimum performance and hence this ratio was utilized for further studies.
- (ii) The synthesized PUs were successfully characterized by the conventional analytical and spectroscopic techniques. The various properties such as physical, mechanical, thermal and biodegradation confirmed the suitability of this polymer as matrix for nanocomposite preparation.
- (iii) The modification of the HBPU with the commercially available epoxy resin and poly(amido amine) hardener system significantly improved the properties, especially mechanical properties, thermal stability, chemical resistance and shape memory behavior. The HBPU modified by 20% of epoxy resin showed optimum performance and therefore this composition was only employed for further investigations.
- (iv) Modified HBPU/OMMT nanocomposites were successfully prepared by *ex-situ* and *in-situ* techniques. The nanocomposites exhibited improvements in performance characteristics. It was observed that most of the properties of the nanocomposites prepared by *in-situ* technique were superior to that of the nanocomposites prepared by *ex-situ* technique.
- (v) The modes of modification of the OMMT by HBPA and their consequent nanocomposites have profound influence on the performance characteristics.

The prepared nanocomposites possess enhanced properties, especially the improvements in thermal and flame retardancy was remarkable.

- (vi) HBPU is better matrix for the preparation of silver nanocomposites than the linear analog. The well dispersed and highly stable nanoparticles of silver, and iron based nanocomposites showed better properties than the pristine polymer. The antimicrobial silver nanocomposites also exhibited adequate biodegradation.
- (vii) The HBPU/MWCNT nanocomposites showed excellent improvements in the properties like mechanical, thermal, rheological and shape memory behavior. They also showed higher biodegradation and more cytocompatibility nature compared to the pristine HBPU.
- (viii) The rheological behaviors of the above nanocomposites confirmed the presence of strong interactions between fillers and the matrices.
- (ix) The different nanocomposites have high potential to be used as advanced surface coating materials, adhesives, highly thermo-stable materials, antimicrobial biomaterials, free radical scavenging materials and shape memory biomaterials.

Thus in a nut shell, the prime achievement of the present investigation is the successful exploitation of a less significant renewable raw material to scientifically important products with great impact.

9.2. Future Directions

There are few future scopes of *Mesua ferrea* L. seed oil based HBPU nanocomposites to be worth mentioned for further studies.

- (i) The comprehensive study with theoretical modeling on the reinforcement action of the nanoclay could be carried out to deduce the exact mechanism of the nanofillers.
- (ii) Different types of hyperbranched amine could be used to modify the hydrophilic clay and the effect of modification on the properties of nanocomposites could be investigated.
- (iii) *Mesua ferrea* L. seed oil based HBPU nanocomposites could be evaluated by *in-vitro* and *in-vivo* tests for different biomedical applications.
- (iv) Waterborne vegetable oil based HBPU nanocomposites could be prepared.

List of Publications

In International Journals

1. **Deka, H.**; Karak, N. Bio-based hyperbranched polyurethanes for surface coating applications. *Prog. Org. Coat.* **66**, 192-198 (2009)
2. **Deka, H.**; Karak, N. Vegetable oil-based hyperbranched thermosetting polyurethane/clay nanocomposites. *Nanoscale Res. Lett.* **4**, 758-765 (2009)
3. Deka, G.; **Deka, H.**; Karak, N. Free radical scavenging magnetic iron-based nanoparticles in hyperbranched and linear polymer matrices. *J. Macromol. Sci., Part A* **46**, 1128-1135 (2009)
4. **Deka, H.**; Karak, N.; Kalita, R.D.; Buragohain, A.K. Biocompatible hyperbranched polyurethane/multi-walled carbon nanotube composites as shape memory materials. *Carbon* **48**, 2013-2022 (2010)
5. **Deka, H.**; Karak, N. Shape-memory property and characterization of epoxy resin-modified *Mesua ferrea* L. seed oil-based hyperbranched polyurethane. *J. Appl. Polym. Sci.* **116**, 106-115 (2010)
6. **Deka, H.**; Karak, N. Bio-based hyperbranched polyurethane/clay nanocomposites: adhesive, mechanical, and thermal properties. *Polym. Advan. Technol.* (2010) (DOI: 10.1002/pat.1603)
7. **Deka, H.**; Karak N.; Kalita, R.D.; Buragohain, A.K. Bio-based thermostable, biodegradable and biocompatible hyperbranched polyurethane/Ag nanocomposites with antimicrobial activity. *Polym. Degrad. Stab.* (2010) (DOI: 10.1016/j.polymdegradstab.2010.06.017)
8. **Deka, H.**; Karak N. Influence of highly branched poly(amido amine) on the properties of hyperbranched polyurethane/ clay nanocomposites. *Mater. Chem. Phys.* (2010) (DOI: 10.1016/j.matchemphys.2010.06.002)
9. **Deka, H.**; Karak N. Rheological study of vegetable oil based hyperbranched polyurethane/ MWCNT nanocomposites. (communicated)
10. **Deka, H.**; Karak N. Rheological behavior of epoxy modified bio-based hyperbranched polyurethane/clay nanocomposites. (communicated)
11. Kumar, A.; Deka, M.; **Deka, H.**; Karak, N. Ionic transport studies in novel hyperbranched/clay nanocomposite gel polymer electrolytes. (communicated)
12. Deka, M.; Kumar, A.; **Deka, H.**; Karak, N. Electrical and electrochemical studies of PvdF/clay nanocomposites gel electrolyte for application in Li-ion batteries. (communicated)

Conference Presentation (Published as Proceeding)

1. Deka, H.; Karak, N. Synthesis and prospect of vegetable oil based highly branched polyurethane. *International Conference on Frontiers in Polymer Science and Technology (POLY 2007)*, Guwahati, Assam, November (2007)
2. Karak, N.; Deka, H. Hyperbranched polyurethane/clay nanocomposites. *International Conference on Polymer Blends, Composites, IPNs, Membranes, Poly Electrolytes and Gels: Macro to Nano Scales (ICBC 2008)*, Kottayam, Kerala, September (2008)
3. Karak, N.; Deka, H.; Dutta, S. Vegetable oil based hyperbranched and conventional resinous polyurethane/clay thermosetting nanocomposites. *International Conference on Nanostructured Materials and Nanocomposites (ICNM 2009)*, Kottayam, Kerala, April (2009)
4. Deka, H.; Karak, N. Fluorescence characteristic of hyperbranched polyurethane/silver nanocomposites. *National Seminar on Photonics and Quantum Structures (NSPQS 2009)* Tezpur University, Assam, November (2009)
5. Karak, N.; Mahapatra, S.S.; Dutta, S.; Deka, H.; Konwar, U.; Das, G.; Konwar, R. Polymer nanocomposites-multifaceted advanced materials for today's society. *National Seminar on Photonics and Quantum Structures (NSPQS 2009)* Tezpur University, Assam, November (2009)
6. Deka, H.; Karak, N. Bio based hyperbranched polyurethane/clay nanocomposites and their prospects. *International Conference on Advanced Nanomaterials and Nanotechnology (ICANN 2009)* IIT Guwahati, Assam, December (2009)